Studies of dye sensitised photovoltaic cells

Shaw, Nicola Jane

Award date:
1999

Awarding institution:
University of Bath

STUDIES OF DYE SENSITISED PHOTOVOLTAIC CELLS

Submitted by Nicola Jane Shaw
for the degree of PhD
of the University of Bath
1999

ProQuest LLC
789 East Eisenhower Parkway
P.O. Box 1346
Ann Arbor, MI 48106-1346

Index

Acknowledgements

Acknowledgements

I would like to thank my supervisor Professor Laurie Peter for all the help, advice, guidance and encouragement he has given throughout the duration of my studies. Special thanks are due to Mike Bailes for all the technical support and Evgueni Ponomarev for computer software used with the IMPS measurements. I would also like to thank the past and present members of the L. M. P. Group at Bath in particular Eric, Günter, Jason, Greg, Rob, Mark, Anthony, José, Sabino, David, Siva, Laurent, Rachel, Gabriella and Gareth for making my time in Bath an enjoyable experience. Thanks must also go to Pam Croft without whom the group could not function.

Thanks are due to the Institut für Angewandte Photovoltaic (INAP) for supplying photovoltaic cells and to Professor Heiland (University of Achen) for supplying the zinc oxide single crystals.

This work would not have been possible without the funding from the Engineering and Physical Sciences Research Council (EPSRC) and The University of Bath.

Thanks must also go to the Winchester Road contingent: Andy, Deb, Bill, Pippa, Jon, Peter & Alex for putting up with me for 3 years.

Finally a big thank you to my family for supporting me over the years and particularly to Howard who has been a continued source of encouragement to me.

Abstract

Studies of Dye Sensitised Photovoltaic Cells

Abstract
Studies of Dye Sensitised Photovoltaic Cells

Steady state and modulation techniques have been used to characterise the properties of dye-sensitised nanocrystalline photovoltaic cells.

The active electrodes were prepared by deposition of a thin (~10 micron) layer of nanocrystalline TiO_2 on fluorine doped tin-oxide coated glass using a sol-gel technique. The TiO_2 was sensitised with cis-di(thiocyanato)-N,N'-bis(2,2-dicarboxylate)ruthenium(II). The electrolyte consisted of methylhexylimidazolium iodide, iodine, 4-tert-butylpyridine and acetonitrile. Thin layer cells were fabricated by sealing with polyethylene hot melt.

The generation and transport of electrons in the cells was characterised by photoelectrochemical impedance spectroscopy (PEIS), intensity modulated photocurrent spectroscopy (IMPS) and intensity modulated photovoltage spectroscopy (IMVS). The kinetics of the regeneration reaction were studied on fluorine doped tin-oxide glass alone and coated with platinum (heat deposited or sputtered) using electrochemical impedance spectroscopy (EIS).

The PEIS data were fitted to a model consisting of the impedance of the counter electrode in series with an impedance representing the illuminated dye-sensitised TiO_2 electrode. The IMPS data were fitted using expressions derived from the continuity equation describing the generation, collection and decay of electrons in the sensitised film. IMVS data were fitted to obtain values of the electron lifetime.

The EIS studies of the kinetics of the iodide/tri-iodide reaction showed that the reaction is very fast on platinum or platinum doped tin-oxide glass but very slow on fluorine doped tin-oxide glass alone.

Electron transport and back reaction with tri-iodide were both found to depend on light intensity. The diffusion coefficient of electrons, D_n was found to depend on the illumination intensity according to the power law $D_n \propto I^{0.6}$. The electron lifetime was found to obey the power law $\tau_n \propto I^{-0.53}$. Since D_n increases with light intensity whereas τ_n decreases, the electron diffusion length $L_n=(D_n\tau_n)^{1/2}$ varies only weakly with light intensity ($L_n \propto I^{-0.03}$). Therefore the incident photon to current conversion efficiency (IPCE) of the cells is almost independent of intensity.

Chapter 1

Introduction

Index

Chapter 1 Introduction

1.1 Solar energy conversion

The increase in population and the rapid consumption of fossil fuels and non-renewable energy has made it necessary to look towards other forms of energy. There is much interest in renewable energy sources as this would be a permanent solution. Solar energy conversion has several advantages as it is a relatively cheap renewable energy source. Photovoltaic systems are in general, quiet, require little maintenance, have no critical size and are environmentally friendly.

The solar spectrum changes depending on air mass. Factors effecting the air mass include atmospheric conditions such as the relative quantities of water, ozone, oxygen, carbon dioxide and dust. The solar spectrum reaching the earth is defined as AMn where $n = 1/\cos\theta$ (θ = the angle between the suns position and zenith). Hence solar spectra are referred to as AM1, AM2, AM3 etc. The spectrum of AM1.5 light is shown in Figure 1.1

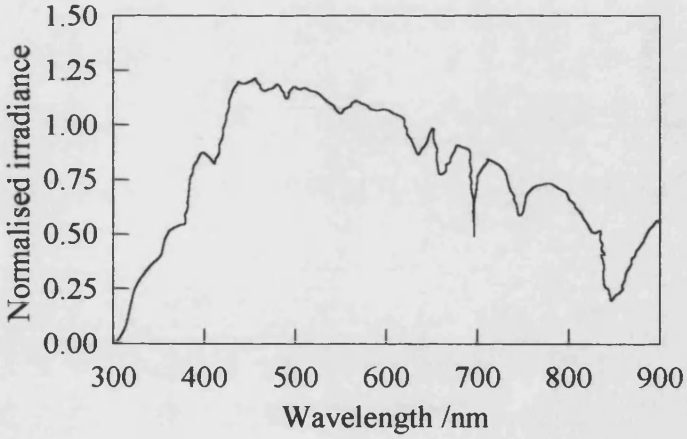

***Figure 1.1** Spectrum of AM1.5 light [1].*

1.2 Photovoltaic parameters.

The effectiveness of a solar cell can be defined quantitatively by the parameters listed in the table below. A typical current voltage curve for a dye sensitised solar cell showing some of the parameters is shown in Figure 1.2.

Parameter	*Definition*
Short circuit current (I_{sc})	Current flow at 0V applied voltage under illumination
The open circuit voltage (V_{oc})	Voltage at which there is no net current flowing through the device under illumination.
IPCE (Φ)	Ratio of electron flux under short circuit conditions to the incident photon flux. It is a dimensionless quantity between 0 and 1 but is often expressed as a percentage. $IPCE = \frac{I_{sc}}{qI_oA}$ (A= electrode area, I_o= incident photon flux, q = elementary charge)
The power output (P)	$P = I \times V$
Fill Factor	$FF = \frac{P_{max}}{I_{sc} \times V_{oc}}$

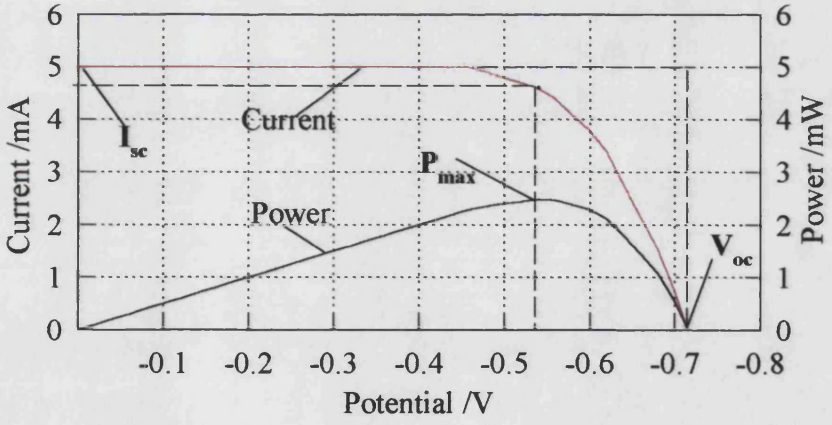

***Figure 1.2** Photocurrent voltage curve and calculated power output (2.84 mW) for a dye sensitised solar cell under illumination. I_{sc}= 5mA, V_{oc}= 0.72V, maximum power = 2.84 mW, Fill Factor =0.79.*

1.3 Early studies of photosensitisation

In the late 60's and early 70's much research was concerned with sensitising wide band-gap, single crystal semiconductors with dye molecules. Zinc oxide was used frequently, and reports of sensitisation with a range of dyes including rhodamine B, riboflavin, chlorophyll derivatives and ferrocyanide can be found in the literature [2,3,4,5,6,7,8]. Sensitisation effects have also been found using the single crystal semiconductors cadmium sulphide [9], and gallium phosphide [10].

1.4 Sensitisation mechanisms

1.4.1 Charge transfer

When a dye adsorbed at the surface of an n-type semiconductor absorbs a photon, an electron in the HOMO is promoted to the LUMO. If the LUMO is above the level of the conduction band in the semiconductor, it may be energetically more favourable for the electron to transfer into the semiconductor rather than for the electron to transfer back to the HOMO. This photoinjection process is possible because there is a high density of vacant sites in the semiconductor. Thus electron transfer between the dye and the semiconductor takes place (Figure 1.3). k_1 is the excited state lifetime quenching rate (injection rate) and k_2 is the process defined by the lifetime of the excited state in the absence of electron transfer quenching. This process results in the dye being oxidised.

$$D \xrightarrow{h\upsilon} D^*$$

$$D^* \rightarrow D^+ + e_{cb.}$$

Electron injection into the conduction band of a semiconductor has been observed, for example with zinc oxide and rhodamine B [11].

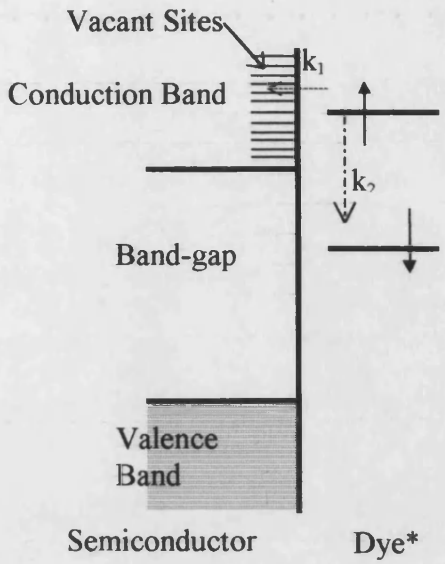

Figure 1.3 *Electron injection by an electronically excited dye molecule into the conduction band of a semiconductor.*

Similarly if the LUMO of the dye lies in the band-gap and the HOMO lies below the valence band edge, then hole injection into (electron capture from) the valence band is possible. This results in the dye being reduced i.e.

$$D \xrightarrow{h\upsilon} D^*$$

$$D^*e_{vb} \rightarrow D^- + h^+_{vb}$$

and is shown in Figure 1.4. Electron capture from the valence band (hole injection into the valence band) of a semiconductor has been observed, for example with gallium phosphide and cryptocyanine [10].

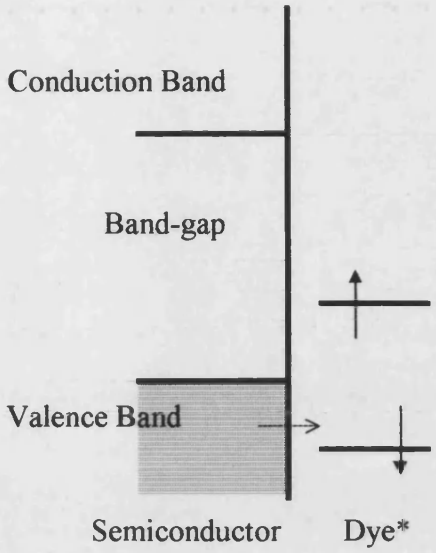

Figure 1.4 *Hole injection (electron capture) by an electronically excited dye molecule into the valence band of a semiconductor.*

If a metal rather than a semiconductor is used electron injection still occurs above the Fermi level, but the reverse reaction is likely to occur almost simultaneously and therefore no net effect will be observed. This is shown in Figure 1.5.

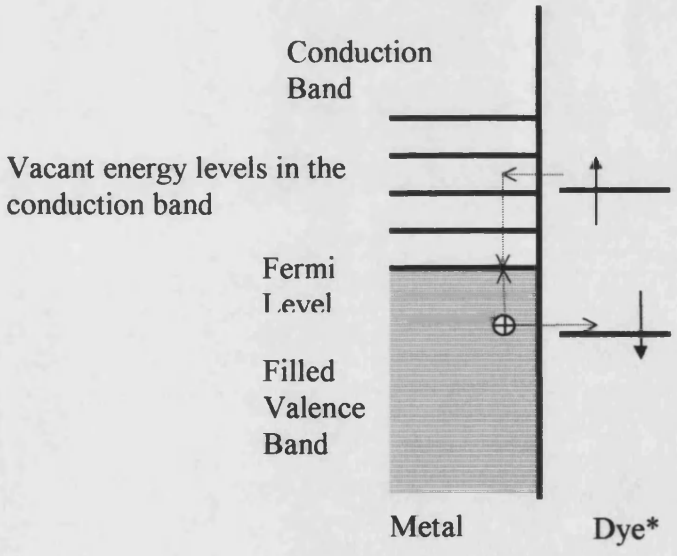

Figure 1.5 *The result of electron injection into the conduction band of a metal.*

1.4.2 Energy transfer

It is possible that when a dye is adsorbed onto the surface of a semiconductor, energy transfer rather than charge transfer occurs. The initial step, the excitation of the sensitising dye, is the same for both mechanisms. For energy transfer (see Figure 1.6) the excited electron, which is now in the LUMO of the dye, falls back into the HOMO of the dye. If the semiconductor has energy levels that have the same energy difference as the HOMO and LUMO of the dye, the energy generated when the electron returns to the ground state of the dye, can be absorbed by the semiconductor. In this case an electron will be promoted from the valence band into an acceptor level in the conduction band. For the next part we shall assume that the energy levels of the dye are in a similar in position to those for hole injection into the valence band (Figure 1.4). Once an electron is in the conduction band, it may transfer to the LUMO of the dye (in which case the corresponding hole will be collected as cathodic photocurrent) and the dye will become reduced. The result is then the same as hole injection (Figure 1.4). Energy transfer has been found to occur with eosin and p-GaP [10]. Other p-type semiconductors (such as SiC, which has a larger band-gap than GaP), show large sensitisation currents with eosin and therefore support the view that energy transfer rather than charge transfer is present in the case of eosin and p-GaP. The electron may of course recombine with the hole in the valence band and thus the excess energy will be dissipated in the lattice.

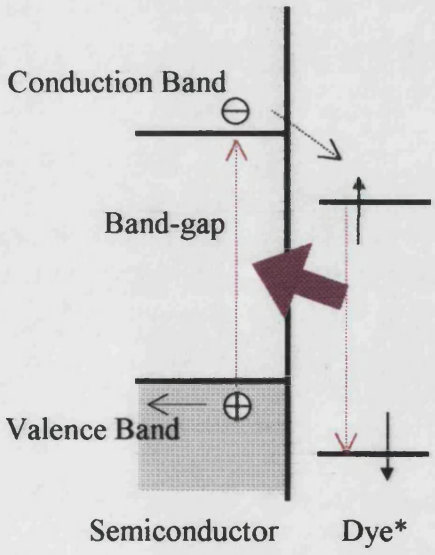

***Figure 1.6** Energy transfer by an electronically excited dye molecule producing a hole in the valence band of a semiconductor.*

Similarly if the HOMO and LUMO of the dye were positioned as those for electron injection into the conduction band (Figure 1.3), energy transfer would produce an anodic current with electron capture from the dye resulting in oxidation of the dye (Figure 1.7).

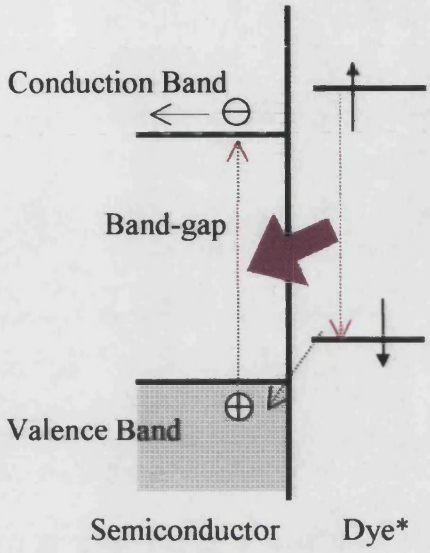

Figure 1.7 *Energy transfer by an electronically excited dye molecule producing an electron in the valence band of a semiconductor.*

1.5 Energy transfer or charge transfer?

Energy transfer depends on the density of energy levels within the semiconductor with the same energy difference as the sensitising dye. The greatest number of energy levels are available in the valence and conduction bands of a semiconductor. Therefore if the energy difference between the HOMO and LUMO of the adsorbed dye is greater than, or equal to, the energy of the semiconductor band-gap, the probability of energy transfer is much higher than charge transfer. Energy transfer is therefore expected when the fluorescence spectra of the excited dye and the absorbency spectrum of the semiconductor overlap [10 and refs. therein.]. If the mechanism is charge transfer then a sensitisation current will be observed at wavelengths where the dye absorbs light.

1.6 Supersensitisation

Supersensitiation is the increase in the sensitisation photocurrent by the addition of a reducing agent in the case of electron injection or an oxidising agent in the case of hole injection [3]. Supersensitisation is only possible for charge transfer mechanisms. The mechanisms of supersensitisation for electron and hole injection are shown in Figure 1.8 and Figure 1.9.

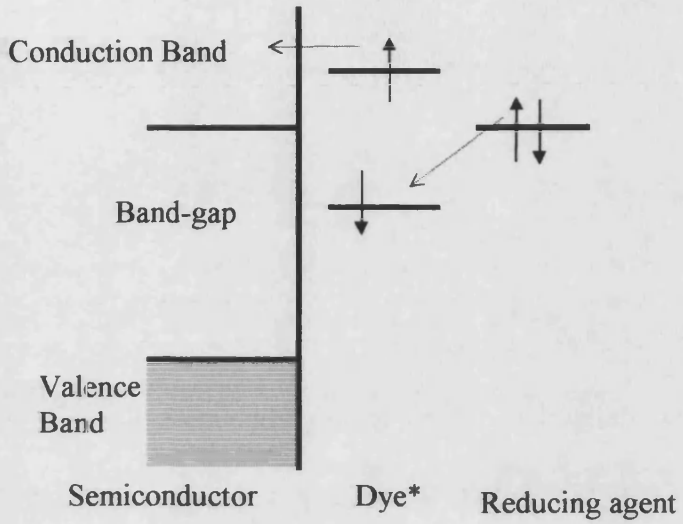

Figure 1.8 *Supersensitisation by a reducing agent of electron injection into the conduction band of a semiconductor. An example of supersensitiation of electron injection into the conduction band is zinc oxide, rose bengal and hydroquinone [11].*

In Figure 1.8 the reducing agent places electrons into the HOMO of the excited dye molecule. This causes the electron transfer from the LUMO of the excited dye to be made easier. This is because of two reasons: Firstly the electron energy levels have moved to a higher energy as a result of the reduction. Secondly the electron lifetime of the electron in the LUMO has been increased due to the electron that has transferred from the reducing agent into the HOMO of the dye. There is also a possibility that the electron from the reducing agent does not initially transfer completely but forms a charge transfer complex with the excited dye molecule. An analogous mechanism occurs when an oxidising agent is used for hole injection. (Figure 1.9)

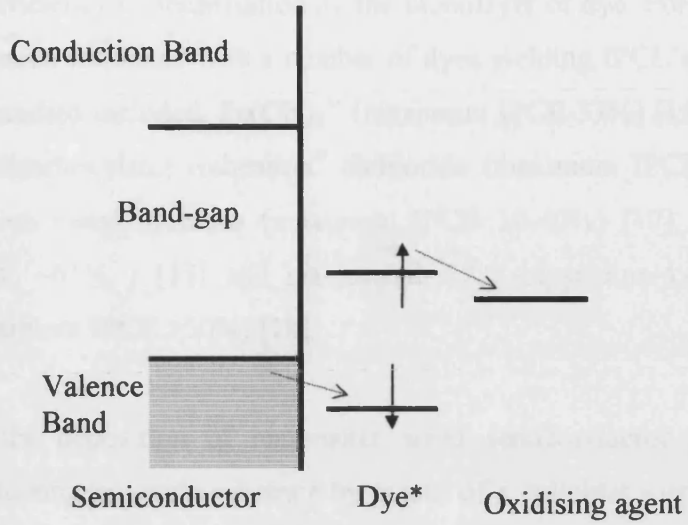

***Figure 1.9** Supersensitisation by an oxidising agent of hole injection into the valence band of a semiconductor. An example of supersensitiation for hole injection into the valence band is p-gallium phosphide, N,N'-diethylpseudoisocyanine and oxygen [3].*

1.7 Effects of surface area

Sensitisation of single crystal semiconductors generally results in low incident photon to current conversion efficiencies (IPCE). It has been observed that longer etching of the surface of GaP produces a rougher surface. This surface pre-treatment yields a higher IPCE at the wavelength of dye adsorption than other surface pre-treatments [10]. The increase in the photocurrent with surface area also gives evidence that only dye molecules that are in intimate contact with the electrode surface are able to partake in the sensitisation. This implies that the charge injection into the semiconductor is limited to the first monolayer of absorbed dye.

In order to obtain larger sensitisation currents, a larger surface area is required. Colloidal particles in solution have shown larger sensitisation effects, for example, on the addition of titanium dioxide particles to solutions of tris-(2,2'-bipyriding-4,4'-dicarboxylate) ruthenium^{II} dichloride [12], phenyl fluorone [13] and a chlorophyll analogue [14], a substantial decrease in the emission spectrum was observed.

Polycrystalline titanium dioxide electrodes can be prepared by the deposition of a layer of TiO_2 onto titanium sheet or rod. The porous film consisting of nanometer sized

particles have a surface area 1000 times the geometric area. This results in a large increase in the efficiency of sensitisation by the monolayer of dye. Polycrystalline TiO_2 electrodes have been sensitised with a number of dyes yielding IPCE's between 10 and 70%. The dyes studied included: $Fe(CN)_6^{4-}$ (maximum IPCE 37%) [15, 16], tris (2,2'-bipyridine-4,4'-dicarboxylate) ruthenium^{II} dichloride (maximum IPCE >40%) [12], a range of transition metal cyanides (maximum IPCE 10-40%) [17], phenyl fluorone (maximum IPCE ~65%) [13] and cis-diaquabis(2,2'-bipyridine-4,4'-dicarboxylate) ruthenium^{II} (maximum IPCE >50%) [18].

More recently the deposition of nanometer sized semiconductor particles onto a transparent conducting tin oxide substrate by means of a colloidal suspension [1,19,20] or in some cases of TiO_2 prepared via hydrolysis of $TiCl_3$ [21, 22] has become popular. This is particularly useful for solar energy conversion as the transparent substrate allows light to be absorbed through the oxide film. Thin films of SnO_2 deposited onto conducting glass have been sucessfully sensitised with a range of dyes including chlorophyll b, bis(2,2'-bipyridine-4,4'-dicarboxylate) ruthenium^{II} crown ether linked cyanine dyes [1,23, 24]. Zinc oxide thin films have also been sensitised with ruthenium based dyes [25, 26]. It should be noted that with the exception of titanium dioxide, sensitisation effects on thin films of semiconductor rarely yield IPCE values that exceed 20%.

1.8 Time scale for electron injection

Electron injection from an excited dye molecule into the conduction band of a TiO_2 semiconductor particle has been shown to take place in the pico second time domain [27, 28 and references therein]. Electron injection is several thousand times faster [28] than recombination of the injected electron with the oxidised state of the dye, which is a multiexponential process that occurs typically on a micro to millisecond time scale [27].

1.9 Dye sensitised thin layer solar cells

A dye sensitised nanoporous TiO_2 semiconductor thin film has been employed by Grätzel and co workers to form a regenerative solar cell with a maximum IPCE of over 80% [29]. A schematic diagram of the cell is shown in Figure 1.10.

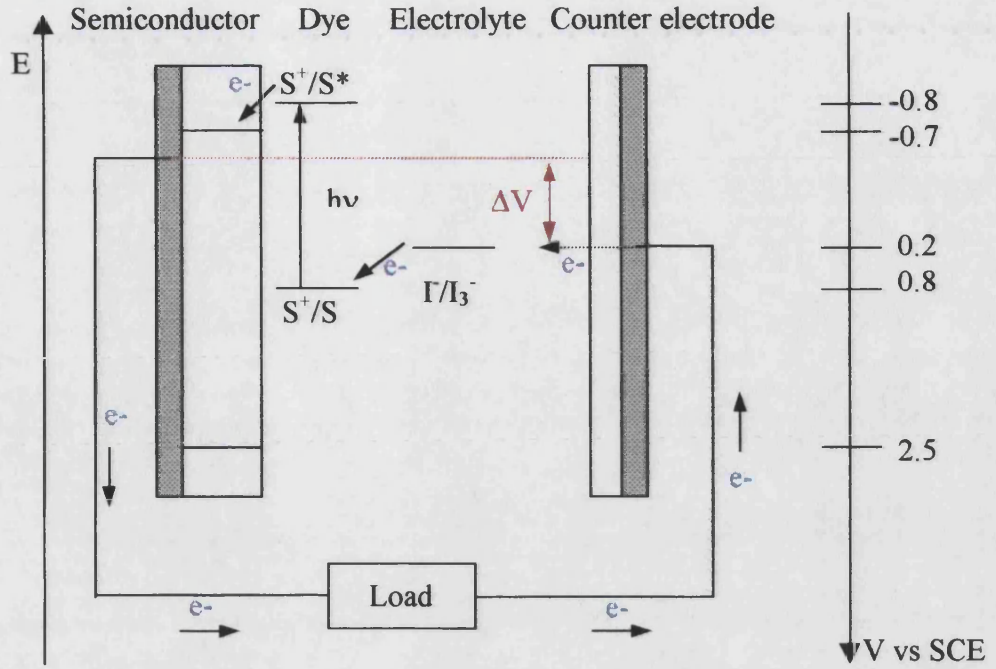

***Figure 1.10** Schematic diagram of a dye sensitised solar cell [28].*

The cell consists of a nanoporous TiO_2 layer deposited onto conducting tin oxide glass. The TiO_2 layer is sensitised by a ruthenium based dye. The counter electrode is platinum sputtered conducting tin oxide. The electrolyte contains iodide ions as a reducing agent.

The primary difference between a dye sensitised solar cell and a conventional p-n junction solar cell is that the dye sensitised cell separates the function of the light absorption and the charge carrier transport. The whole process has similarities to photosynthesis. The dye absorbs the sunlight and uses the light energy to induce an electron transfer reaction. This is analogous to the function of chlorophyll in a leaf. The TiO_2 membrane acts as a support for the dye, accepts electrons into the conduction band and provides a medium by which electrons can be transported to the back contact. This is analogous to the biological lipid membrane in a leaf. Electron transfer from iodide in solution regenerates the dye, the counter electrode then regenerates the iodide. Back reaction between the oxidised state of the dye and the electron injected into the conduction band can only occur at the interface because the hole is localised on the dye molecule. This localisation of the hole reduces the rate of the back reaction significantly. The ratio of injection into the conduction band and back reaction of the injected electrode is large, typically $\geq 1 \times 10^3$. This large ratio means that an electrostatic

field is not required to collect the injected electrons. A high efficiency is achieved, as the ratio of the forward to back reaction is high.

Further developments aimed at excluding the liquid electrolyte from the cell have been made. Tennakone [30, 31] has employed p-CuI deposited on to the dye sensitised TiO_2 layer, but only low conversion efficiencies were obtained. More recently, Grätzel has demonstrated the use of an amphorous organic hole transport material, 2,2'7,7'-tetrakis(N,N'-di-*p*-methoxyphenyl-amine)9,9'-spirobifluorene (OMeTAD). A monochromatic IPCE of 33% was obtained in this case [32]. Results presented in this thesis are concerned with dye sensitised solar cells with a liquid electrolyte.

1.10 Dye characteristics

Ruthenium based dyes have been employed in the dye sensitised solar cell as they have been shown to be very stable. RuL_3 (L=2,2'-bipyridyl-4, 4'-dicarboxylate) was the first dye of this type to be used with high surface area films. This dye survived intense illumination over a period of nine months without significant loss of cell performance (this is calculated to be ~5×10^7 redox cycles) [28]. Other organic dyes were noted to undergo photobleaching after about 1×10^4 cycles.

The ruthenium based dyes have a high ratio of electron injection to back reaction [28]. It is believed that this is because the orbitals for the back electron transfer reaction overlap less favourably with the wave function of the electrons in the conduction band. Carboxylate ligands on the ruthenium complex attach the dye onto the surface. These ligands give a good electronic coupling between the π^* orbital of the excited complex and the 3d wave function of the TiO_2 film, hence electron injection is fast. The back reaction involves a d-orbital localised on the ruthenium, and this orbital has a poor overlap with the wave function of the conduction band electrons. In addition to this poor overlap, the orbitals on the ruthenium contract once an electron has been transferred from the dye to the TiO_2, making it even more difficult for the back reaction to occur. This leads to a slow back reaction and light induced charge separation is achieved on kinetic grounds [28].

Dyes such as chlorophyll derivatives [33,34], tri-nuclear ruthenium complexes [35] and osmium complexes [36] have all been investigated, however mono-nuclear ruthenium

based dyes in general produce a better overall photoresponse. Although RuL_3 is very stable and produces a large IPCE, it does not however, have a good overlap with the visible spectrum [28]. It was found that dyes with the general formula cis-X_2bis(2,2'-bipyridyl-4,4'-dicarboxylate) ruthenium(II) where X = Cl^-, Br^-, I^-, CN^- and SCN^- have a more favourable overlap with the solar spectrum [1]. $RuL_2(NCS)_2$ for example has a high IPCE over the majority of the visible spectrum. Cis-X_2bis(2,2'-bipyridyl-5,5'-dicarboxylate) ruthenium(II) compounds in general absorb more light at longer wavelengths, however the enhanced photoresponse at the longer wavelengths was offset by a much lower photocurrent efficiency at shorter wavelengths [37].

1.11 Electron transport and back reaction within the TiO_2 nanocrystalline film

The IPCE depends on both the rate of electron transport within the film (the diffusion coefficient of electrons) and the lifetime on the electrons in the film (which is related to the rat of the back reaction of the electrons). The diffusion coefficient and the lifetime of the electrons can be combined to obtain the diffusion length of the electrons, which is the square root of the product of the diffusion coefficient and the lifetime of the electrons.

Electron transport

Within a nanocrystalline semiconductor thin film there is no band bending, due to the small size of the colloidal particles. For this reason diffusion rather than migration is responsible for electron transport throughout the film. Nanocrystalline films are unique in that they allow electrolyte to penetrate throughout the porous network of particles to the back contact. Södergren et al [38] have used UV light to generate electron hole pairs in the nanocrystalline TiO_2 film. They assume that the diffusion length of the electrons is constant and fit the current voltage characteristics for electrolyte electrode and substrate electrode illumination.

Intensity modulated photocurrent spectroscopy measurements using UV light on un-dyed TiO_2 thin films show that ω_{min} increases with background light intensity [39]. Simple diffusion control within a nanoporous GaP system shows no intensity dependence of ω_{min} [40] and thus it is clear that for nanoporous TiO_2 systems trapping and recombination of the photogenerated electrons must be considered [39,41].

The photocurrent transient response in dye sensitised systems is slow, whereas the electron injection from the dye into the nanocrystalline system occurs on a pico second time scale. This implies that the electron transport within the film dominates the transient photocurrent response. Measurements indicate that the rise time of the transients depends on the intensity of the incident light with an exponent of –0.6 to -0.8 [42]. Intensity modulated photocurrent spectroscopy measurements of the system indicates the same power law dependence of the time constant [42, 43].

Results presented in this thesis show that modelling of the IMPS response for a range of intensities can be used to obtain the diffusion coefficient of the photo-injected electrons. The IMPS responses for substrate and electrolyte illumination show different characteristics, and modelling of the substrate and electrolyte responses at the same intensity give diffusion coefficients that are in agreement. It was found that in order to obtain a good fit between the experimental and the theoretical results it is important to take the capacitance and resistance of the TiO_2 layer into account. Typical diffusion coefficients are of the order 5×10^{-5} cm^2s^{-1}. This result is 4 orders of magnitude lower than values estimated for electrons in single crystal anatase [44] and sputtered thin films [45]. The diffusion coefficient calculated from photocurrent transients is typically $1. \times 10^{-5}$ cm^2s^{-1}[46]. The IMPS responses at potentials other than short circuit can be fitted by taking into account the changes in the capacitance value of the film.

Electron lifetime and back reaction

The relatively slow diffusion of electrons within the TiO_2 films means that an electron generated within a film will take several milliseconds to diffuse to the back contact. Despite this long transit time, the short circuit collection efficiency of injected electrons still exceeds 90%. This means that the lifetime (τ_n) of the injected electrons exceeds the transit time needed to diffuse to the back contact. At open circuit the electrons are not collected at the contact but undergo back reactions with the I_3^- or the oxidised state of the dye. Intensity modulated photovoltage spectroscopy (IMVS) has been used to derive the electron lifetime under open circuit conditions. The lifetime is noted to depend on the illumination intensity and on the concentration of the I_3^- in solution [47].

The accumulation of electrons in the conduction band in the absence of dye has been monitored spectroscopically [48,49]. Electron accumulation in the conduction band was achieved by controlling the potential of the electrode. Electrons in dye sensitised nanocrystalline systems have been monitored by choosing a wavelength in the near infra red, that lies beyond the dye absorption onset. In recent studies, Franco et al [50] used intensity modulated visible light to excite the dye molecules and monitored the film transmittance in the IR. Results indicated that substantial electron accumulation occurs in the TiO_2 film even under short circuit conditions, and the majority of electrons detected appear to be trapped. They show that under strong accumulation conditions the injection efficiency of the dye is decreased from 1 at short circuit to 0.3 at open circuit. This is in agreement with work by Haque et al [51] who showed that the recombination of injected electrons is strongly dependant on the bias voltage of the electrode.

Electrochemical impedance spectroscopy measurements presented in this thesis support the accumulation of electrons at open circuit. The capacitance calculated at open circuit is of the order of several milli-Farads compared to micro-Farads at short circuit. Illumination of the cell increases the capacitance under both short circuit and open circuit conditions.

1.12 Factors effecting the IPCE

Studies of the photocurrent action spectra for electrolyte electrode and substrate electrode illumination of dye sensitised nanocrystalline films have established that film thickness, electron scavengers in the electrolyte and surface treatments were all found to influence the IPCE [52]. Electron scavengers such as O_2 and iodine lower the IPCE when measurements are made in a conventional 3-electrode cell rather than in a thin layer sealed 2-electrode solar cell. Surface treatment with organics such as pyridine increase the IPCE. It is thought that they adsorb onto vacant sites on the TiO_2 surface and block the back reaction of the injected electrons with the oxidised state of the dye or other solution species [52]. It is reported that substrate electrode illumination produced higher photocurrents than electrolyte electrode illumination because the electrons are generated close to the back contact [38,52] and therefore do not have far to diffuse before they are collected. Electrons generated near to the electrolyte electrode interface must diffuse through the film in order to be collected and thus more have the opportunity to recombine.

1.13 References

1. Nazeeruddin, M. K.; Kay, A.; Rodicio, I.; Humphry-Baker, R.; Müller, E.; Liska, P.; Vlachopoulos, N.; Grätzel, M. *J. Am Chem. Soc.* **1993**, *115*, 6382

2. Gerischer, H. *Surface Science* **1969**, *18*, 97.

3. Tributsch, H.; Gerischer, H. *Ber. Bunsenges. Phys. Chem.* **1969**, *73*, 850.

4. Tributsch, H.; Calvin, M. *Photochem. Photobiol.* **1971**, *14*, 95.

5. Freund, T. *Surface Science* **1972**, *33*, 295.

6. Pettinger, Von B.; Schöppel, H.-R.; Gerischer, H. *Ber. Bunsenges. Phys. Chem.* **1973**, *77*, 960.

7. Pettinger, Von B; Schöppel, H.-R.; Gerischer, H. *Ber. Bunsenges. Phys. Chem.* **1974**, *78*, 450.

8. Danzmann, H. J.; Hauffe, K. *Ber. Bunsenges. Phys. Chem.* **1975**, *79*, 438.

9. Watanabe, T.; Fujishima, A.; Honda, K. *Ber. Bunsenges. Phys. Chem.* **1975**, *79*, 1213.

10. Memming, R.; Tributsch, H. *J. Phys. Chem.* **1971**, *75*, 562.

11. Gerischer, H.; Tributsch, H. *Ber. Bunsenges. Phys. Chem.* **1968**, *72*, 437.

12. Desilvestro, J.; Grätzel, M.; Kavan, L.; Moser, J.; Augustynski, J. *J. Am. Chem. Soc.* **1985**, *107*, 2988

13. Frei, H.; Fitzmaurice, D. J.; Grätzel, M. *Langmuir* **1990**, *6*, 198

14. Kamat, P. V.; Chauvet, J-P.; Fessendan, R. W. *J. Phys. Chem.* **1986**, *90*, 1389

15. Vrachnou, E.; Vlachopoulos, N.; Grätzel, M. *J. Chem. Soc., Chem. Commun.* **1987**, 868

16. Vrachnou, E.; Liska, P.; McEvoy, A. J.; Grätzel, M. *Surface Science*. **1987**, *189/190*, 823

17. Vrachnou, E.; Grätzel, M.; McEvoy, A. J. *J. Electroanal. Chem.* **1989**, *258*, 193

18. Liska, P.; Vlachopoulos, N.; Nazeeruddin, P. C.; Grätzel, M. *J. Am. Chem. Soc.* **1988**, *110*, 3686

19. O'Regan, B.; Moser, J.; Anderson, M.; Grätzel, M. *J. Phys. Chem.* **1990**, *94*, 8720.

20. Bedja, I.; Hotchandani, S.; Carpentier, R.; Fessenden, R. W.; Kamat, P. V. *J. App. Phys.* **1994**, *75*, 5444

21. Kavan, L.; O'Regan, B.; Kay, A.; Grätzel, M. *J. Electroanal. Chem.* **1993**, *346*, 291

22. Kavan, L.; Stoto, T.; Grätzel, M.; Fitzmaurice, D.; Shklover, V. *J. Phys. Chem.* **1993**, *97*, 9493

23. Bedja, I.; Hotchandani, S.; Kamat, P. V. *J. Phys. Chem.* **1994**, *98*, 4133

24. Nasr, C.; Hotchandani, S.; Kamat, P. V.; Das, S.; Thomas, K. J.; George, M. V.; *Langmuir* **1995**, *11*, 1777

25. Redmond, G.; Fitzmaurice, D.; Grätzel, M. *Chem. Mater.* **1994**, *6*, 686

26. Bedja, I.; Kamat, P. V.; Hua, X.; Lappin, A. G.; Hotchandani, S. *Langmuir* **1997**, *13*, 2398

27. Tachibana, Y.; Moser, J. E.; Grätzel, M.; Klug, D. R.; Durrant, J. R. *J. Phys. Chem.* **1996**, *100*, 20056

28. Hagfeldt, A.; Grätzel, M. *Chem. Rev.* **1995**, *95*, 49

29. O'Regan, B.; Grätzel, M. *Nature* **1991**, *353*, 737

30. Tennakone, K.; Kumara, G. R. R. A.; Kumarasinghe, A. R.; Wijayantha, K. G. U.; Sirimanne, P. M. *Semicond. Sci. Technol.* **1995**, *10*, 1689

31. Tennakone, K.; Kumara, G. R. R. A.; Wijayantha, K. G. U. *Semicond. Sci. Technol.* **1996**, *11*, 1737

32. Bach, U.; Lupo, D.; Comte, P.; Moser, J. E.; Weissörtel, F.; Salbeck, J.; Spreitzer, H.; Grätzel, M. *Nature* **1998**, *395*, 583

33. Kay, A.; Grätzel, M. *J. Phys. Chem.* **1993**, *97*, 6272

34. Kay, A.; Humphry-Baker, R.; Grätzel, M. *J. Phys. Chem.* **1994**, *98*, 952

35. Nazeeruddin, M. K.; Liska, P.; Moser, J.; Vlachopoulos, N.; Grätzel, M. *Helvetica Chimica Acta.* **1990**, *73*, 1788

36. Grätzel, M. *Platinum Metals Rev.* **1994**, *38*,151

37. Argazzi, R.; Bignozzi, C. A.; Heimer, T. A.; Castellano, F. N.; Meyer, G. J. *Inorg. Chem.* **1994**, *33*, 5741

38. Södergren, S.; Hagfeldt, A.; Olsson, J.; Lindquist, S. E. *J. Phys. Chem.* **1994**, *98*, 5552

39. De Jongh, P. E.; Vanmaekelbergh, D. *Phys. Rev. Lett.* **1996**, *77*, 3427

40. Vanmaekelbergh, D.; Iranzo Marín, F.; van de Lagemaat, J.; *Ber. Bunsenges. Phys. Chem.* **1996**, *100*, 616.

41. De Jongh, P. E.; Vanmaekelbergh, D. *J. Phys. Chem. B* **1997**, *101*, 2716

42. Cao, F.; Oskam, G.; Meyer, G. J.; Searson, P. C. *J. Phys. Chem.* **1996**, *100*, 17021

43. Dloczik, L.; Ileperuma, O.; Lauermann, I.; Peter, L. M.; Ponomarev, E. A.; Redmond, G.; Shaw, N. J.; Uhlendorf, I. *J. Phys. Chem. B* **1997**, *101*, 10281

44. Forro, L.; Chauvet, O.; Emin, D.; Zuppiroli, L.; Berger, H.; Lévy, F. *J. Appl. Phys.* **1994**, *75*, 633

45. Tang, H.; Prasad, K.; Sanjinés, R.; Schmid, P. E.; Lévy, F. *J. Appl. Phys.* **1994**, *75*, 2042

46. Solbrand, A.; Lindström, H.; Rensmo, H.; Hagfeldt, A.; Lindquist, S. E. *J. Phys. Chem. B* **1997**, *101*, 2514

47. Schlichthorl, G.; Huang, S. Y.; Sprague, J.; Frank, A. J. *J. Phys. Chem. B* **1997**, *101*, 8141

48. O'Regan, B.; Grätzel, M.; Fitzmaurice, D. *J. Phys. Chem.* **1991**, *95*, 10525

49. Rothenberger, G.; Fitzmaurice, D.; Grätzel, M. *J. Phys. Chem.* **1992**, *96*, 5983

50. Franco, G.; Gehring, J.; Peter, L. M.; Ponomarev, E. A.; Uhlendorf, I.; *J. Phys. Chem. B* **1999**, *103*, 692

51. Haque, S. A.; Tachibana, Y.; Klug, D. R.; Durrant, J. R.; *J. Phys. Chem. B* **1998**, *102*, 1745

52. Lindström, H.; Rensmo, H.; Södergren, S.; Solbrand, A.; Lindquist, S. E. *J. Phys. Chem.* **1996**, *100*, 3084

Chapter 2

Fundamentals of semiconductor electrochemistry

Index

Chapter 2 – Fundamentals of Semiconductor Electrochemistry

2.3 The Band Model

It is possible to describe electrical conduction in solids using the band model. The band model can be derived from molecular orbital (MO) theory and the discrete energy levels in atoms. In a solid these energy levels overlap to form a continuum known as a band. The bonding orbitals form the valence band and the anti bonding orbitals the conduction band Figure 2.1.

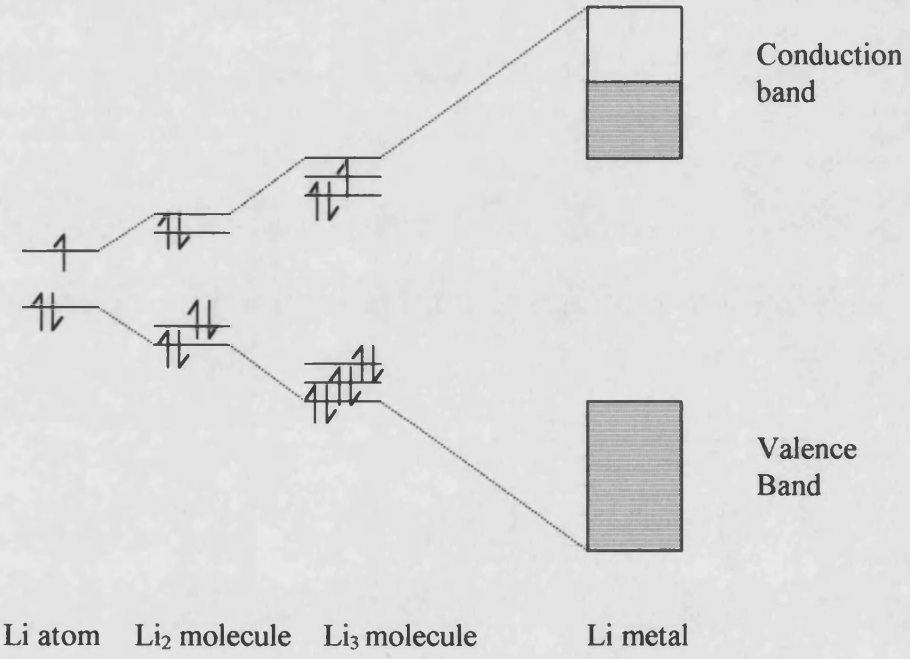

***Figure 2.1** An example of how molecular orbitals overlap to form the band structure of lithium metal.*

Where there is a partially filled band, movement of electrons is possible and conduction can take place. The electrons can be excited thermally or by an electric field to more energetic energy levels within the band allowing electron movement throughout the solid. This occurs at all temperatures above 0 K. Electrons occupying these orbitals are effectively de-localised throughout the solid. In semiconductors and insulators a forbidden region lies between the valence band and conduction band (Figure 2.2). This

forbidden region is known as the band-gap, and it is analogous to the gap between atomic energy levels. For a perfect crystal there are no energy levels in the band gap. Metals have a band-gap, but they conduct as they have a partially filled band that is situated above the bandgap. They are distinguished by their high electrical and thermal conductivity at ambient temperatures.

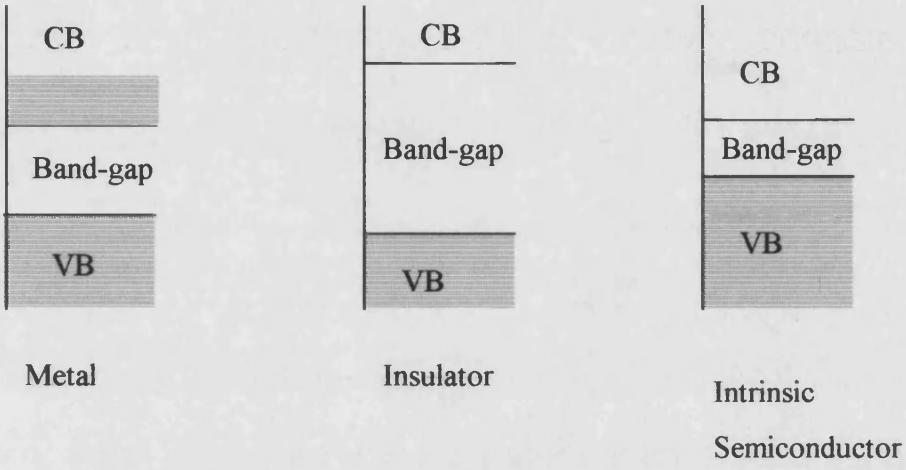

***Figure 2.2** A schematic diagram of the band structure of metals, insulators and intrinsic semiconductors (electron occupancy shown for 0 K)*

At 0 K insulators do not display any conduction because the valence band is filled completely and the conduction band is empty. The higher energy levels needed for conduction are not accessible due to the large band-gap.

Intrinsic semiconductors are characterised by a small band-gap that requires a small amount of energy to cross. For this reason they act as insulators at low temperatures but at higher temperatures the electrons can be excited across the band-gap and conduction occurs.

For a semiconductor the conductivity increases as the temperature rises because more electrons are thermally excited to the conduction band (Figure 2.3).

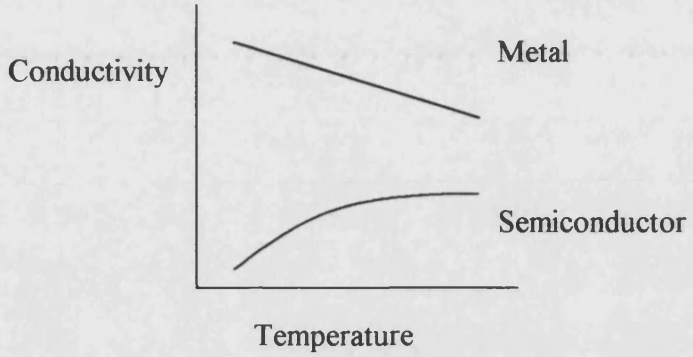

Figure 2.3 *Schematic diagram showing the effect of temperature on the conductivity of a metals and semiconductors.*

For every electron excited to the conduction band, a vacancy is left in the valence band. These vacancies are known as holes and provide a site for an electron from a neighbouring atom to move into. This results in motion of the hole. It is simpler to visualise this as the hole moving throughout the valence band rather than as a cascade of electron movement. It can be shown that the collective movement of electrons in the valence band corresponds to the movement of a virtual particle of opposite sign (the hole).

Photoexcitation

Conduction occurs when light with energy greater than that of the band-gap is incident on the semiconductor. The light excites an electron from the valence band into the conduction band leaving a hole in the valence band. This process is known as photoexcitation. (Figure 2.4)

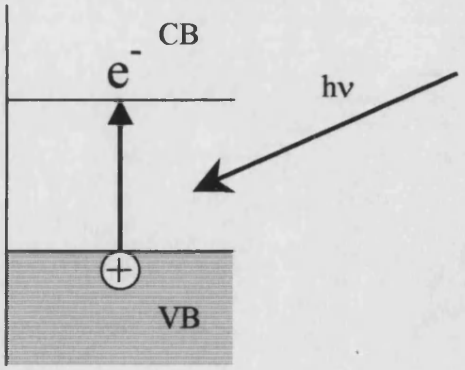

Figure 2.4 *Photoexcitation of an electron from the valence band into the conduction band, forming an electron hole pair.*

Photoexcitation of an electron from the valence band to the conduction band leaves holes in the valence band and fills sites in the conduction band. As electrons are now free to move conduction can occur. The use of photoconduction has been employed in photovoltaic cells where the absorption of light produces electron hole pairs in the semiconductor.

Extrinsic semiconductors.

It is possible to incorporate a small amount of group 13 or group 15 atoms into the group 4 semiconductor i.e. silicon. This process is known as doping. The addition of group 13 atoms (i.e. boron, aluminium, gallium) to the silicon will result in the silicon being electron deficient. The energy levels of the vacant site lie just above the valence band. These vacant levels can accept electrons from the valence band. It takes substantially less energy for an electron to be promoted to these energy levels than to the conduction band, and thus these energy levels (acceptor levels) accept valence band electrons, even at low temperatures. This results in vacancies, 'holes', in the valence band. Since electron movement is now possible within the valence band conduction occurs. This is known as p-type semiconductivity as the electron vacancy is responsible for conduction. If group 15 atoms (i.e. phosphorous, and arsenic) are incorporated into the lattice of silicon, the energy level of the extra electron is located just below the conduction band. Using a small amount of thermal energy it is possible for the electron to be promoted into the conduction band, so that conduction occurs. This is known as n-type semiconductivity as conduction occurs by the electrons in the conduction band.

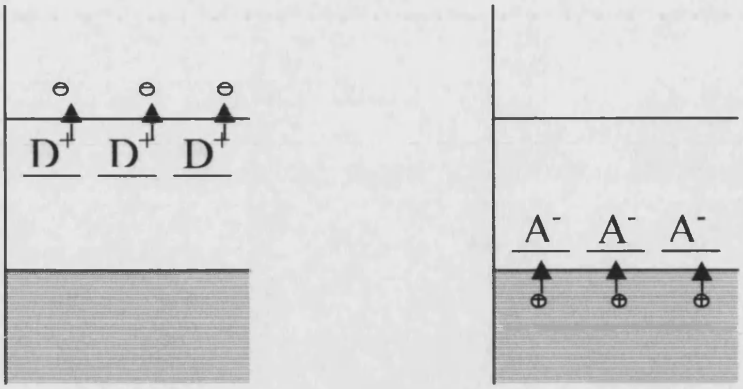

Figure 2.5 *Extrinsic n and p type semiconductors. Diagrams showing the donor and acceptor levels.*

The Fermi-Dirac Function

At any temperature the electron distribution within a solid is described by Fermi-Dirac statistics. At 0 K, all energy levels above the Fermi level are unoccupied and all those below are occupied. The Fermi-Dirac statistics describe the distribution of electrons and holes in the available energy levels in a solid. The probability that an energy level of energy E is occupied by an electron at a given temperature, is given by the Fermi Dirac Function:

$$f(E) = \frac{1}{\left[1 + \exp^{\frac{(E-E_F)}{k_B T}}\right]} \qquad (2.1)$$

E_F =Fermi energy

k = Boltzmann constant

T = Temperature

It follows that the probability of finding an electron at the Fermi energy E_F is ½. For energies above E_F, the probability decreases exponentially. For $E>>E_F$ then the Fermi Dirac function transforms to the Boltzmann function:

$$f(E) \cong e^{\frac{-E-E_F}{k_B T}} \qquad (2.2)$$

This is illustrated in the diagram below. (Figure 2.6)

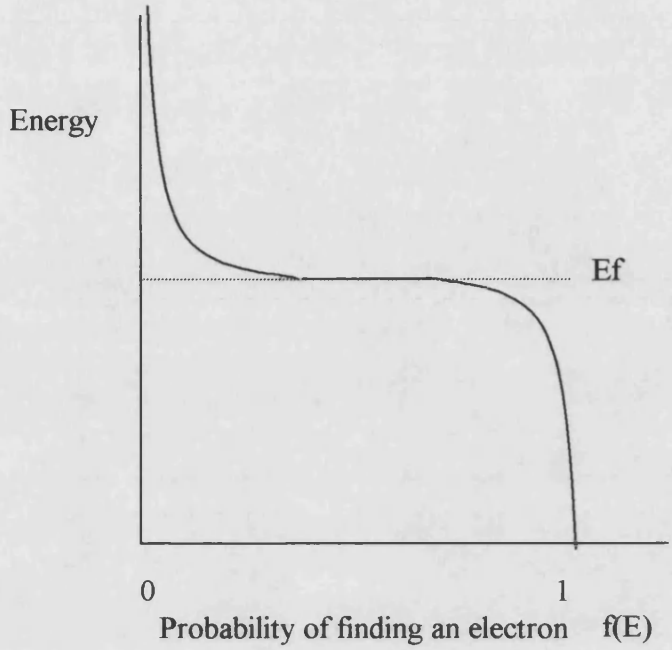

Figure 2.6 *The occupation probability of electrons. The Fermi Dirac Function.*

The Fermi energy is equivalent to the electrochemical potential of electrons in the solid. The electrochemical potential is defined as:

$$\mu_A = \mu_A^{\theta} + \frac{k_B T}{q} \ln \frac{n}{n_o} - q\Phi \qquad (2.3)$$

μ_A = Electrochemical potential

μ_A^{θ}= standard chemical potential

If two metals are placed in contact with each other, one Fermi level will initially be higher than the other. (Figure 2.7)

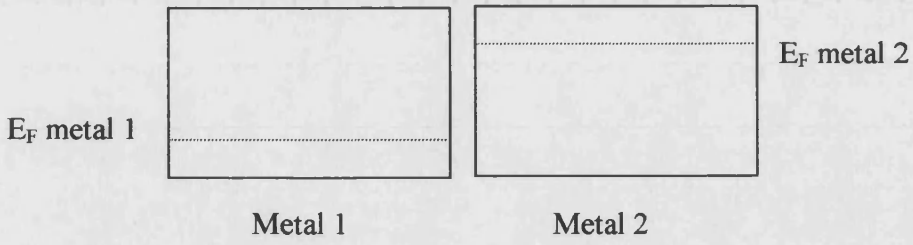

Figure 2.7 *Diagram showing the Fermi levels of 2 different metals before placing in contact with each other.*

It is energetically favourable for electrons to move from metal 2 into metal 1 until both the Fermi levels become equal. This leads to a potential difference across the interface as there are now more electrons in metal 1 so it will have a negative surface charge, whereas metal 2, now electron deficient, will have a positive charge. This is the origin of the contact potential:

$$\Delta\Phi = q\Delta E_F \tag{2.5}$$

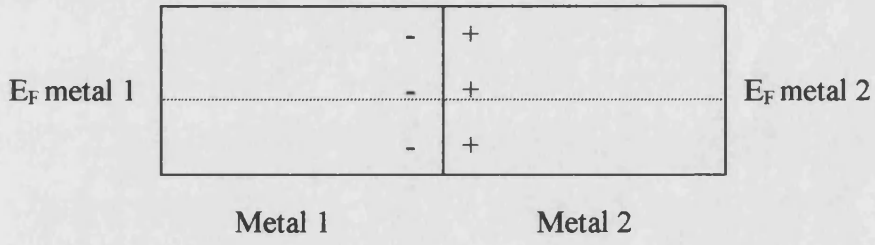

Figure 2.8 *Diagram showing the formation of positive and negatively charged surfaces arising from equalisation of the Fermi level in both metals.*

The Fermi energy in a metal is located within the conduction band. In cases where the valence band is filled and the conduction band is empty the Fermi level is located in the centre of the band-gap as is the case of an insulator or intrinsic semiconductor. For doped semiconductors the Fermi level is close either to the conduction band or valence band depending on the type of doping i.e.

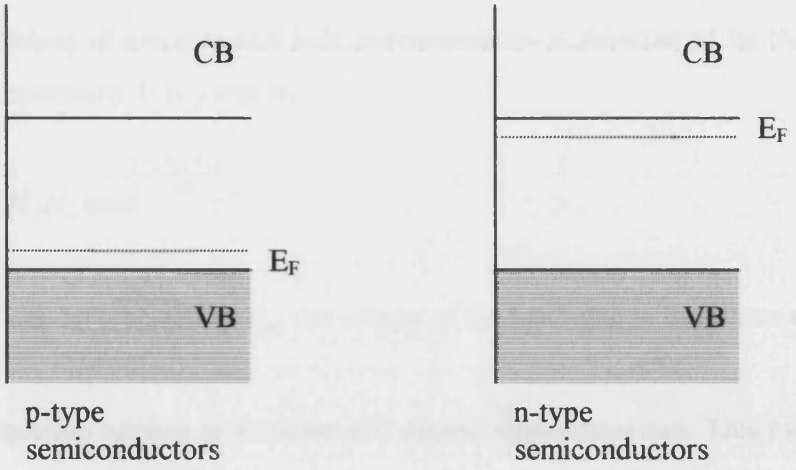

Figure 2.9 *Location of the Fermi level in n and p type semiconductors.*

In cases where a large density of electrons is present in the conduction band (or holes to the valence band), the Fermi level will lie in the band itself. The semiconductor is said to be 'degenerate' under these conditions.

For semiconductors, E_F determines the density of electrons in the conduction band and valence band. When the Fermi energy is more than a few kT from either the conduction band or the valence band, the Fermi Dirac function can be simplified and expressions obtained for both holes in the valence band and electrons in the conduction band. The expressions are given below:

$$n = N_c \exp\left[\frac{-(E_c - E_F)}{k_B T}\right] \tag{2.5}$$

and

$$p = N_v \exp\left[\frac{-(E_F - E_v)}{k_B T}\right] \tag{2.6}$$

Here:

n = density of electrons in the conduction band

p = density of holes in the valence band

N_c and N_v = Density of energy levels in the conduction and valence bands.

k_B = Boltzmann constant

T = Temperature in Kelvin

The product of electron and hole concentrations is determined by the band-gap energy and temperature. It is given by:

$$np = N_c N_v \exp\left[\frac{-(E_c - E_v)}{kT}\right] \tag{2.7}$$

$E_c - E_v$ can be replaced by E_g, the energy of the band gap in the above equation

This equation applies to intrinsic and doped semiconductors. This means that for an n-type sample p tends to small values since n is determined by the doping density Nd.

Non equilibrium conditions

The Fermi energy is useful to describe equilibrium conditions. In practice equilibrium conditions are rarely observed, as many situations involve carrier injection or illumination. which both rely on minority carriers (in a p-type semiconductor these are electrons and in an n-type material they are holes). The density of these minority carriers is dependent on the kinetics of the system and the lifetime of the carriers (The lifetime is the time that the carriers have before they are annihilated by recombination with majority carriers). In order to describe non-equilibrium conditions concept of the 'quasi Fermi level' has been introduced. The quasi Fermi levels for electrons ($_nE_f$) and holes ($_pE_f$) are used to describe the density of carriers in doped semiconductors under non equilibrium conditions (for example under illumination). $_nE_f$ and $_pE_f$ replace E_f in equations 2.5 and 2.6 above and then describe the non-equilibrium density of electrons and holes. Illumination with supra band-gap light will increase the minority carrier concentration by many orders of magnitude. Quasi Fermi levels are particularly useful when dealing with reactions of minority carriers.

2.4 Theory of Steady State Techniques

2.4.1 Capacitance-Voltage measurements

In doped semiconductors in the dark, only the majority carriers are available to take part in any electron transfer reactions and thus the electrolyte junction behaves as a diode.

Under reverse bias (depletion) conditions the electrode exhibits blocking behaviour. A convenient method of characterising the semiconductor-electrolyte interface is to measure the capacitance as a function of applied potential. There are several capacitances present at the semiconductor-electrolyte junction. These are the diffuse double layer capacitance C_D, the surface states capacitance C_{ss}, the Helmholtz layer capacitance C_H and the space charge capacitance C_{SC}. C_D and C_H are both on the electrolyte side of the interface and are both in series with C_{SC}. Under depletion conditions, the measured capacitance is dominated by the space charge capacitance (C_{SC}) as C_D and C_H are both much larger than C_{SC}:

$$Cmeas = (C_{SC}^{-1} + C_H^{-1} + C_D^{-1})^{-1}$$

$$Csc << C_H, C_D \quad \text{i.e. } C_{SC}^{-1} >> C_H^{-1}, C_D^{-1}$$

The surface states capacitance is in parallel with the space charge capacitance. This can be neglected when $\omega >> 1/R_{ss}C_{ss}$. Using high frequencies results in not enough time for charge to be exchanged with the surface state.

The capacitance of the space charge region is given by the Mott-Schottky relationship:

$$C_{sc}^{-2} = \left(\frac{2}{qN_{sc}\kappa\varepsilon_o A^2}\right)\left(V_m - V_{fb} - \frac{kT}{q}\right) \tag{2.8}$$

Where:- q = electronic charge

N_{sc} = donor density in cm^{-3}

ε_o = permittivity of free space

V_m = applied DC potential versus the reference electrode

V_{fb} = flatband potential

A^2 = electrode area

k_B = Boltzmann constant

κ = relative permittivity of semiconductor

It follows that $1/C^2$ varies linearly with applied potential. Extrapolation can be used to obtain the flat band potential. The donor density of the semiconductor can be calculated

from the gradient. A plot of this type is known as a Mott-Schottky plot. It is obtained for n-type samples under anodic bias in the absence of light and for p-type samples under cathodic bias in the absence of light. The potential where there is no excess charge in the semiconductor is known as the flat band potential since the bands do not bend (Figure 2.10) If the potential of an n-type electrode is made more positive than the flat band potential, electrons are withdrawn from the surface and the positively charged ionised donor species form a space charge region (SCR). The size of the SCR is much larger than the Helmholtz double layer. The potential drop across the SCR is the applied potential minus the flatband potential.

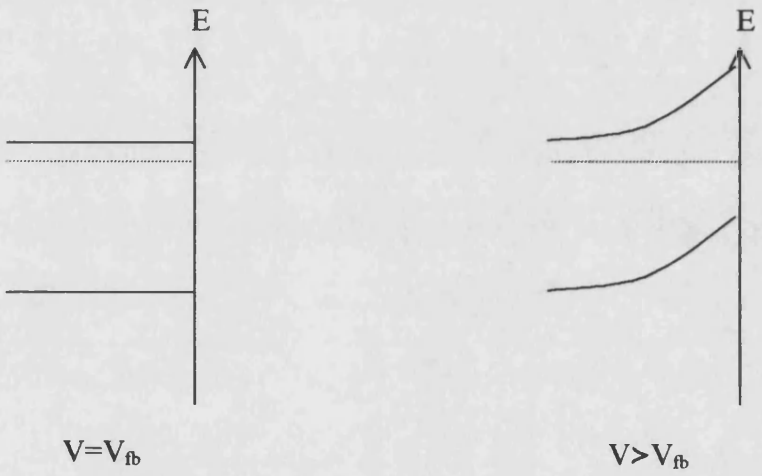

Figure 2.10 *Effects of applying an external potential to an n-type semiconductor.*

The flat band potential may shift as a result of surface, chemical and dipole modifications or Fermi level pinning. The latter effect is caused by the storage of electronic charge by surface states, which produces a drop in potential across the Helmholtz layer. This charge changes with applied potential. For a high density of surface states there is a large potential drop across the Helmholtz layer, but the potential drop across the semiconductor remains constant when the electrode potential is changed. (Figure 2.11)

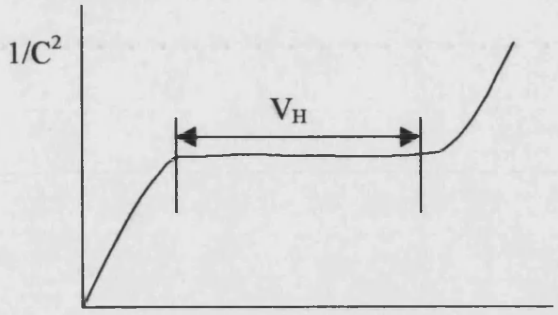

Figure 2.11 *Fermi level pinning. Large potential drop across the Helmholtz layer. Potential drop across the bulk semiconductor remains constant.*

The Fermi level is said to be pinned as only the band edge moves with the applied potential.

The C_d often varies with frequency and this can lead to complications when determining the doping density and flat band potential. It has been noted that many semiconductors behave as one of two types 'A' or 'B' [1]. Type A produce Mott-Schottky plots that are parallel over a range of frequencies and therefore give frequency dependent flatband potentials. Type B are not parallel but converge to a single flat band potential. Mott-Schottky plots may be non-linear. If this is the case the flat band potential and the donor density cannot be determined with any reliability as it is not possible to measure the gradient or to extrapolate. Explanations have been suggested for this such as dielectric relaxation of surface states in the surface layer [1] and slow response to the applied potential of the charge carriers in the depletion layer (deep donors) [2].

2.4.2 Photocurrent Spectroscopy

When a solid absorbs a photon of sufficient energy, an electron hole pair is formed. In the case of a metal, when the electron is excited from a filled state it leaves an electron vacancy below the Fermi level. An electron from a higher energy level can rapidly fill this vacancy thus inducing a cascade of electron movement. For this reason electron hole recombination is highly probable. Thus the quantum efficiencies of photoelectrochemical reactions at illuminated metal electrodes tend to be very small. However in the case of a semiconductor, once the electron is excited electron hole recombination is more difficult

as a forbidden band separates the electron from the hole. The minority carrier is not stable and will eventually recombine. The recombination process for a minority carrier within the bulk region of the semiconductor is pseudo first order, and is characterised by the minority carrier lifetime τ. Under illumination, it is primarily the photogenerated minority carriers that participate in photoelectrochemical reactions, In the dark it is primarily the majority carriers that take part in reactions.

Under illumination, the electron transfer rate is dependent on the concentration of minority carriers at the interface. This in turn depends on the potential, the illumination intensity, the concentration of redox species and the rate constant for interfacial electron transfer. For an n-type semiconductor, holes generated by the absorption of light can be collected at the interface by diffusion and migration. For depletion conditions, the electric field within the space charge region (SCR) drives holes to the surface where they can participate in electron reactions. Holes that are generated within the bulk of the semiconductor can diffuse to the edge of the SCR and then be transported to the interface or lost via recombination within the bulk. The generation /collection problem is described by the following characteristic lengths:

The width of the SCR (W)

$$W = \left(\frac{2\Delta\phi_{sc}}{\varepsilon\varepsilon_0 q N_d} \right)^{\frac{1}{2}} \tag{2.9}$$

the penetration depth of the light $1/\alpha$

and the diffusion length of the holes L_p

$$L_p = (D_p \tau_p)^{\frac{1}{2}}$$

$\Delta\phi_{ms}$ = potential difference across the SCR

ε = relative permitivity of the solid

N_d = doping density

α = absorption coefficient

τ_p = hole lifetime

D_p = hole diffusion coefficient

When an electric field is present, band bending occurs and the minority carriers (n-type = holes, p-type = electrons) move towards the semiconductor electrolyte interface and react with the lattice or the electrolyte. The majority carriers move into the semiconductor. This is shown below Figure 2.12.

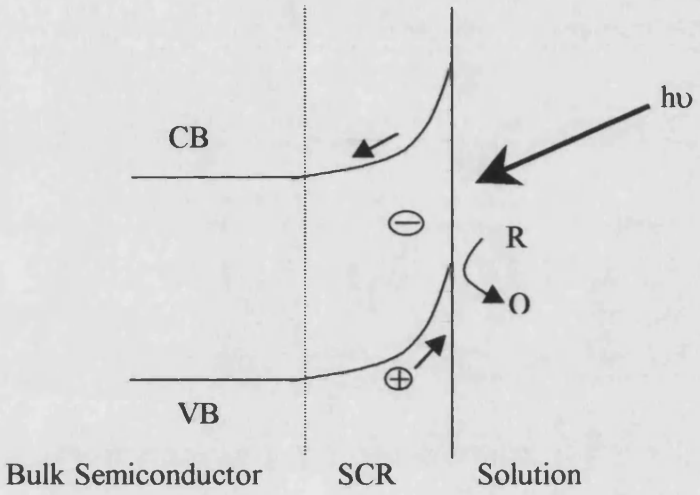

Figure 2.12 *n-type semiconductor electrolyte junction under illumination.*

The collection of minority carriers from the charge free region of the semiconductor depends on the lifetime τ, and the diffusion coefficient D, of the carriers. The carrier collection is given in terms of the minority carrier diffusion length.

$$L=(\pi D\tau)^{1/2} \tag{2.10}$$

Carriers created within this distance from the edge of the space charge region can contribute to the photocurrent. It is possible to calculate the photo current conversion efficiency Φ by using the Gärtner equation.

$$\Phi = \frac{j_{photo}}{qI_o} = 1 - \frac{\exp^{-\alpha W}}{1+\alpha L} \tag{2.11}$$

Where:

j_{photo} = the photocurrent density

I_o = the incident photon flux density corrected for reflection losses

Φ = the photocurrent conversion efficiency

α = the absorption coefficient

W = the width of the space charge region

L = the diffusion length of the minority carriers

q =electronic charge

For a single crystal semiconductor at large band bending the collection efficiency approaches unity *i.e.* no recombination takes place.

The value of Φ calculated from the Gärtner equation will be the maximum conversion efficiency as there is no term present to account for any recombination in the space charge region or at the interface. A plot of $-\ln(1-\Phi)$ versus W is linear with a slope proportional to the absorption coefficient and an intercept dependent on αL. Close to the flat band potential, the plot deviates from linearity as recombination at the at the surface is more significant. Fig 2.11 shows the ideal Gärtner equation response and the effect of surface recombination. The Gartner equation does not contain any information about the electron transfer kinetics as it involves assumptions about the boundary conditions. Under steady state conditions the rate of arrival from the bulk, and the rate of removal (by electron transfer or recombination) determine the concentration of holes at the surface. It is important to use low light intensities in studies of recombination kinetics so that the constant band bending approximation is valid i.e. it can be assumed that W is independent of I_0. Electron transfer is restricted to a small reaction volume defined by the tunnelling distance δ. The steady state concentration of holes in this region can be calculated from the flux of holes to the surface, g, by using the following equation:

$$\frac{\partial p_{x=0}}{dt} = g - k_p P_{x=0}[red] = \frac{\partial p_s}{\partial t} \qquad (2.12)$$

$p_{x=0}$ = concentration of holes at x=o

$\delta P/\delta t$ = change in concentration of holes at x=o with respect to time

g = flux of holes

k_p = rate constant for holes

[Red] = concentration of the reduced species

$\delta p_s/\delta t$ = change in concentration of holes within the solid with respect to time

i.e.

$$p_{x=0} = g - k_p p_{x=0}[\mathrm{Red}] = 0 \tag{2.13}$$

$$g = k_p p_x[\mathrm{Red}] \tag{2.14}$$

$$p_{x=0} = \frac{g}{k_p[\mathrm{Red}]} \tag{2.15}$$

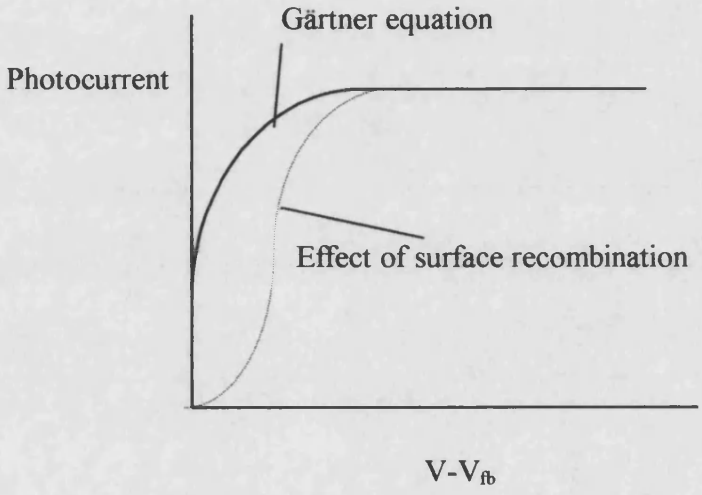

Figure 2.13 *The photocurrent voltage curve for an ideal system (no recombination – the Gärtner equation) and the effect of surface recombination on the shape of this curve.*

2.5 Recombination Processes

Recombination is the process where a photo-generated electron-hole pair annihilate. This process can occur at a recombination centre. A recombination centre is a site that can trap charge carriers from each band. Usually these centres are fully occupied by majority carriers. In the case of recombination, the centre first traps a minority carrier, then the majority carrier occupies the site so that recombination occurs. The lifetime (τ) of the minority carriers is the time the photo-excited carriers exist before recombining.

Defects are important as they provide a preferential starting point for many surface reactions, also a change in the electronic properties of the crystal is sometimes evident.

Vacancies are missing atoms in the crystal lattice. Cation vacancies act as electron acceptors and anion vacancies act as donors. An interstitial atom is an atom that is located at an interstitial site between lattice atoms. It can act as an electron donor.

Dislocations and Grain boundaries are particularly important at the solution/electrolyte interface as they may provide energy levels in the band-gap region, current flow along the grain, charge trapping sites, paths of easy diffusion and providing active sites at the interface for surface active reactions. A dislocation is a linear defect, which occurs when there is an extra half plane of atoms. This results in one of the atoms not having the full compliment of nearest neighbours and hence is able to act as an electron donor or acceptor. A line of atoms that are poorly co-ordinated, enable donor and acceptor levels to be present in the band-gap. As the dislocation results in atoms whose bonds are highly strained, atoms and vacancies are able to move much easier than those in the bulk. Grain boundaries are formed at the interface of two orientations of crystal lattice. These can behave as an accumulation of dislocations

A trap is the term used to describe energy levels deep within the band-gap where an electron or hole may be localised for a period of time. They can form due to defects or impurities within the crystal. Good insulators tend to have a high level of trapping centres.

2.6 Charge Transport

Diffusion

Diffusion arises from uneven concentration distributions and occurs to maximise entropy. The diffusion rate at a given point depends upon the concentration gradient at that point. This follows Fick's first law:

$$J = -D\frac{\partial[B]}{\partial x} \tag{2.16}$$

J = diffusional flux

[B] = concentration of B

D = diffusion coefficient

x = distance

The change in concentration at a given point as a function of time can be derived from Fick's first law. It is the difference in the flux of B entering a plane (x) and leaving through a different plane located at x + δx (δx) during a given time. This can be written as:

$$\frac{\partial[B]}{\partial t} = D\left(\frac{\partial^2[B]}{\partial x^2}\right) \tag{2.17}$$

This is Fick's second law.

Migration

The external electric field that exists at the electrode solution interface (δϕ/δx) results from the drop in potential between the two phases ($\Delta\phi_{ms}$). This field exerts electrostatic forces on charged species at the interface. This results in movement of ions to/from the electrode surface. This effect is known as migration. It can be described mathematically as:

$$J_m = -u[B]\frac{\partial\phi}{\partial x} \tag{2.18}$$

J_m = migratory flux

u = ion mobility

[B] = concentration of B

δϕ/δx = charge on the interface

The ionic charge, the size and the solution viscosity determine the ion mobility (u).

Charge transport within a semiconductor.

Within the space charge region (SCR) of a semiconductor, migration is the primary form of transport due to the high electric charge and potential gradient. In the neutral region there is no significant charge or potential difference, so that diffusion is the primary mode of transport for charge carriers. At the flat band potential migration disappears and the primary mode of transport is diffusion

Electron transfer at a semiconductor/electrolyte junction.

Electron Transfer in a metal/redox system occurs near the Fermi level. As the electron density in a metal is constant, electron transfer is characterised by a first order heterogeneous rate constant (cm s^{-1}). Changes in electrode potential across the interface result in a change in the activation energy of the process, and an exponential dependence of the rate constant on potential is observed. These considerations lead to the well known Butler Volmer and Tafel relationships used in electrode kinetics.

For the case of a semiconductor electrolyte junction, an n-type electrode is considered. In the dark, electron transfer is dependent on both the concentration of redox species in solution and on the density of electrons in the semiconductor. The electron density in the semiconductor is potential dependent. For depletion conditions, the majority of the potential drop is located within the solid so that the activation energy for electron transfer is independent of potential but the density of electrons does depend on a potential. Electron transfer at semiconductor electrodes is therefore characterised by second order heterogeneous rate constant (cm^4 s^{-1}). Under depletion conditions, electrons are removed from the surface so that electron transfer rate constants of outer sphere reactions can be measured more easily than at metals. Ideally situation, the electron concentration at the surface should vary exponentially with potential. This can be described by the Boltzman equation:

$$n_{x=0} = n_{bulk} e^{\frac{-q(V-V_{fb})}{kT}} \qquad (2.19)$$

$n_{x=0}$ = surface concentration of electrons

n_{bulk} = bulk concentration of electrons

q = charge

V = potential

V_{fb} = flatband potential

k = boltzmann constant

T = temperature

Electron transfer rate constants can therefore be determined directly from steady state current voltage characteristics by selecting a particular potential range.

2.7 Charge Transport within Nanocrystalline Solids

Nanocrystalline solids display unusual properties as they possess a three-dimensional semiconductor electrolyte interface. They consist of an array of interconnected particles and as such have a large surface area. This structure enables electrolyte to penetrate throughout the semiconductor through to the back contact.

The Helmholtz double layer is able to extend throughout the large internal surface area of the nanoporous electrode, so that the electrode may behave as a supercapacitor under accumulation conditions. Where the Helmholtz layer dominates the capacitance, the internal surface area can be estimated by measuring the capacitance [3].

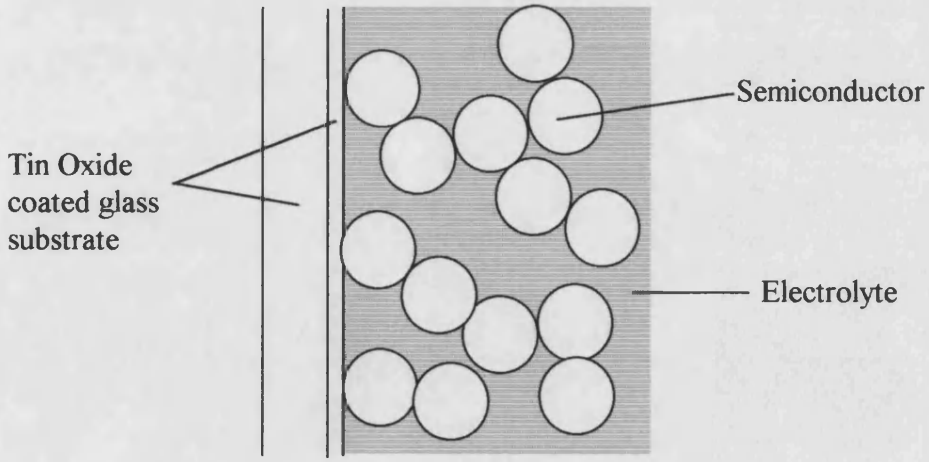

Figure 2.14 *Interpenetrating phases of a nanocrystalline semiconductor and electrolyte.*

Nanocrystalline systems contain particles that are typically several nanometers in size, the particles are too large to exibit quantum size effects but due to their size they cannot be treated in the same was as bulk semiconductors. The Debye length (L_D) is given by:

$$L_D = \left(\frac{kT\varepsilon\varepsilon_0}{q^2 N} \right) \tag{2.20}$$

here:

ε = permitivity of the semiconductor

ε_0 = permiativity of free space

N = doping density

The Debye length in a nanocrystalline semiconductors is usually larger than the particle diameter, in this case no appreciable potential difference is generated within the particles by ionised donor and acceptor sites. For this reason no space charge layer and no band bending will be present [4]. The absence of electric fields within the nanocrystalline structure is important for charge transport within these systems. The driving force for the charge movement in these systems is by an electron concentration gradient.

As the primary means of transport within a nanocrytstalline system is diffusion, the diffusion length (L_n) of the photoinjected electron is therefore important. The diffusion length is given by:

$$L_n = (D\tau)^{\frac{1}{2}} \tag{2.21}$$

Here D is the diffusion coefficient of the electrons and τ is the lifetime of the electrons. The lifetime of the electrons is determined by the recombination rate. Because charge separation is not influenced by an electric field, the probability of recombination is increases as the film thickness increases as the electron has to travel through more particles (and consequently grain boundaries) to reach the back contact. The interpenetrating electrolyte typical of a nanoporous system, screens the charge present on neighbouring particles, so that a high amount of charge can be stored within a nanoporous structure.

Electrons travel through nanoporous system and may be temporarily trapped at the surface or in the bulk of the interconnecting particles. This trapping will slow down the diffusion of electrons through the film. Similarly polarisation of the solvent molecules may have the same effect. These effects are highly probable within a nanoporous network due to the high surface area to volume ratio of the structure. The diffusion coefficients of electrons within TiO_2 nanocrystalline structures are reported to be significantly slower [5,6,7] than those within bulk TiO_2.

As the potential of the substrate where the electrons are collected is increased the electron concentration at the collection point will also increase. This is shown in Figure 2.15. As the potential increases the electron concentration gradient (n_0 to n) of the film becomes shallower which gives less efficient charge transport. At open circuit there is no appreciable gradient and therefore the electrons remain in the film and are not collected.

Further investigations of the semiconductor electrolyte interface and charge transport within nanocrystalline systems are needed as detailed mechanisms are not known although hopping mechanisms have been suggested [8, 9].

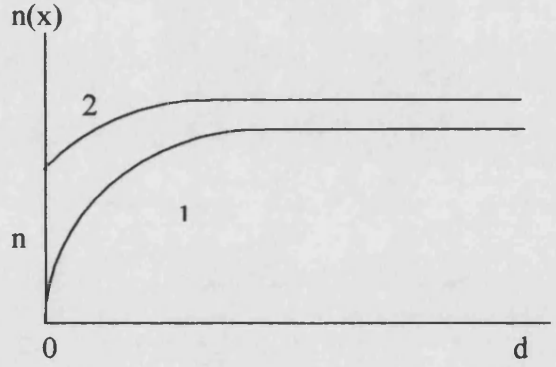

Figure 2.15 *Electron concentration profile of a nanocrystalline electrode under illumination. Curve 1 shows the electrode at short circuit conditions and curve 2 show the result of a potential increase at the substrate, d is the film thickness.*

The Grätzel cell [10] uses nanostructured materials because of the large surface area to volume ratio. In Grätzel cells the surface is covered by a monolayer of dye, which absorbs visible light, it follows that a high surface area is essential in the conversion efficiency of these cells.

2.8 References

1. Dutroit, G. C. et al. *Ber. Bunsenges. Phys. Chem.* **1975**, *79*, 1206

2. Goosens, A. *J. Electroanal. Chem.* **1991**, *27*, 317

3. Peter,LM; Riley, DJ; Wielgosz, RI. *Appl. Phys. Lett.* **1995**, *66*, 2355

4. Albery, W. J.; Bartlett, P. N. *J. Electrochem. Soc.* **1984**, *131*, 315

5. Cao, F; Meyer, G; Oscam, G; Searsons, P.C. *J. Phys. Chem.* **1996**, *100*, 17021

6. Solbrand, A: Lindstrom, H; Rensmo, H; Hagfelt, A; Lindquist, SE; Sodergren, S. *J. Phys. Chem. B* **1997**, *101*, 2514

7. Dloczik, L.; Ileperuma, O.; Lauermann, I.; Peter, L. M.; Ponomarev, E. A.; Redmond, G.; Shaw, N. J.; Uhlendorf, I. *J. Phys. Chem. B* **1997**, *101*, 10281

8. Könenkamp, R.; Henninger., R.; Houer, P. *J. Phys. Chem.* **1993**, *97*, 7328

9. Kay, A.; Humphry-Baker, R.; Grätzel, M. J. *Phys. Chem.* **1994**, *98*, 952

10 O'Regan, B.; Grätzel, M. *Nature* **1991**, *353*, 737

General references

Morrison, S. R. *Electrochemistry at semiconductor and oxidised metal electrodes*, **1980,** Plenum, New York,

Peter L. M; in *Comprehensive chemical kinetics 29, New techniques for the study of electrodes and their reactions, Ch. 8 Photocurrent spectroscopy*. Ed. Compton, R. G. **1989,** Elsevier, Amsterdam

Peter, L. M.; Vanmaekelbergh, D., **in press,** in *Advances in electrochemical science and engineering* Vol 6. Ed. Alkire, R. C.; Kolb, D. M., VCH, Weinheim.

Chapter 3

Theory of dynamic techniques

Index

Chapter 3 Theory of dynamic techniques

3.1 *An introduction to AC theory*

A sinusoidal voltage can be represented by the equation below:

$$V = \Delta V \sin \omega t \qquad (3.1)$$

or

$$V = \Delta V e^{iwt} \qquad (3.2)$$

Where: ω = angular frequency

V = instantaneous value of the voltage

ΔV = the maximum amplitude

This sinusoidal voltage can be represented by a sine wave with respect to time or as a phasor (rotating vector) as shown in the figure below

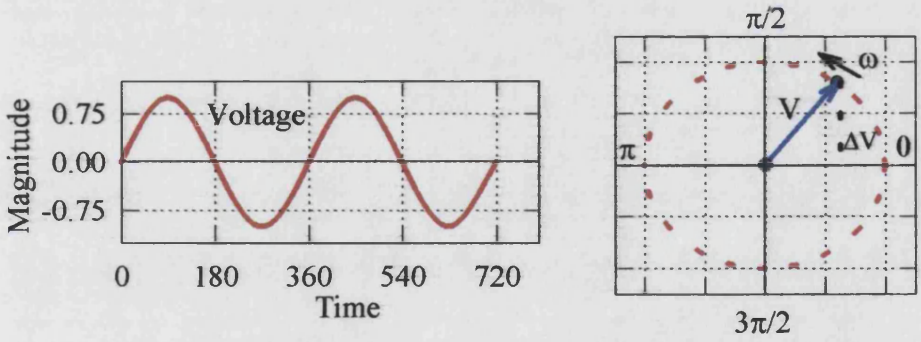

Figure 3.1 *Time axis and phasor representation for a sinusoidal wave.*

When analysing linear circuits it is usual to describe a relationship between voltage and current. If the voltage is sinusoidal the current will usually be sinusoidal and of the same frequency. In most cases the amplitude and the phase will be different. The current in this type of system can be represented by the following equation:

$$i = \Delta i \sin(\omega t + \theta) \qquad (3.3)$$

This is shown graphically in both time axis and phasor representation in Figure 3.2

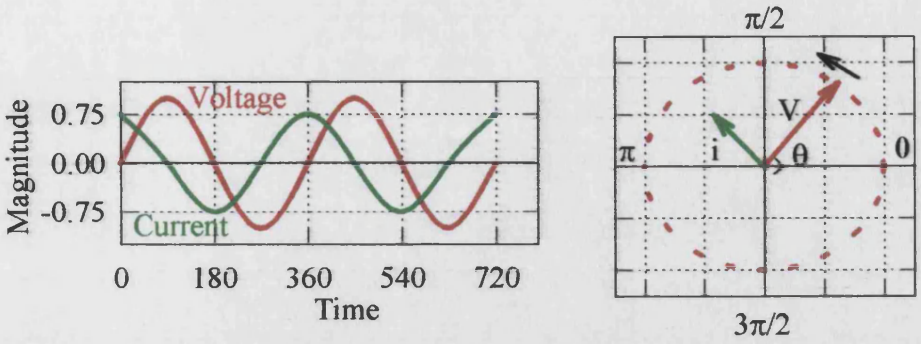

Figure 3.2 *Equivalent representations in time axis and phasor representation of current and voltage relationship showing a 90° phase shift. The current is leading the voltage.*

It should be noted that the phase shift of the current with respect to the voltage is 90° and that it is leading the voltage. It should also be noted that the amplitude of the current is not equal to the amplitude of the voltage.

Resistor

If a sinusoidal voltage is applied to a resistor the current response obeys Ohm's law (V=iR). The current and voltage are directly proportional and both signals are in phase. This is shown in time axis and phasor notation below.

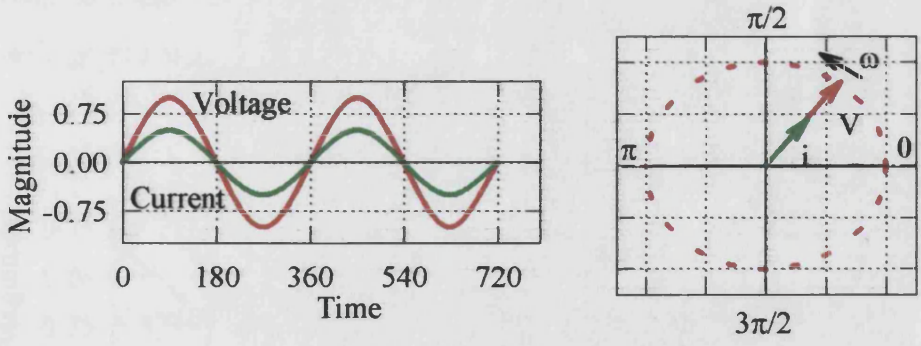

Figure 3.3 *Time axis and phasor notation showing the current response to applied voltage of a resistor.*

Capacitor

For a capacitance we must first define the current as a function of the capacitance. The charge on the plates (q) is given by the capacitance multiplied by the voltage:

$$q = CV \tag{3.4}$$

The current is the rate of change of charge with respect to time and thus differentiating yields:

$$i = \frac{dq}{dt} = C\frac{dV}{dt} \tag{3.5}$$

Hence:

$$i = \omega C \Delta V \cos(\omega t) \tag{3.6}$$

or:

$$i = \omega C \Delta V \sin\left(\omega t + \frac{\pi}{2}\right) \tag{3.7}$$

$1/\omega C$ can be written as X_c which is the capacitive reactance giving:

$$i = \frac{\Delta V}{X_c}\sin\left(\omega t + \frac{\pi}{2}\right) \tag{3.8}$$

It should be noted that in this case there is a phase shift of $\pi/2$ (90°) and the phasor and time axis graphs show this.

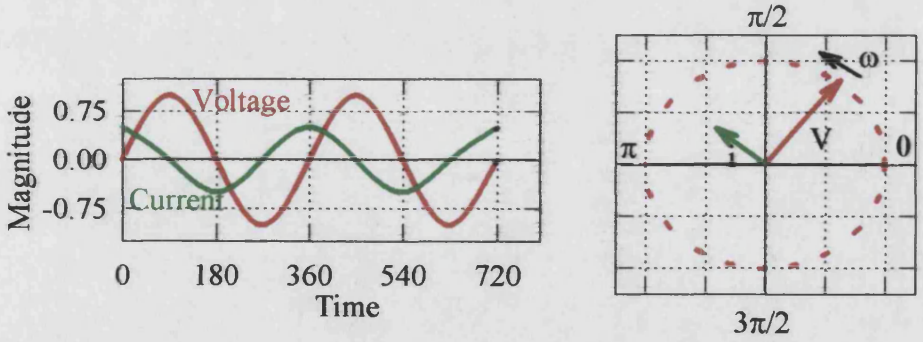

Figure 3.4 *Time axis and phasor notation for the current response to applied voltage of a capacitor.*

It can be seen that equation (3.8) is similar in form to ohms law but instead of using the resistance R the capacitive reactance (X_c) is used and there is a phase shift of $\pi/2$. It is

possible to use complex notation ($j=\sqrt{-1}$) such that the data can be represented on a Nyquist plot and the phase angle is accounted for. The equation then becomes:

$$V = -jX_c i \tag{3.9}$$

$$\frac{V}{i} = -jX_c \tag{3.10}$$

3.2 *Impedance*

The ratio of the voltage to current is the impedance (Z). In general it is a vector quantity (*i.e.* it has magnitude and phase). It can be represented as a vector on a complex plane plot. It is possible to represent an array of vectors on a complex plane plot in the form of a Bode plot. A Bode plot shows the information regarding the magnitude and phase of the vector as a function of frequency.

For a resistor the impedance Z is simply the resistance. It can be shown on a complex plane plot as a single point on the real axis. A resistance is not frequency dependent and as such will be represented by a horizontal line on a bode plot. This is shown in Figure 3.5.

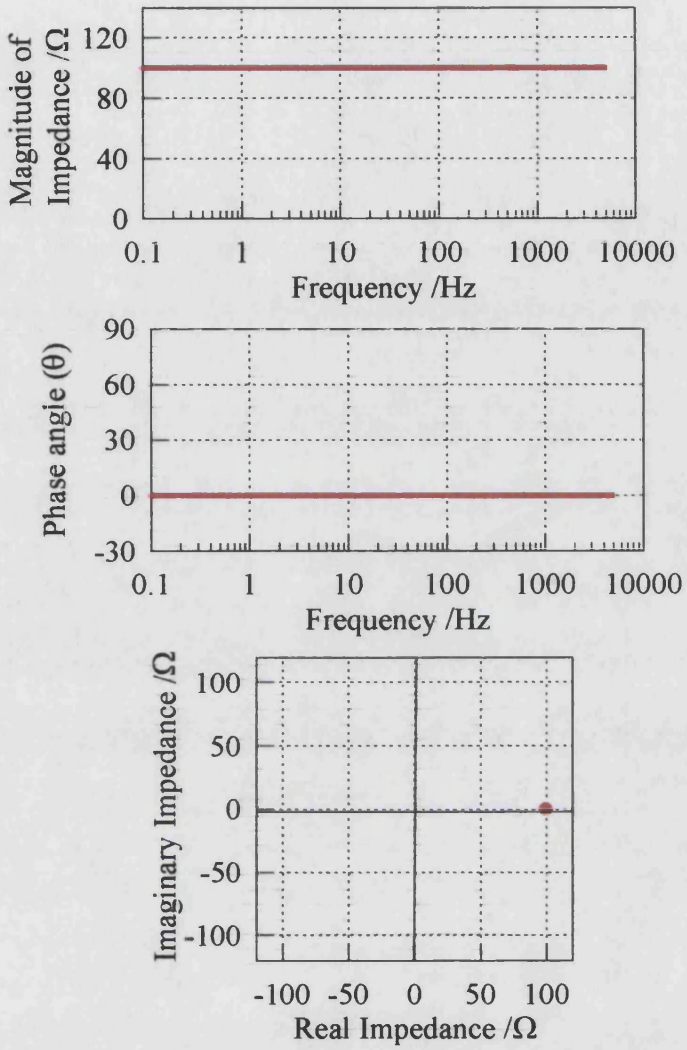

Figure 3.5 *Impedance of a resistor shown as a Bode plot and on a complex plane plot.*

For a capacitor the impedance is defined as -jXc which is frequency dependent. This is shown in the complex plane plot as a straight line down the origin to infinity the Bode plot is also shown in Figure 3.6.

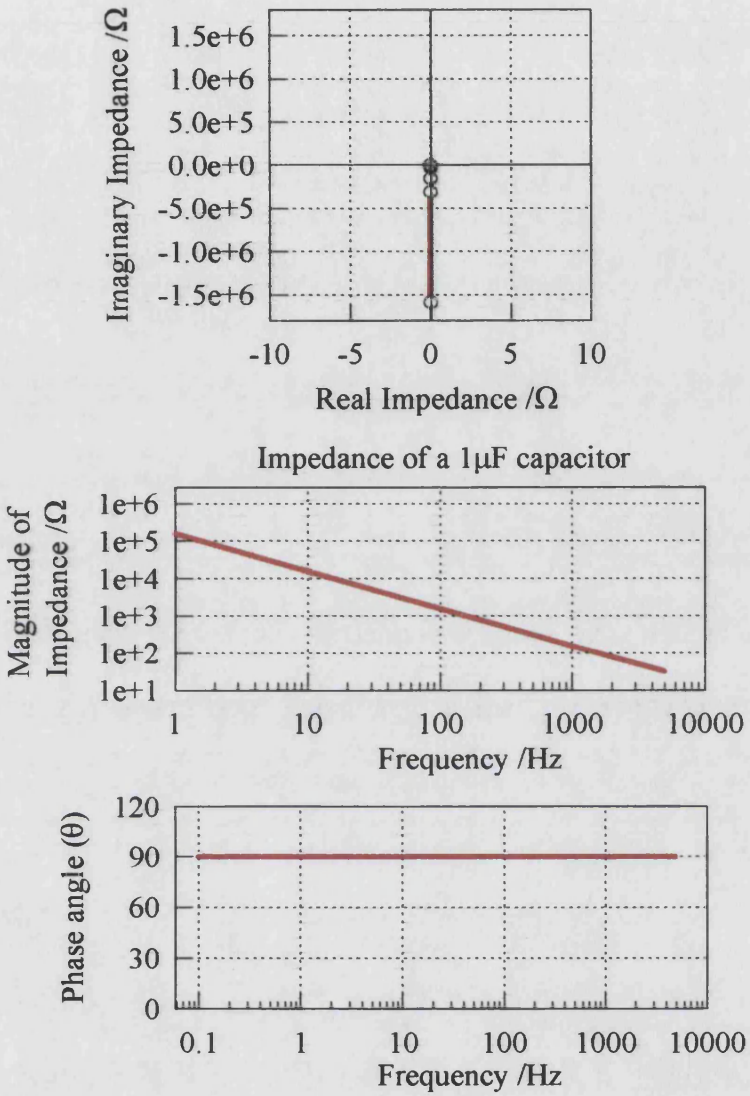

Figure 3.6 *Impedance of a 1μF capacitor displayed on a complex plane and Bode plot.*

For systems where resistors and capacitors are both present the total impedance is calculated using Kirchoffs laws. Kirchoffs laws state that the current at any junction in a circuit must be equal to zero and that all the sum of the potential differences around any complete loop of circuit is zero.

For a series circuit of a resistor and capacitor the current can only travel one way. This means that it must pass through both the resistor and capacitor. Therefore the impedance must be simply the resistance of the resistor (R) plus resistance of the capacitor (X_c):

$$Z = R - jX_c \qquad (3.11)$$

This response gives a vertical line on the Nyquist plot corresponding to the summation of the impedance of the resistor and the impedance of the capacitor.

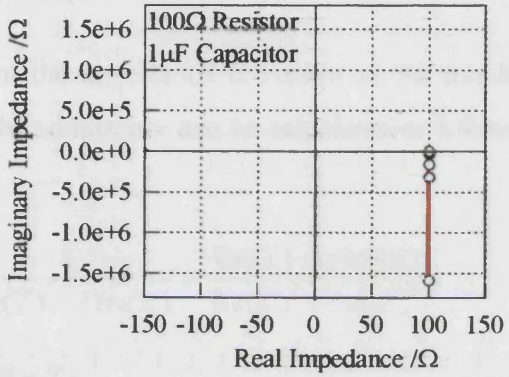

Figure 3.7 *Complex plane plot for a 100Ω resistor and 1μF capacitor in series.*

As the current passes through both the resistor and capacitor the phase shift (θ) will be equal to $\tan^{-1}$ (Xc/R). This is shown in Figure 3.8.

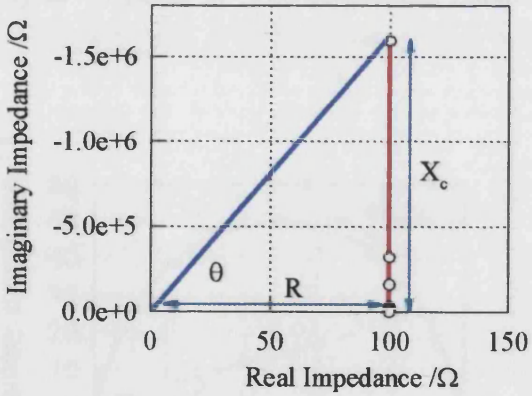

Figure 3.8 *Diagram to illustrate the calculation of the phase angle from a complex plane plot at a particular frequency.*

For a parallel circuit the current has several paths by which it can travel through the circuit components. At low frequencies the majority of the current will travel through the resistor whereas as at high frequencies the current will travel mostly through the capacitor. The real and imaginary components of the impedance (Re(Z) and Im(Z)) for the system are calculated by equation (3.12) shown below. This has a similar form to the equation defining the addition of resistances in a parallel circuit.

$$\frac{1}{Ztot} = \frac{1}{\mathrm{Re}(Z)} + \frac{1}{j\,\mathrm{Im}(Z)} = \mathrm{Y} \qquad (3.12)$$

The reciprocal of the impedance is known as the admittance. The real and imaginary components of the admittance can be calculated as follows:

$$\frac{1}{Ztot} = \mathrm{Y} = \frac{1}{\mathrm{Re}(Z) + j\,\mathrm{Im}(Z)} = \frac{\mathrm{Re}(Z) - j\,\mathrm{Im}(Z)}{\mathrm{Re}(Z)^2 + \mathrm{Im}(Z)^2} \qquad (3.13)$$

$$\mathrm{Re}(\mathrm{Y}) = \frac{\mathrm{Re}(Z)}{\mathrm{Re}(Z)^2 + \mathrm{Im}(Z)^2} \qquad (3.14)$$

$$\mathrm{Im}(\mathrm{Y}) = \frac{-\mathrm{Im}(Z)}{\mathrm{Re}(Z)^2 + \mathrm{Im}(Z)^2} \qquad (3.15)$$

This gives a complex plane plot representation of a semicircle with a phase angle varying from 0 (low f) to 90 (high f). The semicircle maximum $\omega = (1/RC)^2$, where $\omega = 2\pi f$ (f=frequency).

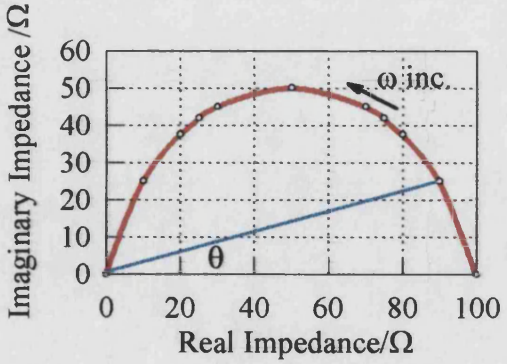

Figure 3.9 *Complex plane plot of the impedance of a circuit with a resistor and capacitor in parallel.*

3.3 *Electrochemical impedance spectroscopy (EIS) and photo electrochemical impedance spectroscopy (PEIS).*

3.2.2 Electrochemical impedance spectroscopy

Electrochemical Impedance Spectroscopy (EIS) involves superimposing a small AC potential perturbation on to a DC potential. This potential is then applied to the sample electrode via a potentiostat. The real and imaginary components of the impedance are recorded as a function of frequency.

Electrochemical systems are non-linear, however impedance measurements are still valid providing the modulation used is small enough such that the response can be linearised. All the circuit components we have previously discussed assume that there is a linear correlation between current and potential. In general the current of an electron transfer reaction follows the Butler-Volmer equation.

$$j = j_0\left[\exp\left(\frac{(1-\alpha)nF}{RT}\eta\right) - \exp\left(-\frac{\alpha nF}{RT}\eta\right)\right] \qquad (3.16)$$

Where:

j	= Current
j_0	= Exchange current density
F	= Faraday constant
n	= Number of electrons
α	= Transfer coefficient
η	= Overpotential
R	= Gas constant
T	= Temperature

For small perturbations about the equilibrium potential we can define the Faradaic Resistance by linearising the exponential terms as shown below and diagrammatically in Figure 3.10.This linearisation is only valid when:

$$\frac{\alpha nF}{RT}\eta << 1 \qquad (3.17)$$

i.e.

$$\eta << \frac{RT}{\alpha nF} \qquad (3.18)$$

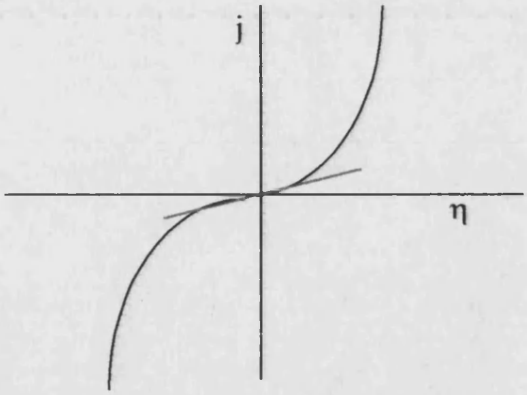

Figure 3.10 *Linearisation of the Butler-Volmer relationship for small values of the overpotential*

For small values of x e^x can be written as:

$$e^x = 1 + x + \frac{x^2}{2} + \frac{x^3}{3} + \frac{x^4}{4} \ldots\ldots \qquad (3.19)$$

If we ignore all the higher order terms we can define the exponential as:

$$e^x \approx 1 + x \qquad (3.20)$$

If we apply this approximation to the Butler Volmer equation we get:

$$j = j_0 \left[\left(1 + \frac{(1-\alpha)nF}{RT}\eta \right) - \left(1 - \frac{\alpha nF}{RT}\eta \right) \right] \qquad (3.21)$$

$$j = j_0 \left[\frac{(1-\alpha)nF}{RT}\eta + \frac{\alpha nF}{RT}\eta \right] \qquad (3.22)$$

This can be re written as:

$$j = \frac{j_0 nF}{RT}\eta \qquad (3.23)$$

Rearranging gives:

$$\frac{\eta}{j} = \frac{RT}{nFj_0} = R_f \qquad (3.24)$$

here:

R_f = Faradaic resistance

R = Gas constant

It is possible to see that for small values of x the i-v curve can be linearised and represented by a resistance.

In all electrochemical cells there will be a region at the interface where ions may accumulate or deplete from their bulk values. This region, known as the double layer, is capable of storing charge and as such will have a capacitance associated with it. If the interface behaves as a simple capacitor then the capacitance will be described by the following equation:

$$C = \frac{q}{V} \qquad (3.25)$$

The charge on the plates of the capacitor is directly proportional to the applied potential and thus the equation can be used to calculate the capacitance. This relationship implies that the capacitance is constant and does not change with the applied potential. This holds true for linear circuits however, when dealing with electrochemical circuits the capacitance changes with applied potential. The capacitance of an electrochemical system is determined by the size of the double layer that will change with applied potential. It is therefore appropriate to use the term differential capacitance defined as:

$$C_d = \frac{\delta q}{\delta V} \qquad (3.26)$$

For small values of potential (close to 0) it is possible to use linear expressions to calculate the capacitance and the impedance.

For potentials other than zero, EIS superimposes a small AC perturbation of the potential onto a larger DC potential. The real and imaginary components of the current and potential are measured and used to calculate the real and imaginary impedance. The AC potential must be small enough so that it is possible to linearise the equations describing the perturbation.

If we take the Butler-Volmer equation which defines the current as a function of potential:

$$j = j_0\left[\exp\left(\frac{(1-\alpha)nF}{RT}\eta\right) - \exp\left(-\frac{\alpha nF}{RT}\eta\right)\right]$$

(3.27)

For a small perturbation about some DC potential, not equal to the equilibrium potential can be shown to induce a small perturbation in the current Figure 3.11

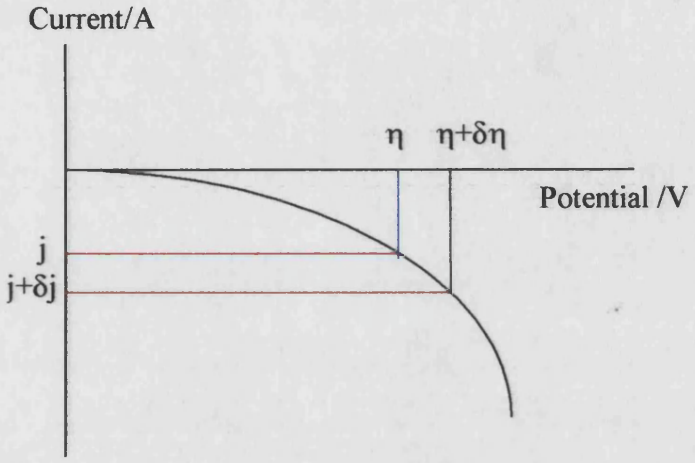

Figure 3.11 *A small perturbation about a potential other than the equilibrium potential*

For a small perturbation δη about a large DC overpotential η we can write:

$$j+\delta j = j_0\left[\exp\left(\frac{(1-\alpha)nF}{RT}(\eta+\delta\eta)\right)-\exp\left(-\frac{\alpha nF}{RT}(\eta+\delta\eta)\right)\right] \qquad (3.28)$$

At a large overpotential the Tafel approximation is valid, thus for an anodic process the equation can be written as:

$$j+\delta j = j_0\left[\exp\left(\frac{(1-\alpha)nF}{RT}(\eta+\delta\eta)\right)\right] \qquad (3.29)$$

this can be re written as:

$$j+\delta j = j_0\left[\exp\left(\frac{(1-\alpha)nF}{RT}\eta\right)\times\exp\left(\frac{(1-\alpha)nF}{RT}\delta\eta\right)\right] \qquad (3.30)$$

Expanding the exponential term containing δη and linearising we obtain:

$$j+\delta j = j_0\left[\exp\left(\frac{(1-\alpha)nF}{RT}\eta\right)\times\left(1+\frac{(1-\alpha)nF}{RT}\delta\eta\right)\right] \qquad (3.31)$$

$$j+\delta j = j_0\left[\exp\left(\frac{(1-\alpha)nF}{RT}\eta\right)+\exp\left(\frac{(1-\alpha)nF}{RT}\eta\right)\times\left(\frac{(1-\alpha)nF}{RT}\delta\eta\right)\right] \quad (3.32)$$

It follows that:

$$\delta j = j_0\left[\exp\left(\frac{(1-\alpha)nF}{RT}\eta\right)\times\left(\frac{(1-\alpha)nF}{RT}\delta\eta\right)\right] \quad (3.33)$$

This can be re written using j rather than j_0 as follows:

$$\delta j = j\frac{(1-\alpha)nF}{RT}\delta\eta \quad (3.34)$$

Thus the admittance is given by:

$$\frac{\delta j}{\delta\eta} = \frac{(1-\alpha)nF}{RT}j \quad (3.35)$$

And the impedance is given by:

$$\frac{\delta\eta}{\delta j} = \frac{RT}{(1-\alpha)nFj} = R \quad (3.36)$$

From the above it is possible to see how the current and voltage associated with an electrochemical cell may be represented as an impedance provided the excitation signal has a small amplitude.

Consider the simplest circuit for an electrochemical cell, with no diffusion to and from the electrode surface. This simple system will have several impedances associated with it. The solution resistance (R_s) is in series with the Faradaic resistance (R_f) which is in parallel with the double layer capacitance (C_{dl}) this is shown in Figure 3.12:

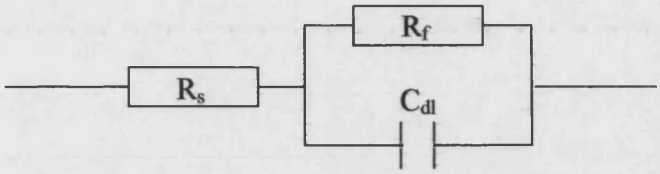

Figure 3.12 *Equivalent circuit representation for a simple electrochemical cell.*

The impedance of the equivalent circuit for the electrochemical cell can be calculated by:

$$Z_{tot} = Z_{real} + jZ_{imag} \tag{3.37}$$

$$Z_{real} = R_s + \frac{Rf}{1+\omega^2 C_{dl}^{\ 2} R_f^{\ 2}} \tag{3.38}$$

$$Z_{imag} = \frac{C_{dl} R_f^{\ 2} \omega}{1+\omega^2 C_{dl}^{\ 2} R_f^{\ 2}} \tag{3.39}$$

When plotted on a complex plane plot the output is a semicircle shifted by a constant along the real axis. If $\omega \rightarrow 0$ (the low frequency limit) it is possible to determine the impedance is simply the total resistance (R_s+R_f), if $\omega \rightarrow \infty$ the impedance is simply the R_s, at the maximum of the semicircle $\omega_{max}=1/R_fC_{dl}$. From these three cases it is possible to easily determine the values of R_s, R_f and C_{dl}.

3.2.3 Photo-electrochemical impedance spectroscopy

Photo-electrochemical impedance spectroscopy (PEIS) is similar as a small AC potential perturbation is superimposed onto a DC potential and is applied to a sample electrode. The difference is that the sample is illuminated during measurements. The technique is similar in interpretation, however it is possible to study photo-electrochemical processes.

Under illumination the total current is a function of the dark current and the photocurrent. In the simplest case the current produced due to the illumination is a constant for all values of the potential as shown in Figure 3.13.

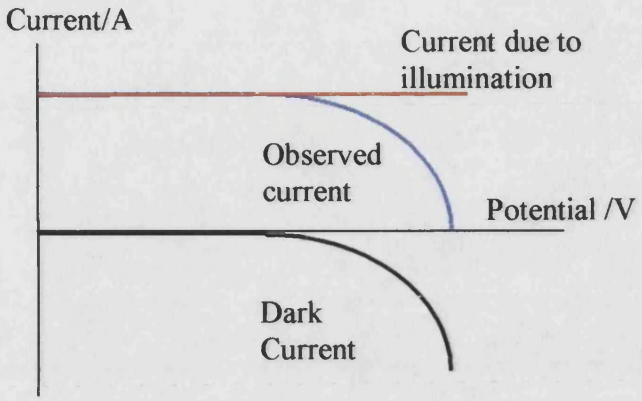

Figure 3.13 *The simplest case: the observed current is a function of the dark current plus the current due to illumination where the current due to the illumination is constant for all values of the potential.*

In this simple case the shape of the dark current curve determines the shape of the total current voltage curve. If a small AC potential perturbs the system the response under illumination will be the same for both the illuminated and the dark response because it is only the dark current that is dependent on potential .

In a system where the photo-current is not constant for all values of the potential, the impedance will not be the same in the dark and under illumination. This is because both the dark current and the current due to illumination are dependent on potential. This is shown in Figure 3.14.

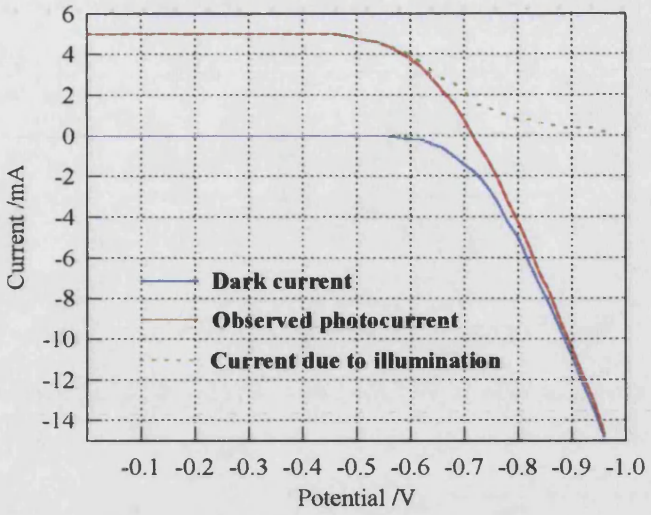

Figure 3.14 *The case where the observed photocurrent is a function of the dark current and the current due to illumination when both the dark current and the current due to illumination are both dependent on potential.*

3.4 *Intensity Modulated Photocurrent Spectroscopy (IMPS)*

3.2.1 Theory

Intensity Modulated Photocurrent Spectroscopy (IMPS) is a dynamic technique that involves the sinusoidal modulation of the intensity of a light source superimposed on a constant illumination. Modulation of the light source can be achieved by the use of an acousto-optic modulator or a light emitting diode driven by a frequency response analyser or lock in amplifier. The time dependent illumination is of the form:

$$I(t) = I_0 + \delta I_0 \sin \omega t \qquad (3.40)$$

or

$$I(t) = I_0 + \delta I_0 e^{i\omega t} \qquad (3.41)$$

A frequency response analyser is used to record the real and imaginary components of the modulated photocurrent. The response is measured over a range of frequencies.

Consider the situation within a bulk semiconductor under depletion conditions where illumination produces electron hole pairs. When surface recombination occurs, the IMPS response is composed of two components, the first being associated with the flux of the photo-generated minority carriers and the second with the flux of majority carriers involved in surface recombination. The two currents have opposite signs and are generally not in phase with each other. The kinetics of recombination determines the phase and magnitude of the signal at each frequency. A complex plane plot is used to analyse the frequency dependence of the photocurrent. Complex plane plots of IMPS responses usually extend into at least two quadrants as the phase shifts associated with the RC time constant and with the recombination kinetics have opposite signs. It is possible to relate the photocurrent transient response to chopped illumination to the IMPS response.

If we recall from chapter 2 the photocurrent voltage characteristics (Figure 3.15), the ideal response where recombination is not present follows the Gärtner equation. In reality however, recombination is encountered and the response is lower than predicted by the Gärtner equation in the photocurrent onset region.

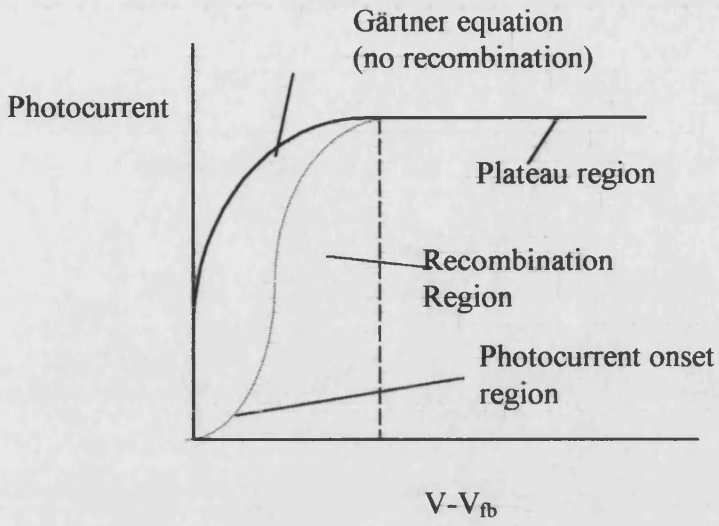

Figure 3.15 *Photocurrent voltage curve showing the predicted response by the Gärtner equation.*

Case 1 – No recombination and no RC attenuation

When recombination and RC attenuation are both negligible *i.e.* in the plateau region of the photocurrent voltage curve, the photocurrent transient is observed to be square. The corresponding IMPS plot is a single point on the real axis at Φ=1 (Φ is defined as the incident photon to current conversion efficiency corrected for reflection losses. See Figure 3.16).

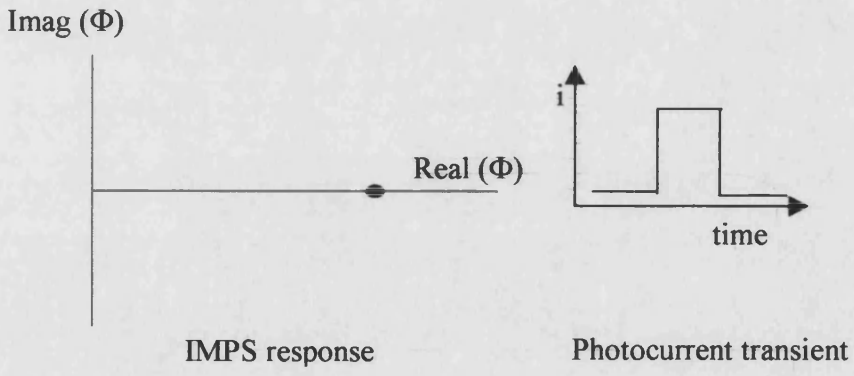

Figure 3.16 *Case 1 no recombination and no RC attenuation.*

The location of the point on the real axis corresponds to the value of the steady state photocurrent conversion efficiency.

Case 2 – Finite Recombination and negligible RC attenuation

If surface recombination occurs, for example in the photocurrent onset region of the photocurrent voltage curve, the photocurrent transient exhibits a sharp spike initially and then levels out. The corresponding IMPS response is a semicircle in the positive upper quadrant. The maximum real intercept is the initial (instantaneous) photocurrent and the lower real intercept is the steady state photocurrent. Figure 3.17. On illumination the photogenerated holes move quickly to the semiconductor surface aided by the electric field. This takes typically less than 10^{-9} s, and causes the initial sharp current spike. Some of these holes then become trapped at the surface, which induces electrons in the conduction band to back react with the trapped holes. This creates a current of opposite sign. This current reduces the current from the transport of holes and the result is a decay in the overall current. The current then levels out to a steady state value. when the light is switched off, the current overshoots in the opposite direction as the remaining trapped holes react with electrons.

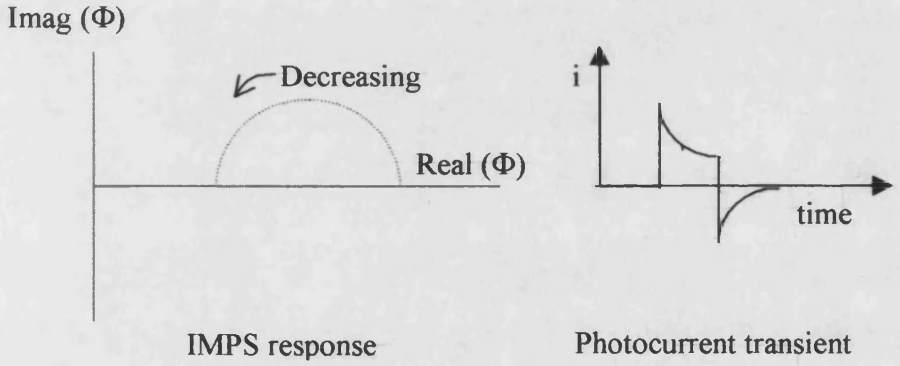

Figure 3.17 *Case 2- recombination with no RC attenuation*

Case 3 – Negligible recombination and finite RC attenuation

For the case in which surface recombination is negligible the IMPS response will fall in the lower quadrant. The low frequency intercept on the real axis is equivalent to a quantum efficiency of 1. At higher frequencies the response is attenuated due to the RC time constant of the system. The plot passes through a minimum of $\omega=1/RC$. This corresponding transient rises towards a maximum as shown in Figure 3.18.

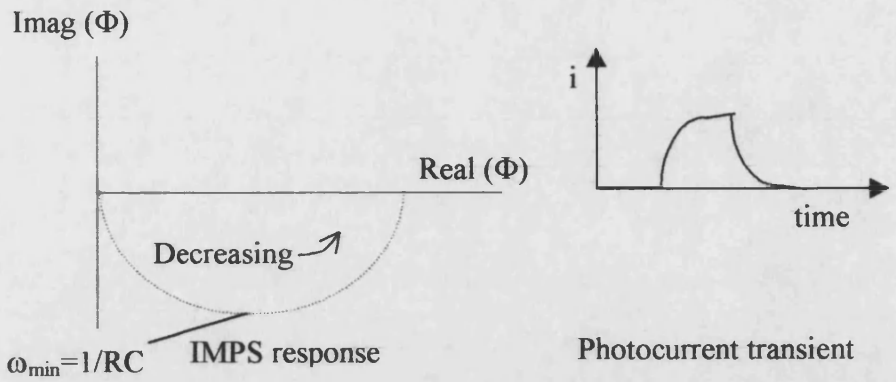

Figure 3.18 *Case 3- Negligable recombination and finite RC attenuation*

Case 4 Recombination and RC attenuation both present

It is clear that the result is from a combination of cases 2 and 3. The IMPS and transient responses for this case are shown in Figure 3.19.

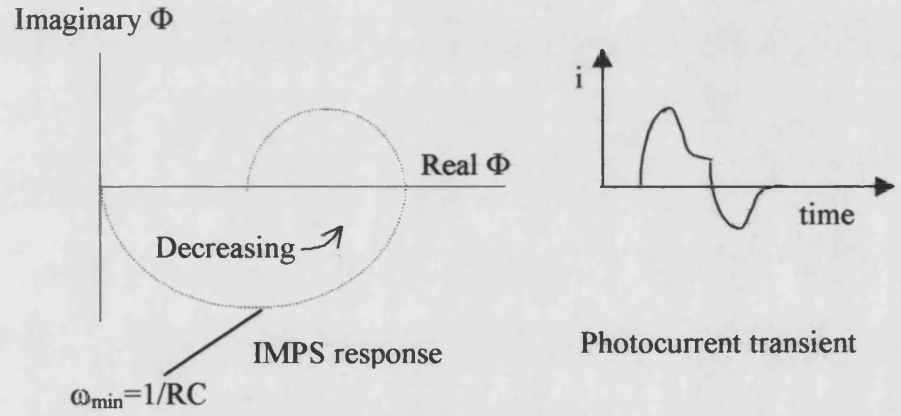

Figure 3.19 *Case 4- Recombination and RC attenuation both present.*

Recombination processes cause problems when determining the minority carrier diffusion length from steady state photocurrent measurements using the Gärtner equation. The high frequency intercept of the photocurrent, obtained from the IMPS plots, can be used instead of the steady-state value in order to determine the diffusion length. This has been demonstrated by Peat & Peter [1].

For dye sensitised cells

The response for a thin film dye sensitised solar cell contrasts with minority carrier photocells as the IMPS response always appears in the lower half of the complex plane and is determined by the diffusion coefficient and the lifetime of the photo-generated electrons.

3.2.4 Model of electron generation and collection in nanocrystalline cells.

It is assumed that due to the nanocrystalline particles and the interpenetrating solvent, the internal electric field within the film is negligible. Electron transport within the film must then be dominated by diffusion. This is expected to be coupled with relaxation of the ionic atmosphere of the electrolyte. This is a novel situation and is very different from conventional p-n junction solar cells. In a p-n junction solar cell or a Shottky barrier cell an electric field is present and therefore migration is the major form of charge transport. As electron diffusion in nanocrystalline TiO_2 cells is slow, reaction of the electrons from the TiO_2 or SnO_2 with I_3^- must also be slow enough such that electrons injected by the dye are collected efficiently.

The steady state response of the i-V characteristics of dye sensitised nanocrystalline cells has been discussed by Södergren et al [2]. They derived the solutions of the steady state generation/collection equation for mobile excess electrons.

$$\frac{\partial n}{\partial t} = D\frac{\partial^2 n}{\partial x^2} - \frac{n-n_o}{\tau} + \alpha I_0 e^{-\alpha x} \qquad (3.42)$$

Here n is the local electron concentration and n_o is the equilibrium electron concentration in the dark. D is the diffusion coefficient of electrons, τ is the electron lifetime determined by the back reaction with iodide, α is the absorption coefficient determined by the surface area/volume ratio and the dye coverage of the nanocrystalline electrode and I_o is the incident photon flux corrected for reflection losses. The first term on the right hand side of equation (3.42) is a diffusion term from Ficks second law. The second term accounts for photo injected electrons that react with the tri-iodide before reaching the collection pane. The electron lifetime τ, is the inverse of the pseudo first order rate constant for the electron/tri-iodide reaction, n-n_o is the excess electron

concentration. The final term is the rate of electron generation by the photosensitisation process where the light is incident from the substrate side. (For cases where the light is incident from the electrolyte side, x in the exponent is replaced by $(d-x)$. Light scattering is not considered but may be incorporated by the use of an effective absorption coefficient.

Illumination of the cell from either side was considered. The illumination geometry for each is shown below Figure 3.20.

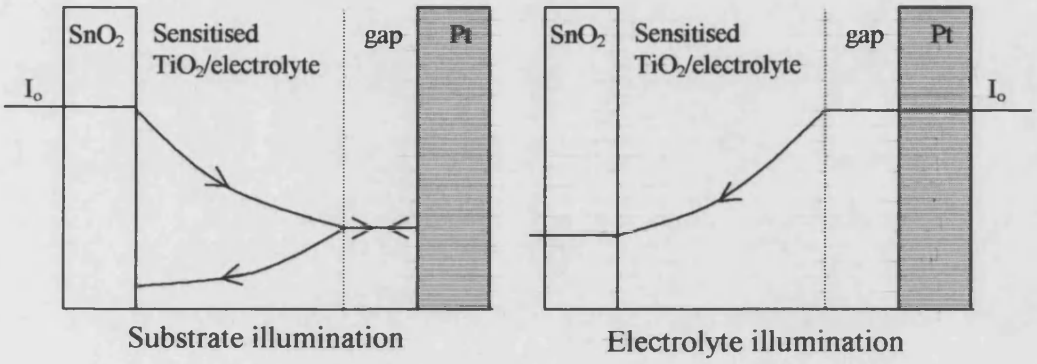

Figure 3.20 *Illumination geometry from substrate and electrolyte illumination*

In order to develop a model it is necessary to make a number of assumptions [3]. These are listed below:

The thin film of TiO_2 is uniformly sensitised with dye.
The absorption coefficient is independent of distance.
Light absorption within the electrolyte is neglected, and any scattering is taken into account by defining an effective absorption coefficient.
The electrolyte penetrates throughout the porous layer and hence injected electrons are screened by the solution.
The lifetime of the excess electrons within the TiO_2 is determined by reaction with I_3^-.
Regeneration of dye from the oxidised state by reaction with I^- is fast.
Change in the concentration of I^-/I_3^- within the pores is neglected.
The effective diffusion coefficient is related to electron trapping by the following equation:

$$D_{eff} = D\frac{n_{free}}{n_{total}} = D\frac{k_{detrap}}{k_{trap} + k_{detrap}} \qquad (3.43)$$

We consider that electrons diffuse through the TiO_2 film to the back contact and may be extracted over a potential dependent energy barrier. It is assumed that extraction over this barrier has a potential dependent rate constant k_{ext}. If k_{ext} is very large, then every electron that reaches the back contact is extracted immediately. This situation is the diffusion limited case as the rate determining step for electron extraction is the time taken for the electron to reach the back contact. If the converse is true and k_{ext} is small, then electron extraction may become rate limiting. This situation is the kinetically limited (recombination limited) case. The reverse process of electron injection from the SnO_2 into the TiO_2 can be described by a potential rate constant k_{inj}.

$$k_{ext} = k^0{}_{ext} e^{\left[\frac{-q\beta V}{kT}\right]} \qquad (3.44)$$

$$k_{inj} = k_{inj} e^{\left[\frac{-q(1-\beta)V}{kT}\right]} \qquad (3.45)$$

These expressions are analogous to the equations developed for the electron transfer of an electron from solution to an electrode (i.e. the Butler Volmer equation, equation (3.46)) Here V is the cell voltage and β is analogous to the transfer coefficient used in electrode kinetics.

$$i_{net} = i_e\left[\exp\left(\frac{\beta zF\eta}{RT}\right) - \exp\left(\frac{-(1-\beta)zF\eta}{RT}\right)\right] \qquad (3.46)$$

The model shown below has been used to describe the TiO_2/SnO_2 junction within the dye sensitised cell. Figure 3.21.

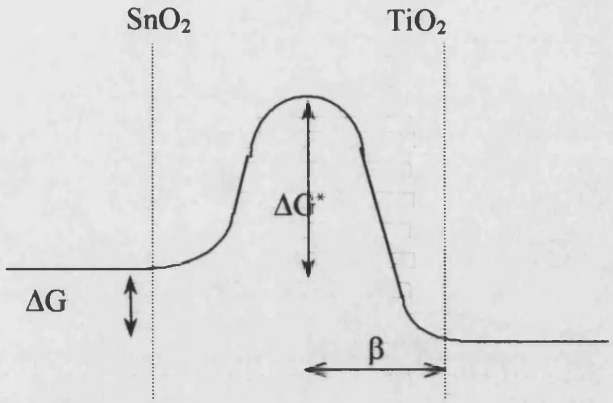

Figure 3.21 *Reaction co-ordinate across the TiO_2 /SnO_2 interface.*

The geometry of the interface is far more complex than a simple metal solution interface. Within a dye sensitised cell there are three phases associated with the back contact. These are the conducting tin oxide, the dye sensitised TiO_2 nanoparticles and the electrolyte. The TiO_2 nanoparticles are sintered onto the conducting tin oxide glass and form a network system of interconnected particles these particles are surrounded by electrolyte. [Figure 3.22]

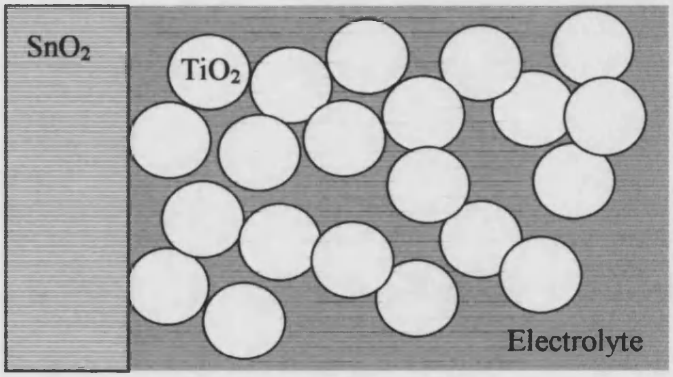

Figure 3.22 *Schematic diagram of a nanocrystalline TiO_2 electrode.*

There is also the possibility that an insulating layer of TiO_2 is located between the nanocrystalline particles and the tin oxide to prevent reaction of the electrolyte with the tin oxide. This three-phase system enables the electrolyte to shield electrons in the nanoporous TiO_2. Evidence suggests [4] that a potential drop within a nanoporous network does not occur at the electrode solution interface, as with conventional metal electrodes. In a nanoporous system the ions within the electrolyte are free to move, when a negative potential is applied to the back contact the ions can move towards the

back contact and shield the charge. This results in the potential difference being dropped mainly near to the substrate hence the nearer to the back contact the bigger the potential difference between the solution and the semiconductor. The potential drop within a nanocrystalline system can influence ΔG_{act}^{*}, it is clearly not as straightforward as the case of a metal/solution interface where the potential drop is located between the OHP and the metal electrode.

The photocurrent conversion efficiency (Φ_ω) for the dye sensitised system is defined as:

$$\Phi(\omega) = \frac{j_{photo}}{qI_0} \tag{3.47}$$

The general solution for substrate illumination is [3]:

$$\Phi(\omega) = \frac{\alpha}{\alpha+\gamma} \cdot \frac{e^{\gamma d} - e^{-\gamma d} + 2\alpha \dfrac{e^{-\alpha d} - e^{-\gamma d}}{\gamma - \alpha}}{e^{\gamma d} + e^{-\gamma d} + \dfrac{D\gamma}{k_{ext}}\left(e^{\gamma d} - e^{-\gamma d}\right)} \tag{3.48}$$

For the diffusion limited case:

$$\Phi(\omega) = \frac{\alpha}{\alpha+\gamma} \cdot \frac{e^{\gamma d} - e^{-\gamma d} + 2\alpha \dfrac{e^{-\alpha d} - e^{-\gamma d}}{\gamma - \alpha}}{e^{\gamma d} + e^{-\gamma d}} \tag{3.49}$$

For electrolyte side illumination the following holds:

$$\Phi(\omega) = \frac{\alpha}{\alpha+\gamma} \cdot \frac{e^{(\gamma-\alpha)d} - e^{-(\gamma+\alpha)d} + 2\alpha \dfrac{e^{(\gamma-\alpha)d} - 1}{\gamma - \alpha}}{e^{\gamma d} + e^{-\gamma d} + \dfrac{D\gamma}{k_{ext}}\left(e^{\gamma d} - e^{-\gamma d}\right)} \tag{3.50}$$

The diffusion-limited case is given by:

$$\Phi(\omega) = \frac{\alpha}{\alpha+\gamma} \cdot \frac{e^{(\gamma-\alpha)d} - e^{-(\alpha+\gamma)d} + 2\alpha \dfrac{e^{(\gamma-\alpha)d} - 1}{\gamma - \alpha}}{e^{\gamma d} + e^{-\gamma d}} \tag{3.51}$$

Where:

$$\gamma = \sqrt{\frac{1}{D\tau} + \frac{i\omega}{D}} \qquad (3.52)$$

DC solutions can be obtained noting that for $\omega=0$:

$$\gamma = \sqrt{\frac{1}{D\tau}} \qquad (3.53)$$

It should be noted that in the diffusion limited case the DC solutions obtained by setting $\omega=0$ are the same as those derived by Södergren et al [2].

The open circuit voltage is defined by j=0 *i.e.* when $0=j_{photo}+j_{dark}$. Both the photocurrent and the dark current are determined by the solutions of the diffusion equations for electrons. For simplicity the case where trapping does not influence the shape of the IMPS plot but does influence the electron lifetime and effective diffusion coefficient will be discussed.

The capacitance and the electrode/solution resistance attenuate the frequency dependent photocurrent measured in the external circuit. (In practice the resistance is mainly the sheet resistance of the SnO_2 coated glass.) In general the IMPS response Φ_{ext} is given by:

$$\Phi_{ext}(\omega) = \Phi_{int}(\omega)A(\omega) \qquad (3.54)$$

Where:

$$A = \frac{1 - j\omega RC}{1 + \omega^2 R^2 C^2} \qquad (3.55)$$

A is defined as the RC attenuation factor and Φ_{int} is the conversion efficiency (Φ_{int} is the internal conversion efficiency = current/(incident photon flux –transmitted light – reflected light). As there are many variables within the system the effects of changing values of components is shown below. The plots were produced using a programme written by E. A. Ponomarev. Unless stated, no RC component was accounted for.

3.2.5 *Predictions of the model*

The diffusion length

The diffusion length (L) is related to the distance that can be travelled by an electron before it reacts with the tri-iodide. It is defined by the following equation.

$$L = \sqrt{D_n \tau}_n \qquad (3.56)$$

Here D_n is the diffusion coefficient for the electrons in the film and τ_n is the lifetime of the photo-generated electrons determined by the back reaction with the I_3^- and it is assumed to be pseudo first order due to the large excess of electrons in the conduction band.

It is possible for the diffusion length to be changed in the model by changing either the diffusion coefficient or the lifetime of the injected electrons. If the diffusion length is much larger than the film thickness, all of the injected electrons will be collected successfully. This will give a conversion efficiency (Φ) of 1. Conversely if τ_n is much smaller than the film thickness, most of the electrons will react with the tri-iodide or the oxidised state of the dye and not be collected. This results in a low conversion efficiency.

Illumination from the substrate side

For this geometry, light is absorbed primarily near to the collecting contact, so that many of the electrons do not have far to diffuse before they are collected. The absorption of light produces a concentration gradient of electrons, which are being constantly extracted at the substrate. If the diffusion length is large, then most of the electrons diffuse to the back contact and are extracted. This is shown for various diffusion lengths in Figure 3.23. The IMPS response for this case is shown in Figure 3.24.

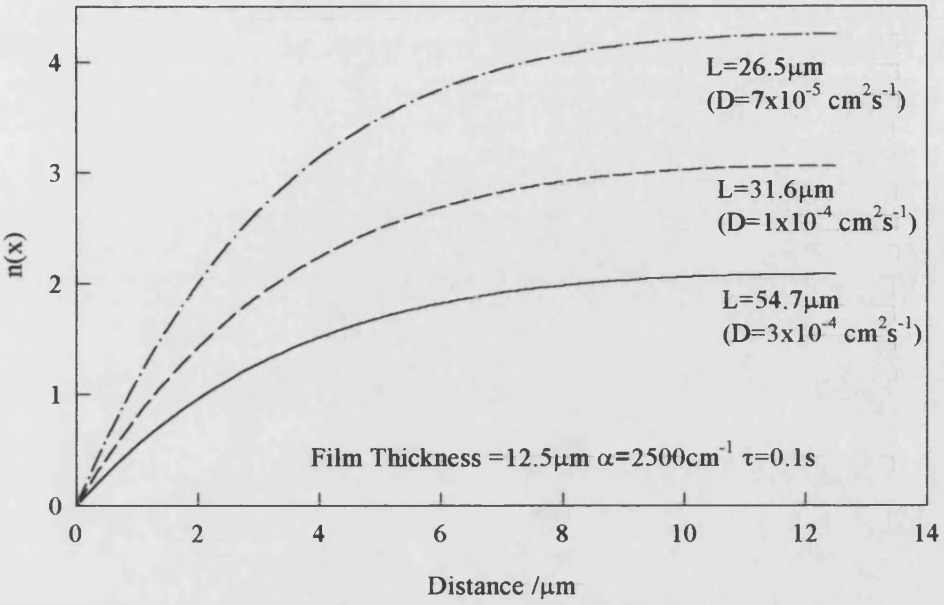

Figure 3.23 *Substrate side illumination. L_n>Film Thickness*

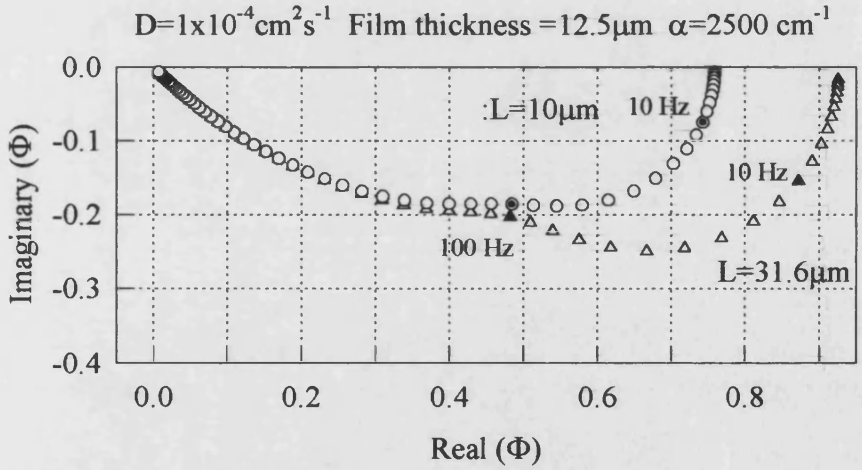

Figure 3.24 *IMPS for the case where L_n>film thickness*

When the diffusion length is less than the film thickness, the collection efficiency for electrons is lowered. This is shown in Figure 3.25. It should be noted that a maximum is present in this case, which increases as L decreases. The presence of the maximum

means that electrons generated beyond the maximum will diffuse away from the collection plane rather than towards it (Figure 3.26). The IMPS response for the above cases is shown in Figure 3.27. It can be seen that Φ is less than 1 and decreases with decreasing L.

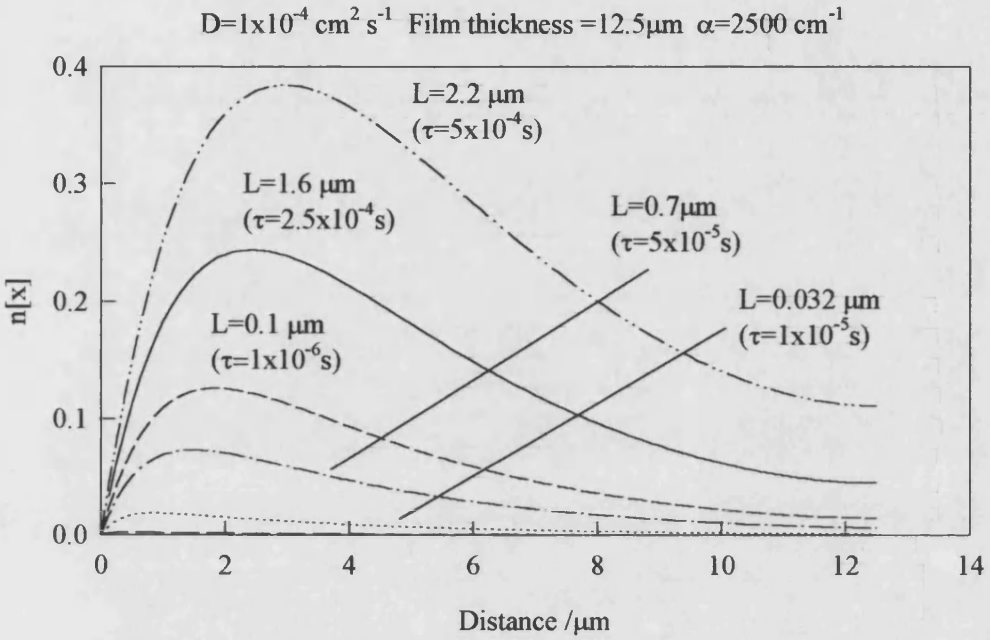

Figure 3.25 *Electron concentration profiles as a function of electron diffusion length for substrate side illumination Ln< film thickness. (τ_n changed).*

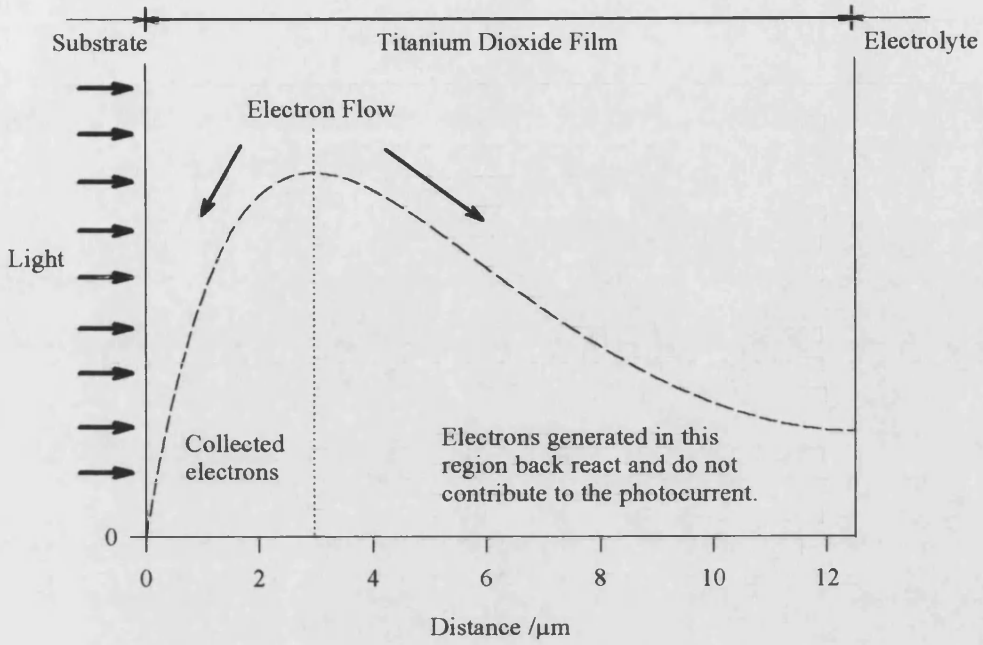

Figure 3.26 *Diagram showing electron flow in a nanocrystalline solar cell when the diffusion length is smaller than the film thickness.*

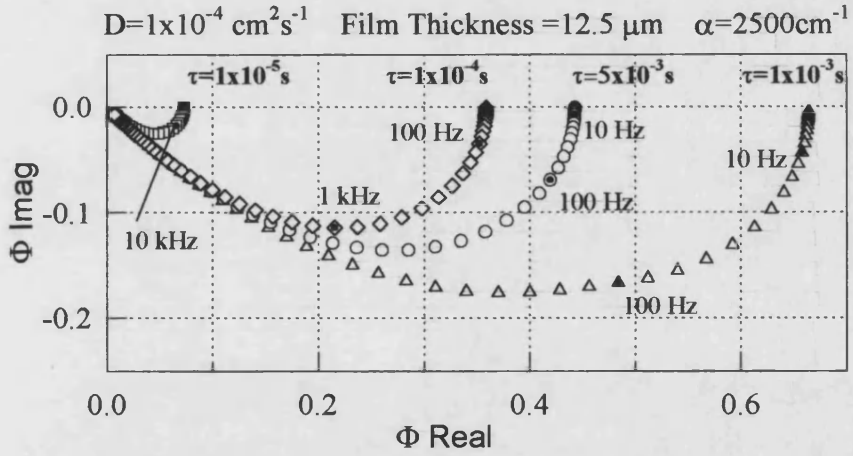

Figure 3.27 *IMPS L<film thickness*

It is worth noting at this point that all the IMPS plots calculated for substrate side illumination display a 45° slope at high frequencies. This slope is characteristic of diffusion controlled electron extraction. It should also be noted that when $\Phi \cong 1$, ω_{min} is

determined only by D, whereas when Φ is much less than 1, ω_{min} is determined only by τ, At intermediate values ω_{min} depends on both D and τ.

Illumination from the electrolyte side

For this geometry, most of the electrons are generated furthest from the collection plane. For the electrons to be collected they have to diffuse through the majority of the film. The concentration gradient moves electrons towards the substrate all the time as a large number of electrons are generated furthest from the substrate. At large diffusion lengths there is less of a gradient (Figure 3.28) because the electrons move faster and are extracted. As L decreases, the electrons move more slowly, thus the gradient is steeper the sagging effect demonstrated in Figure 3.29 is caused due to loss of electrons in transit.

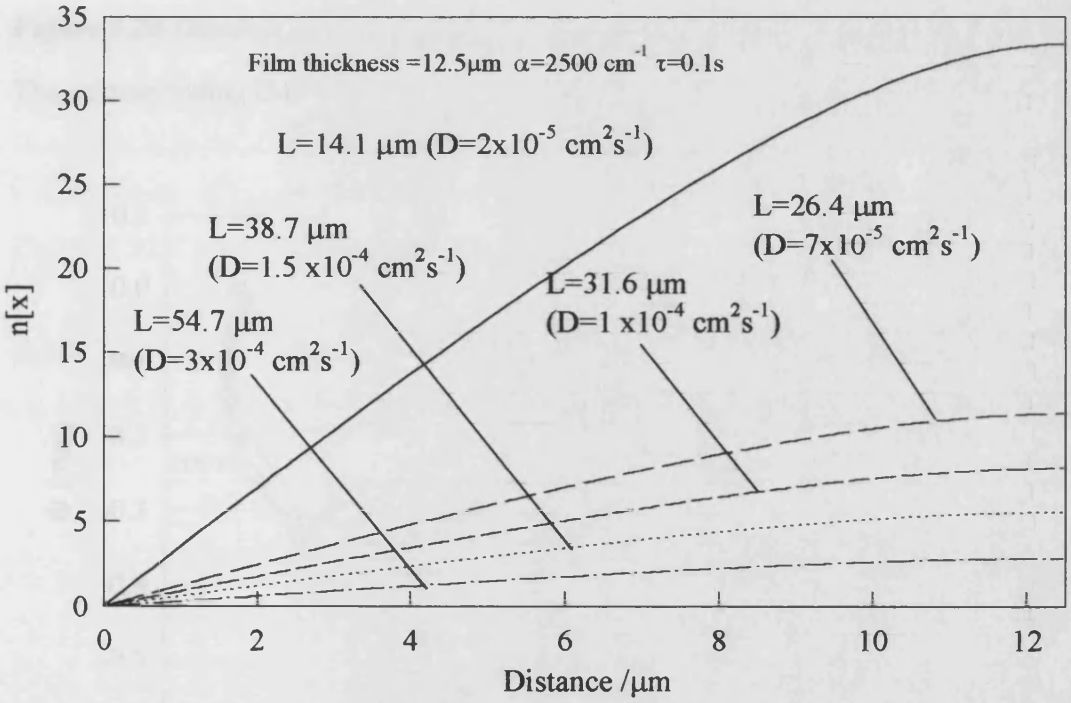

Figure 3.28 *Illumination from the electrolyte side L_n> film thickness*

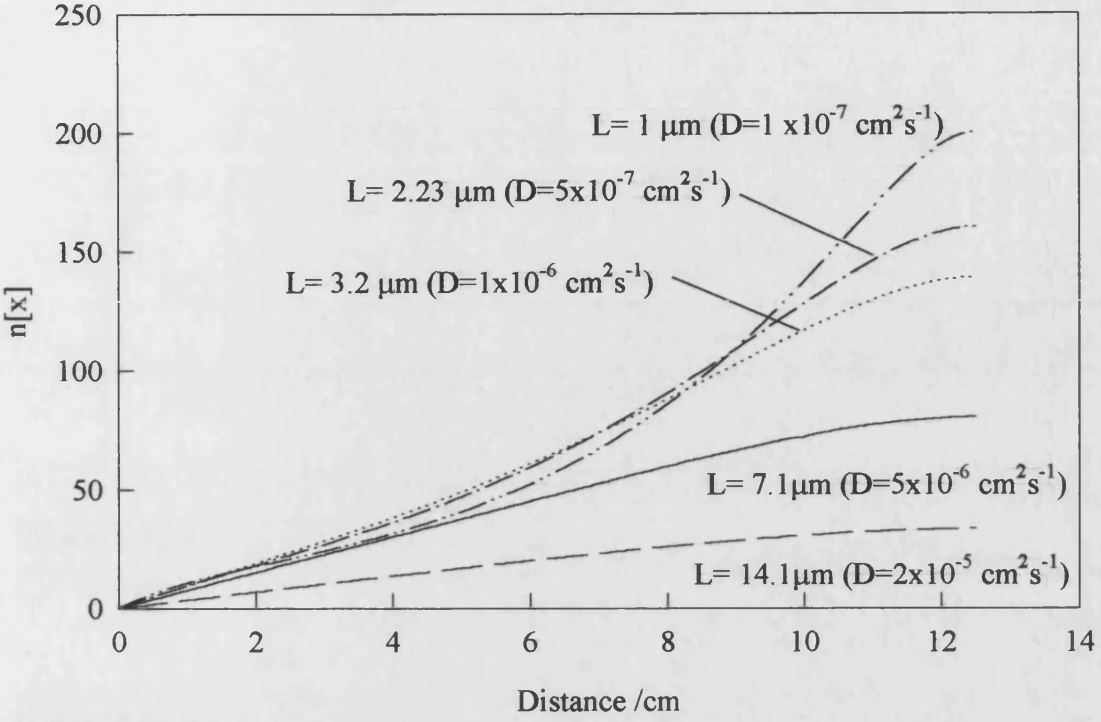

Figure 3.29 *Illumination from the electrolyte side L_n<< film thickness*

The corresponding IMPS plots are shown in Figure 3.30 and Figure 3.31.

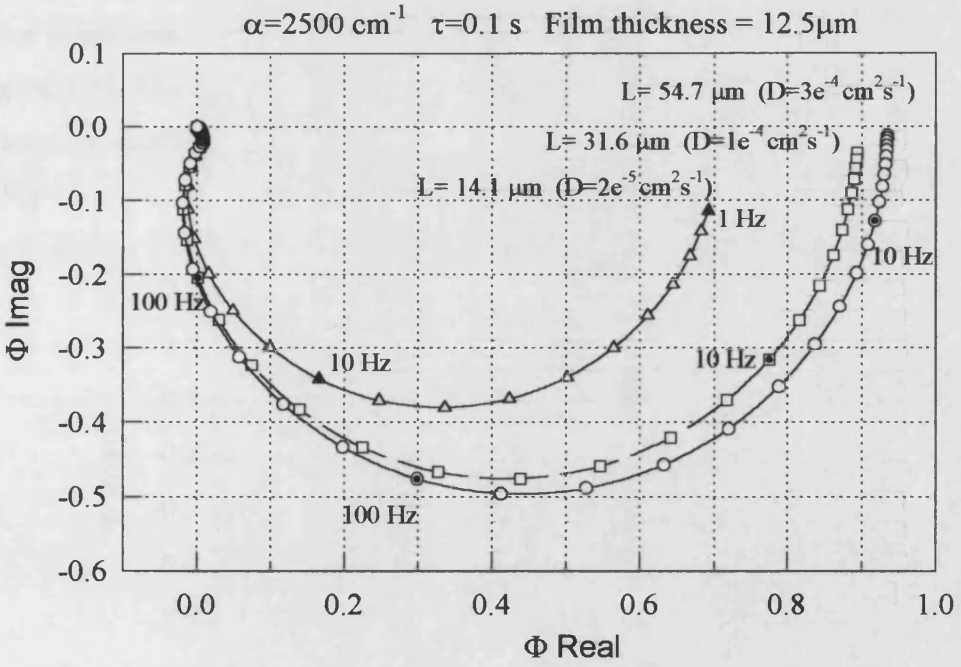

Figure 3.30 *IMPS plot for electrolyte side illumination for the case where Ln> film thickness.*

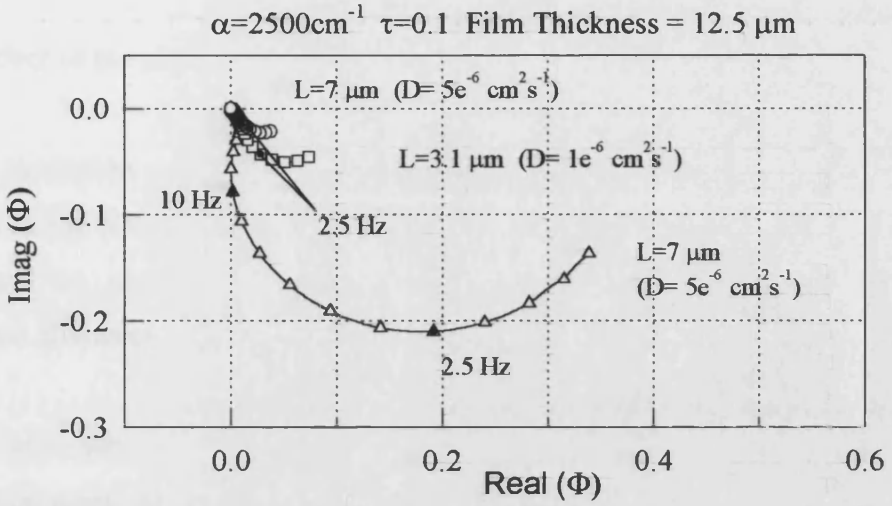

Figure 3.31 *IMPS plot for electrolyte side illumination for the case where L_n<<thickness.*

It should be noted that at high frequencies the IMPS response begins to spiral into the origin. This becomes more evident as the absorption coefficient increases as it is due to the delay caused by electrons travelling through the film. In the Grätzel cell, absorption coefficients are of the order of 10^3 and the effect is not expected. The spiral effect is more prominent with absorption coefficients of the order of 10^5 as shown below in Figure 3.32. The spiralling effect is therefore expected when using UV excitation as the absorption coefficient is much higher [5]. This has been shown by Vanmaekelbergh et al [6].

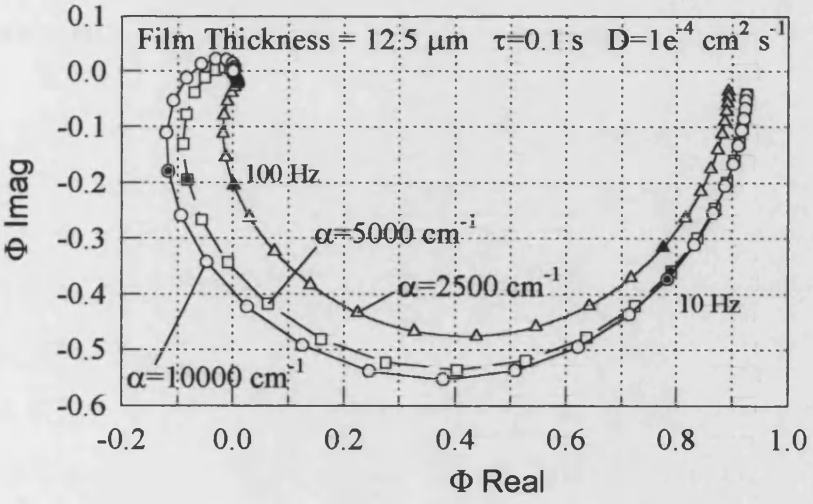

Figure 3.32 *High absorption coefficient*

The effect of the absorption coefficient

If the absorption coefficient (α) is small, not much light will be absorbed, and this results in the conversion efficiency being low (i.e. $\Phi<<1$). If the unabsorbed light is corrected for, and the diffusion coefficient and electron lifetime are high, then the quantum efficiency (Q.E.) should be close to unity.

If α is large, substrate illumination will generate the majority of the electrons near to the collection point, whereas with electrolyte illumination most electrons will be generated at the surface of the film. In this case electron transport through the film will be more important for electrolyte illumination than substrate illumination.

The effect of the extraction rate constant

If the extraction rate constant is large (Figure 3.33 and Figure 3.34) then electrons will be extracted as soon as they reach the back contact. A high electron extraction rate constant implies that the activation energy for the extraction is small. This will result in the diffusion-limited case.

If the extraction rate constant is small, the activation energy is large (Figure 3.33 and Figure 3.34) then the electrons accumulate at the collection point. Due to the slow extraction rate the electrons recombine with the oxidised state of the dye or tri-iodide and thus Φ is lower. Transport to the back contact is not as important because the extraction rate rather than the diffusion coefficient determine the response.

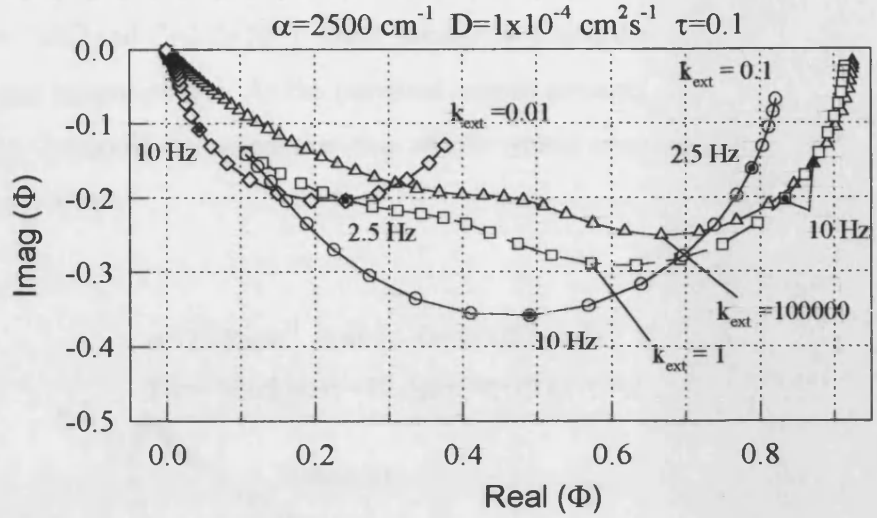

Figure 3.33 *Substrate illumination. The effect of k_{ext}.*

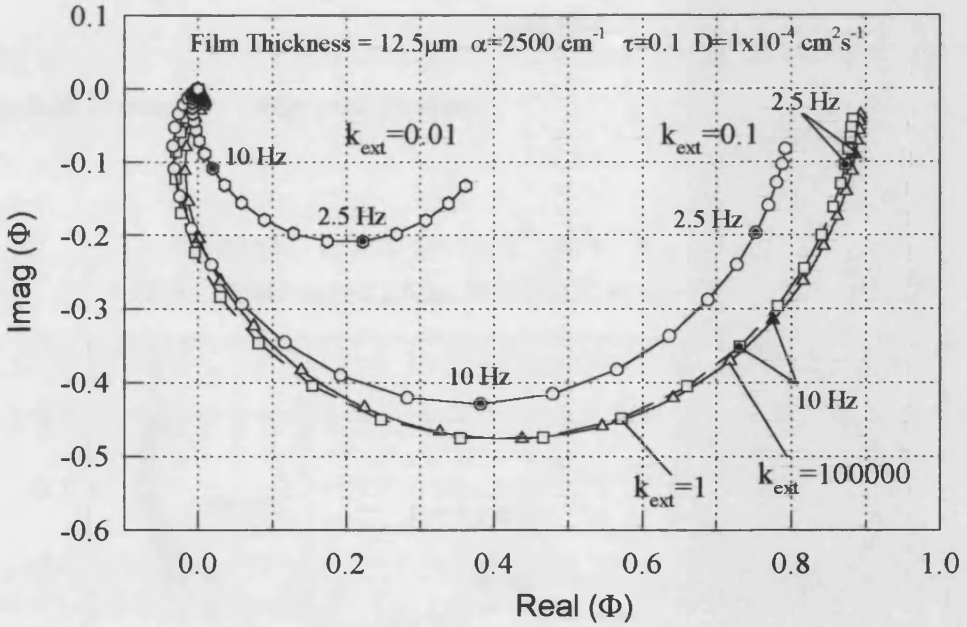

Figure 3.34 *Electrolyte illumination. The effect of k_{ext}.*

The effect of the RC time constant

The majority of the effect of the RC time constant is noted to occur at high frequency. When The RC attenuation factor is taken into account, the characteristic 45° slope noted under diffusion controlled conditions is not seen, instead a bulge is present in this area (Figure 3.35.) If the capacitance is increased ω_{min} decreases and the whole IMPS

response becomes dominated by the RC time constant (Figure 3.36). Typical values at 0v are R=10Ω and C=2.2×10^{-5}F these values were also determined independently from Impedance measurements. As the potential moves towards open circuit the capacitance increases. It should be noted that this effect would obscure any effect indicative of kinetic extraction.

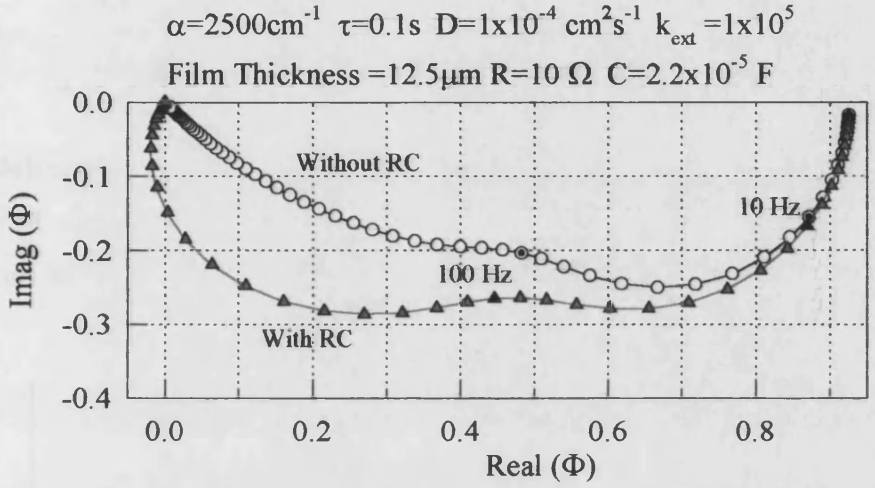

Figure 3.35 *Presence of bulge and 45 slope*

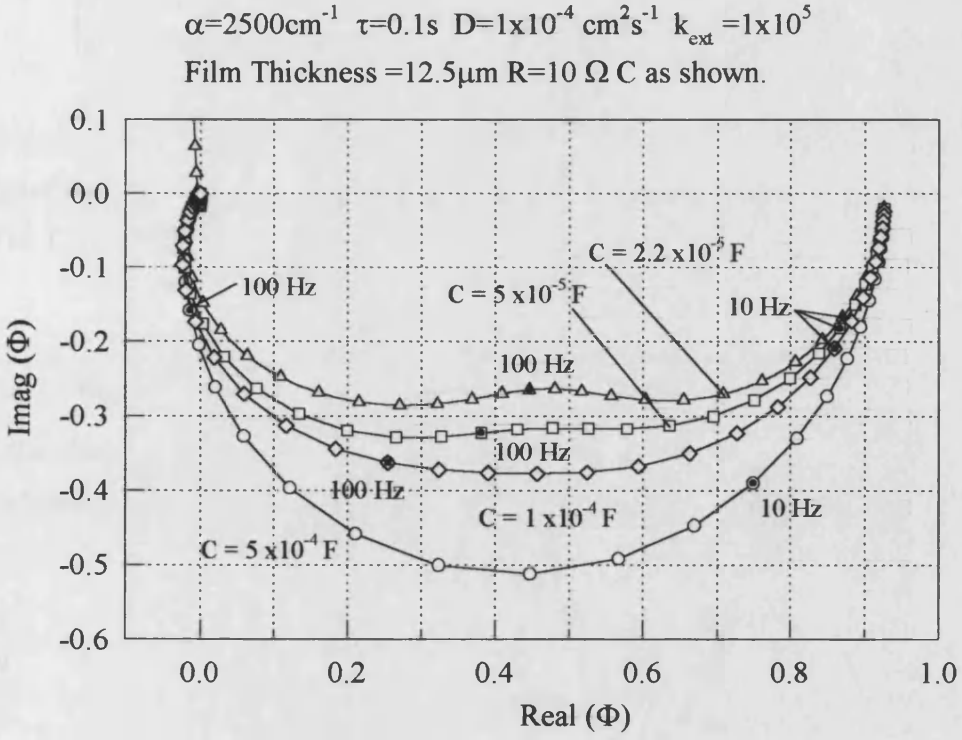

Figure 3.36 *Effect of IMPS with increasing Capacitance.*

3.5 *Intensity modulated photovoltage spectroscopy (IMVS)*

3.3.1 Definitions

3.3.1.1 The Fermi level (E_F)

The Fermi Dirac distribution defines the probability of the occupancy of electron energy levels. The Fermi Dirac distribution is:

$$f(E) = \frac{1}{1 + e^{\left(\frac{E - E_F}{kT}\right)}} \qquad (3.57)$$

This defines the Fermi level of electrons in the TiO_2, this is a measure of the Gibbs free energy of electrons in the film. In the dark it is in equilibrium with the Fermi level of electrons in the SnO_2 and the electrolyte. This is shown diagrammatically below:

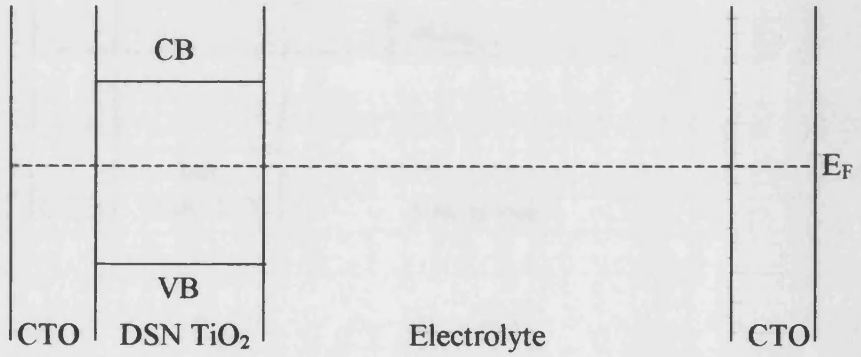

Figure 3.37 *The Fermi level of electrons in a nanocrystalline solar cell in the dark. CTO: Conducting tin oxide, DSN: Dye sensitised.*

3.3.1.2 The Quasi Fermi Level ($_nE_F$)

In the dark under conditions of thermal equilibrium the number of electrons in the conduction band of the TiO_2 is given by:

$$\frac{n_0}{N_c} = e^{-\frac{(E_C - E_F)}{kT}} \qquad (3.58)$$

Here Nc is the density of states in the conduction band and E_C is the conduction band energy. Under illumination, the electron population within the semiconductor increases and can be written as $n_o + \Delta n$, where Δn is an increase in the electron concentration by illumination. The increase in the electron concentration results in an upward movement in the Fermi level of the TiO_2. This new level is termed the quasi Fermi level, ${}_nE_F$. The total (non equilibrium) electron density defines the quasi Fermi level for electrons ${}_nE_F$:

$$\frac{n_o + \Delta n}{N_c} = e^{\frac{-(E_C - {}_nE_F)}{kT}} \qquad (3.59)$$

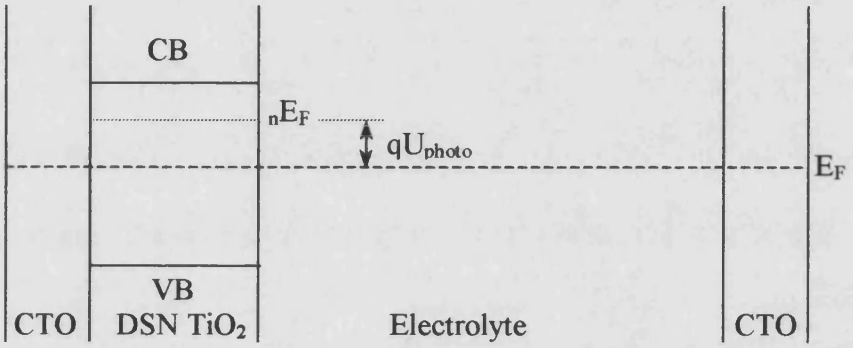

Figure 3.38 *The quasi Fermi level of electrons in a dye sensitised solar cell under illumination at open circuit.*

3.3.1.3 The Photovoltage

The photovoltage is a measure of the change in the Fermi level of the TiO_2. It is related to the change in the Fermi level by equation 3.60. Equation 3.60 is only valid when the distance dependence of the quasi Fermi level (${}_nE_F$) is neglected *i.e.* at open circuit and when $\alpha d=1$. Under short circuit conditions, a diffusion gradient is present and the excess electron concentration tends to 0 at the substrate, so that ${}_nE_F$ is distance dependent.

$$qU_{photo} = {}_nE_F - E_F \qquad (3.60)$$

If we now consider δU_{photo} as a small amplitude change in the photovoltage, this corresponds to a modulation of ${}_nE_F$. This is shown diagrammatically in Figure 3.39.

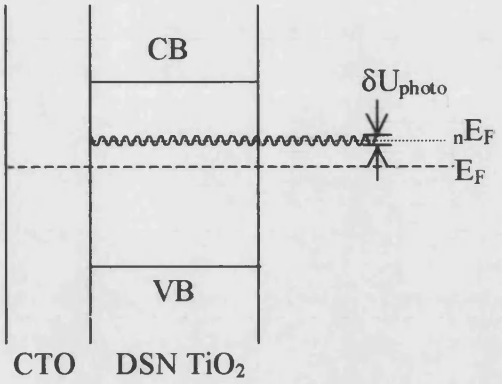

Figure 3.39 *A small amplitude change in the photovoltage* δU_{photo}.

3.3.1.4 The conduction band capacitance C_{CB}

The conduction band capacitance C_{CB} [7,8] is defined as the change in charge accumulated in the conduction band on illumination. The relationship between this and the photovoltage can be derived as follows: [8].

Equation (3.60) enables equation (3.59) to be written as follows:

$$\frac{n_o + \Delta n}{N_c} = e^{\frac{-(E_C - E_F - qU_{photo})}{kT}} = e^{-\left(\frac{E_C - E_F}{kT}\right)} e^{\frac{qU_{photo}}{kT}} \qquad (3.61)$$

If as in the case of IMVS, a small periodic modulation of the intensity is superimposed onto the background DC illumination. Equation (3.61) becomes:

$$\frac{n_o + \Delta n + \delta n}{N_c} = e^{-\left(\frac{E_C - E_F}{kT}\right)} e^{\left(\frac{qU_{photo}}{kT}\right)} e^{\left(\frac{q\delta U_{photo}}{kT}\right)} \qquad (3.62)$$

(δn is the periodic component of the excess electron density).

Due to the small amplitude modulation it is possible to linearise the final term of equation (3.62) by expansion of the exponential, to give:

$$\frac{\delta n}{N_c} = e^{-\left(\frac{E_C - E_F}{kT}\right)} e^{\left(\frac{qU_{photo}}{kT}\right)} \frac{q\delta U_{photo}}{kT} \qquad (3.63)$$

δQ_{CB}, the modulation of the conduction band electron density per unit area in a film with thickness d, is given by equation (3.64).

$$\delta Q_{CB} = qd\delta n = \frac{q^2 dN_C}{kT} e^{-\left(\frac{E_C - E_F}{kT}\right)} e^{\left(\frac{qU_{photo}}{kT}\right)} \delta U_{photo} \qquad (3.64)$$

Franco *et al* [8] define the conduction band capacitance as: (equation (3.65))

$$C_{CB} = \frac{q^2 N_C d}{kT} e^{-\left(\frac{E_C - E_F}{kT}\right)} e^{\left(\frac{qU_{photo}}{kT}\right)} \qquad (3.65)$$

Substitution of equation (3.65) into equation (3.64) yields the relationship between conduction band capacitance and intensity modulated photovoltage.

$$\delta Q_{CB} = C_{CB} \delta U_{photo} \qquad (3.66)$$

3.3.1.5 Trap capacitance (C_t)

Although the preceding discussion defined the conduction band capacitance there is no information regarding the proportion of free and trapped electrons. In the dark at equilibrium the trapped electron density is given by the following:

$$n_t^0 = \int_{E_V}^{E_C} N(E) f(E) dE \approx \int_{E_V}^{E_F} N(E) dE \qquad (3.67)$$

N(E) is the density of states function for traps located in the band gap.

When the cell is illuminated the quasi Fermi level ${}_nE_F$ determines the trapped electron density (as shown in Figure 3.40) and n_t under open circuit conditions is given by equation (3.68) (${}_nE_F$ is once again assumed to be independent of distance).

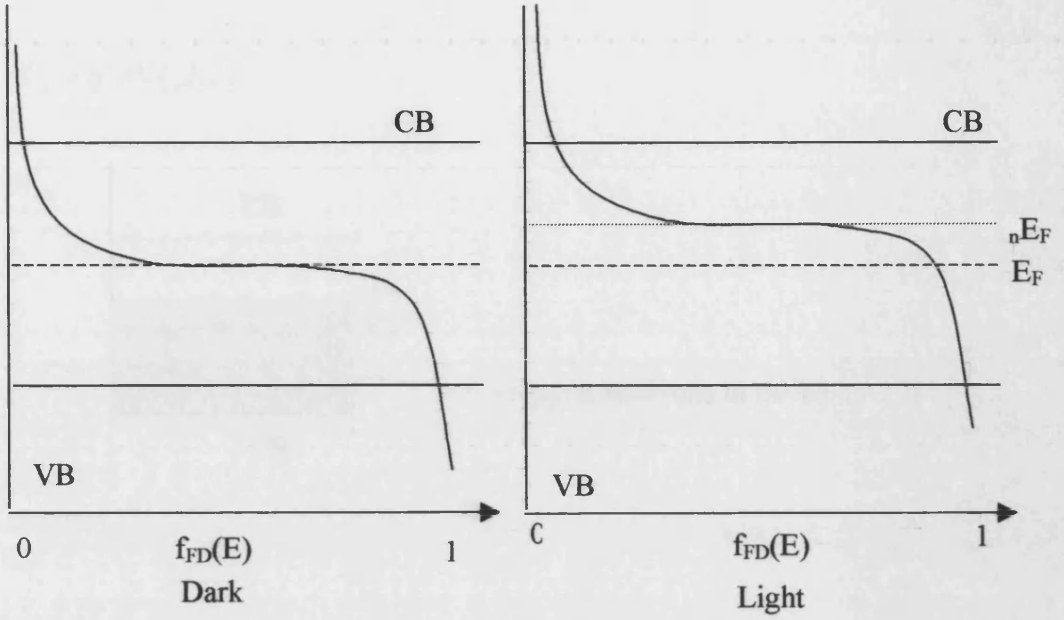

Figure 3.40 *Change in the occupation of the conduction band under illumination.*

$$n_t = \int_{E_V}^{{}_nE_F} N(E).d(E) \qquad (3.68)$$

The change in the electron density for a small optical perturbation of the electron quasi Fermi level is thus:

$$\delta n_t = N({}_nE_F)\delta_{{}_n}E_F = N({}_nE_F)q\delta U_{photo} \qquad (3.69)$$

Here $N({}_nE_F)$ is the density of electron traps at ${}_nE_F$.

The modulated-trapped charge per unit area in a film of thickness d is given by equation (3.70).

$$qd\delta n_t = q^2 dN({}_nE_F)\delta U_{photo} \qquad (3.70)$$

Equation (3.71) can be used to define the trap capacitance C_t. Schlichthörl *et al* [7] introduced the concept of the surface state capacitance, however as the electrons are not necessarily trapped at the surface, this may be misleading. The trap capacitance produced by electrons in traps in the band-gap region under illumination. It is determined by the Fermi level of electrons. This is shown in Figure 3.41.

$$C_t = q^2 dN({}_nE_F) \tag{3.71}$$

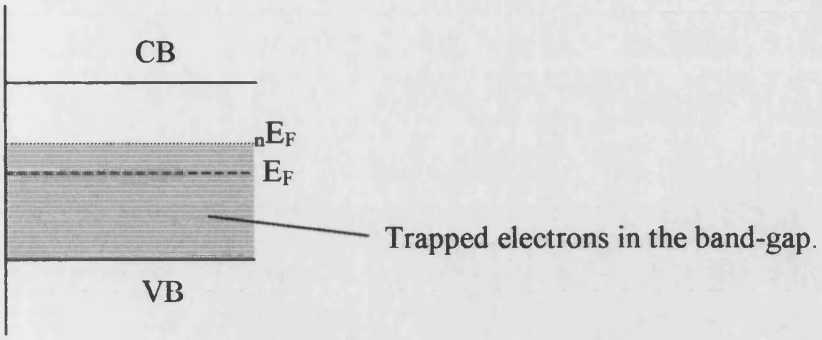

Figure 3.41 *The origin of Ct*

Equation (3.71) allows the intensity-modulated photovoltage and the perturbation of trapped charge density to be written as:

$$\delta Q = C_t \delta U_{photo} \tag{3.72}$$

3.3.1.6 The total photomodulated charge

The total photomodulated charge in the nanocrystalline electrode is thus given by equation 8.17.

$$dQ_{total} = (C_{CB} + C_t)\delta U_{photo} = C_{total}\delta U_{photo} \tag{3.73}$$

Thus under illumination:

$$C_{total} = C_{CB} + C_t \tag{3.74}$$

This defines the total photocapacitance of the electrode.

3.3.2 Trap distribution

Trapping has been discussed using a simple single level trap model these are shown as discrete energy levels in the band-gap. (Figure 3.42)

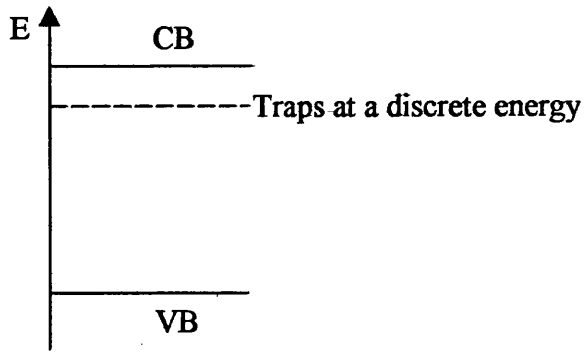

Figure 3.42 *Simple trap distribution in a semiconductor. All at a discrete energy within the band-gap.*

In reality this type of distribution does not occur. Traps are generally located throughout the band-gap in a distribution. Possible distributions for traps within the band-gap are described below.

Continuous trap distribution: This distribution is present when the probability of finding an electron in a trap is the same for all energies within the band-gap (Figure 3.43).

Exponential trap distribution: This exponential trap distribution indicates that there are many shallow traps located just below the conduction band but very few deep traps located near to the valence band (Figure 3.43).

Gaussian: With a Gaussian trap distribution the majority of the traps are located in the centre of the band-gap with few very deep or very shallow traps (Figure 3.43).

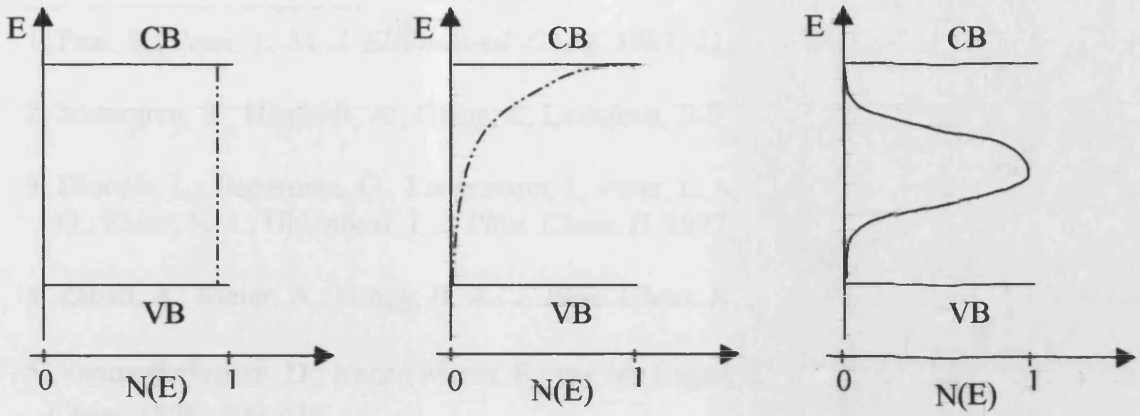

Continuous distribution Exponential distribution Gaussian distribution

Figure 3.43 *Trap distributions in a semiconductor band-gap.*

Other distributions

For some cases it is possible to have several trap distributions present within the band-gap. This is the case for amorphous silicon that has both a gaussian and exponential distribution. This is shown below in Figure 3.44.

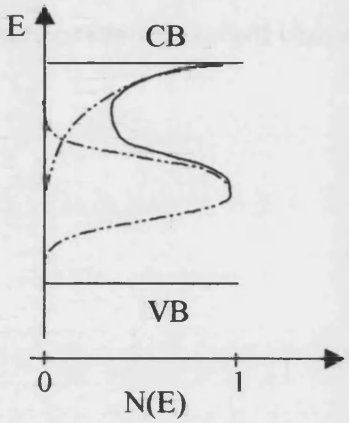

Figure 3.44 *Diagramatic representation of a band-gap containing both a gaussian and exponential trap distribuion.*

It is possible to define C_t as a function of the quasi Fermi level ($_nE_F$). If this is done over a large range of quasi Fermi levels then the trap distribution can, in principle, be obtained.

3.6 *References*

1. Peat, R.; Peter, L. M. *J. Electroanal. Chem.* **1987**, *228*, 351

2. Södergren, S.; Hagfeldt, A.; Olson, J.; Lindquist, S-E.; *J. Phys. Chem.* **1994**, *98*, 5552

3. Dloczik, L.; Ileperuma, O.; Lauermann, I.; Peter, L. M.; Ponomarev, E. A.; Redmond, G.; Shaw, N. J.; Uhlendorf, I. *J. Phys. Chem. B.* **1997**, *101*, 10281

4. Zaban, A.; Meier, A.; Gregg, B. A.; *J. Phys. Chem. B* **1997**, *101*, 7985

5. Vanmaekelbergh, D.; Iranzo Marín, F.; van de Lagemaat, J. *Ber. Bunsenges. Phys. Chem.* **1996**, *100*, 616

6. De Jongh, P. E.; Vanmaekelbergh, D. *Phys. Rev. Lett.* **1996**, *77*, 3427

7. Schlichthorl, G.; Huang, S. Y.; Sprague, J.; Frank, A. J. *J. Phys. Chem. B.* **1997**,*101*, 8141

8. Franco, G.; Gehring, G.; Peter, L. M.; Ponomarev, E. A.; Uhelendorf, I. *J. Phys. Chem. B.* **1999**, *103*, 692

General references

Southampton Electrochemistry Group, **1985**, *Instrumental methods in electrochemistry*, Ellis-Horwood, Chitchester.

Fisher, A. C. ; **1996**, *Electrode Dynamics*, Oxford University Press, Oxford

Chapter 4

Experimental methods

Index

Chapter 4 Experimental methods

4.1 Techniques

4.1.1 Capacitance voltage measurements

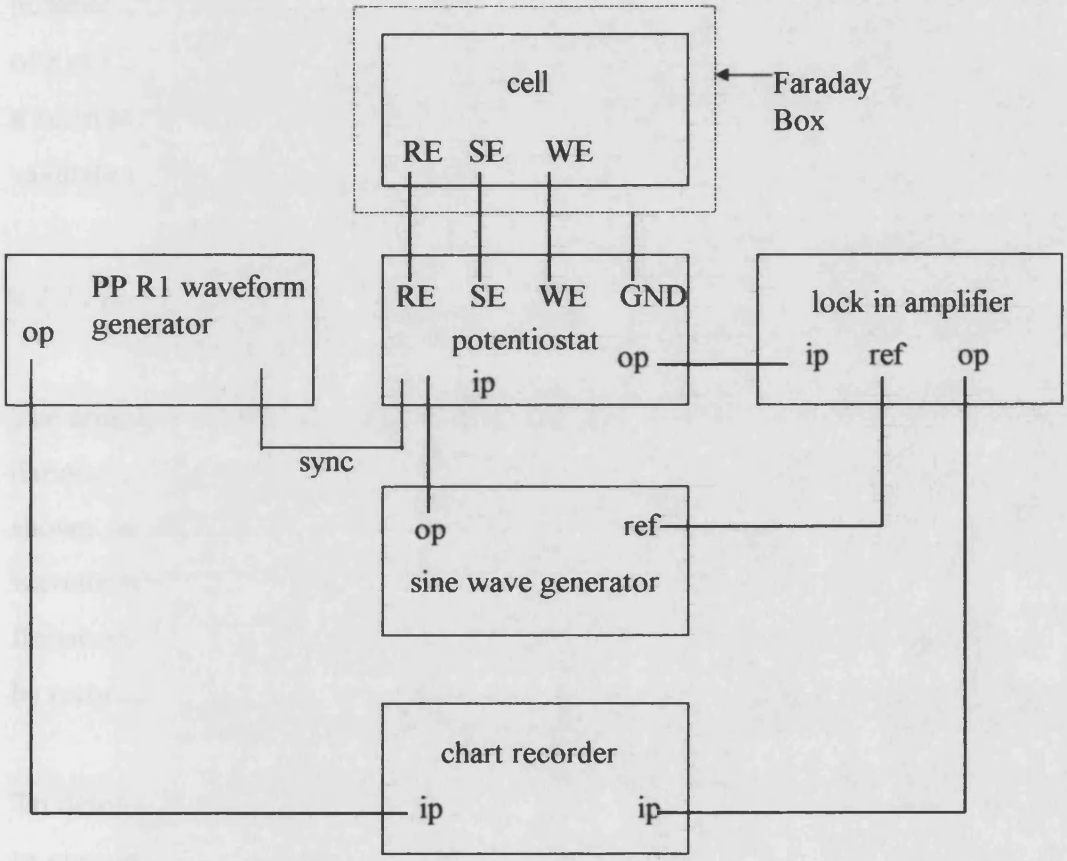

Figure 4.1 *Experimental set-up for capacitance voltage measurements*

The experimental set-up is shown in Figure 4.1. The cell is connected to a potentiostat via the reference electrode (RE), secondary or counter electrode (SE or CE) and the working electrode (WE). The potentiostat applies a potential as determined by the PPR1 waveform generator connected to the input. The PPR1 is programmed to scan a potential range and is

therefore also connected to the x input of the chart recorder. A sine wave generator is also connected to the potentiostat input. This is used to apply an AC potential to the sample. A synchronous signal is fed into the reference input of a lock in amplifier. The potentiostat output is fed into the lock in amplifier, which monitors only the signal with the same frequency as the reference. This means that only the current due to the AC signal is measured. This has advantages in that the signal to noise ratio improves and thus it is possible to measure much smaller signals. The 90° out of phase component of the admittance of a cell is related to the capacitance by $Y=j\omega C$ when dealing with a simple parallel circuit of a resistor and capacitor. Capacitance and resistance boxes (precision 5 %) were used to calibrate the equipment prior to use.

4.1.2 Photocurrent voltage measurements

The sample under investigation is connected to the potentiostat as the working electrode and illuminated with chopped illumination at a known wavelength. The experimental set-up is shown in Figure 4.2. A potential sweep is applied to the potentiostat from the PPR1 waveform generator. The photocurrent produced by the sample will be at the same frequency as the illumination. The use of a lock in amplifier enables small photocurrents to be recorded.

To determine the monochromatic conversion efficiency (also known as the incident photon to current conversion efficiency IPCE), the cell is replaced with a calibrated silicon diode. The diode is connected via a current amplifier to the lock in amplifier and the output recorded. The monochromatic conversion efficiency can be calculated from the following equation:

$$IPCE_{\lambda} = \frac{i_{\lambda,sample}}{i_{\lambda\,diode}} \times \Phi_{\lambda,diode} \qquad (4.1)$$

here : i_{λ} = current at wavelength λ, $\Phi_{\lambda,diode}$ = diode conversion efficiency at wavelength λ

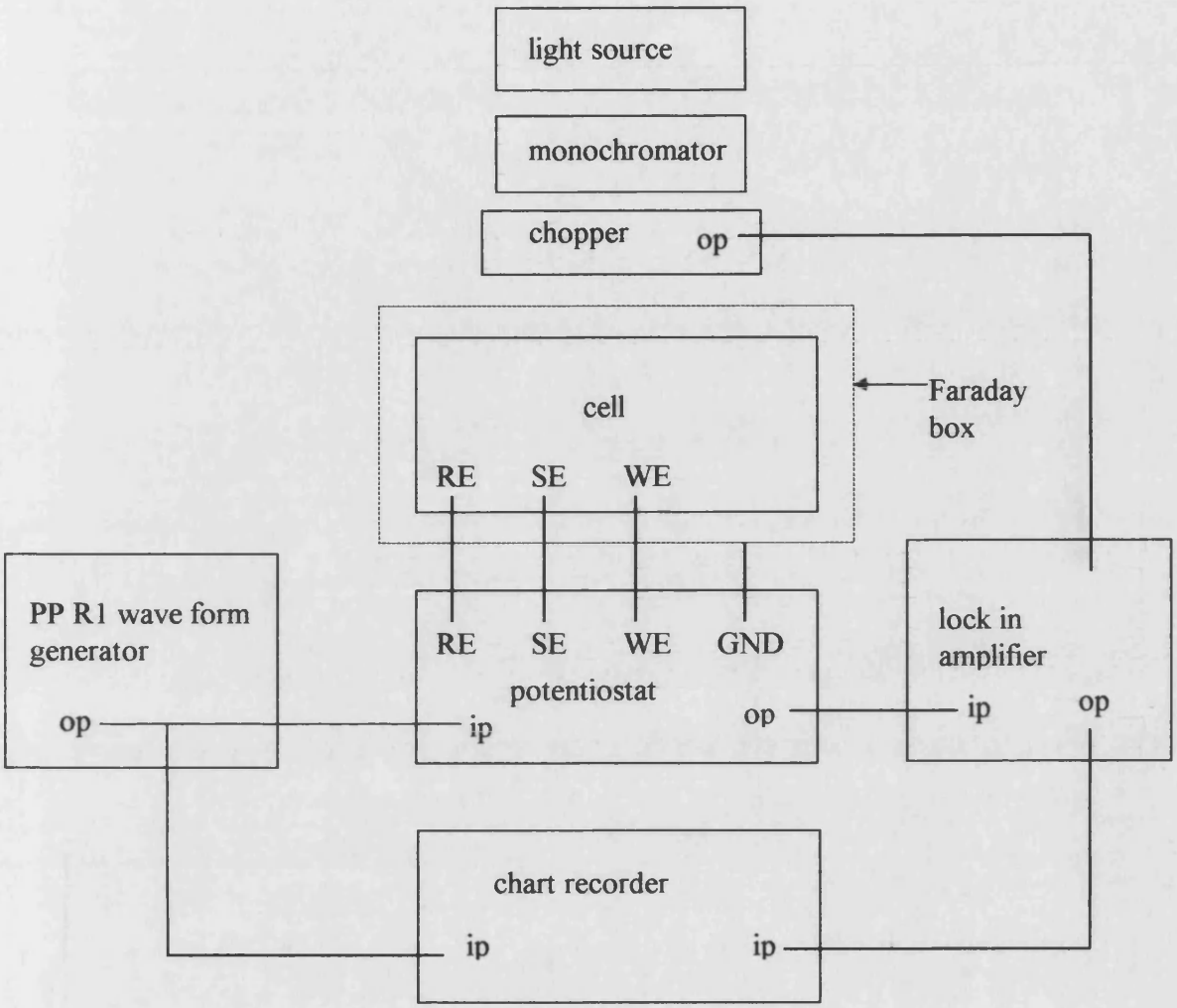

Figure 4.2 *Experimental set-up for Photocurrent Voltage measurements*

A similar set-up to Figure 4.2 was used for two electrode measurements, except that the reference and counter electrodes on the potentiostat were connected together. For experiments using complete dye sensitised cells, no chopper was used because the cell response was very slow. In cases where white light illumination was used this was via a tungsten halogen lamp with no monochromator.

4.1.3 Photocurrent spectroscopy

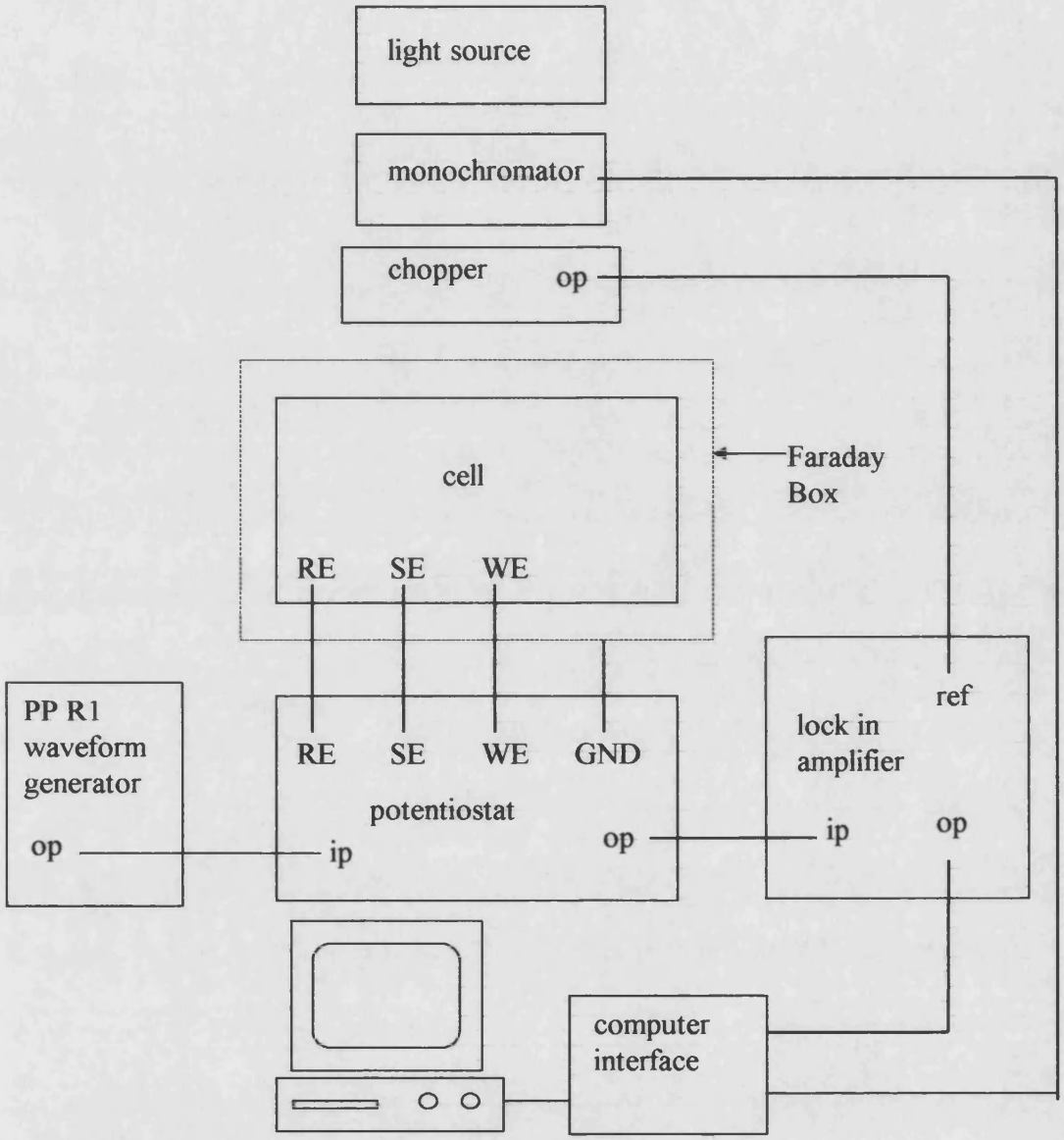

Figure 4.3 *Experimental set-up for photocurrent spectroscopy*

Photocurrent spectroscopy involves measuring the photocurrent of a sample as a function of wavelength. The potential of the sample is held constant and the wavelength of the light is scanned over the range of interest. The monochromator was interfaced to a BBC microcomputer to enable automatic scanning of the wavelength. The output of the lock in

amplifier was connected to the computer to enable data processing. The computer records the photocurrent at each wavelength. The sample was then replaced by a calibrated diode connected to a current amplifier, (the diode conversion efficiency at each wavelength is stored in the computer), and photocurrent of the diode recorded directly without the use of the chopper or lock in amplifier. The photocurrent of the sample was then converted to the conversion efficiency at each wavelength using (4.1), and a spectrum of the monochromatic conversion efficiency was obtained.

For complete dye sensitised thin layer cells, the counter electrode and reference electrode inputs are connected together and the potentiostat operates in the two-electrode mode. For these measurements no chopper or lock in amplifier were used and the photocurrent was recorded via a current amplifier by the computer. The conversion efficiencies were obtained by the use of a calibrated diode as with the three-electrode system.

4.1.4 Impedance measurements

A small-modulated potential is superimposed onto a DC potential by a Solartron 1250 frequency response analyser. This potential is then applied to the sample via a potentiostat or Solartron 1286 electrochemical interface depending on the software used. The real and imaginary components of the impedance are recorded as a function of frequency by the computer controlled Solartron 1250. The programme converts the inputs into impedance by dividing potential by the current, (*i.e.* the input AC potential divided by the output AC current). The software used for these measurements was either the "Z-plot" software with the appropriate apparatus as shown in Figure 4.4 or a conventional potentiostat and a programme written by E.A. Ponomarev and M. Bailes.

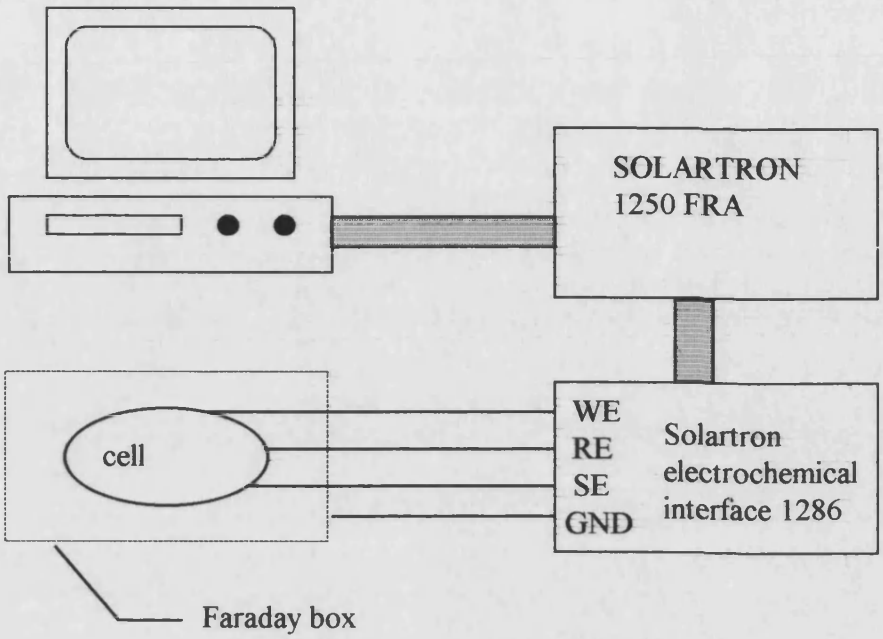

Figure 4.4 *Set-up for electrochemical impedance spectroscopy using the Solartron 1286 and the Z-plot software*

If a two electrode system was used the reference and secondary electrode inputs were connected together. The remainder of the set-up was as described for the three-electrode system.

4.1.5 Photoelectrochemical impedance spectroscopy measurements (PEIS).

The operation of this set-up is similar to the EIS set-up described previously. The only modification is that the sample is illuminated with a constant white light source (tungsten halogen lamp) throughout the duration of the measurement. The impedance measured by this system is the impedance under illumination *i.e.* the photo-electrochemical impedance.

4.1.6 ***Intensity modulated photocurrent spectroscopy (IMPS).***

A small-modulated (sinusoidal) current was applied to an LED by a Solartron 1250 frequency response analyser. This produced a sinusoidal light intensity as a function of time

(AC illumination). White light from a tungsten halogen lamp was used as a constant background illumination (DC illumination). The DC illumination is much greater than the AC illumination. A DC potential is applied to the sample via a potentiostat operating in the two-electrode mode, the real and imaginary components of the photocurrent are recorded as a function of frequency. A computer was used to control the Solartron 1250 and to record the output. The experimental set-up is shown in Figure 4.5.

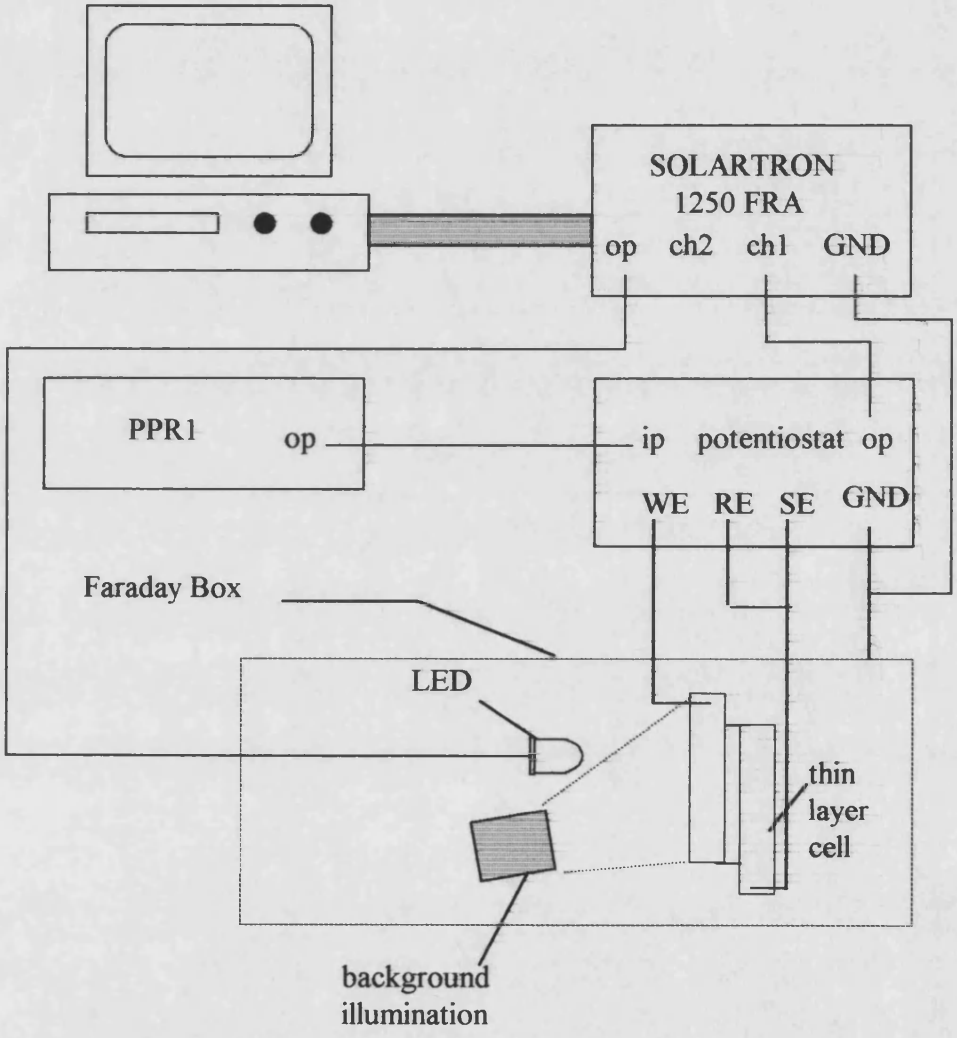

Figure 4.5 *Experimental set-up for IMPS*

4.1.7 Intensity Modulated Photovoltage Measurements (IMVS)

A small-modulated (sinusoidal) current was applied to an LED by a Solartron 1250 frequency response analyser. This produced a sinusoidal light intensity as a function of time (AC illumination). White light from a tungsten halogen lamp was used as a constant background illumination (DC illumination). The working electrode and the counter electrode of the cell under investigation were connected to the inputs of a high impedance differential amplifier (Stanford Research Systems SR 560). The set-up is shown in Figure 4.6. The real and imaginary components of the photovoltage were recorded as a function of frequency. The software used for these measurements was written by E.A. Ponomarev and M. Bailes.

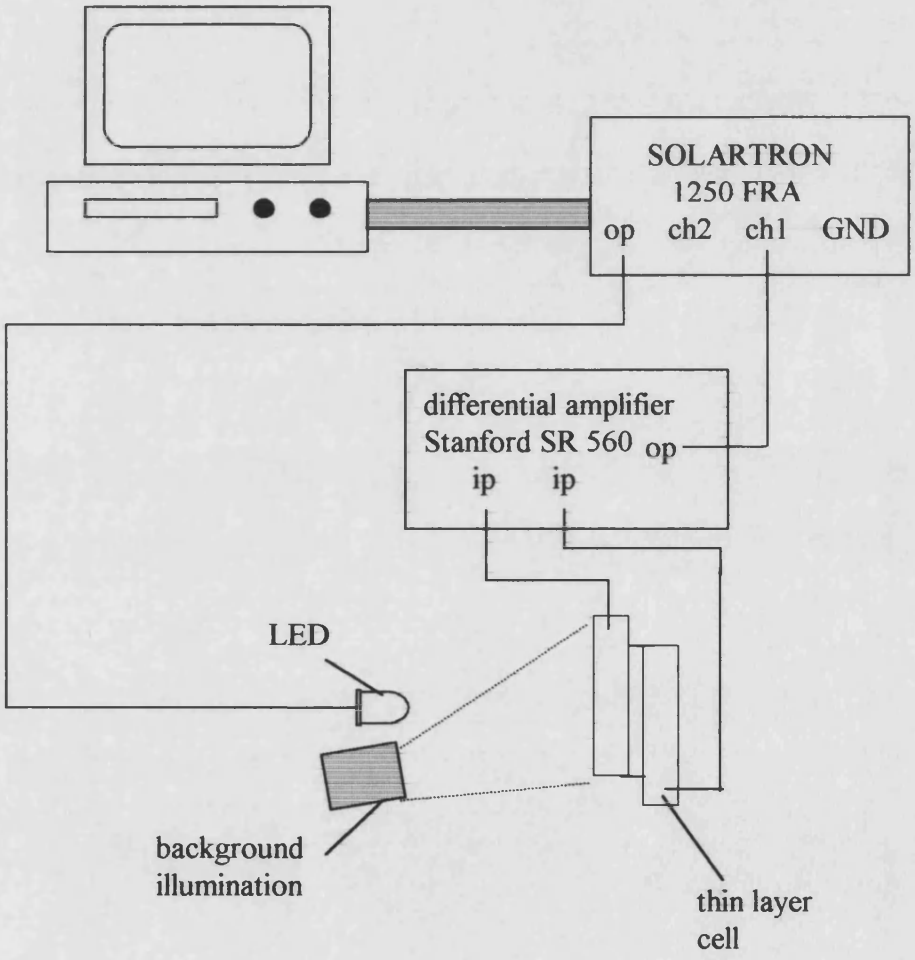

Figure 4.6 *Experimental set-up for IMVS*

4.2 *Experimental details*

4.2.1 Zinc Oxide Crystals

4.2.4.1 ***Electrode preparation***

Zinc oxide crystals were obtained from Professor Heiland (University of Achen). These needle like crystals (approx. 2mm in diameter and 3cm long) were cut perpendicular to the C axis to expose the 0001 and the $000\bar{1}$ faces of zinc and oxygen atoms respectively. These crystals were mounted in 'Kel-F' holders with epoxy cement, the contact was made with gallium-indium eutectic and silver paint. The mounted crystals were then polished with alumina (1 μm) using water as a lubricant before etching in concentrated hydrochloric acid. Electrochemical etching in neutral potassium chloride at reverse bias under UV illumination was subsequently performed.

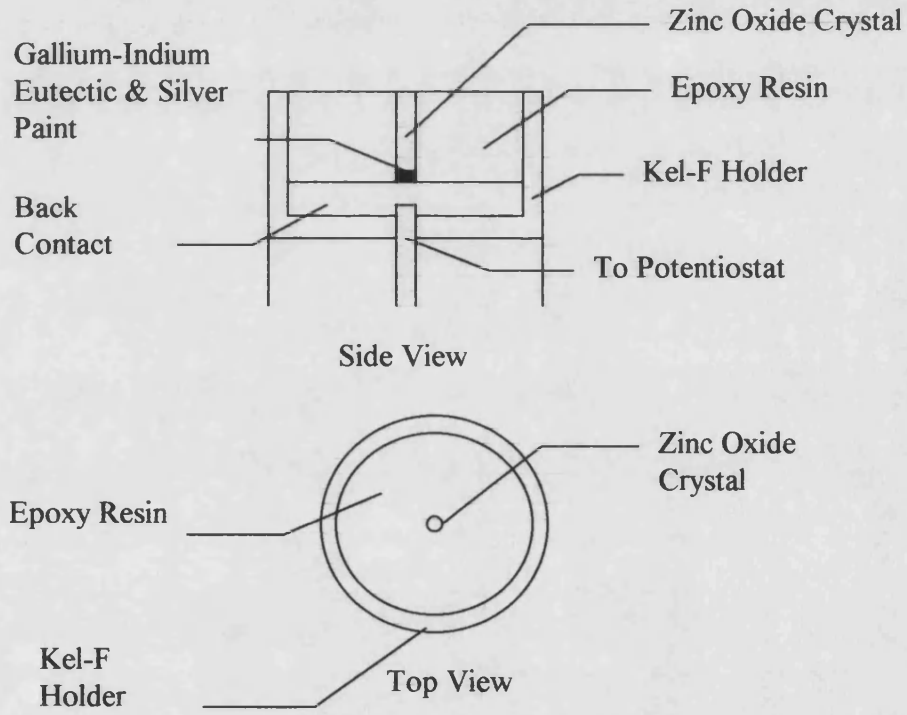

Figure 4.7 *Diagram of mounted zinc oxide crystals.*

4.2.2 Preparation of TiO_2 electrodes

The basis of this method was developed by Grätzel et al [1]. P25 Degussa powder (6g) was ground with 2ml of a mixture of 10% acetyl acetone and water until pale green in colour. The acetyl acetone prevents re-aggregation of the particles. Once the shear forces in the viscous paste dispersed the powder, it was diluted slowly with water (8ml) under continued grinding. A few drops of Triton-X100 (a detergent) was added to facilitate spreading. Scotch clear tape was used to mask off an area of conducting glass and the paste was spread using a glass rod. Once the paste was dry, the tape was removed, and the electrode was fired for 30 minutes in air at 450°.

4.2.3 Synthesis of $RuL_2Cl_2.2H_2O$

This was prepared following the method recorded by Liska et al [2]. $RuCl_3$ (60mg, Aldrich) and 2,2'-bipyridine-4,4'-dicarboxylic acid (113mg, Aldrich) were refluxed in DMF (20ml) for six hours. Argon was continually bubbled through the reaction mixture. Once cool, the resulting solution was filtered to remove any traces of RuL_3 (where L=2,2'-bipyridine-4,4'-dicarboxylic acid). The majority of the DMF was removed using a rotary evaporator. Acetone was added and the reaction mixture was placed on ice. A deep red/burgundy precipitate formed. The precipitate was vacuum filtered and the dye crystals collected. Elemental analysis was carried out and the UV visible spectrum of the dye in ethanol was obtained.

Elemental analysis

	C	H	N
Calculated %	41.379	2.873	8.045
Actual %	39.4	4.20	9.31

UV/Visible Absorbency Spectrum

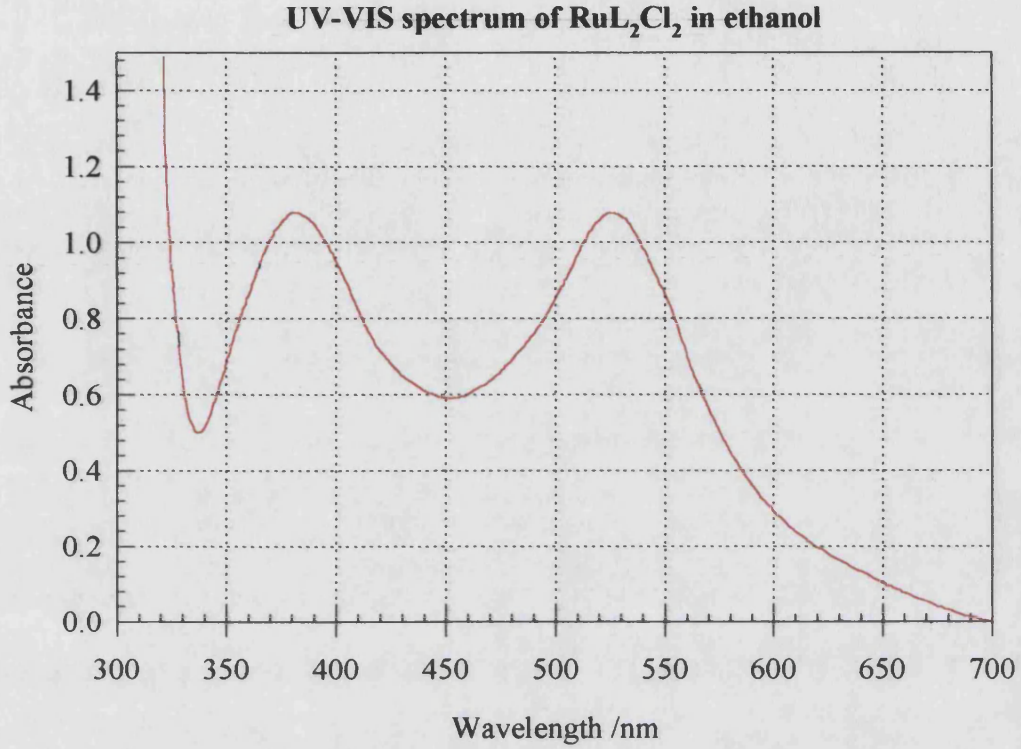

Figure 4.8 *The UV visible absorbency spectrum of 9×10^{-6}M solution of $RuL_2Cl_2.2H_2O$ in ethanol. Recorded in a 1cm cell.*

	Peak 1	Peak 2	Peak 3
Wavelength of peak (literature) /nm [1]	534	385	309
Wavelength of actual peak /nm	530	582	309

The elemental analysis results indicate that it is very probable that solvent molecules are present. DMF would increase substantially the percentage of H and to a smaller extent the percentage of N present. The percentage of C would remain about the same. Despite this, the percentage of C would seem to indicate that the di-substituted complex has been formed rather that the mono or tri substituted complex. The absorbency spectrum shows good

agreement with the published data [1], which indicates that the desired complex has been formed and the elemental analysis result is not as expected only due to the presence of solvent molecules. The first peak in the absorbency spectrum does appear to be slightly blue shifted, although this could be because the peak is quite broad.

4.2.4 Preparation of platinum mirror counter electrode

The vacuum sputtering system was set-up to sputter platinum by inserting the platinum disc into the correct area. A clean degreased piece of fluorine doped 8-10Ωcm^{-2} tin oxide glass (previously cut to the required size for the cell) was placed, tin oxide side up, in the sample area of the sputtering machine and the lid closed securely. The air was removed from the sample area and the system was flushed with argon twice. The argon was pumped out until the required vacuum was obtained. The sputtering mechanism was then allowed to operate for the required length of time. Care was taken not to contaminate the surface of the electrode.

4.2.5 Preparation of transparent platinum counter electrode

Hexachloroplatinic acid was dissolved in isopropanol yielding a 5 mmol dm^{-3} solution. A small amount (5µl cm^{-2}) of this solution was placed onto a clean, degreased piece of conducting tin oxide glass. The solution was spread over the surface and left to dry protected from contamination under a watch glass. Once dry the electrode was fired at 400°C for 30 minutes.

4.2.6 Fabrication of the dye sensitised nanocrystalline TiO_2 cell

The cell was prepared following procedures similar to those used in the fabrication of the INAP cells. (Details of the INAP cells can be found in section 4.2.8). The cell consists of 2 electrodes, a dye-sensitised electrode and a platinum electrode. The platinum electrode has two holes drilled in opposite corners as shown in Figure 4.9 . Pieces of 'surlyn™' (Dupont, a thin polymer film) are cut to the required size and placed around the working electrode area, on the conducting tin oxide glass. The platinum-coated electrode was then placed over

the dye-sensitised electrode, slightly offset to allow for contacts to be made to each electrode. The electrodes were clamped together and heat was applied via a soldering iron, to the glass to melt the surlyn™ and bond the electrodes together. The cell was left clamped until the surlyn™ had set. The cell was filled with electrolyte via the holes in the platinum electrode. The holes were sealed with microscope cover slips bonded to the electrodes with surlyn™. Sealing wax was applied to the bonded edges and over the cover slips to aid sealing

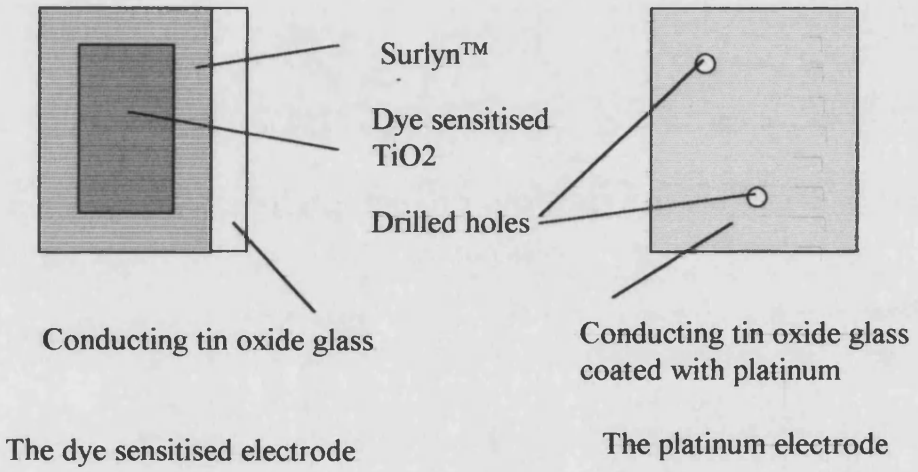

Figure 4.9 *The electrodes that form the completed dye sensitised cell.*

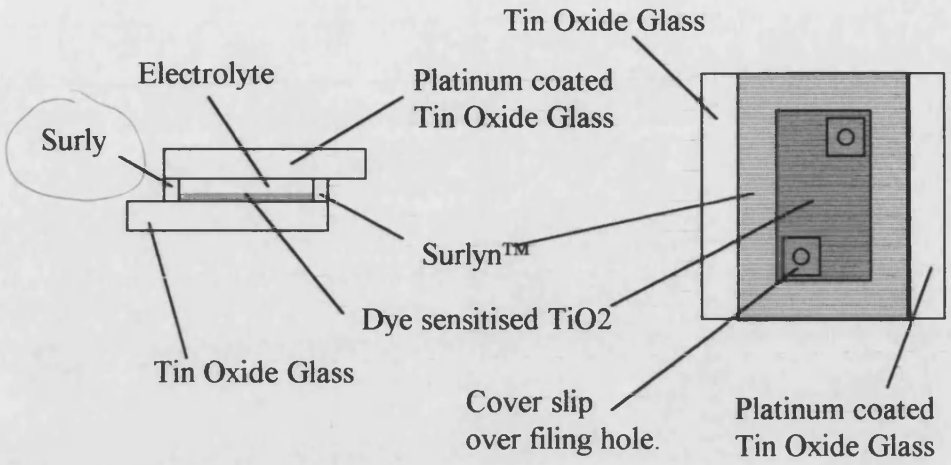

Figure 4.10 *The completed cell*

4.2.7 Cell details.

As the dye N3 was not available at the time of initial studies, the dye used for the cell was $RuL_2Cl_2.2H_2O$ (where L=2,2'-bipyridine-4,4'-dicarboxylicacid). This was chosen as it exhibits sensitisation on nanocrystalline TiO_2 and can be easily prepared. It has the disadvantage that it does not give efficiencies as high as dyes used currently by Grätzel and co-workers. This was prepared as described above. The TiO_2 film was placed into a 1×10^{-3} mol dm^{-3} ethanolic solution of $RuL_2Cl_2.2H_2O$ and left for 48 hours. On removing, the film was deep burgundy in colour. The film was dried and a thin layer cell constructed (as detailed above) using a sputtered platinum counter electrode. The electrolyte used consisted of 0.5M lithium iodide, 40mm iodine, and 0.1M tertbutyl pyridine in dry acetonitrile.

4.2.8 INAP cell details

These optimised cells were prepared at the Institut für Angewandte Photovoltaik (INAP). The nanocrystalline layer was prepared from a colloidal TiO_2 dispersion obtained by hydrolysis of titanium isopropoxide. The preparation method of O'Regan and Gratzel [3] was modified to give only the anatase modification. Screen printable pastes were obtained by drying the colloidal dispersions and grinding the powder with pine oil. The resulting paste was screen printed onto conducting tin oxide glass (TEC 8, fluorine doped SnO_2 on 3mm float glass purchased from Libby Owens Ford) and fired at 450°C yielding TiO_2 films between 5 and 15 μm. The nanocrystalline films were dipped into a 3×10^{-4} mol dm^{-3} ethanolic solution of cis-di(thiocyanato)-N,N'-bis(2,2'-dicarboxylate)ruthenium(II) for 2 hours. The counter electrode was either sputtered platinum (150nm) or a thermally deposited transparent layer of platinum (preparation is described above). A thin layer cell was prepared as described in section 4.2.6, however transparent polyethylene (PE) hot melt replaced the 'surlyn™' and sealing wax. The electrolyte used was composed of methylhexylimidazolium iodide (MHImI) prepared according to the method given by Papageorgiou et al [4], iodine (Fluka), 4-tert-butyl pyridine and acetonitrile (Fluka and distilled under nitrogen before use).

4.3 References

1. Nazeeruddin, M. K.; Kay, A.; Rodicio, I.; Humphry-Baker, R.; Müller, E.; Liska, P.; Vlachopoulos, N.; Grätzel, M. *J. Am. Chem. Soc.* **1993**, *115*, 6382.

2. Liska, P.; Vlachopoulos, N.; Nazeeruddin, M. K.; Comte, P.; Grätzel, M. *J. Am. Chem. Soc.* **1988**, *110*, 3686

3. O'Regan, B.; Grätzel, M. *Nature* **1991**, *353*, 737

4. Papageorgiu, N.; Athanassov, Y.; Armand, M,; Bonhote, P.; Petterson, H.; Azam, A.; Grätzel, M. *J. Am. Chem. Soc.* **1993**, *143*, 3099

Chapter 5

Steady state photo-electrochemistry

Index

Chapter 5 Steady state photo-electrochemistry

5.1 Preliminary studies and steady state measurements

This chapter aims to serve firstly as an introduction to sensitisation and secondly to present steady state measurements on thin layer dye sensitised TiO_2 cells. Sensitisation is illustrated with results from a model system, zinc-oxide single crystal sensitised with a Rhodamine dye. It was found that the sensitisation efficiency was limited by monolayer dye coverage. The use of a thin film of semiconductor oxide particles increases the surface area and hence the efficiency. The characterisation and performance of a dye sensitised TiO_2 thin layer cell, constructed in our laboratory, is presented and compared to that of an optimised (INAP) cell. The effects of the addition of t-butyl pyridine to the electrolyte of the optimised thin layer cell discussed in the final part of the chapter.

5.2 Measurements on Zinc Oxide – A model system

Mott-Schottky plots of the zinc oxide single crystal used for sensitisation experiments are shown in Figure 5.1. They were used to calculate the doping density and the flat band potential of the crystal.

Rhodamine 6G (Rh6G) was used to sensitise the zinc oxide. It was chosen as it is similar in structure to rhodamine B which was used in early sensitisation work in the late sixties and early seventies [1,2,3,4,5]. More recently rhodamine 6G was noted to sensitise porous silicon [6]. The absorbance spectrum for rhodamine 6G in methanol is shown in Figure 5.2. Photocurrent spectra zinc oxide sensitised with several concentrations of rhodamine 6G is shown in Figure 5.3.

Mott-Schottky plots of zinc oxide single crystal (zinc face).
0.5M sodium sulfate after photoetching.

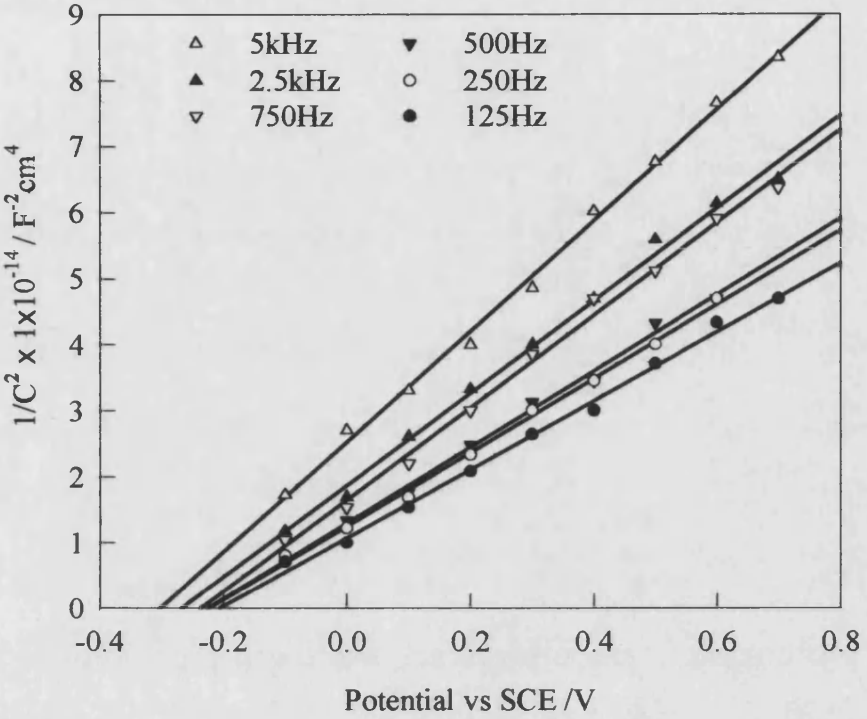

Figure 5.1 *Mott-Schottky plots of zinc oxide single crystal in 0.5 mol dm^{-3} sodium sulfite after photoetching at reverse bias.*

The doping density of the zinc oxide single crystal is calculated from the Mott-Shottky equation:

$$C_{sc}^{-2} = \left(\frac{2}{qN_{sc}\kappa\varepsilon_o A^2}\right)\left(V_m - V_{fb} - \frac{kT}{q}\right) \qquad (5.1)$$

Where:- q = electronic charge

N_{sc} = donor density in cm^{-3}

ε_o = permeativity of free space

V_m = applied DC potential versus the reference electrode

V_{fb} = flatband potential

A^2 = electrode area

k_B = boltzmann constant

κ = relative permiativity of semiconductor

Doping density and flat band potential at each frequency are given in the table below.

Frequency /Hz	Flat band potential /V	Doping density $\times 10^{-16}$ /cm^2
125	-0.20	3.06
250	-0.20	2.66
500	-0.25	2.79
750	-0.25	2.25
2500	-0.28	2.24
5000	-0.30	1.87

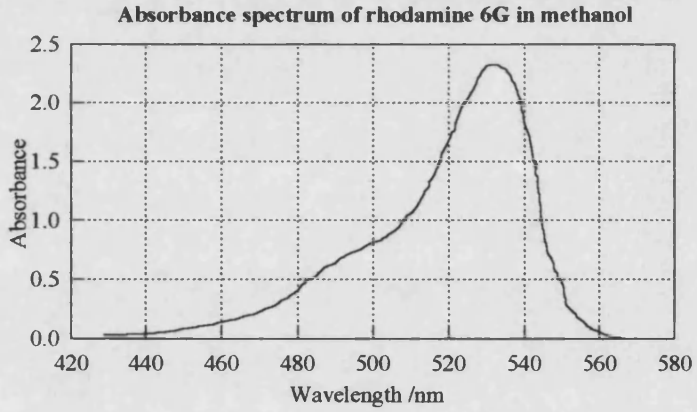

Figure 5.2 *Absorbency spectrum of a 2×10^{-5} mol dm^{-3} solution of rhodamine 6G in methanol. Measured using a Perkin Elmer 330 double beam infra red spectrophotometer.*

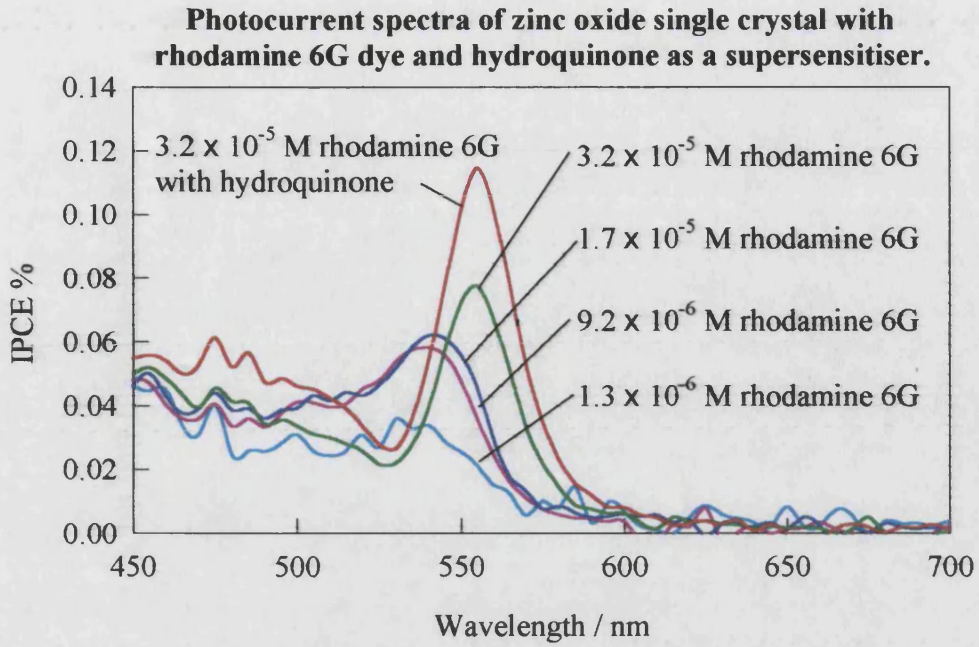

Figure 5.3 *Photocurrent spectra of zinc oxide single crystal sensitised with solutions of rhodamine 6G. Hydroquinnone was added to effect supersensitisation. 1 M KCl was used as background electrolyte in all cases. Spectra were recorded at no applied potential. The SCE was used as a reference electrode.*

Discussion

The Mott-Shottky plots of the zinc oxide single crystal are included to show the characteristics of the single crystal used in the sensitisation experiments. The linearity of the plots shows that the surface of the crystal does not have many defects. The plots show some frequency dependence especially at the higher frequencies, despite this, values of the doping density and flatband potential could still be obtained. The doping density is of the order $2\text{-}3\times10^{16}cm^{-2}$ and the flat band potential lies between –0.2 V and –0.25 V. These values are within the same region as those measured by Li [7].

The absorption spectrum Figure 5.2 shows that the maximum absorbency occurs between 520 and 540nm, this is in the visible region of the electromagnetic spectrum and is therefore useful for solar energy conversion.

The Rh6G solution sensitised the zinc oxide, however the efficiency was very low. This was primarily due to the smooth zinc oxide surface (low surface area) and monolayer

coverage of dye. Multi-layer coverage would not increase the efficiency as the system works because the dye molecule is close contact with the zinc oxide so that electrons can transfer across the interface. The mechanism for sensitisation can be described as follows:

Step 1: Rh6G molecules diffuse to the surface of the zinc oxide.
Step 2: Rh6G molecules adsorb onto the surface of the zinc oxide
Step 3: Light excites an electron from the HOMO of the Rh6G into the LUMO.
Step 4: The electron from the LUMO of the dye is injected into the CB of the Zinc oxide.
Step 5: The electron is collected in the external circuit as photocurrent.
Step 6: The dye desorbs and diffuses to the counter electrode to be regenerated.
Step 7: A Rh6G dye molecule adsorbs onto the zinc oxide in place of the one that has desorbed.

This mechanism is heavily reliant on Rh6G molecules adsorbing and desorbing, this will reduce the maximum efficiency as no electrons will be injected whilst the adsorption/desorption process is taking place. In order to remove this factor a supersensitiser can be added to the solution. The supersensitiser acts as a source of electrons in solution for the Rh6G, which will no longer have to desorb to be re generated. This will increase the photocurrent. A simplified mechanism for this process is as follows:

Step 1: Rh6G molecules diffuse to the surface of the zinc oxide.
Step 2: Rh6G molecules adsorb onto the surface of the zinc oxide
Step 3: Light excites an electron from the HOMO of the Rh6G into the LUMO.
Step 4: The electron from the LUMO of the dye is injected into the CB of the Zinc oxide.
Step 5: The electron is collected in the external circuit as a photocurrent.
Step 6: An electron from the supersensitiser is injected into the HOMO of the Rh6G. This regenerates the dye and the process from step 3 begins again.
Step7: The oxidised supersensitiser diffuses to the counter electrode.

This mechanism is simplified, it is possible that once the electron from the Rh6G is promoted the electron from the supersensitiser is injected into the dye before the electron from the Rh6G is injected into the zinc oxide. Also the supersensitiser may interact with the Rh6G forming a complex, similar to a charge transfer complex. If this is the case steps regarding the association and dissociation of the supersensitiser and the Rh6G need to be included.

A shift in the sensitisation peak from 525nm to 550nm is evident as the dye concentration increases. This is due to dye in solution that is not adsorbed on to the zinc oxide adsorbing the light before it reaches the adsorbed Rh6G. At low concentrations there are only a few un-adsorbed molecules, but as the concentration increases more molecules are free in solution. If the solution molecules are sufficient in number to absorb a large amount of the light at a particular wavelength, (*i.e.* wavelength 1 in Figure 5.4), then the molecules adsorbed on the zinc oxide will have much less light to adsorb at wavelength 1, thus a reduction of the photocurrent will be seen at wavelength 1. This will have the appearance to 'shifting' the absorption peak (Figure 5.4). Care was taken with these measurements so that the zinc oxide crystal was very close to the cell wall so that the path length of the light was very small.

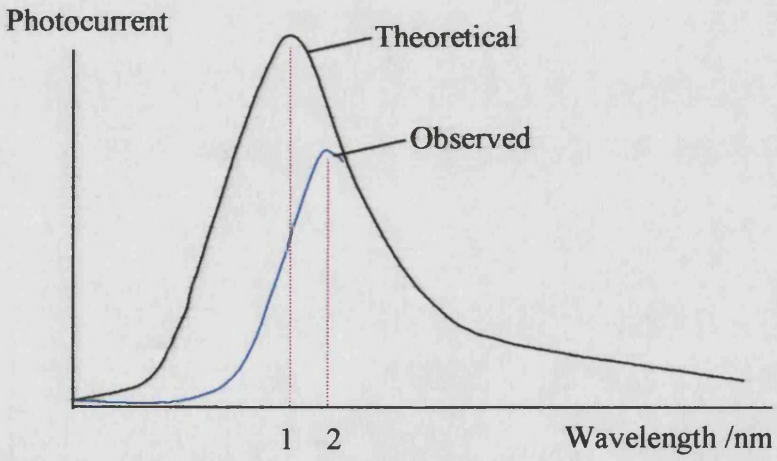

Figure 5.4 *Diagram to show how the peak of the photocurrrent shifts when dye in solution absorbs incident light.*

5.3 Thin Layer cell characteristics

5.3.1 Cell constructed in the laboratory in Bath

Cell NJS1 was used for all measurements in this section. The cell was prepared as described in chapter 4 section 4.2.5. The photocurrent spectrum can be seen in Figure 5.5 and the photocurrent voltage curve in Figure 5.6. Both the photocurrent spectrum and the photocurrent voltage curve were recorded in the two electrode configuration.

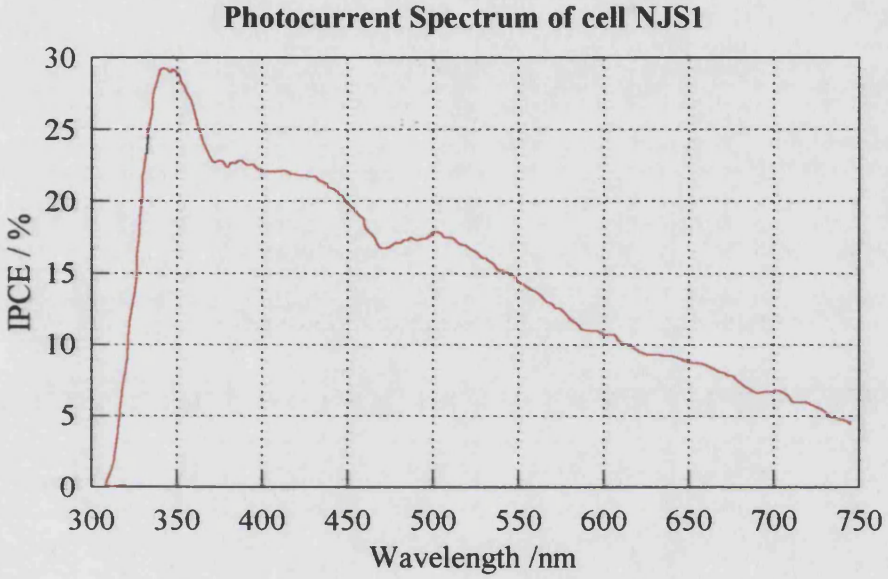

Figure 5.5 *Photocurrent spectrum of cell NJS1. Recorded in the 2-electrode configuration with no chopping at 0V.*

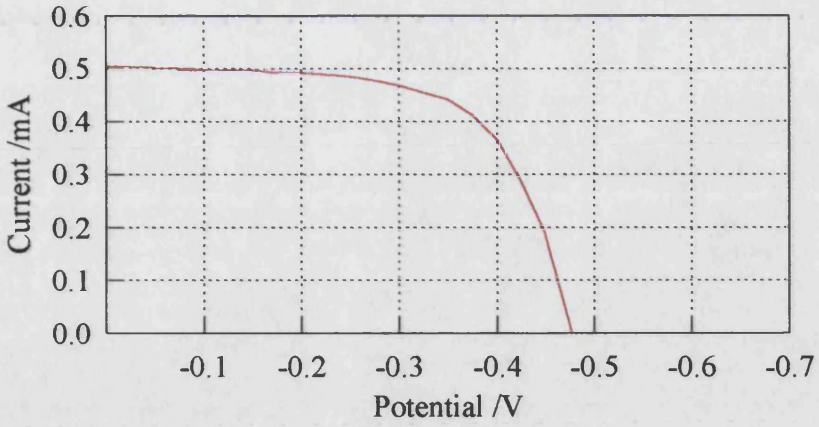

Figure 5.6 *Photocurrent voltage curve of cell NJS 1. Recorded with no chopping in the 2-electrode configuration, illuminated with white light from a tungsten halogen bulb at an intensity equivalent to 0.5mA.*

5.3.3 Optimised cells (INAP cells)

The Photocurrent characteristics for a typical INAP cell can be seen in Figure 5.7 and Figure 5.8.

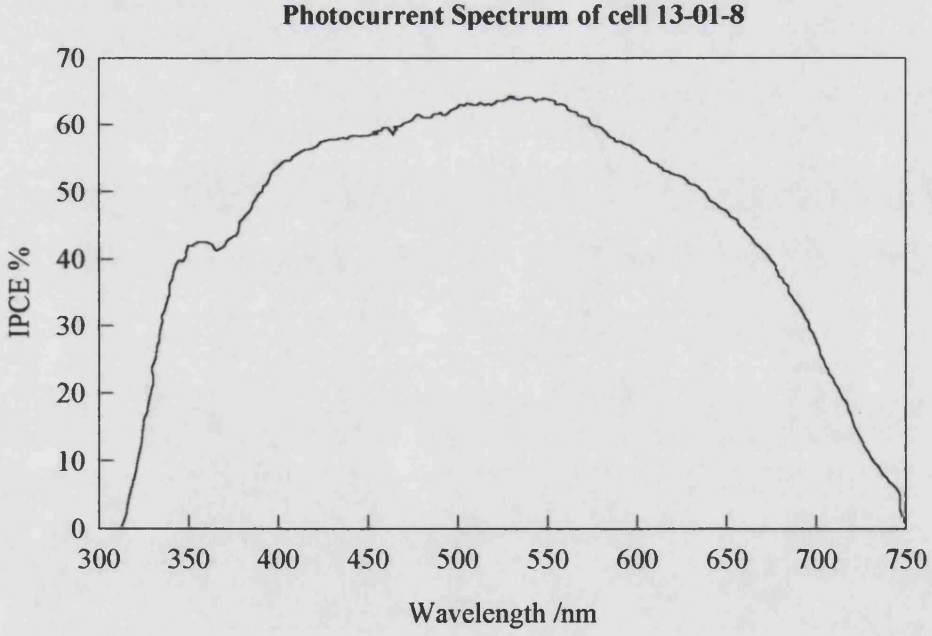

Figure 5.7 *Photocurrent spectrum of cell 13-01-8. Recorded in the 2-electrode mode with no chopping at 0V.*

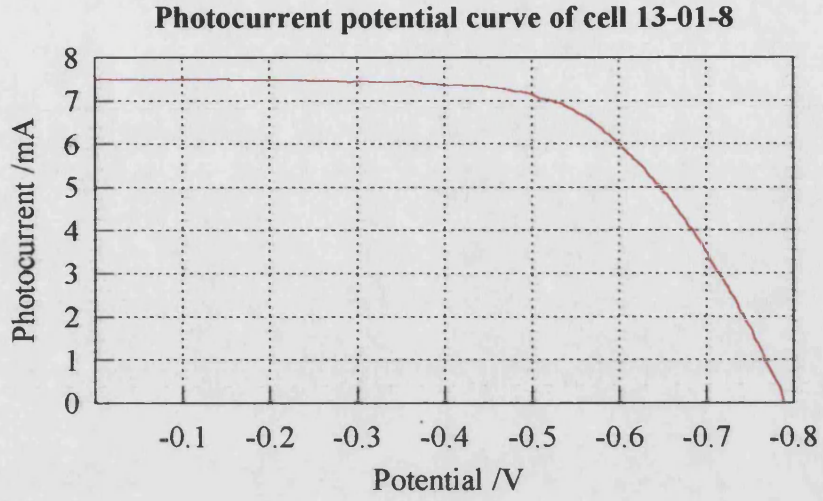

Figure 5.8 *Photocurrent voltage curve of cell 13-01-8. Recorded with no chopping in the 2-electrode mode, illuminated with white light from a tungsten halogen bulb at an intensity equivalent to 7mA.*

Discussion

The photocurrent spectrum of cell NJS 1 exhibits 3 broad overlapping peaks. The peak at 350nm is photocurrent caused by UV illumination as the band gap of TiO_2 is in this region. The broad peaks at 425 nm and 500 nm are photocurrent, produced as a result of the dye adsorbing the light and injecting electrons into the TiO_2. The spectrum above 400 nm is similar in shape to the absorbance spectrum (see chapter 4 figure 4.8) of the sensitising dye used to construct the cell, however the peaks are noted to be broader and shifted slightly to a higher wavelength. The spectrum tails off after 550 nm. The maximum IPCE of the cell in the region of the sensitisation is 23%. The photocurrent voltage curve of the cell at a short circuit current of 0.5mA gives an open circuit voltage of –0.475V.

It must be realised that if any part or system within the cell does not function well the IPCE will be effected dramatically. For example if the dye does not sensitise well, no matter how good the film, electrolyte and cell construction a low efficiency will always result. If all the systems have a low efficiency, the effect of this on the total cell efficiency will be dramatic. For example take a cell constructed of a dye, a film and a collection contact. Say the efficiency of the dye to inject excited electrons into the conduction band of the TiO_2 is 50%, the film transports 50% of injected electrons to the

back contact and that the back contact only collects 50% of the electrons that are transported to the back contact. This will mean that of, say 100 electrons that are initially excited, 50 will reach the CB of the TiO_2, 25 will then reach the back contact and only 12.5 will be collected. It is possible to see that from this simple calculation, if each system operated with 50 % efficiency only 12.5% of the initial electrons that were excited would actually be collected in the external circuit. This calculation only takes into account four systems and does not take into account light that is not absorbed by the dye or regeneration of dye. By following the same logic, it is possible to see that if any one of the systems was 10% efficient, and all others were 100% efficient the cell would only be 10% efficient.

As stated earlier the maximum IPCE obtained for cell NJS1 was 23% there are several reasons why the efficiency is lower than cells prepared by Grätzel's group or by the INAP. Firstly the dye used in cell NJS1 was not the same dye as that used in the Grätzel or INAP cells, the dye used in cell NJS1 was $RuL_2Cl_2.2H_2O$ where $L=C_{10}H_6N_2(COOH)_2$, the cells manufactured by INAP and Grätzel use cis-di(thiocyanato)-N,N-bis(2,2'-dicarboxylate)ruthenium(II). This dye contains 2 SCN groups as ligands, which are thought to assist with the electron injection into the TiO_2. At the time of making cell NJS1 this dye was not commercially available and took several difficult steps to synthesise, for this reason, it was decided to use $RuL_2Cl_2.2H_2O$ which is easier to synthesise but not as efficient at injecting electrons into TiO_2. Secondly the TiO_2 film was made using Degussa P25 powder, this has been used in some early research by Grätzel and co workers but, more recently the hydrolysis of titanium isopropoxide has become more popular. Thirdly the electrolyte contained lithium iodide as the source of iodide ions, the INAP cells contained methylhexylimidazolium iodide. Lithium was used as it was readily available methylhexylimidazolium iodide must be synthesised. The lithium may have made a difference to the performance of the cell however it is unlikely that the difference would be large, as it is the iodide that is involved in the dye regeneration mechanism not the counter ion. Finally sealing of the cell was also a problem, as the electrolyte would react with most epoxy based glues. Surlyn™ was used however leakage was still a problem and sealing wax was applied to prevent leakage. This method of sealing was fine for short periods of time (a few days) however; over longer periods of time (weeks) the cell

leaked. The open circuit voltage of the cell at an intensity equivalent to i_{sc} of 0.5mA was -0.475V, the INAP cell at the same intensity had an open circuit voltage of –0.530V. Cell NJS 1 has a smaller open circuit voltage than the INAP cell however, this is most probably due to the differences in the cell composition.

The INAP cell gives a broad shape, which is due to the absorption spectrum of the dye used. The response of the INAP cell extends to much longer wavelengths because of the absorption spectrum of the dye used. The IPCE is 60% in the sensitisation region and has an open circuit voltage of –0.530V at an intensity equivalent to i_{sc} of 0.5mA. The high IPCE indicates that all the systems within the cell work efficiently. The use of the dye cis-di(thiocyanato)-N,N-bis(2,2'-dicarboxylate)ruthenium(II), that is now commercially available, (Solaronix SA, Switzerland) and the TiO_2 film preparation that involves screen-printing techniques. Cell sealing involved the use of polyethylene hot melt which, in general, works well over long periods of time (a year). The open circuit voltage at an intensity equivalent to 0.5mA is –0.53V this increases as the light intensity increases (at an intensity of 7 mA, V_{oc} = -0.79V).

5.4 Effect of t-butyl pyridine on the open circuit voltage.

The study of the effect of the addition of t-butyl pyridine was carried out on INAP cells. The photocurrent wavelength spectra are shown in Figure 5.9. It should be noted that the IPCE is similar for each cell and that as expected the shape of the spectra are very similar. Photocurrent voltage curves for each of the cells in Figure 5.9 are shown in Figure 5.10.

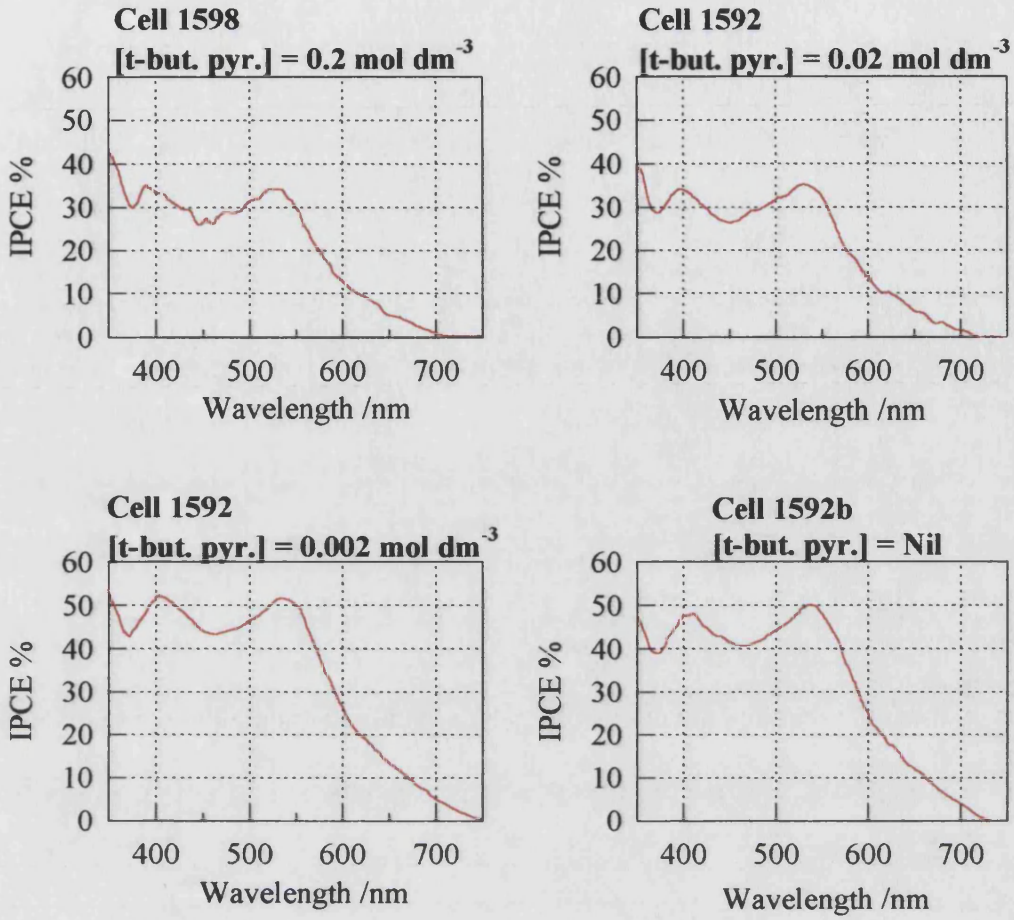

Figure 5.9 *Photocurrent spectra of 4 cells (cells 1598, 1592, 1602, 1592b), each with a different concentration of t-butyl pyridine. Spectra were recorded at short circuit with illumination from a tungsten halogen lamp.*

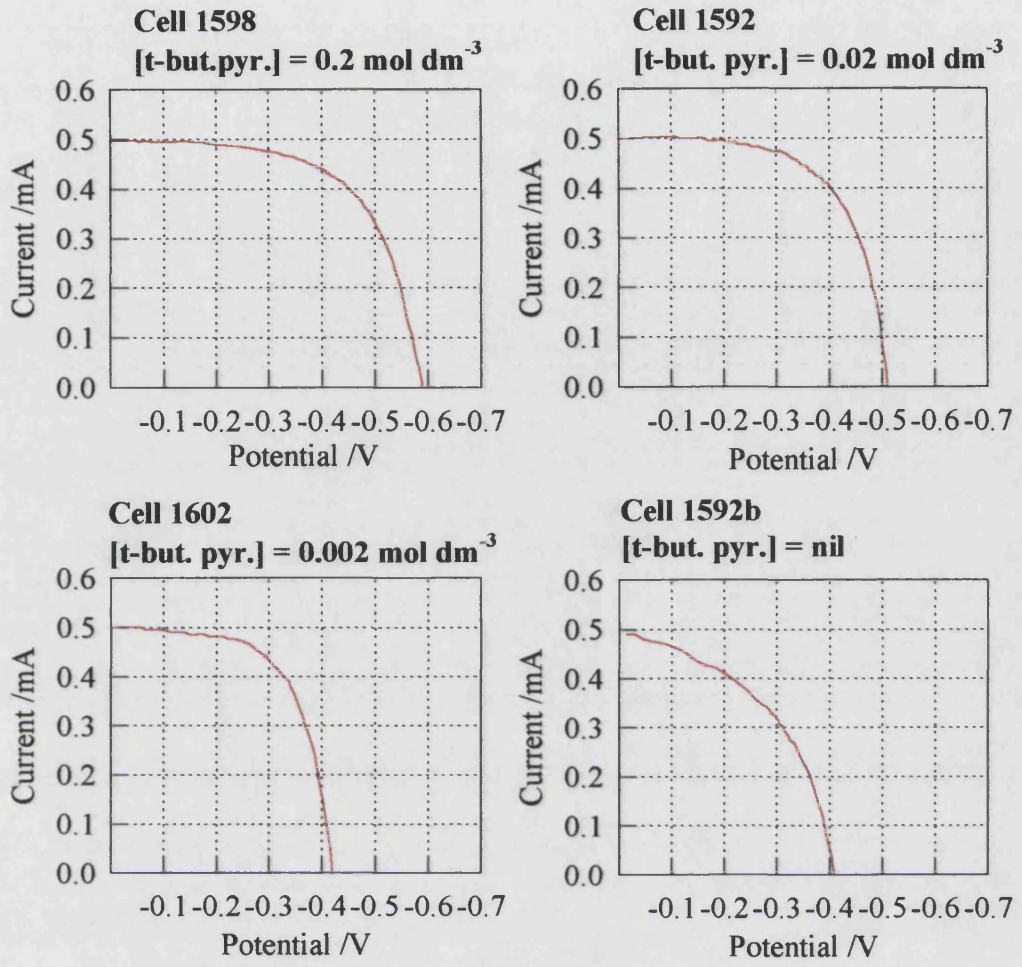

Figure 5.10 *The photocurrent voltage curves of 4 cells (1598, 1592, 1602, 1592b) each with a different concentration of t-butyl pyridine.* I_{sc} *was set to 0.5mA in each case and white light illumination was from a tungsten halogen lamp.*

The table below shows the concentration of t-butyl pyridine, V_{oc} at 3 intensities for each cell used in the experiments. A semi-logarithmic plot of the concentration as a function of the open circuit voltage is displayed in Figure 5.11.

Cell Number	[t-butyl pyridine]	Intensity	V_{oc}	Intensity	V_{oc}	Intensity	V_{oc}
1598	0.2	5mA	-0.685	2.5mA	-0.660	0.5mA	-0.590
1592	0.02	5mA	-0.615	2.5mA	-0.585	0.5mA	-0.513
1602	0.002	5mA	-0.525	2.5mA	-0.495	0.5mA	-0.420
1592b	none	5mA	-0.535	2.5mA	-0.495	0.5mA	-0.410

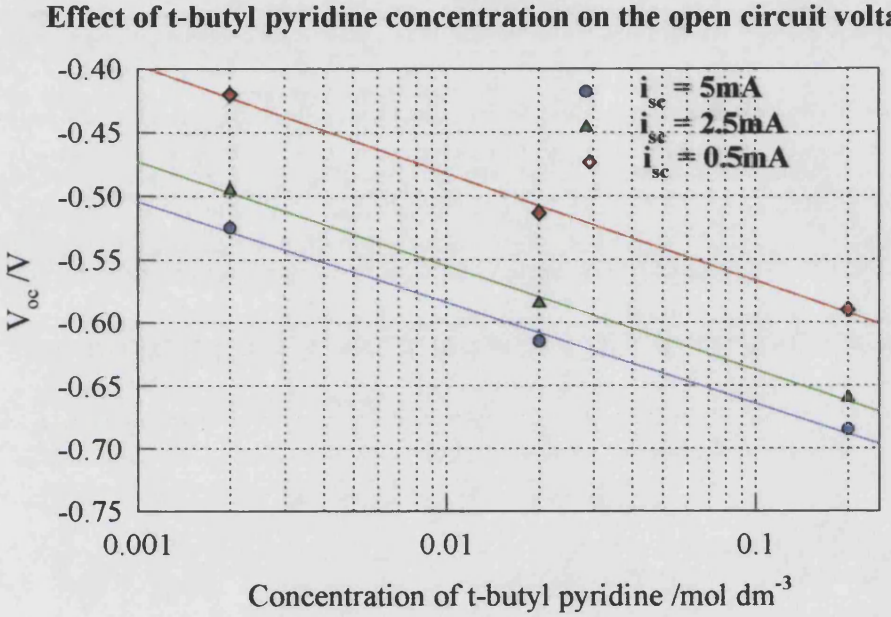

Figure 5.11 *Plot of the effect of t-butyl pyridine on V_{oc} at 3 intensities. (Cells 1598, 1592, 1592b and 1602). White light illumination was from a tungsten halogen lamp.*

Discussion and conclusions

It is noted that as the t-butyl pyridine concentration increases, the open circuit voltage increases. A semi-logarithmic plot of the t-butyl pyridine concentration versus open circuit voltage shows a linear relationship. The gradient of the plot is noted to increase very slightly as the intensity decreases. Only a limited number of cells were available with different concentrations of the t-butyl pyridine and as such the plot has only a few points. It is noted that the shape of the i-v curve is much less 'square' (*i.e.* it will have a much smaller fill factor) when there is no t-butyl pyridine present in the cell.

The open circuit voltage increases with the addition of t-butyl pyridine, this is thought to be because the t-butyl pyridine adsorbs onto vacant sites on the TiO_2 surface. This could block any back reaction of injected electrons with the dye or the electrolyte. These cells were also studied using IMPS measurements however there was no effect on the IMPS response.

5.5 References

1. Gerischer, H.; Tributsch, H. *Ber. Bunsenges. Phys. Chem.* **1968**, *72*, 436

2. Tributsch, H.; Gerischer, H. *Ber. Bunsenges. Phys. Chem.* **1969**, *73*, 251

3. Tributsch, H.; Gerischer, H. *Ber. Bunsenges. Phys. Chem.* **1969**, *73*, 850

4. Pettinger, B.; Schöppel, H.-R.; Gerischer, H. *Ber. Bunsenges. Phys. Chem.* **1973**, *77*, 960

5. Pettinger, B.; Schöppel, H.-R.; Gerischer, H. *Ber. Bunsenges. Phys. Chem.* **1974**, *78*, 450

6. Canham L. T. *Appl. Phys. Lett.* **1993**, *63*, 337

7. Li, J.; PhD Thesis, The University of Southampton, 1984

Chapter 6

Impedance spectroscopy

Index

Chapter 6 Impedance spectroscopy

This chapter presents results obtained for a three-electrode system to characterise three counter electrode materials (tin oxide glass, heat deposited platinum and sputtered platinum). The results show evidence to suggest that sputtered platinum would be the best counter electrode for a dye sensitised solar cell. This chapter also presents impedance results for a complete dye sensitised solar cell. Impedance results were fitted using an equivalent circuit and resistance and capacitance values for the platinum counter electrode and the TiO_2 electrode were calculated at several intensities and potentials.

6.1 *Impedance spectroscopy using the 3 electrode system*

Electrochemical impedance spectroscopy measurements have been made on three counter electrode materials: tin oxide glass, tin oxide glass with a layer of deposited platinum and tin oxide glass with a layer of sputtered platinum. The measurements were fitted to an RC parallel circuit which enabled the exchange current density of the electrolyte to be calculated for each material. The materials were compared for the suitability of the material as an electrode in a dye sensitised cell. The results are displayed as a complex plane plot of the real and imaginary impedance of the system.

6.1.1 Impedance results for the 3 electrode system

Tin oxide glass alone

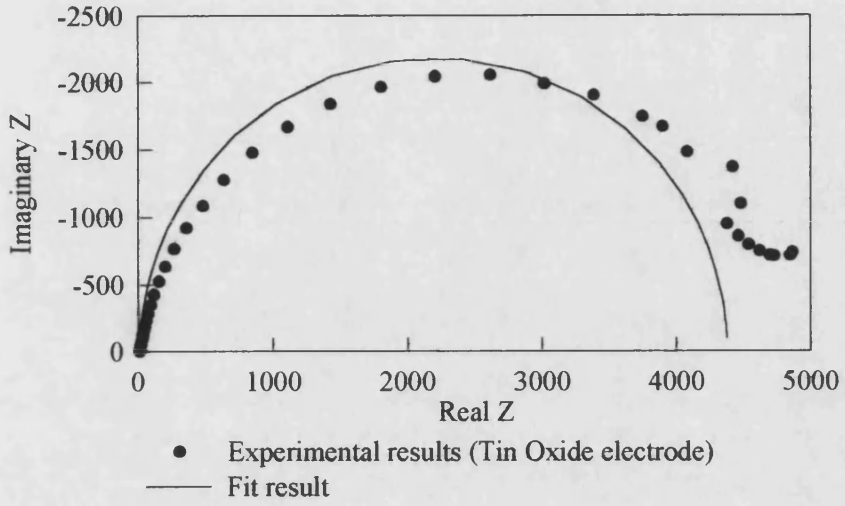

Figure 6.1 *Impedance measurements of the tin oxide glass substrate in a solution of cell electrolyte. Fitting of the semicircle to an RC parallel circuit gives a resistance of 4366 Ω cm^{-2} and a capacitance of 6μF cm^{-2}.*

Tin oxide glass with a layer of heat deposited platinum.

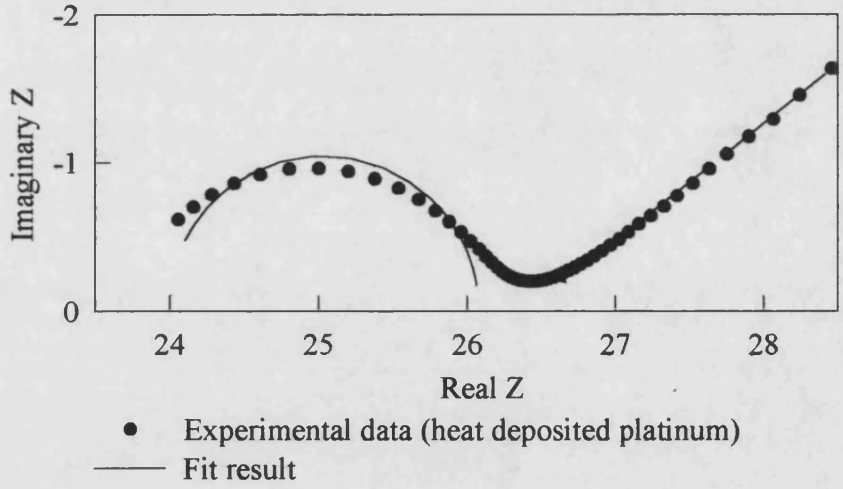

Figure 6.2 *Impedance measurements of the tin oxide glass with a layer of heat deposited platinum in a solution of cell electrolyte. Fitting of the semicircle to an RC parallel circuit gives a resistance of 2.4Ω cm^{-2} and a capacitance of 16μF cm^{-2}.*

Tin oxide glass with a layer of sputtered platinum

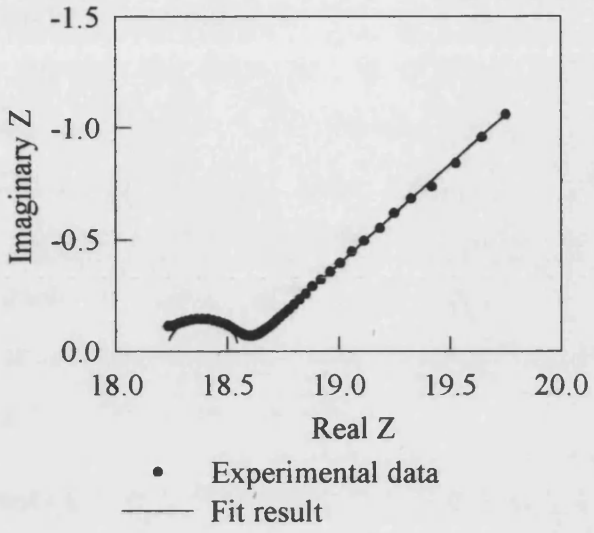

Figure 6.3 *Impedance measurements of the tin oxide glass with a layer of sputtered deposited platinum in a solution of cell electrolyte. Fitting of the semicircle to an RC parallel circuit gives a resistance of 0.3Ω cm^{-2} and a capacitance of 142μF cm^{-2}.*

6.1.2 Calculation of the exchange current density.

The equation below (derived from the Butler Volmer equation) shows the relationship between the faradic resistance and the exchange current density.

$$R_f = \frac{RT}{nFj_o}$$

The table shows the values of exchange current density at equilibrium for the 3 electrodes.

Electrode material	**Faradaic resistance /Ωcm^{-2}**	**Exchange current density /A cm^{-2}**
Tin oxide glass	4366	5.9×10^{-6}
Heat deposited platinum	2.4	0.0107
Sputtered platinum	0.3	0.086

6.2 *Impedance measurements on a complete dye sensitised cell*

Impedance measurements were made in the dark and under illumination for a complete dye sensitised cell. The response was fitted using linear circuit components, and gave a very good fit to the experimental results. The capacitance and resistance values from the fit are assigned to the different interfaces and layers of the cell. The potential and intensity dependence of the capacitance and resistance of the dye sensitised TiO_2 film is discussed. In the dark the capacitance is 14μF at short circuit rising to 1.5mF at open circuit. At an intensity equivalent to i_{sc}=3.5mA, a typical value for the capacitance of the $Ti0_2$ film is 18μF at short circuit rising to 3.0mF at open circuit.

6.2.1 PEIS and impedance spectroscopy model of the dye sensitised solar cell and fitting procedures

There are several interfaces associated with dye sensitised TiO_2 cells, each layer has impedance associated with it. It is therefore possible to devise an equivalent circuit for the cell.

tin oxide glass	dye sensitised nanoporous TiO_2 film	electrolyte	platinum layer	tin oxide glass

Figure 6.4 *Schematic representation of a dye sensitised solar cell.*

The dye sensitised TiO_2 film can be modelled as a resistor and capacitor in parallel as can the platinum layer. The electrolyte is simply equivalent to a series resistor, as is the sheet resistance of the SnO_2 glass. The overall equivalent circuit is therefore thus:

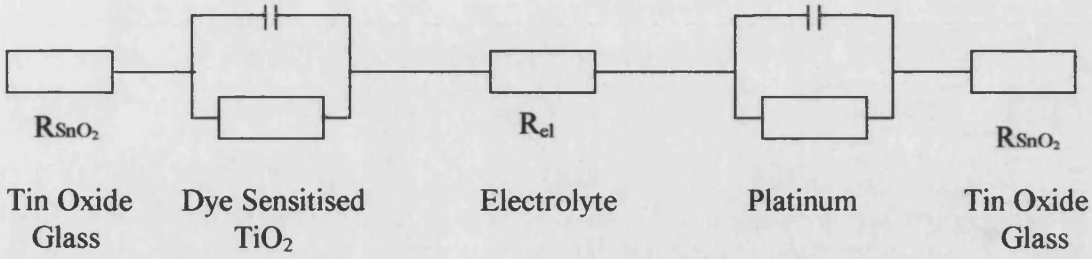

Figure 6.5 *Representation of the dye sensitised solar cell using linear circuit components.*

The EIS output is expected to consist of two semicircles and a small space before them corresponding to the solution resistance plus the resistance of the tin oxide glass. As all the series resistances will appear as one resistance they are termed 'lumped'. The circuit diagram now becomes simplified as we can only measure the lumped resistance not the individual values:

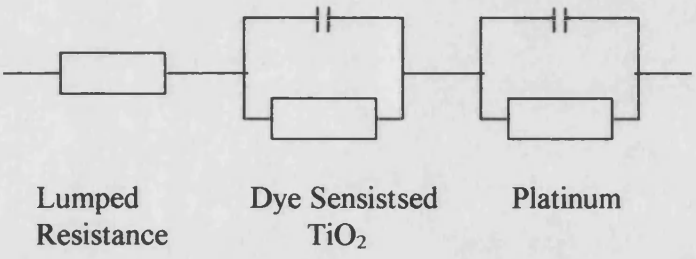

Figure 6.6 *Simplified circuit diagram of a dye sensitised solar cell.*

The results are displayed in the form of Nyquist plots showing the real and imaginary impedance. The fitting of the response was accomplished using Z-plot equivalent circuit fit. The circuit used is described above in Figure 6.6.

6.2.2 Comparison of impedance measurements in the dark and under illumination.

A typical response near to open circuit in the dark is shown in the complex plane plot in Figure 6.8. The impedance results show two semicircles shifted slightly along the x-axis in the complex plane plot. The calculated resistances and capacitances correspond to the following (also shown in Figure 6.7):

R1 = The resistance corresponding to the shift of the semicircles along the x axis
R2 = The resistance corresponding to the high frequency semicircle
R3 = The resistance corresponding to the low frequency semicircle
C1 = The capacitance corresponding to the high frequency semicircle
C2 = The capacitance corresponding to the low frequency semicircle

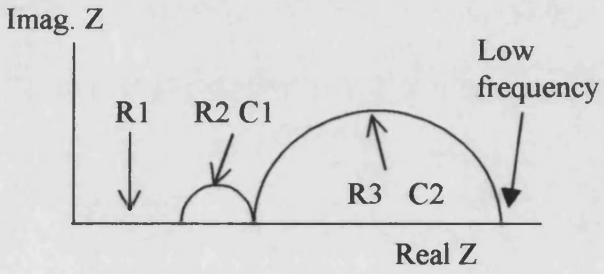

Figure 6.7 *Diagram of the complex plane plot showing the calculated resistances and capacitances.*

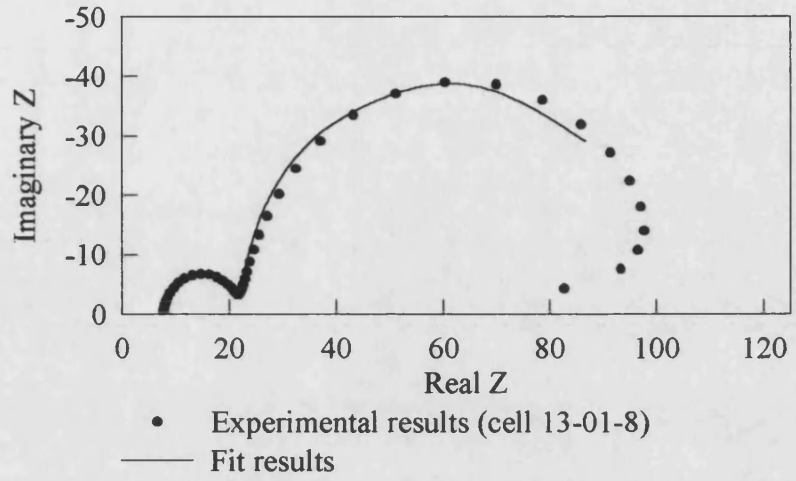

Figure 6.8 *Complex plane plot of the impedance measurements of cell 13-01-8 in the dark potential = -0.7V. Fitting gives R1=8Ω, R2=14Ω, R3=78Ω, C1=16μF and C2=1.5mF*

Bode plots are used alongside complex plane plots to show the accuracy of the fitting (Figure 6.9 and Figure 6.10). The response near open circuit and under illumination can be seen in Figure 6.11 to Figure 6.13.

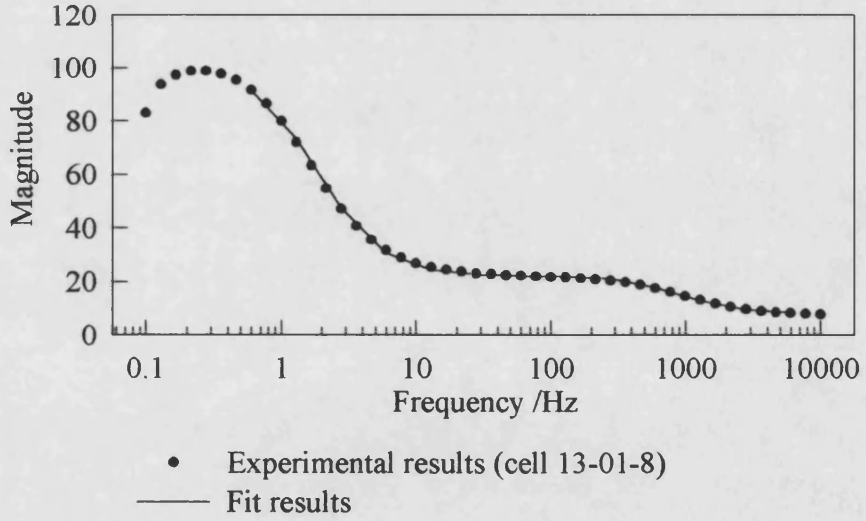

Figure 6.9 *Bode plot of the magnitude of the impedance measurements of cell 13-01-8 in the dark potential = -0.7V. Fitting gives R1=8Ω, R2=14Ω, R3=78Ω, C1=16μF and C2=1.5mF*

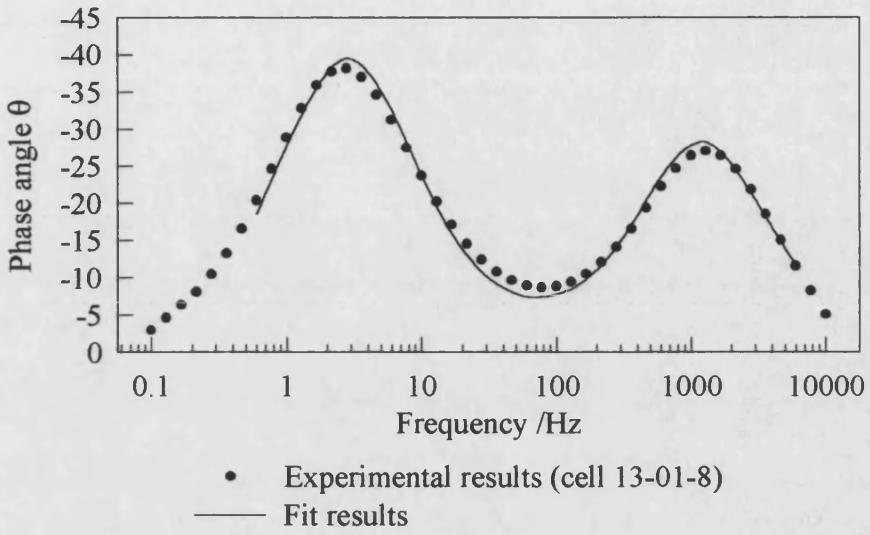

Figure 6.10 *Bode plot of the phase angle of the impedance measurements of cell 13-01-8 in the dark, potential = -0.7V. Fitting gives R1=8Ω, R2=14Ω, R3=78Ω, C1=16μF and C2=1.5mF*

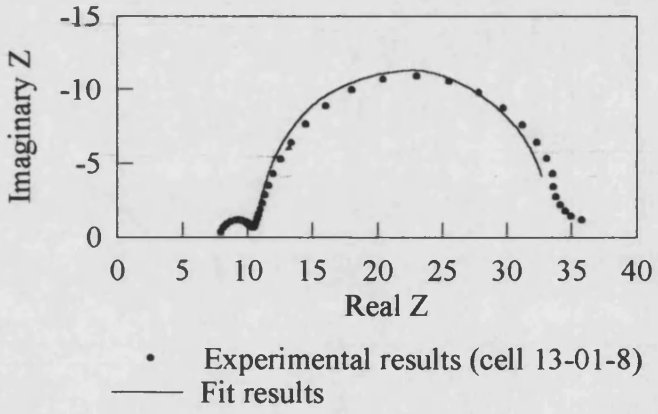

Figure 6.11 *Complex plane plot of the impedance measurements of cell 13-01-8 under illumination i_{sc}=3.5mA, potential = -0.7V. Fitting gives R1=8Ω, R2=3Ω, R3=23Ω, C1=29μF and C2=2.2μF*

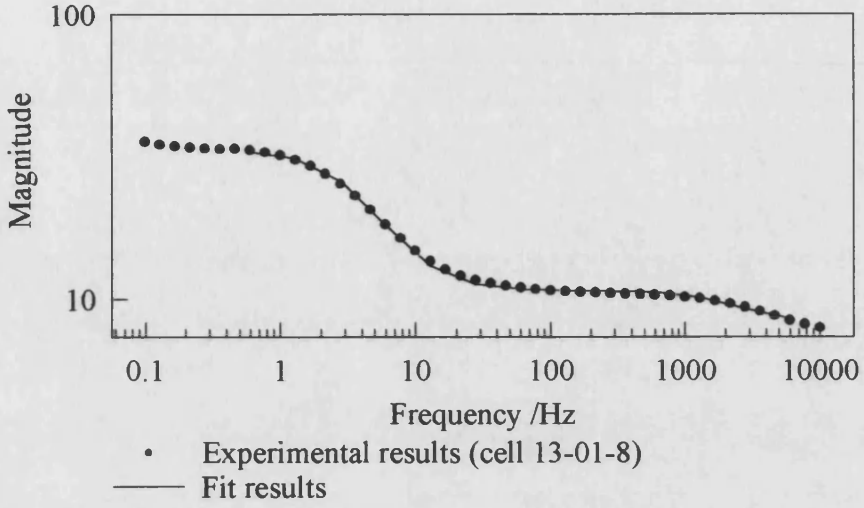

Figure 6.12 *Bode plot of the magnitude of impedance measurements of cell 13-01-8 under illumination i_{sc}=3.5mA, potential = -0.7V. Fitting gives R1=8Ω, R2=3Ω, R3=23Ω, C1=29μF and C2=2.2μF*

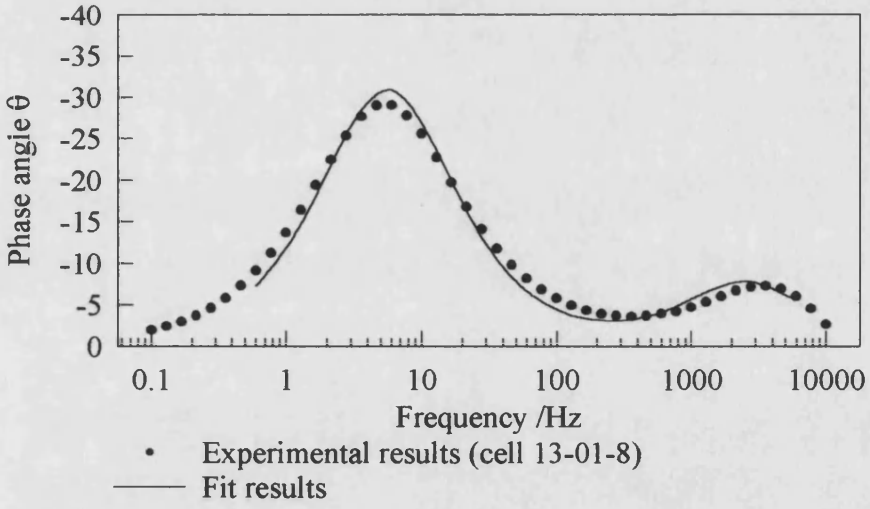

Figure 6.13 *Bode plot of the phase angle of the impedance measurements of cell 13-01-8 under illumination i_{sc}=3.5mA, potential = -0.7V. Fitting gives R1=8Ω, R2=3Ω, R3=23Ω, C1=29μF and C2=2.2μF*

The short circuit response in the dark is shown in Figure 6.14 to Figure 6.16 and under illumination in Figure 6.17 to Figure 6.19.

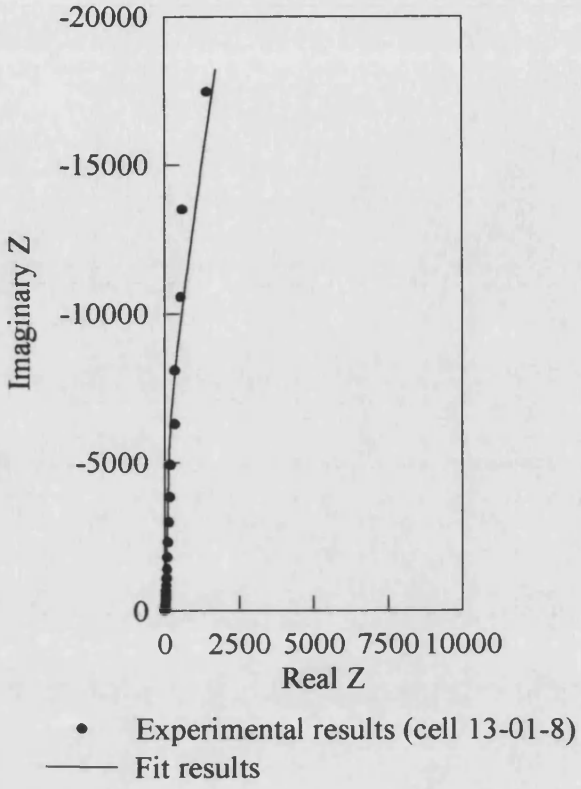

Figure 6.14 *Complex plane plot of the impedance measurements of cell 13-01-8 in the dark potential = 0V. Fitting gives R1=8Ω, R2=24Ω, R3=199,680Ω, C1=13μF and C2=14μF.*

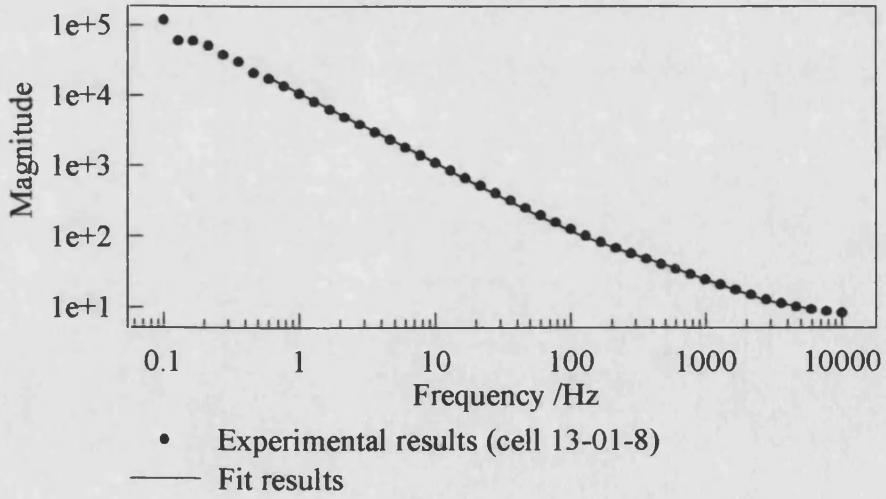

Figure 6.15 *Bode plot of the magnitude of the impedance measurements of cell 13-01-8 in the dark potential = 0V. Fitting gives R1=8Ω, R2=24Ω, R3=199,680Ω, C1=13μF and C2=14μF.*

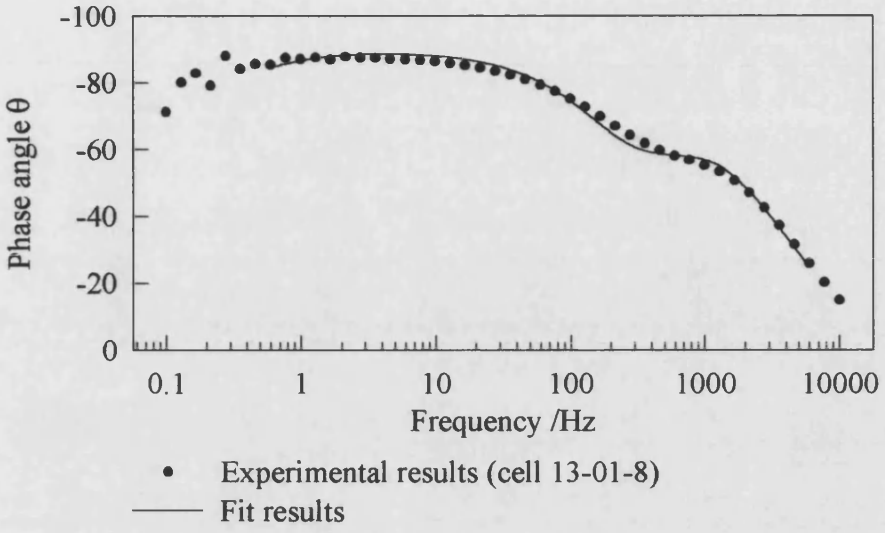

Figure 6.16 *Bode plot of the phase angle of the impedance measurements of cell 13-01-8 in the dark potential = 0V. Fitting gives R1=8Ω, R2=24Ω, R3=199,680Ω, C1=13μF and C2=14μF*

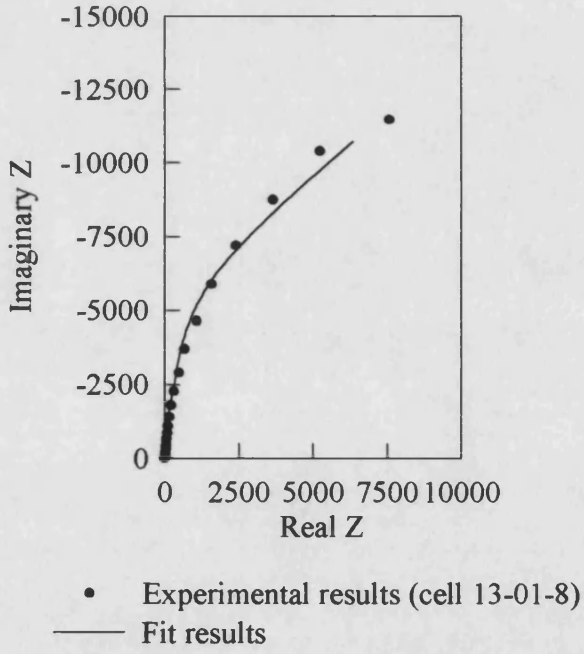

Figure 6.17 *Complex plane plot of the impedance measurements of cell 13-01-8 under illumination i_{sc}=3.5mA, potential = 0V. Fitting gives R1=9Ω, R2=15Ω, R3=24522Ω C1=16μF and C2=18μF*

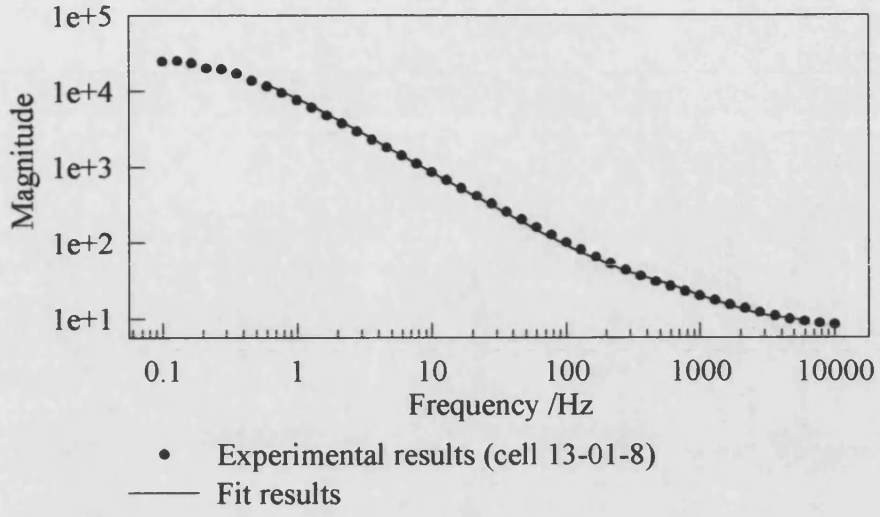

Figure 6.18 *Bode plot of the magnitude of the impedance measurements of cell 13-01-8 under illumination i_{sc}=3.5mA, potential = 0V. Fitting gives R1=9Ω, R2=15Ω, R3=24522Ω C1=16μF and C2=18μF*

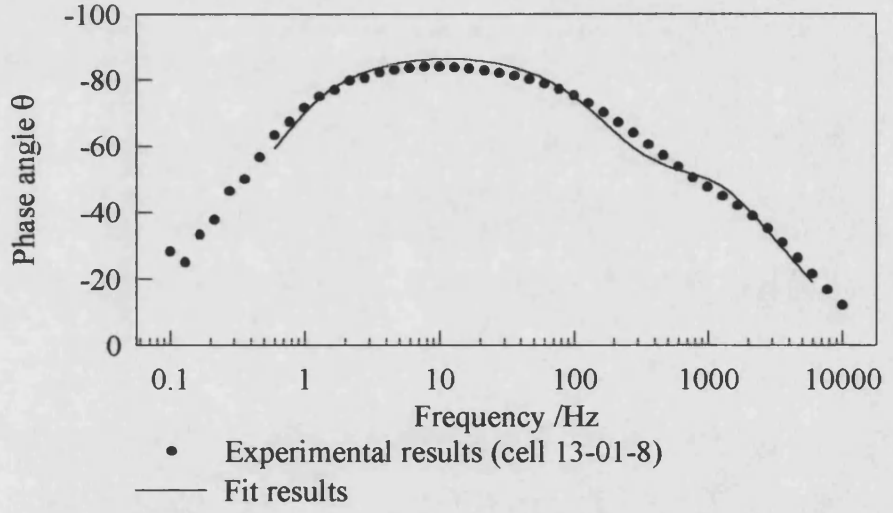

Figure 6.19 *Bode plot of the phase angle of the impedance measurements of cell 13-01-8 under illumination i_{sc}=3.5mA, potential = 0V. Fitting gives R1=9Ω, R2=15Ω, R3=24522Ω C1=16μF and C2=18μF*

The response initially indicates part of a very large (low frequency) semicircle. On enlarging the plot there is evidence that the high frequency semicircle is present as a very small shoulder on the large semicircle. Fitting using the equivalent circuit shown in Figure 6.6 works well and can be seen particularly well in the Bode plot format.

It should be noted that the shape of the response is the same in both the dark and under illumination at the same potential. The capacitance in the dark is lower than the capacitance under illumination and the resistance in the dark is higher than the resistance under illumination.

6.2.3 Potential dependence

As the potential decreases from 0V to –0.7V the impedance response changes from part of a large dominating low frequency semicircle with a very small high frequency semicircle to two clearly defined semicircles. The response in the dark and under illumination at potentials of 0V, –0.4V, –0.6V and –0.7V are shown in Figure 6.20 and Figure 6.21. These results can be fitted with the same equivalent circuit as described in section 6.2.2. Fitting is shown for results in the dark and under illumination at open circuit and short circuit previously in this chapter. (Fitted results at open circuit in the dark and under illumination are displayed in Figure 6.8 to Figure 6.13, fitting results for short circuit in the dark and under illumination are shown in Figure 6.14 to Figure 6.19). The fitting at an intermediate potential in the dark is shown in Figure 6.22 to Figure 6.24 and under illumination in Figure 6.25 to Figure 6.27. Experimental results at potentials other than those discussed here were fitted using the same equivalent circuit. This enabled the plots in Figure 6.37 and Figure 6.40.

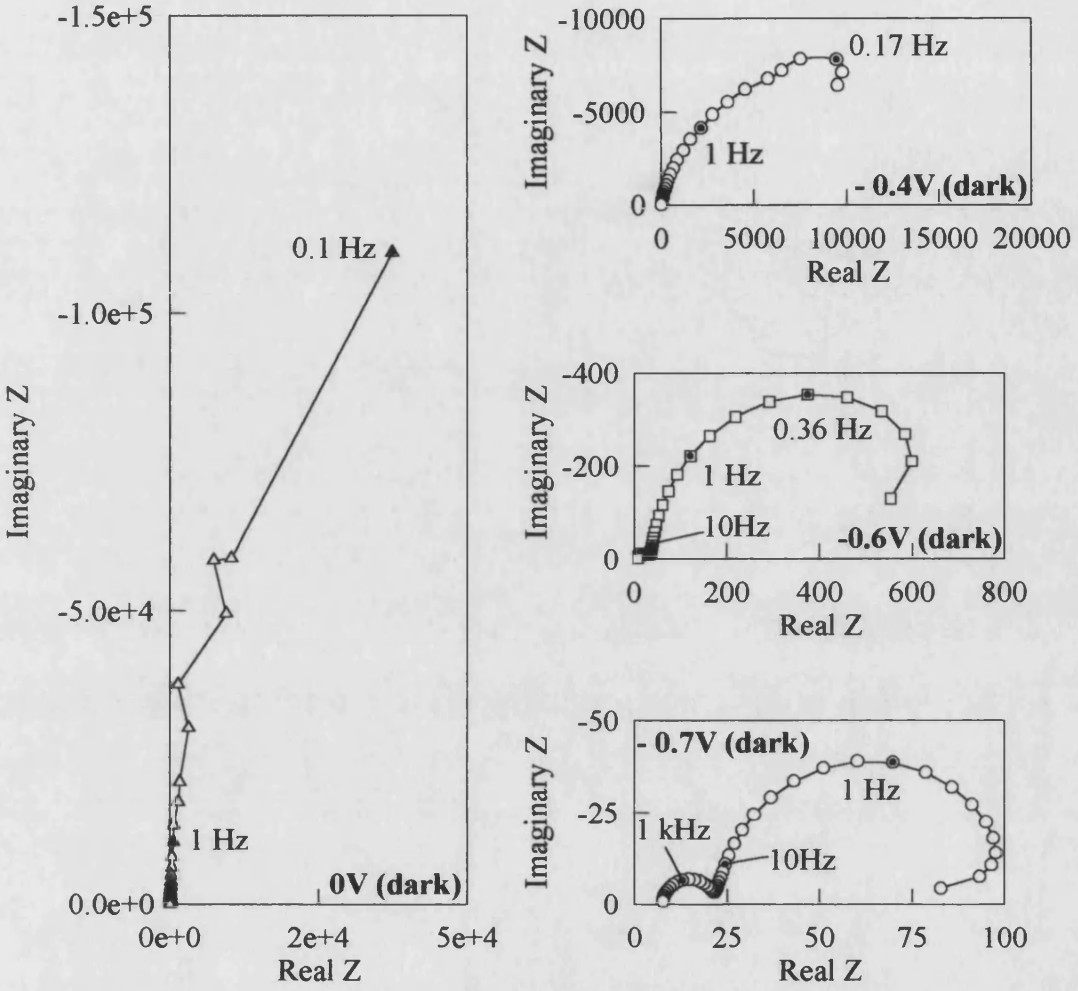

Experimental results (cell 13-01-8) measured in the dark at a range of potentials. (Potential given on each graph)

Figure 6.20 *Complex plane plot of the impedance measurements of cell 13-01-8 in the dark at potentials of 0V, -0.4V, -0.6V and –0.7V.*

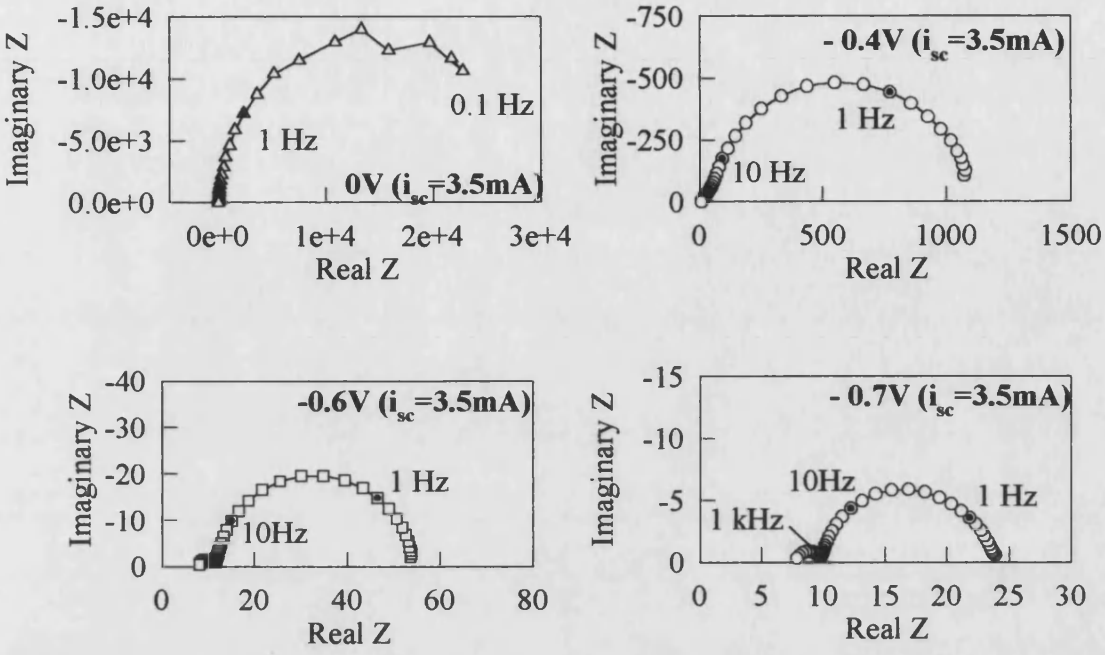

Experimental results (cell 13-01-8) measured under illumination (i_{sc}=3.5mA) at a range of potentials. (Potential given on each graph)

Figure 6.21 *Complex plane plot of the impedance measurements of cell 13-01-8 under illumination (i_{sc}=3.5 mA) at potentials of 0V, -0.4V, -0.6V and –0.7V.*

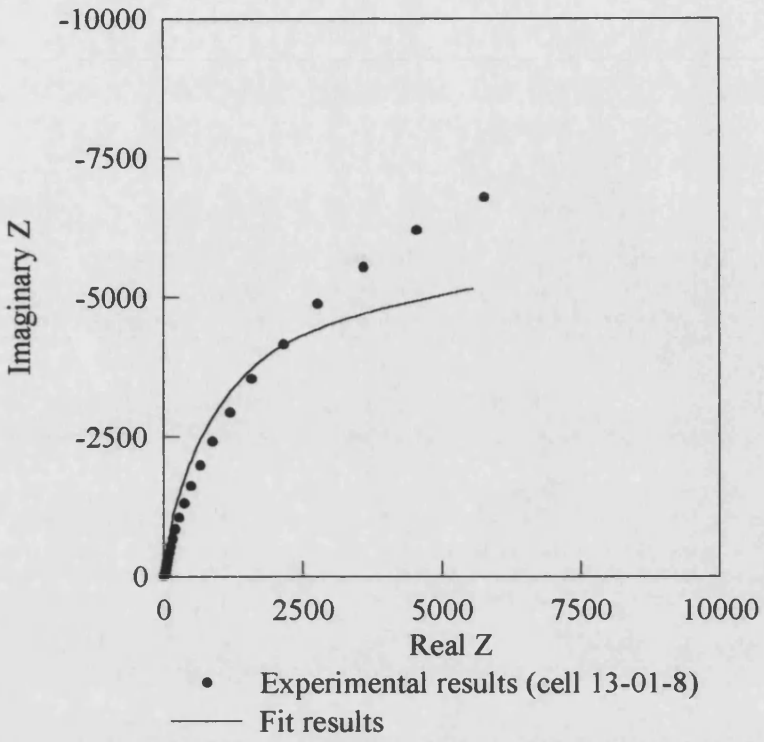

Figure 6.22 *Complex plane plot of the impedance measurements of cell 13-01-8 in the dark, potential = -0.4V. Fitting gives R1=8.5Ω, R2=36Ω, R3=10330Ω C1=13μF and C2=24μF*

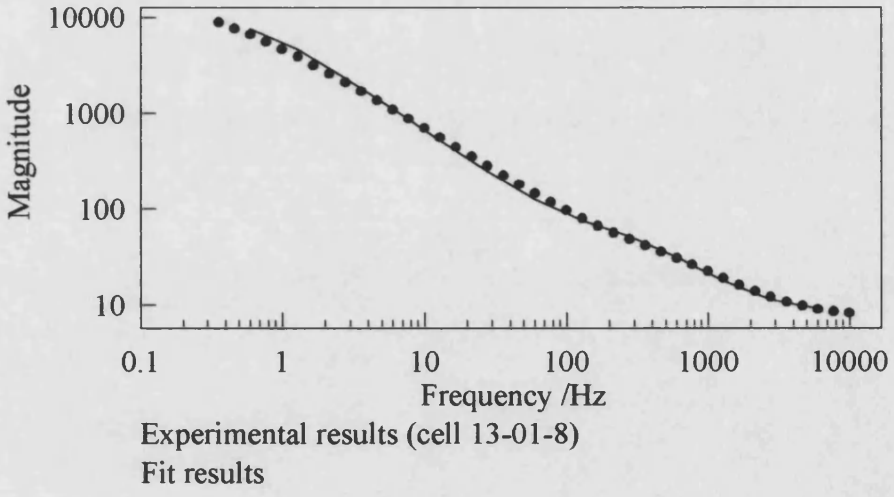

Figure 6.23 *Bode plot of the magnitude of the impedance measurements of cell 13-01-8 in the dark, potential = -0.4V. Fitting gives R1=8.5Ω, R2=36Ω, R3=10330Ω C1=13μF and C2=24μF*

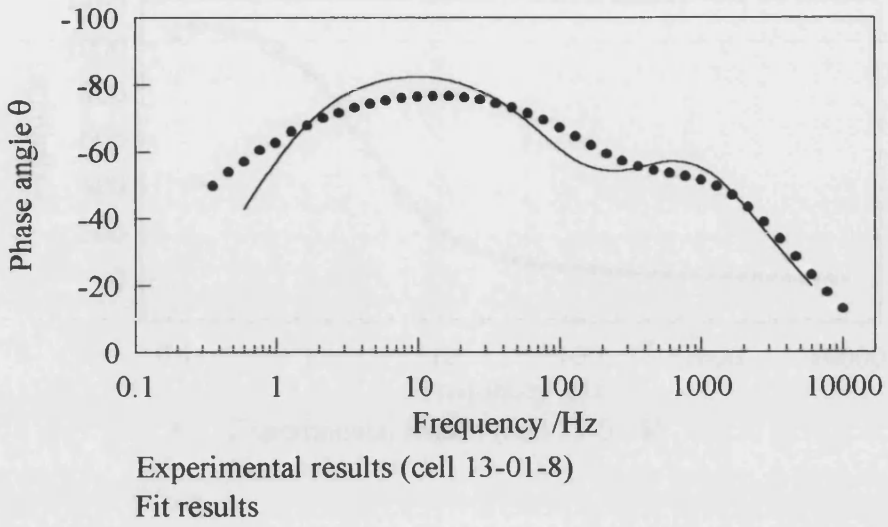

Figure 6.24 *Bode plot of the phase angle of the impedance measurements of cell 13-01-8 in the dark, potential = -0.4V. Fitting gives R1=8.5Ω, R2=36Ω, R3=10330Ω C1=13μF and C2=24μF*

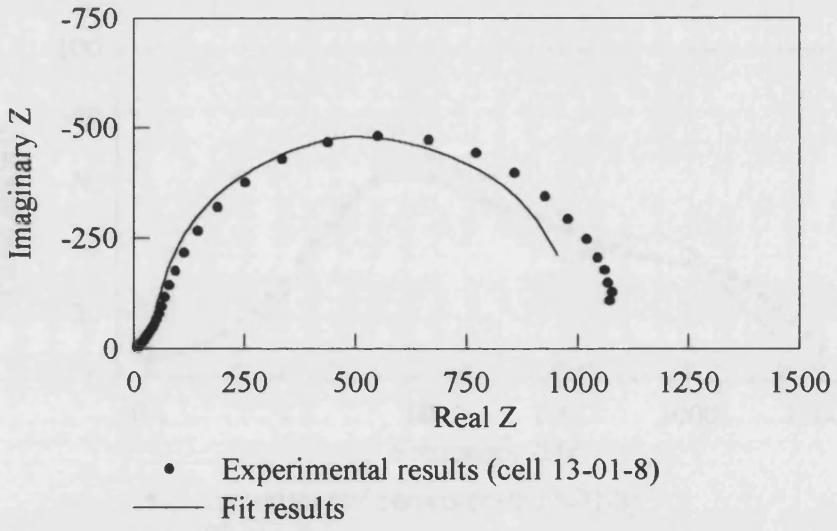

Figure 6.25 *Complex plane plot of the impedance measurements of cell 13-01-8 under illumination i_{sc}=3.5mA, potential = -0.4V. Fitting gives R1=10Ω, R2=31Ω, R3=962Ω C1=17μF and C2=82μF*

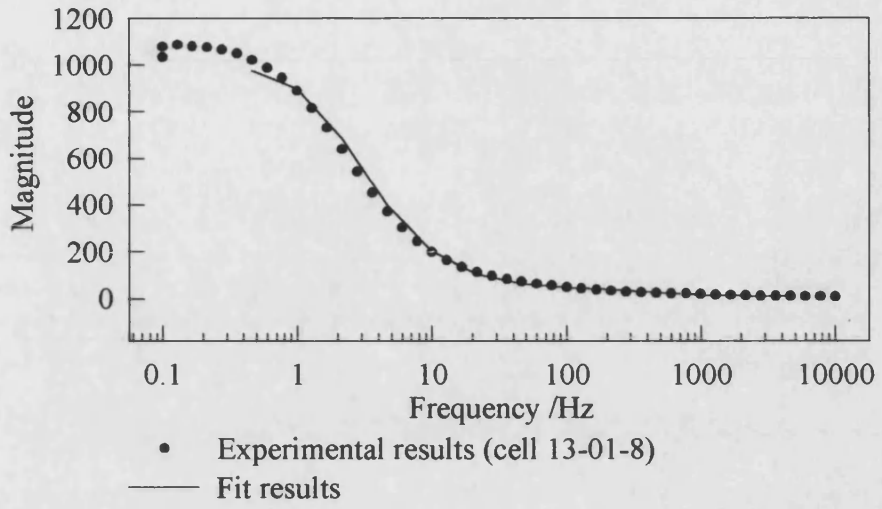

Figure 6.26 *Bode plot of the magnitude of the impedance measurements of cell 13-01-8 under illumination i_{sc}=3.5mA, potential = -0.4V. Fitting gives R1=10Ω, R2=31Ω, R3=962Ω C1=17μF and C2=82μF*

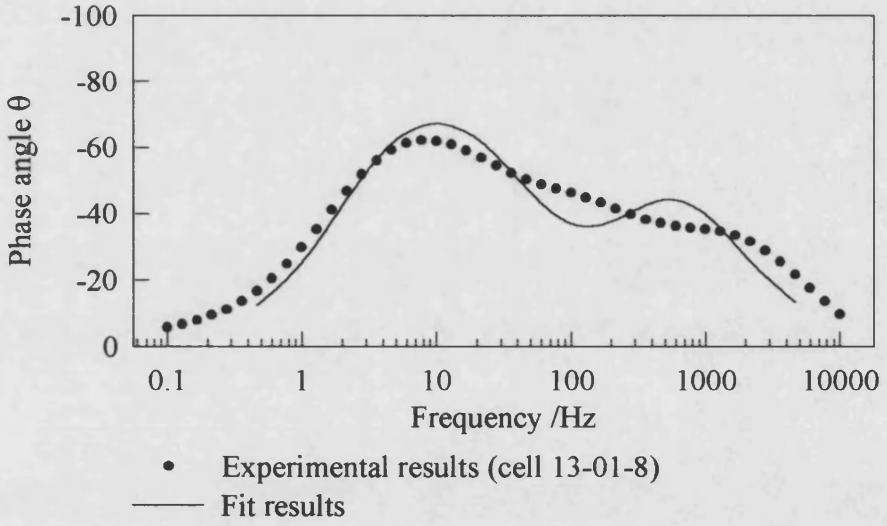

Figure 6.27 *Bode plot of the phase angle of the impedance measurements of cell 13-01-8 under illumination i_{sc}=3.5mA, potential = -0.4V. Fitting gives R1=10Ω, R2=31Ω, R3=962Ω C1=17μF and C2=82μF*

Figure 6.28 to Figure 6.30 show how the resistance (R3), the admittance (1/R3) and the capacitance (C2) of the low frequency semicircle change with applied potential. The capacitance and the admittance were calculated in the dark and at several intensities.

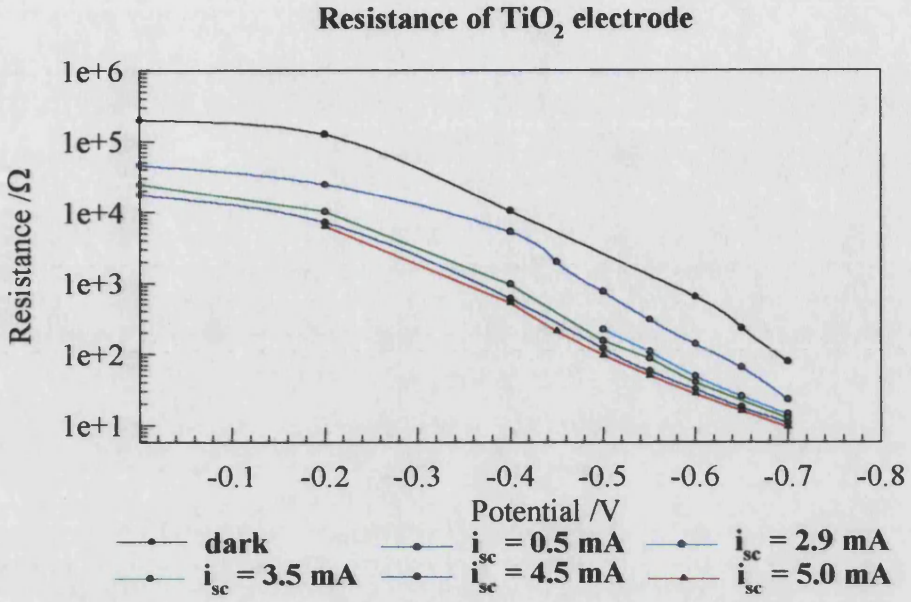

Figure 6.28 *Results calculated from the impedance measurements. The potential dependence of the resistance R3 of the low frequency (TiO_2) semicircle at several intensities.*

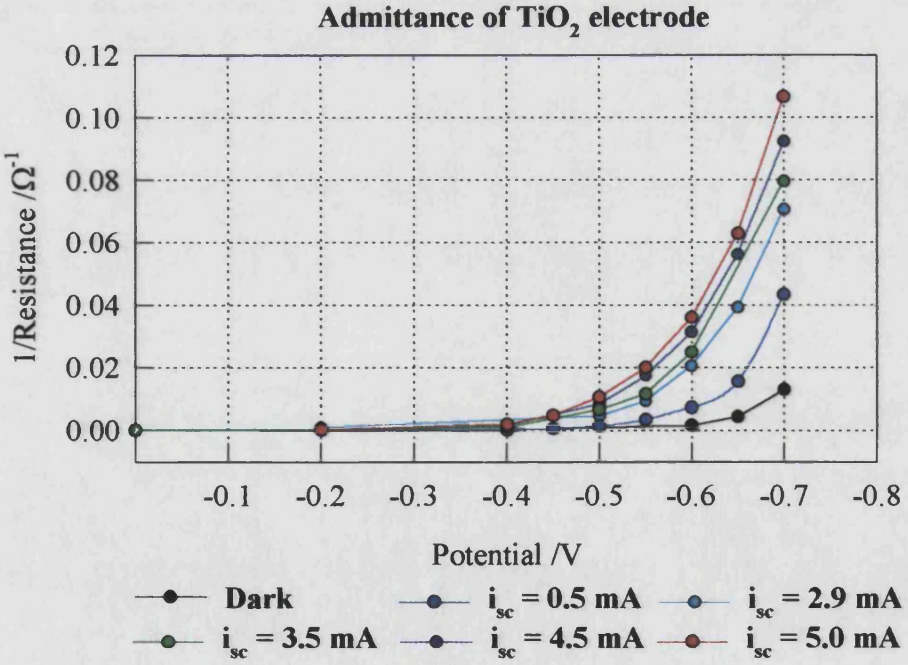

Figure 6.29 *Results calculated from the impedance measurements. The potential dependence of the admittance (1/R3) of the low frequency (TiO_2) semicircle at several intensities.*

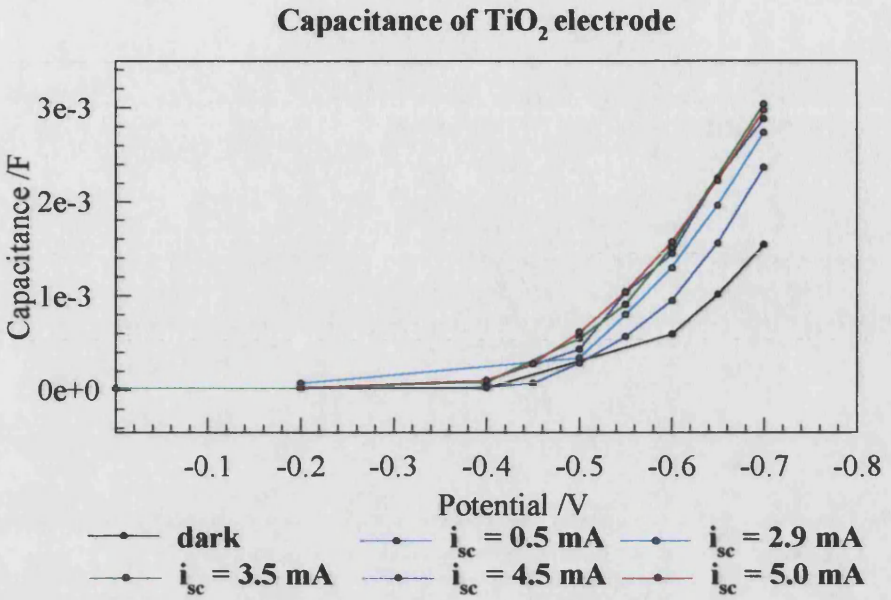

Figure 6.30 *Results calculated from the impedance measurements. The potential dependence of capacitance C2 of the low frequency semicircle at several intensities.*

6.2.4 Intensity dependence

The short circuit current (i_{sc}) has been used as an indirect measure of the intensity, recent work has shown that for dye sensitised TiO_2 systems i_{sc} is directly proportional to the incident light intensity [1]. Figure 6.31 to Figure 6.33 show results for a high light intensity at several potentials, Figure 6.34 to Figure 6.36 show results for a low light intensity at several potentials. The fitting of the plots was identical to the fitting described in section 6.2.1. Fitting of several intermediate light intensities at a range of different potentials was carried out enabling the plots in Figure 6.37 to Figure 6.40. (Fitting of an intermediate intensity can be seen in Figure 6.22 to Figure 6.27).

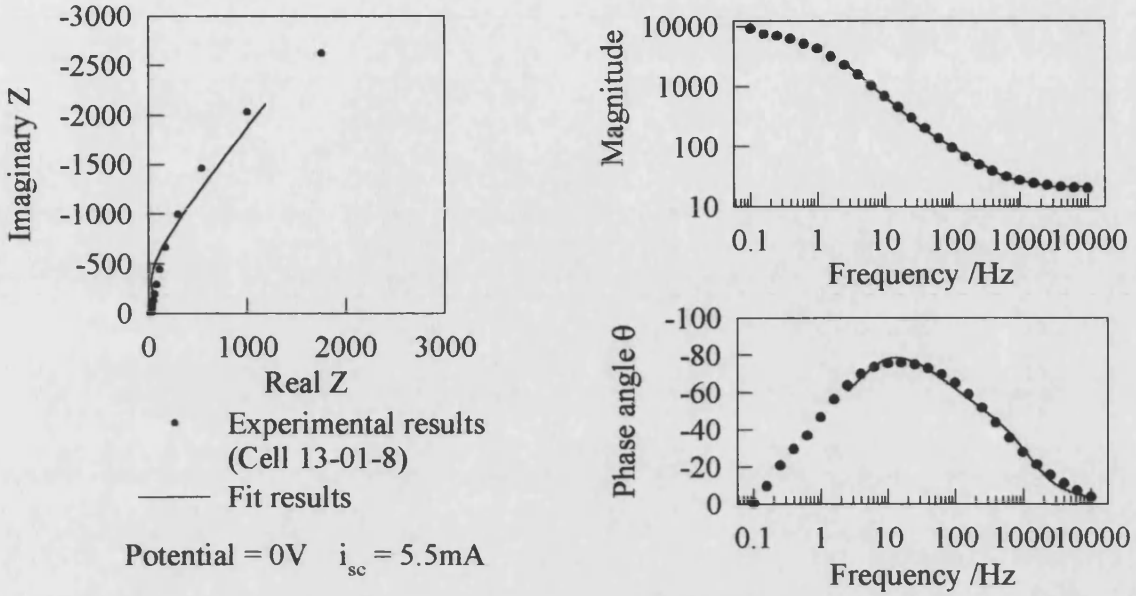

Figure 6.31 *Impedance measurements of cell 13-01-8 under illumination i_{sc}=5.5mA, potential = 0V. Fitting gives R1=21 R2=30 R3=5078Ω C1=30μF and C2=23μF.*

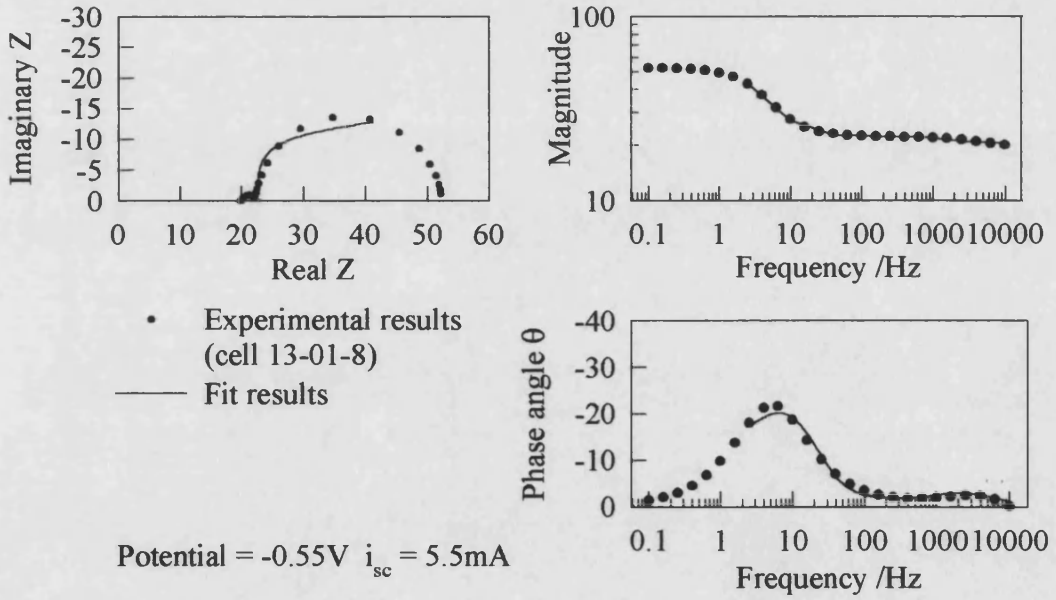

Figure 6.32 *Impedance measurements of cell 13-01-8 under illumination i_{sc}=5.5mA, potential = -0.55V. Fitting gives R1=20Ω, R2=2Ω, R3=28Ω, C1=38μF and C2=1.6mF.*

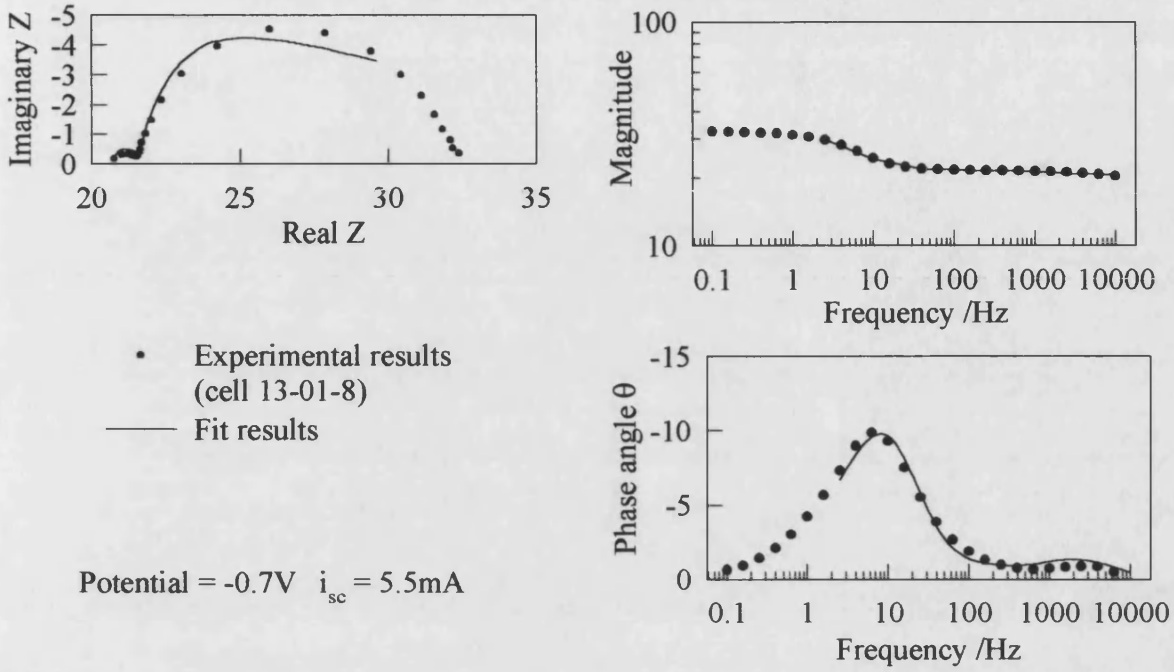

Figure 6.33 *Impedance measurements of cell 13-01-8 under illumination i_{sc}=5.5mA, potential = -0.7V. Fitting gives R1=21Ω, R2=1Ω, R3=9Ω, C1=88μF and C2=2.9mF.*

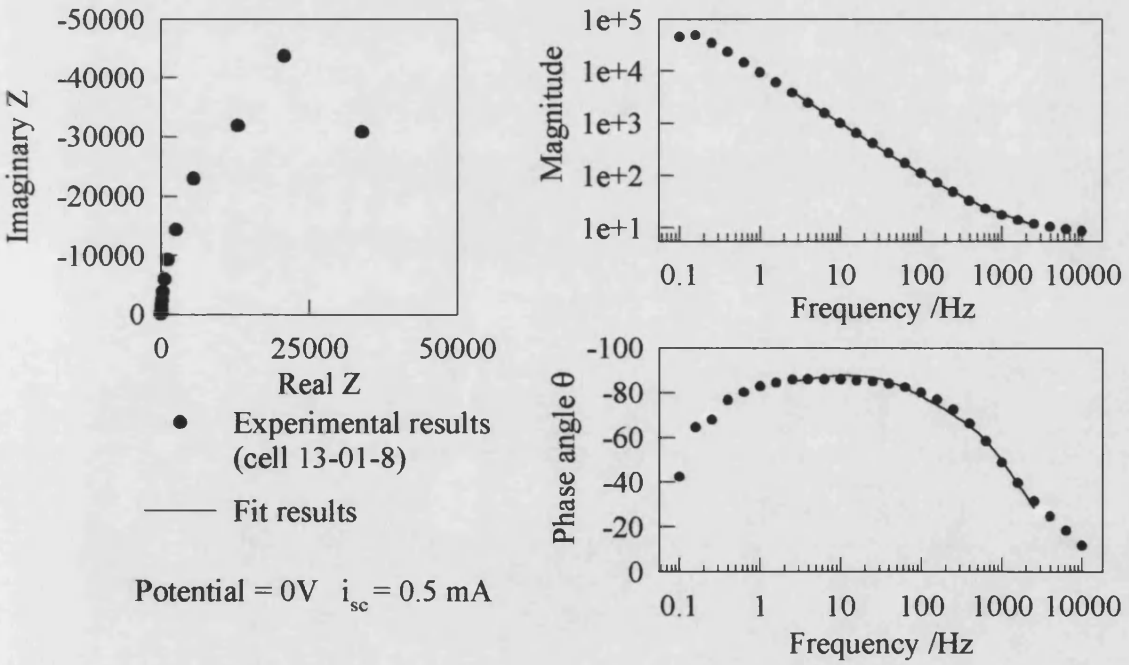

Figure 6.34 *Impedance measurements of cell 13-01-8 under illumination i_{sc}=0.5mA, potential = 0V. Fitting gives R1=8.6Ω, R2=7Ω, R3=46030Ω, C1=25μF and C2=16μF.*

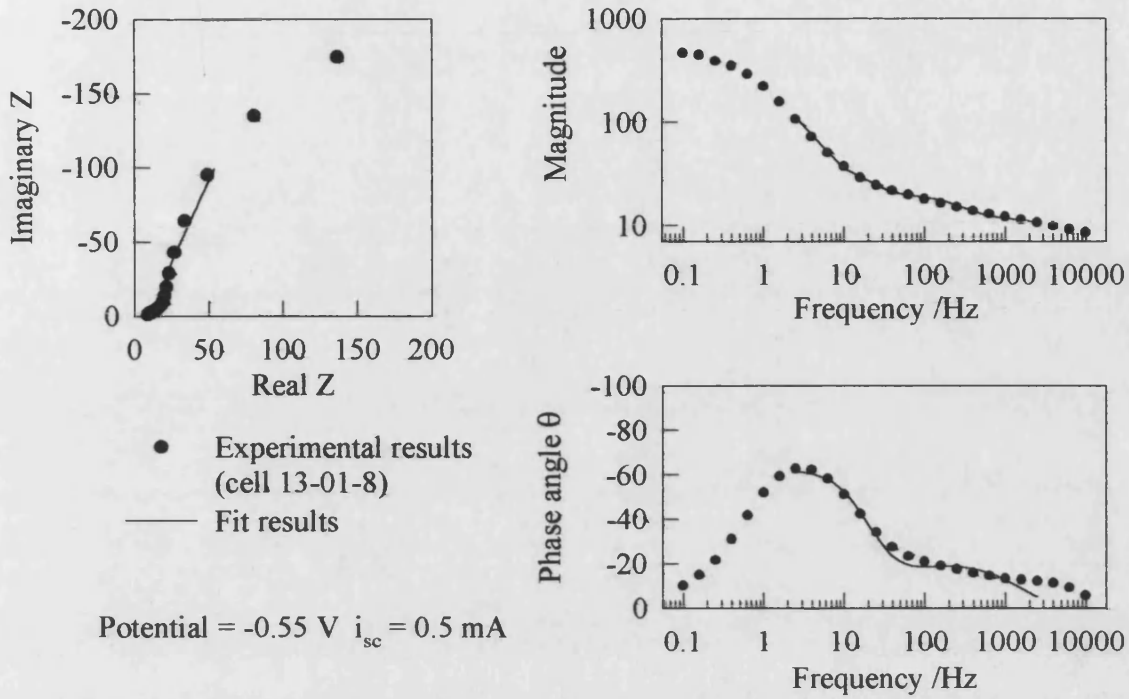

Figure 6.35 *Impedance measurements of cell 13-01-8 under illumination i_{sc}=0.5mA, potential = -0.55V. Fitting gives R1=10Ω, R2=9Ω, R3=320Ω, C1=77μF and C2=0.6mF.*

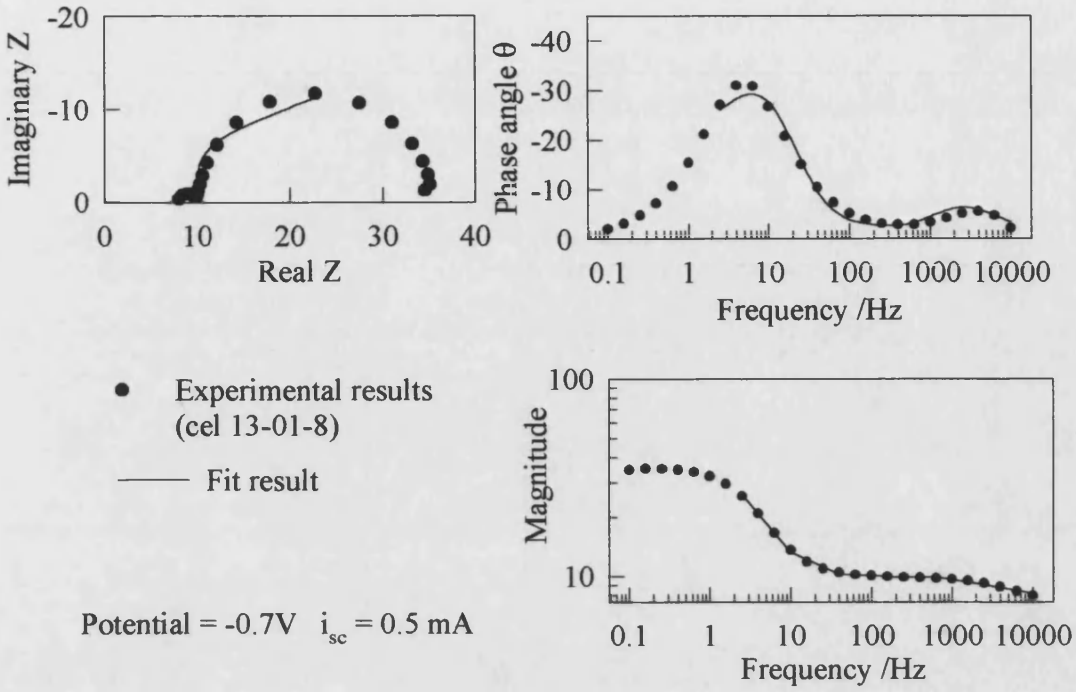

Figure 6.36 *Impedance measurements of cell 13-01-8 under illumination i_{sc}=0.5mA, potential = -0.7V. Fitting gives R1=8Ω, R2=2Ω, R3=23Ω, C1=31μF and C2=2.4mF.*

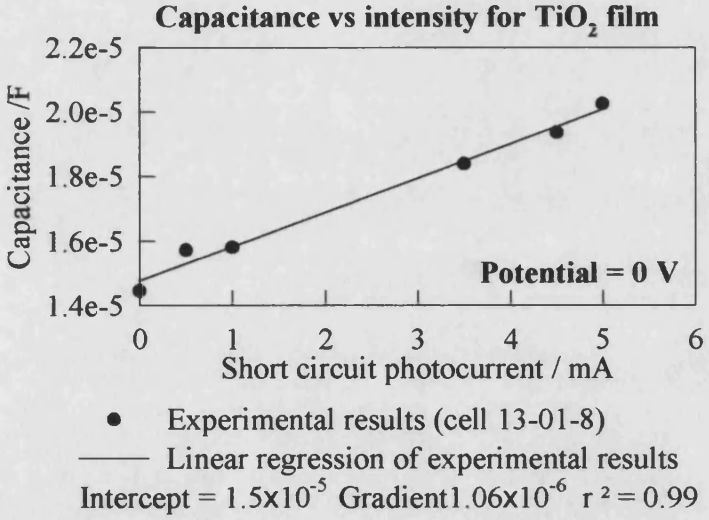

Figure 6.37 *Results calculated from the impedance measurements. The intensity dependence of capacitance C2 of the low frequency semicircle at a potential of 0V.*

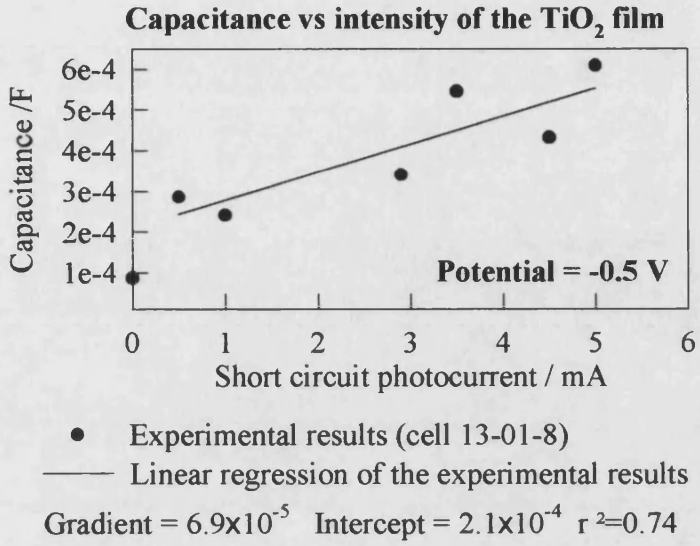

Figure 6.38 *Results calculated from the impedance measurements. The intensity dependence of capacitance C2 of the low frequency semicircle at a potential of –0.5V.*

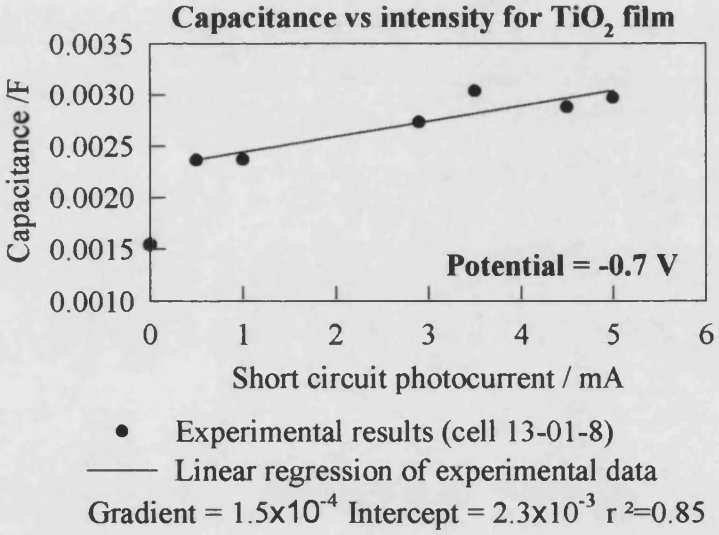

Figure 6.39 *Results calculated from the impedance measurements. The intensity dependence of capacitance C2 of the low frequency semicircle at a potential of –0.7V.*

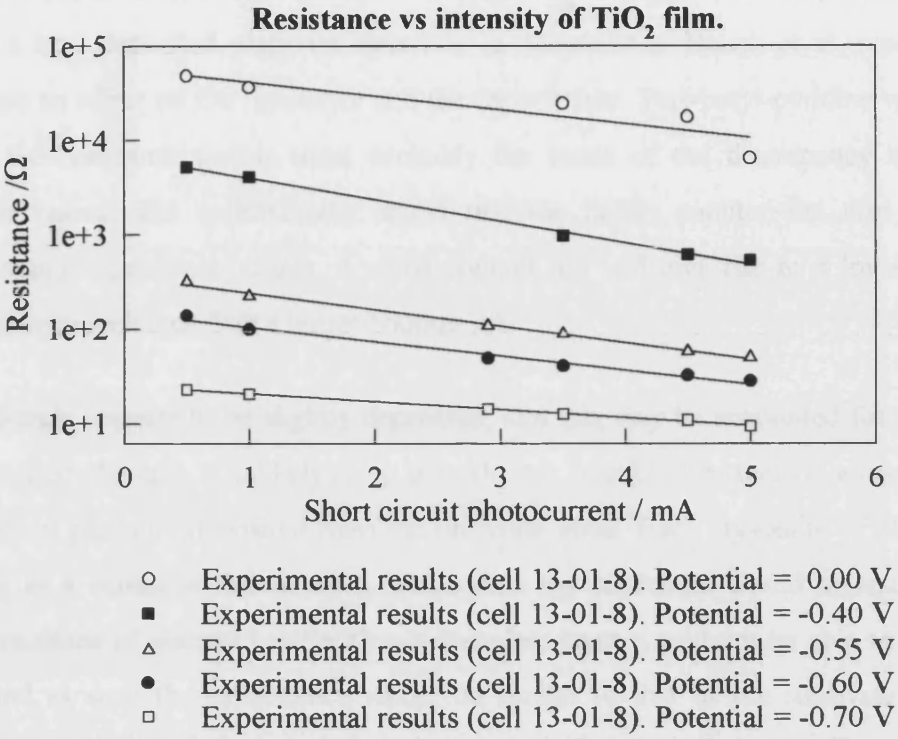

Figure 6.40 *Results calculated from the impedance measurements. The intensity dependence of resistance (R3) of the low frequency semicircle at several potentials.*

6.3 *Discussion*

Three electrode measurements

The impedance of the tin oxide glass in the iodide/triiodide electrolyte is a large semicircle. Fitting using a simple RC parallel circuit gives a capacitance of 9.2 μF and a resistance of 4952Ω. This large resistance corresponds to an exchange current density around 5 μA cm^{-2}. When a layer of platinum is heat deposited onto the surface, the impedance response is a small semicircle at high frequency with an angled line at low frequency (about 40°). The resistance and capacitance calculated from fitting of the semicircle to an RC equivalent circuit are 2.5Ω and 11 μF respectively. The exchange current density is calculated to be 0.01A cm^{-2}. The resistance is almost 2000 times smaller but capacitance is only slightly larger than that of the tin oxide.

Hauch et al [2] have reported a Faradaic resistance of 1.3 Ωcm^{-2} and a capacitance of 13μF cm^{-2} for a heat deposited platinum electrode in Acetonitrile. Hauch et al. report that the solvent has an effect on the resistance and the capacitance. Tert-butyl-pyridine was noted to increase the resistance and is most probably the cause of the discrepancy between the resistance values. The authors also report that the iodide counter ion also effects the resistance and capacitance values. A small counter ion will give rise to a lower resistance and a higher capacitance than a larger counter ion.

The semicircle appears to be slightly depressed, and this may be accounted for because the heat deposited platinum is unlikely to be smooth. It is possible that there is an array of small crystallites of platinum deposited onto the tin oxide glass. Each crystallite of platinum may be acting as a hemispherical microelectrode thus the semicircle would appear depressed. Small crystallites of platinum rather than a complete layer would not be able to store much charge and as such the capacitance would be similar to that of the substrate alone. The capacitance result for the heat deposited platinum verifies this. The angled line appearing at low frequency is indicative of a Warburg impedance. A Warburg impedance is characterised by a 45° line on a complex plane plot. It arises from the diffusion of the electroactive species to the electrode surface. The shift of the response along the x-axis is due to solution resistance.

When a platinum layer is sputtered onto tin oxide glass, the impedance response is similar to that for the heat deposited platinum. A small semicircle at high frequency with an angled line at low frequency (43°) is seen in the complex plane plot. Fitting of the semicircle to a parallel RC equivalent circuit gives a Faradaic resistance of 0.3 Ω cm^{-2} a capacitance of 142 μF cm^{-2}. The exchange current density is calculated to be 0.086 A cm^{-2}. It is noted that the Faradaic resistance is 5 times smaller than the resistance of the heat deposited platinum and 10,000 times smaller than the resistance of the tin oxide alone. The capacitance is ~15 times larger than the capacitance of the tin oxide glass and over 10 times larger than that of the heat deposited platinum. Clearly platinum layer is able to store far more charge than either the heat deposited platinum or the tin oxide alone. A small amount of platinum present on the tin oxide glass decreases the Faradaic resistance dramatically. The semicircle is slightly

depressed and a high capacitance is present both these factors indicate that the surface is unlikely to be smooth. A Warburg impedance is present and in this case is much nearer to ideality (45°).

The exchange current density at the counter electrode is an important factor within a dye sensitised cell. It must be sufficiently high that the regeneration of the iodide is not rate-limiting. The exchange current density determines the shape of the current voltage curve. A diagram of the effect the current voltage curve of a high and low exchange current density and low diffusion coefficients of the iodide are shown in Figure 6.41. A calculated example of this is given in [2]. The diffusion coefficient of the iodide is reported to be 5×10^{-5} cm^2s^{-1} in acetonitrile but only 1×10^{-7} cm^2s^{-1} in 50% methoxypropionitrile and 50% polyethylene glycol 600 [2].

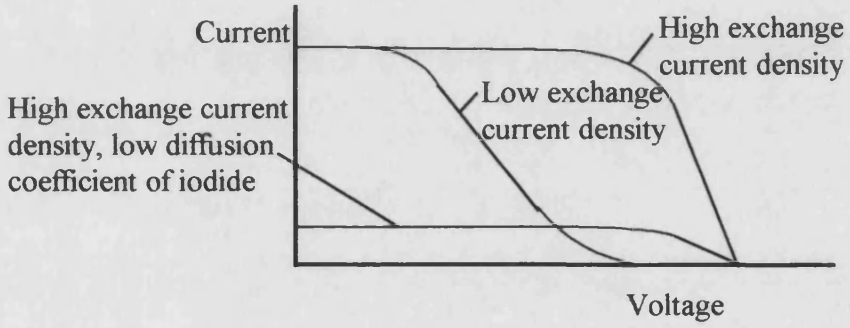

Figure 6.41 *Effect of the exchange current density of the counter electrode and the diffusion coefficient of the iodide ions on the current voltage curve of a dye sensitised solar cell.*

Comparison of three electrode and two electrode measurements

It should be noted that the sputtered platinum result from the three-electrode system is comparable with the small high frequency semicircle seen in the impedance response of a complete (two-electrode) dye sensitised cell. The small semicircle can be attributed to the platinum counter electrode. In the 2-electrode cell (complete dye sensitised cell) it is noted that the small semicircle gives Faradaic resistance values greater than those obtained with the 3-electrode system. This can be accounted for by several reasons: firstly the electrode

used in the complete (2-electrode) cell was not the same electrode that was used in the 3 electrode measurements. To use exactly the same electrode would require the cell to be dismantled, which was not possible, as the cell was needed for other measurements. Secondly the platinum in the 2-electrode cell may have become partly deactivated due to continued use. Some evidence for poisoning of the platinum electrode is given in [2]. Partial deactivation of the platinum may be due to contaminants (possibly from the sealing glue), fragments of the sensitising dye and impurities within the electrolyte adsorbing onto the surface. Over a prolonged period of use, the platinum counter electrode of a cell may become slowly de-activated. This would cause the exchange current density to decrease, the open circuit voltage to decrease and the cell would become inefficient.

The impedance response of a complete dye sensitised cell.

The impedance response of a complete dye sensitised cell (in the dark) at open circuit, shows the presence of two semicircles shifted along the x-axis. The shift along the x-axis is attributed to the solution resistance within the cell. The high frequency semicircle is attributed to the platinum counter electrode (see above). The low frequency semicircle is attributed to the dye sensitised TiO_2 film. The response was fitted using the equivalent circuit described in Figure 6.6. The fitting gave excellent results with small errors. Under illumination, the impedance response still showed evidence of two semicircles and could be fitted using the same equivalent circuit.

Hauch et al [2] have assumed that the high frequency characteristic is associated with the charge transport within the TiO_2 film. They do not take into account that the interface associated with the counter electrode would almost certainly be seen in the impedance results, due to using a two electrode system. The capacitance and resistance values associated with the platinum electrode would seem to agree with the capacitance and resistance values for the high frequency semicircle. Hauch et al. note two low frequency effects depending on the light intensity and the applied potential. They attribute these to the electrical double layer of the TiO_2 film at high light intensities or potentials near to open circuit, or the tin oxide/TiO_2 interface at low light intensities at short circuit or in the dark.

The results presented in this thesis show no evidence of two separate low frequency effects. This suggests that the low frequency event is solely the TiO_2 film and the changes in ω_{max} (and as such in resistance and capacitance) correspond to the charge stored in the film at a particular intensity and potential. As shown, from the results in this thesis there is a significant dependence of the capacitance and resistance (of the low frequency effect) on the potential and light intensity. As the light dependent process is directly associated with the dye sensitised TiO_2 film, it is reasonable to assume that the low frequency effect is primarily due to the dye sensitised TiO_2.

At short circuit (in the dark) the impedance response appears to be simply part of a very large semicircle. However inspection of the impedance Bode plots indicates that there is a high and low frequency response. The low frequency response dominates the complex plane plot, and for this reason Bode plots alongside complex plane plots have been used to show the fitting. Fitting using the same equivalent circuit as above proved successful and good fits were obtained. Under illumination the response showed some evidence of two semicircles particularly at high light intensities. Fitting of the response using the equivalent circuit described above was successful.

The counter electrode

The impedance of the small high frequency semicircle is attributed to the platinum counter electrode. The calculated capacitance and resistance values for this electrode were observed to change slightly with a change in applied potential. The fitting is a possible cause of inaccuracies, particularly at short circuit, as the high frequency semicircle is effectively 'lost' in the large dominating low frequency semicircle. One of the problems with the two electrode configuration is that the potential of the counter electrode is likely to change as a result of current flow even if the electron transfer kinetics are fast. The reason for this is that the iodide/triiodide concentration ratio (and hence the equilibrium Nernst potential) will change from the dark (or open circuit) potential.

Potential dependence of the impedance of the TiO_2 layer.

As the potential approaches open circuit (V_{oc}), the impedance response decreases markedly in magnitude. Initially at short circuit the response appears to be part of a much larger semicircle, but as the potential decreases the response becomes more semicircular and a small hump at the high frequency end becomes apparent. As open circuit is approached two discrete semicircles are evident. The high frequency semicircle (as discussed previously), is attributed to the counter electrode response. The low frequency semicircle is attributed to the response of the TiO_2 film. Resistance and capacitance values for the TiO_2 have been calculated by fitting the impedance response. The resistance of the TiO_2 film is noted to decrease by several orders of magnitude as the open circuit potential is approached. (Figure 6.28 and Figure 6.29) The capacitance of the film is noted to increase as the potential decreases (Figure 6.30). As the potential approaches open circuit, the Fermi level will increase and there will be more electrons in the film, so that the capacitance will increase. If there are more electrons in the film, then it will be much easier for charge to be transported through the film and thus the resistance will be lower than at short circuit.

Intensity dependence of the impedance of the TiO_2 layer.

At a set potential, the capacitance of the film increases linearly with increasing light intensity. The gradient of plots of capacitance vs intensity are noted to increase as the potential approaches open circuit (Figure 6.37 and Figure 6.39). The resistance decreases logarithmically as the intensity increases (Figure 6.40). There is no clear dependence of the gradient on the potential. As the intensity increases more electrons are injected into the conduction band from the dye. An increase in electrons in the TiO_2 means the capacitance of the film will increase. These injected electrons will fill some of the traps in the conduction band. It is therefore easier for electrons to move through the film without being trapped as there are less available traps. This will decrease the resistance of the film.

Potential dependence of the TiO_2 film under illumination

Under illumination, the impedance response at each potential is the same shape but smaller in magnitude than the dark response at the same potential. The capacitance and resistance

values obtained by fitting the impedance response show the same trend as the results obtained in the dark. The capacitance at a particular potential is noted to be higher than the capacitance in the dark (Figure 6.30) and resistance under illumination at a particular potential is noted to be much less than in the dark at the same potential (Figure 6.28 and Figure 6.29).

6.4 *References*

1. Wijayantha, K. G. U. Personal communication, The University of Bath

2. Hauch, A; Kern, R; Ferber, J; Georg, A; Luther, J. *2nd World conference and exhibition on photovoltaic solar energy conversion,* **1998** p260

Chapter 7

Intensity modulated photocurrent spectroscopy (IMPS) and intensity modulated photovoltage spectroscopy (IMVS)

Index

Chapter 7 Intensity modulated photocurrent spectroscopy (IMPS) and Intensity modulated photovoltage spectroscopy (IMVS)

7.1 IMPS results

This section makes a comparison of the theoretically predicted IMPS response with the experimental data obtained. Results from substrate side and electrolyte side illumination are presented and discussed. The diffusion coefficient for electrons is calculated from the frequency minimum of the IMPS response and presented as a function of the absorbed light intensity. The intensity dependence of the system is discussed. The effect of the RC time constant of the system is discussed and included in the fitting of the results. It was found that fitting of the Bode plots is much more accurate than fitting in the complex plane, and that at potentials near to open circuit the RC time constant begins to dominate the response. Typical diffusion coefficients of the cells used are of the order $10^{-5}cm^2s^{-1}$ for a DC light intensity producing DC current of 1mA. In the latter part of the chapter the IMPS results are combined with the photovoltage results to determine the diffusion length of the cells.

7.1.1 Details of fitting procedures

The IMPS data are displayed as a complex plane plot and also in the form of Bode plots. A calculated response is also shown with and without RC attenuation. The use of the Bode plots enables the best fit by eye to be achieved. Values of the electron diffusion coefficients were calculated from the fits.

Several of the parameters used in the calculated response are fixed, either because they have been measured independently or because a reasonable assumption can be made about their order of magnitude. These are as follows: α = $2500cm^{-1}$ (as measured by absorption spectroscopy by INAP prior to cell construction); film thickness = 12.5 μm also measured prior to cell construction by INAP, $\tau \Rightarrow \infty$ where the IMPS response is insensitive to any change in τ and $k_{ext} \Rightarrow \infty$ ($1\times10^5s^{-1}$) which corresponds to the diffusion controlled limit. Where RC attenuation was included, R=10Ω. The diffusion coefficient and the capacitance for each calculation are given on the individual graphs. The short circuit current is an indirect measure of the light intensity.

7.1.2 Comparison of theory and experiment for substrate side illumination of a dye sensitised nanocrystalline cell

It should be noted that on including the RC attenuation, the characteristic 45° slope at high frequency is no longer seen in the simulated complex plane plots. The Bode plots corresponding to the IMPS plot in Figure 7.1 are shown in Figure 7.2 and Figure 7.3.

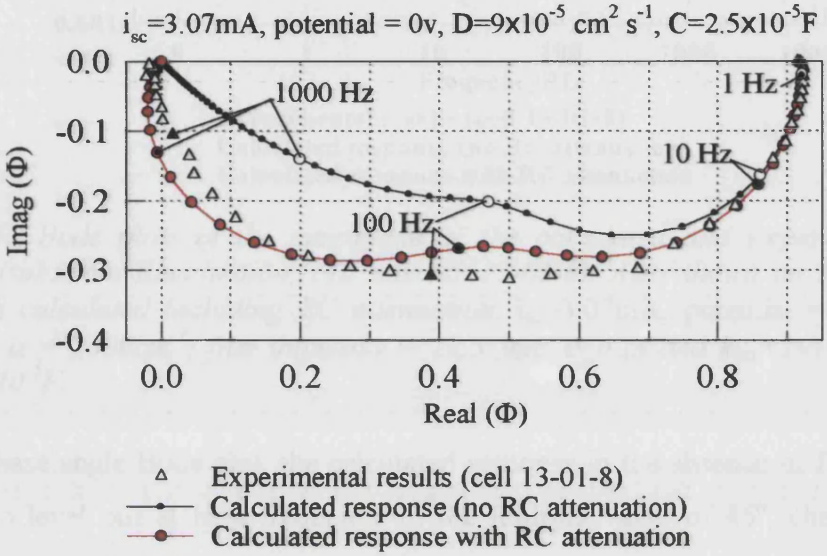

Figure 7.1 *Calculated and experimental short circuit IMPS responses for substrate side illumination of a dye-sensitised solar cell (cell number 13-01-8). Also shown on the plot is the calculated response including RC attenuation.* i_{sc}=3.07mA, potential =0V, D=9×10^{-5} cm^2 s^{-1}, α = 2500cm^{-1}, *film thickness* = 12.5 μm, τ=0.1s *and* k_{ext}=1×10^{5}s^{-1}, R=10Ω, C=2.5×10^{-5}F.

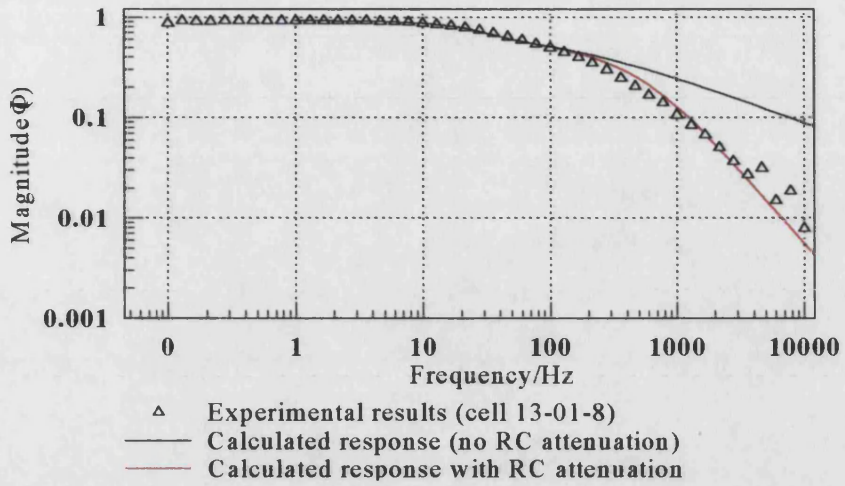

Figure 7.2 *Bode plots of the magnitude of the calculated and experimental IMPS signals (substrate illumination, cell number 13-01-8). Also shown on the plot is the response calculated including RC attenuation.* i_{sc}=3.07mA, potential =0V, D=9×10^{-5} cm^2 s^{-1}, α = *2500cm*$^{-1}$, *film thickness = 12.5* μm, τ=*0.1s and* $k_{ext}=1\times10^5 s^{-1}$, *R=10*$\Omega$, *C=*$2.5\times10^{-5}$*F.*

In the phase angle Bode plot, the calculated response in the absence of RC attenuation begins to level out at high frequency to the limiting value of 45°, characteristic for diffusion control. Where RC attenuation is present, the phase angle continues to increase with increasing frequency. The use of the Bode plots to show how the experimental data fits the predicted value is much better that the complex plane IMPS plot alone.

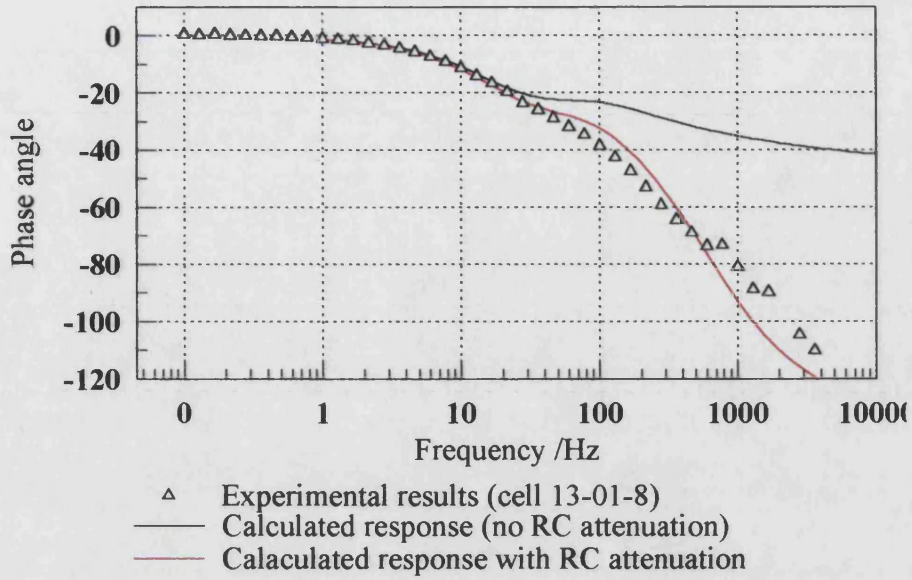

Figure 7.3 *Bode plot of the phase angle of the IMPS response (substrate illumination, cell number 13-01-8). Also shown on the plot is the calculated response including RC attenuation.* i_{sc}*=3.07mA, potential =0V,* $D=9\times10^{-5}$ cm^2 s^{-1}, α *= 2500*cm^{-1}*, film thickness = 12.5* μm, $\tau=0.1s$ *and* $k_{ext}=1\times10^5 s^{-1}$, $R=10\Omega$, $C=2.5\times10^{-5}F$.

7.1.3 Substrate and electrolyte illumination for cell with a transparent counter electrode.

The dye sensitised titanium dioxide film was constructed by INAP, the transparent counter electrode was manufactured in Bath as described in Chapter 4. Results for both substrate and electrolyte side illumination are displayed.

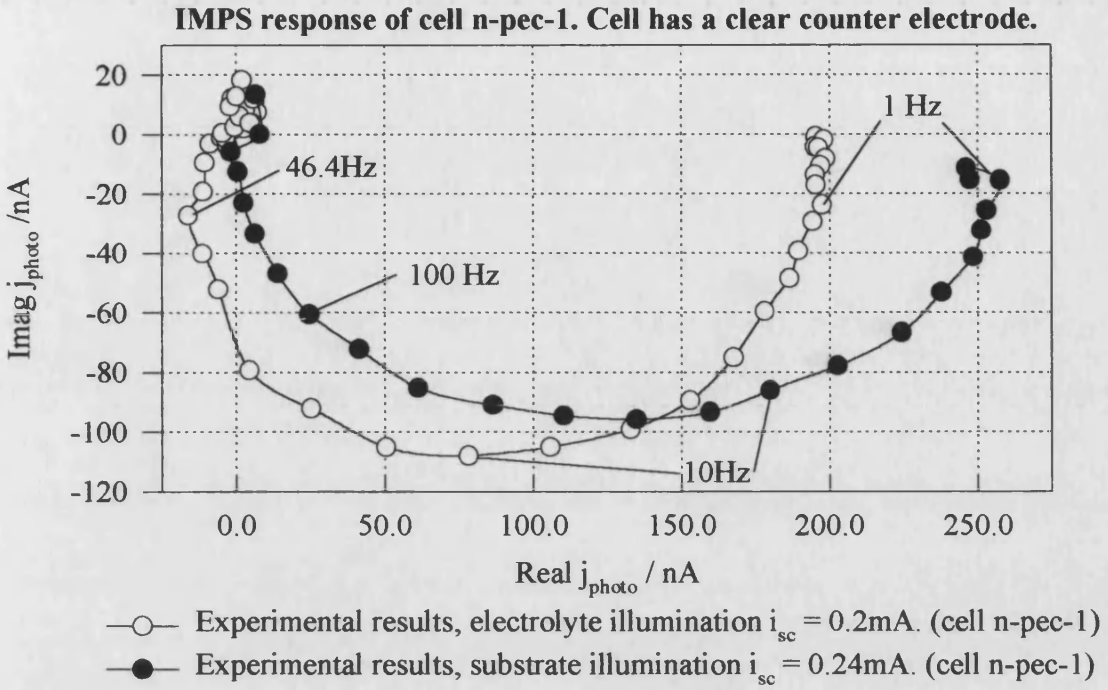

Figure 7.4 *IMPS response for substrate and electrolyte illumination. (Cell n-pec-1).*

For the fitting of the data shown in Figure 7.4, simulations for both substrate side and electrolyte side illumination were performed, and the same values for the variable parameters were used in each case. Figures 7.5 to Figure 7.7 show the fitting for electrolyte side illumination and Figures 7.8 to Figure 7.10 show the fitting for substrate illumination.

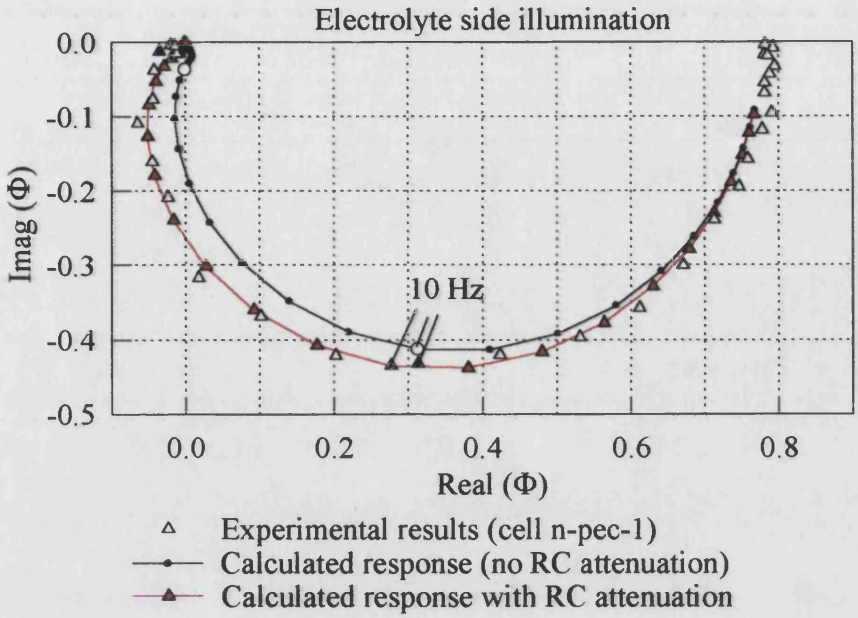

Figure 7.5 *IMPS response for electrolyte illumination of a dye sensitised solar cell with a transparent counter electrode (cell number n-pec-1). Also shown on the plot is the calculated response including RC attenuation.* i_{sc}=0.2mA, potential =0V, D=3×10^{-5} cm^2 s^{-1}, α = *2500cm*$^{-1}$, *film thickness = 12.5μm* τ=*0.1s and* $k_{ext}=1\times10^5 s^{-1}$, *R=10Ω, C=*$1.3\times10^{-4}$*F*

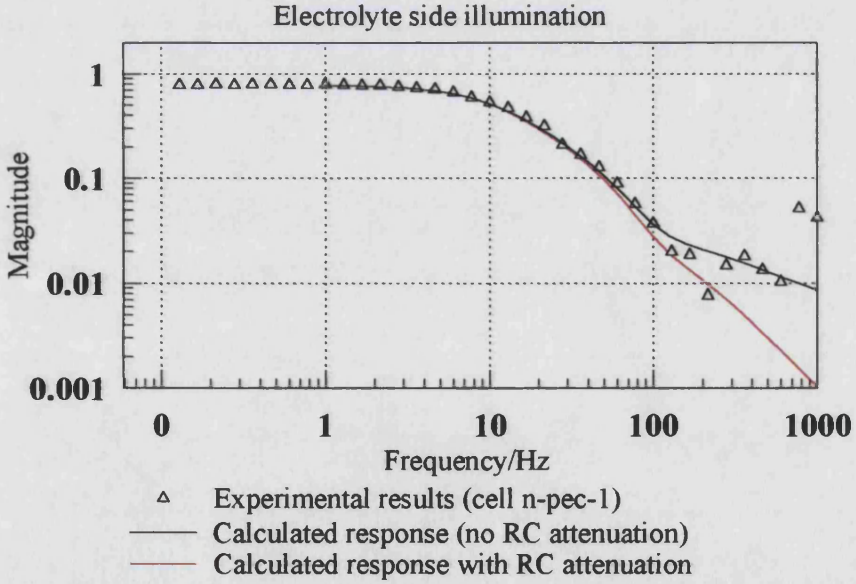

Figure 7.6 *Bode plot of the magnitude of the IMPS signal (electrolyte illumination, cell number n-pec-1). Also shown on the plot is the calculated response including RC attenuation.* i_{sc}=0.2mA, potential =0V, D=3×10^{-5} cm^2 s^{-1}, α = *2500cm*$^{-1}$, *film thickness = 12.5μm* τ=*0.1s and* $k_{ext}=1\times10^5 s^{-1}$, *R=10Ω, C=*$1.3\times10^{-4}$*F*

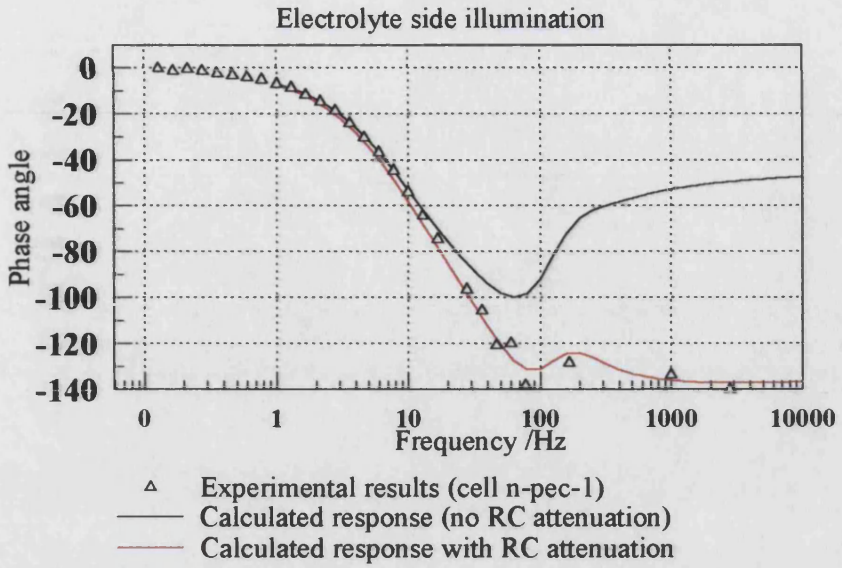

Figure 7.7 *Bode plot of the phase angle of the IMPS signal (electrolyte illumination, cell number n-pec-1). Also shown on the plot is the calculated response including RC attenuation.* i_{sc}=0.2mA, potential =0V, D=3×10^{-5} cm^2 s^{-1}, α = *2500cm*$^{-1}$, *film thickness = 12.5μm* τ=*0.1s and* $k_{ext}=1\times10^5 s^{-1}$, *R=10Ω, C=*$1.3\times10^{-4}$*F*

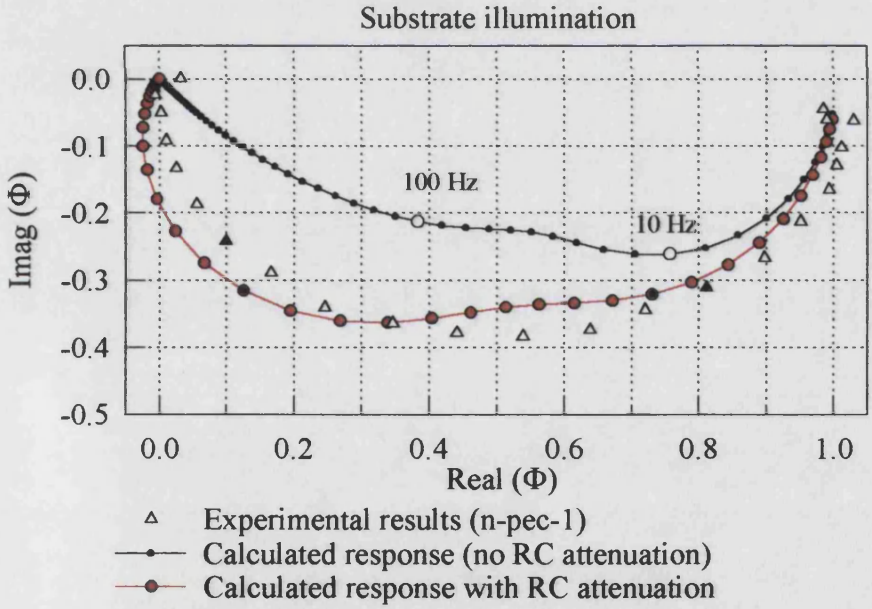

Figure 7.8 *IMPS response for substrate illumination of a dye sensitised solar cell with a transparent counter electrode (cell number n-pec-1). Also shown on the plot is the calculated response including RC attenuation.* i_{sc}=0.2mA, potential =0V, D=3×10^{-5} cm^2 s^{-1}, α = *2500cm*$^{-1}$, *film thickness = 12.5μm* τ=*0.1s and* $k_{ext}=1\times10^5 s^{-1}$, *R=10Ω, C=*$1.3\times10^{-4}$*F*

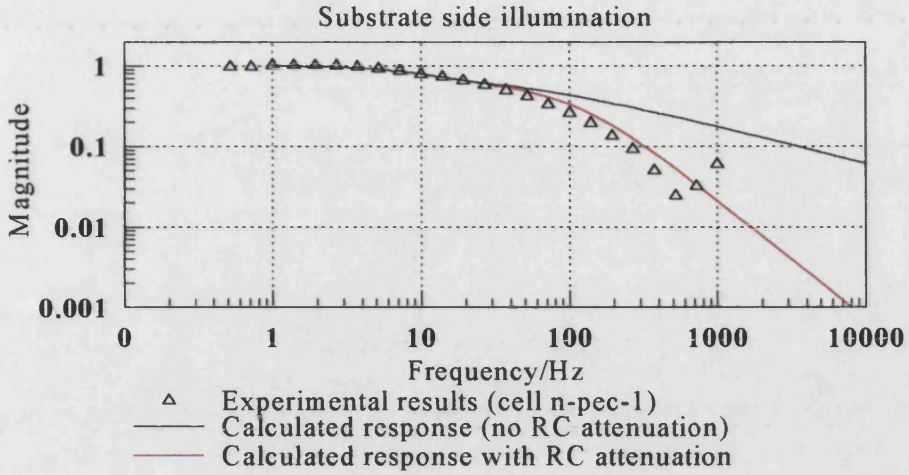

Figure 7.9 *Bode plot of the magnitude of the IMPS signal for substrate side illumination of a dye sensitised solar cell with a transparent counter electrode (cell number n-pec-1). Also shown on the plot is the calculated response including RC attenuation.* i_{sc}=0.2mA, potential =0V, D=3×10^{-5} cm^2 s^{-1}, α = *2500cm*$^{-1}$, *film thickness = 12.5μm* τ=*0.1s and* $k_{ext}=1\times10^5 s^{-1}$, *R=10Ω, C=*$1.3\times10^{-4}$*F*

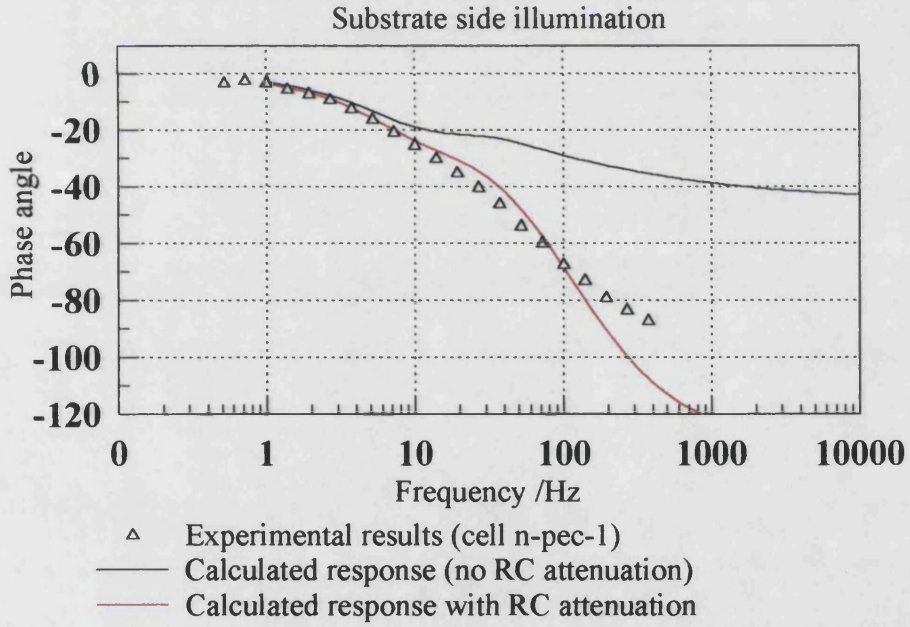

Figure 7.10 *Bode plot of the phase angle of the IMPS signal for substrate side illumination of a dye sensitised solar cell with a transparent counter electrode (cell number n-pec-1). Also shown on the plot is the calculated response including RC attenuation.* i_{sc}=0.2mA, potential =0V, D=3×10^{-5} cm^2 s^{-1}, α = *2500cm*$^{-1}$, *film thickness = 12.5μm* τ=*0.1s and* $k_{ext}=1\times10^5 s^{-1}$, *R=10Ω, C=*$1.3\times10^{-4}$*F*

7.1.4 Intensity dependence of IMPS.

The short circuit current (i_{sc}) is used as a measure of intensity, as it has been shown that for dye-sensitised TiO_2 thin layer cells, i_{sc} is directly proportional to the incident light intensity [1]. Figure 7.11 to Figure 7.16 show results corresponding to a high and low intensity. Figure 7.1 to Figure 7.3 show the response at an intermediate intensity. Measurements at intermediate intensities were also made and the plots obtained underwent the same analysis as the plots above and the parameters of the best fit by eye noted were recorded. This enabled a plot of diffusion coefficient as a function of light intensity to be obtained Figure 7.18.

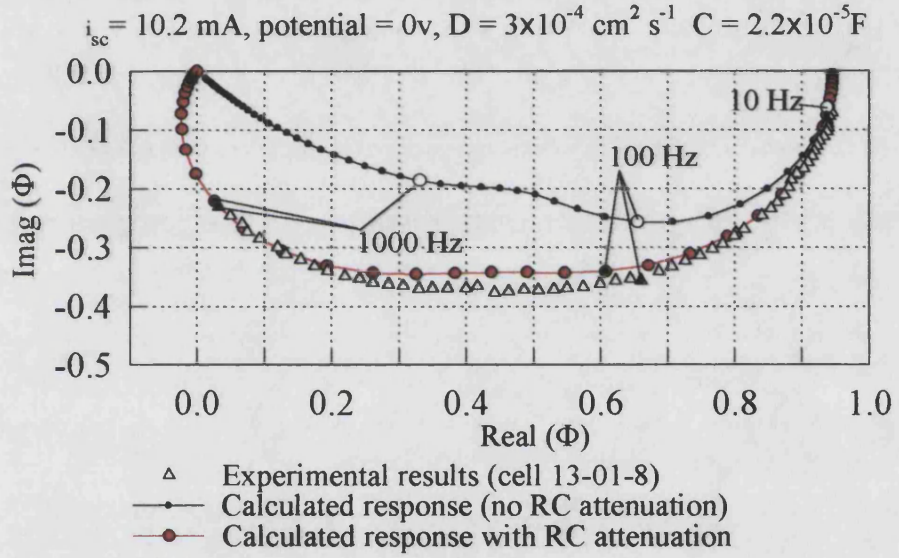

Figure 7.11 *IMPS response for high light intensity. (Substrate side illumination, cell 13-01-8.)* i_{sc}*=10.2mA, potential =0V,* $D=3\times10^{-4}$ *cm*^{2} *s*$^{-1}$, $C=2.2\times10^{-5}$*F,* $\alpha = 2500$*cm*$^{-1}$, *film thickness = 12.5 μm,* $\tau=0.1$*s and* $k_{ext}=1\times10^5$ *s*$^{-1}$, $R=10\Omega$.

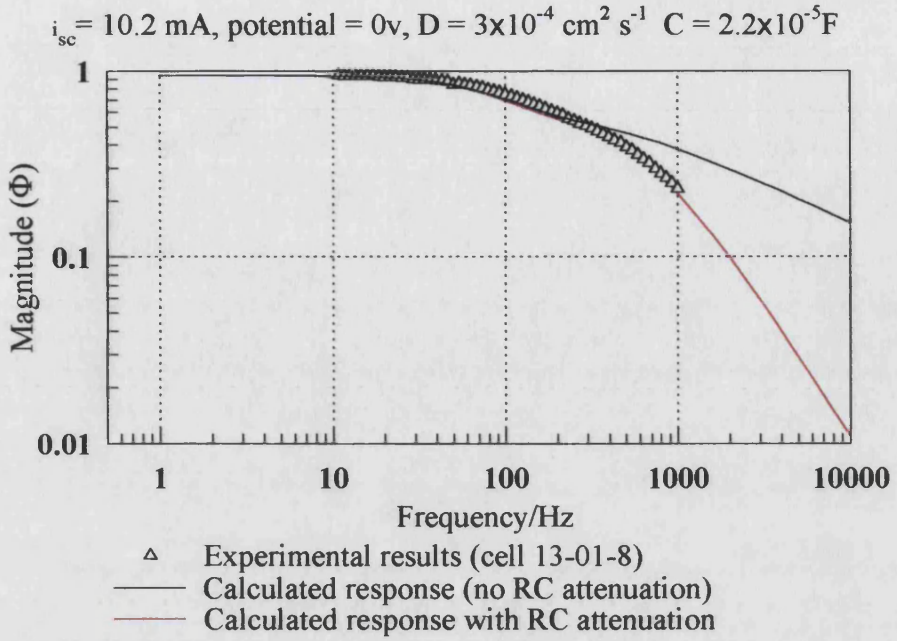

Figure 7.12 *Bode plot of the magnitude of Φ at high light intensity (substrate side illumination, cell 13-01-8.)* i_{sc}*=10.2mA, potential =0V,* $D=3\times10^{-4}$ *cm*^{2} *s*$^{-1}$, $C=2.2\times10^{-5}$*F,* $\alpha = 2500cm^{-1}$*, film thickness = 12.5 μm,* $\tau=0.1s$ *and* $k_{ext}=1\times10^5 s^{-1}$, $R=10\Omega$.

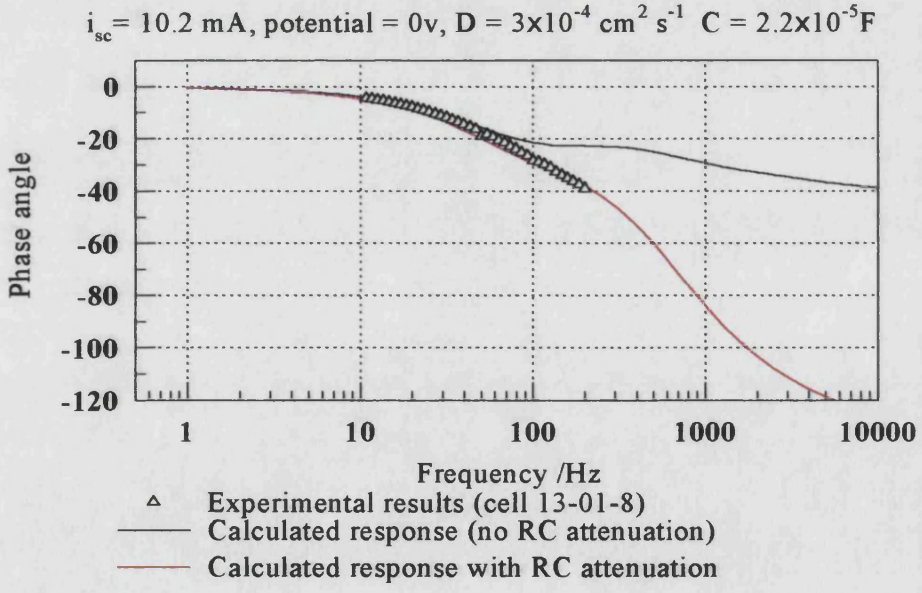

Figure 7.13 *Bode plot of the phase angle of the IMPS response at high light intensity (substrate side illumination, cell 13-01-8.)* i_{sc}*=10.2mA, potential =0V,* $D=3\times10^{-4}$ *cm*^{2} *s*$^{-1}$, $C=2.2\times10^{-5}$*F,* $\alpha = 2500cm^{-1}$*, film thickness = 12.5 μm,* $\tau=0.1s$ *and* $k_{ext}=1\times10^5 s^{-1}$, $R=10\Omega$.

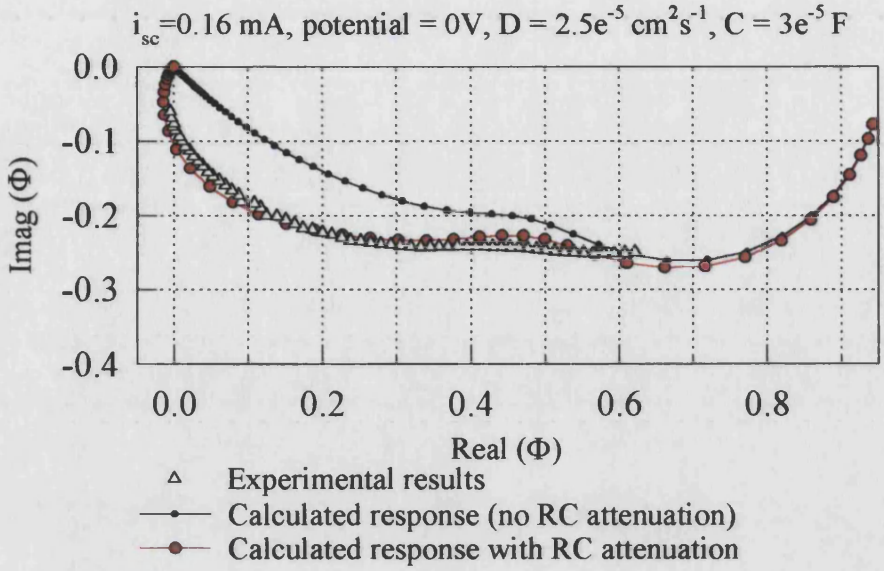

Figure 7.14 *IMPS response at low light intensity (substrate side illumination, cell 13-01-8) i_{sc} =0.16mA, potential =0V, D=1.2×10^{-5} cm^{2}s^{-1}, C=3×10^{-5} F, α = 2500cm^{-1}, film thickness = 12.5 μm, τ=0.1s and k_{ext}=1×10^{5}s^{-1}, R=10Ω*

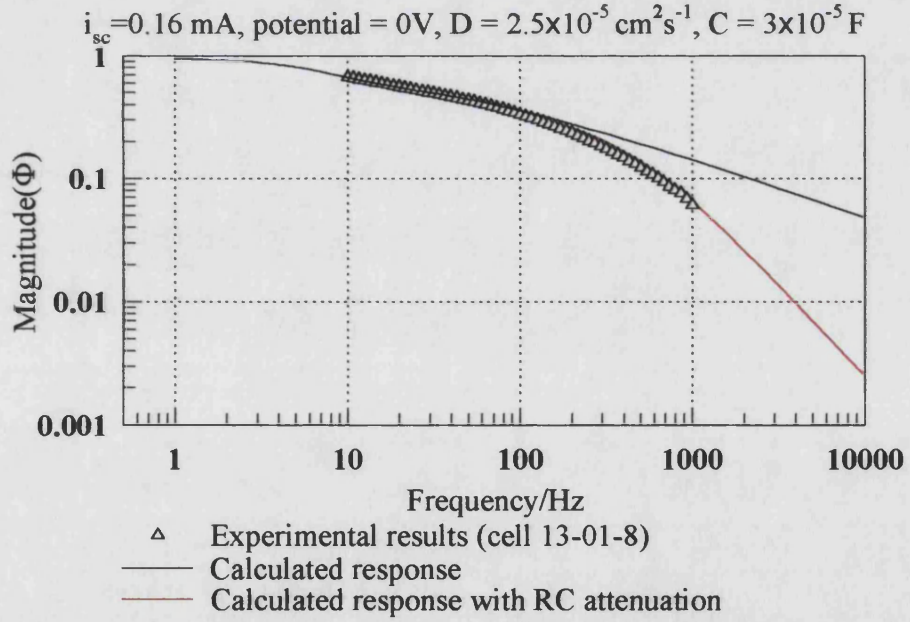

Figure 7.15 *Bode plot of the magnitude of Φ at low light intensity (substrate side illumination, cell 13-01-8) i_{sc} =0.16mA, potential =0V, D=1.2×10^{-5} cm^{2}s^{-1}, C=3×10^{-5} F, α = 2500cm^{-1}, film thickness = 12.5 μm, τ=0.1s and k_{ext}=1×10^{5}s^{-1}, R=10Ω*

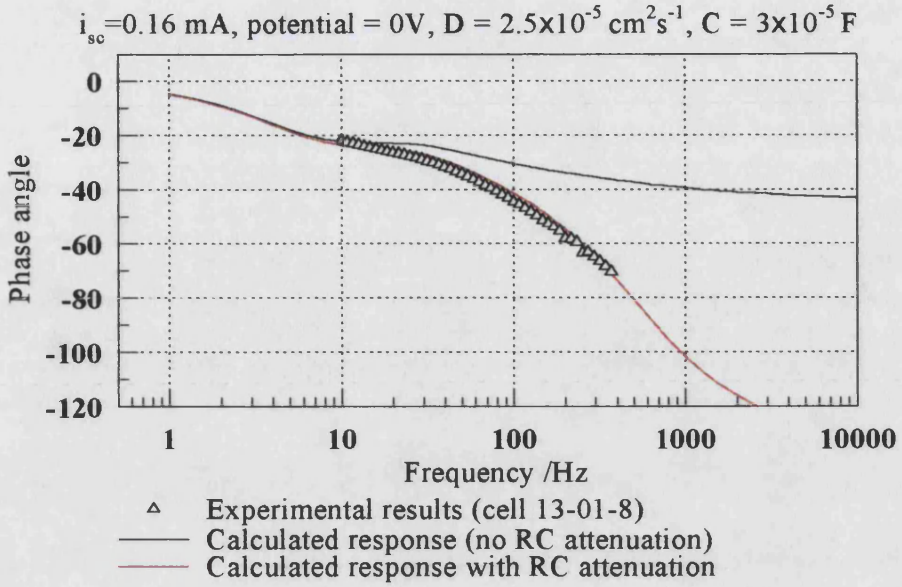

Figure 7.16 *Bode plot of the phase angle of the IMPS response at low light intensity (Substrate side illumination, cell 13-01-8) i_{sc} =0.16mA, potential =0V, D=1.2×10^{-5} cm^{2}s^{-1}, C=3×10^{-5} F, α = 2500cm^{-1}, film thickness = 12.5 μm, τ=0.1s and k_{ext}=1×10^{5}s^{-1}, R=10Ω.*

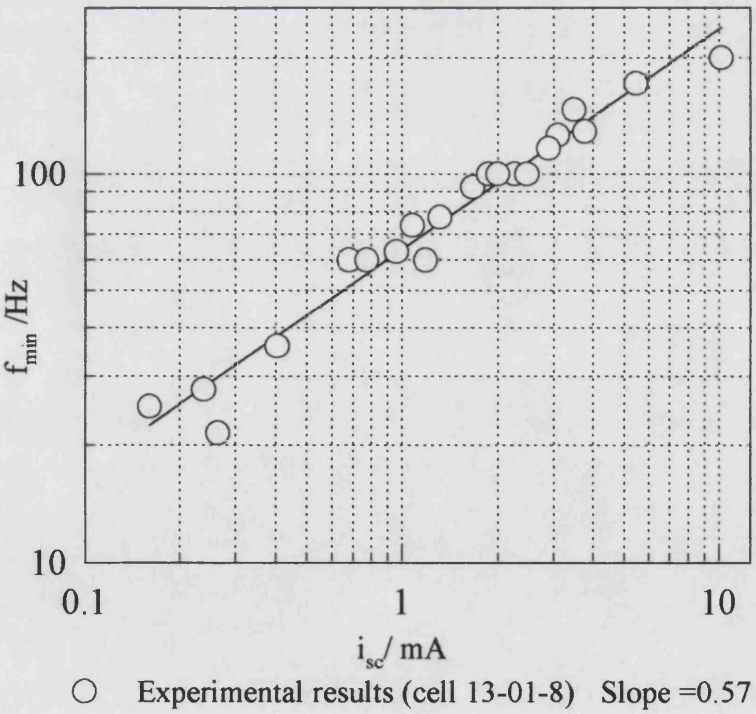

Figure 7.17 *Plot of f_{min} as a function of the short circuit current. (Substrate illumination, $i_{sc} \propto$ light intensity)*

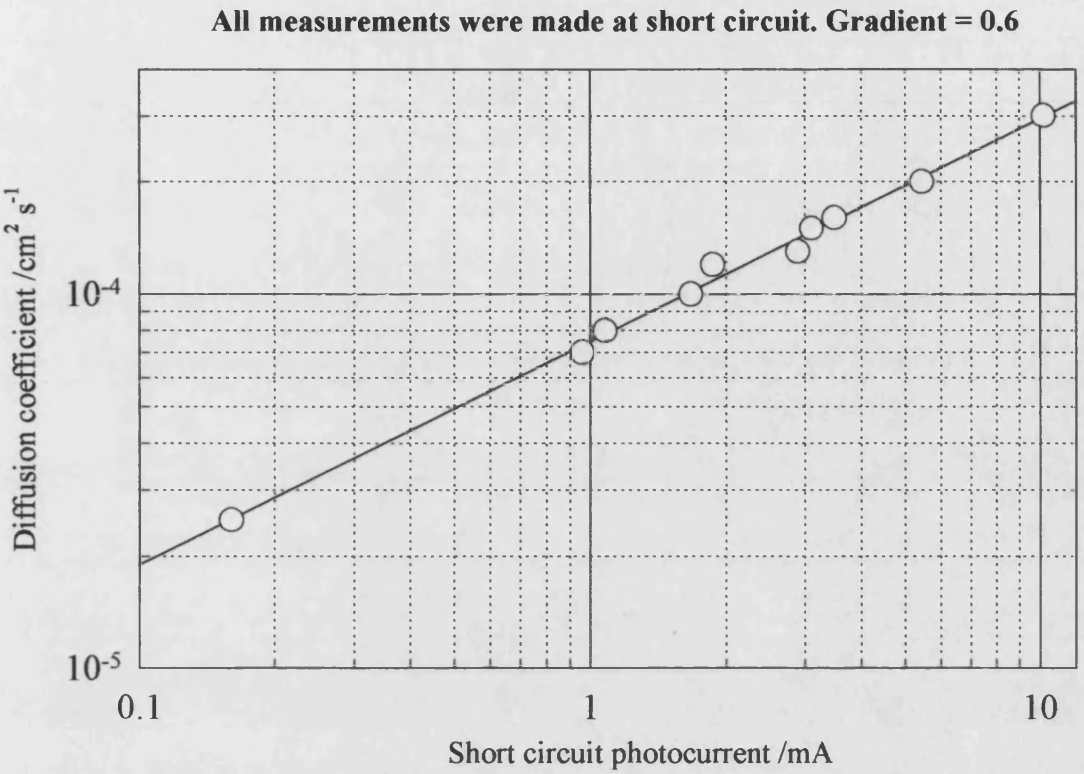

Figure 7.18 *Plot of diffusion coefficient as a function of the short circuit current. (Substrate illumination, $i_{sc} \propto$ light intensity).*

In the plot above (Figure 7.18) D was obtained from the best fit by eye of some of results shown in the preceding plot Figure 7.17. Only some of the points from Figure 7.17 were represented on Figure 7.18 because of the long time consuming fitting procedure.

7.1.5 Potential dependence

As the voltage decreases towards the open circuit voltage (in the region of –0.7V) the IMPS response becomes smaller and more circular. This can be seen in Figure 7.19.

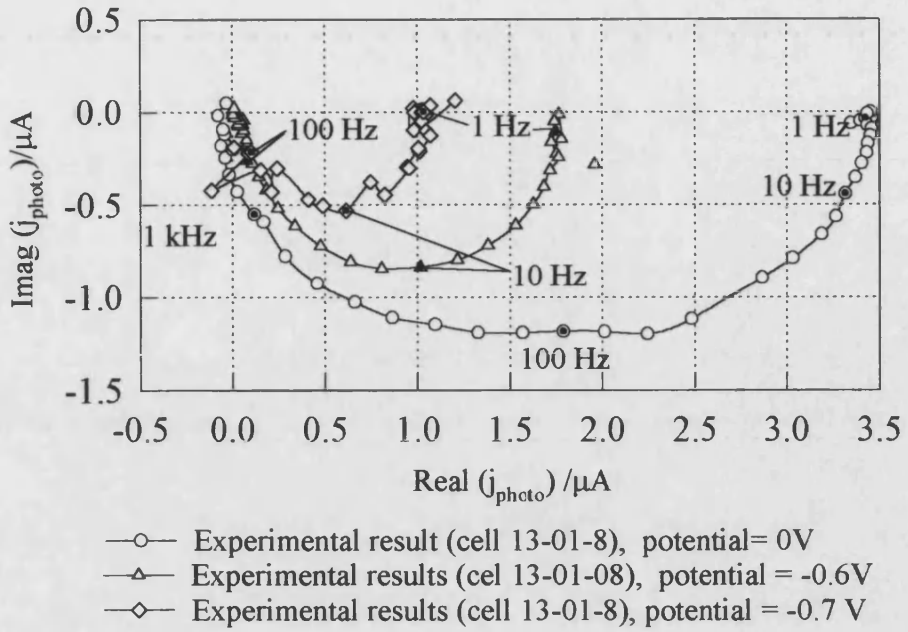

Figure 7.19 *IMPS response at different potentials i_{sc} =6.14 mA.*

The low frequency intercept decreases as the potential approaches open circuit. This is because the back reaction of D^+ with an injected electron increases as the potential approaches open circuit. This process decreases the injection efficiency (η) and is manifest in the decrease in the low frequency intercept of the IMPS response.

To explain the origin of η we need to consider the reactions that are happening. On illumination an electron in injected from the LUMO of the dye into the conduction band of the titanium dioxide:

$Dye^* \rightarrow D^+ + e_{cb}$ Electron injection into conduction band of TiO_2

Next the electron can either back react with D^+ or move through the semiconductor film and be collected. If the electron is collected the dye will be regenerated by the I^-. From this we can make the assumption that the amount of D^+ that reacts with tri-iodide is the same as the amount of electrons injected.

$e_{cb} + D^+ \rightarrow Dye$ Back reaction.

or

$I^- + D^+ \rightarrow Dye$ Regeneration of Dye and electron injection.

The rate of the reactions above can be written as shown below:

Rate of back reaction

$$Rate = k_{back}[D^+][e_{cb}^-] \quad (7.1)$$

Rate of regeneration/injection

$$Rate = k_{back}[D^+][I^-] \quad (7.2)$$

From this we can say that the injection efficiency (η, the number of electrons collected divided by the number of electrons injected) is equal to:

$$\eta = \frac{k_{reg}[I^-][D^+]}{k_{reg}[I^-][D^+] + k_{back}[e_{cb}^-][D^+]} \quad (7.3)$$

$$\eta = \frac{k_{reg}[I^-]}{k_{reg}[I^-] + k_{back}[e_{cb}^-]} \quad (7.4)$$

Under accumulation conditions the process is reported to occur on a nanosecond time scale [2] it is not seen as a separate event only as a decrease in the observed quantum efficiency. η has been shown to be 1 at short circuit and as little as 0.3 at open circuit [3]. The theory for calculating the IMPS response does not incorporate η.

Although the theory for calculating the IMPS plots does not take η into account, it is possible to normalise the actual output by using the following steps. Firstly a simulated best fit by eye response is calculated for the result at short circuit. Secondly, for a result at a potential other than short circuit, the output is rescaled such that the low frequency intercept is the same as that at short circuit. Finally the capacitance is varied until the phase angle of the calculated and real Bode plot is in agreement. Results (complex plane plot, and Bode plots) at three different potentials are shown in Figures 7.20 to Figure 7.28.

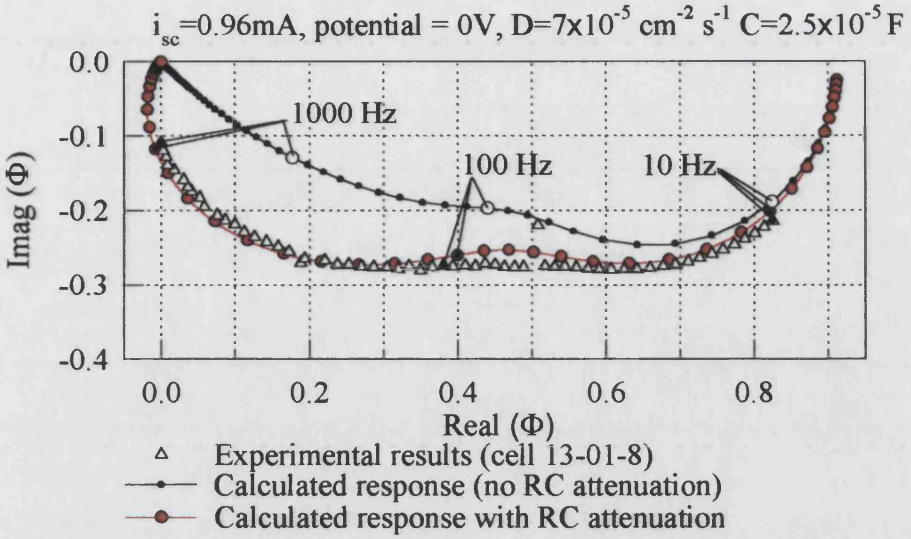

Figure 7.20 *IMPS response for substrate side illumination of a dye sensitised solar cell (cell 13-01-8). i_{sc}=0.96 mA, potential = 0V, D=7×10^{-5} cm^2 s^{-1}, C=2.5e^{-5} F, α = 2500 cm^{-1}, film thickness = 12.5 μm, τ=0.1s and k_{ext}=1×10^{5}s^{-1}, R=10Ω.*

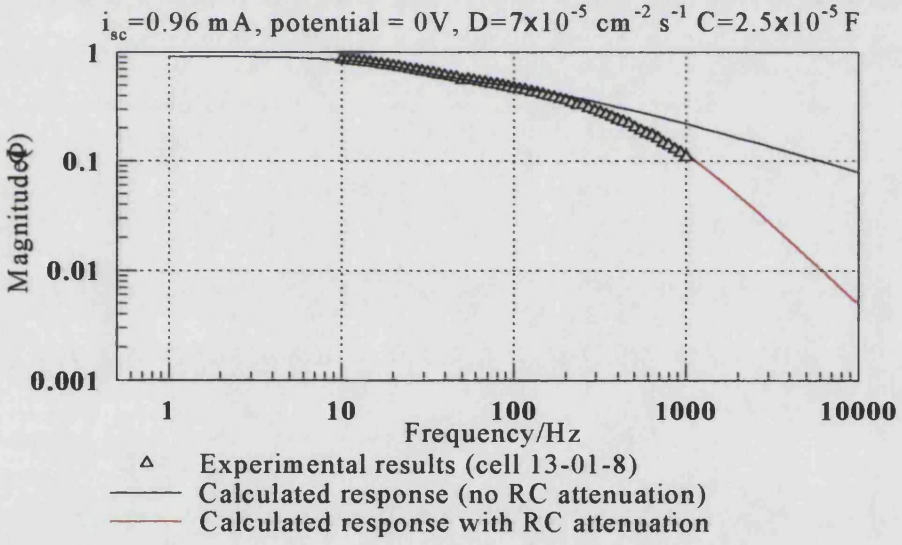

Figure 7.21 *Bode plot of the magnitude of the IMPS signal for substrate side illumination of a dye-sensitised solar cell (cell 13-01-8). i_{sc}=0.96 mA, potential =0V, D=7×10^{-5} cm^2 s^{-1} C=2.5×10^{-5} F, α = 2500cm^{-1}, film thickness = 12.5 μm, τ=0.1s and k_{ext}=1×10^{5}s^{-1}, R=10Ω*

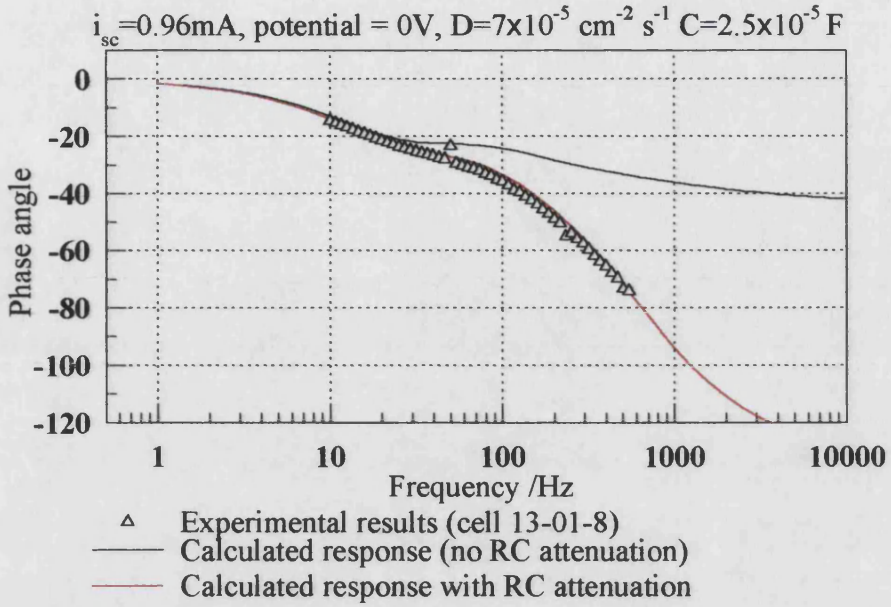

Figure 7.22 *Bode plot of the phase angle for substrate side illumination of a dye-sensitised solar cell (cell 13-01-8). i_{sc}=0.96 mA, potential =0V, D=7×10^{-5} cm^2 s^{-1} C=2.5×10^{-5} F, α = 2500cm^{-1}, film thickness = 12.5 μm, τ=0.1s and k_{ext}=1×10^{5}s^{-1}, R=10Ω.*

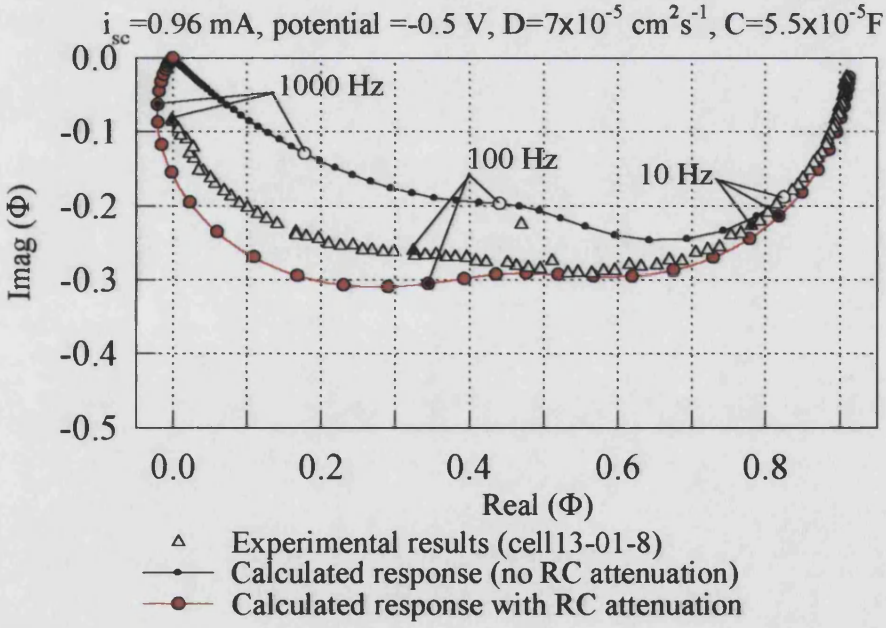

Figure 7.23 *IMPS response for substrate side illumination of a dye sensitised solar cell (cell 13-01-8). i_{sc}=0.96 mA, potential =-0.5V, D=7×10^{-5} cm^2 s^{-1} C=5.5×10^{-5} F, α = 2500cm^{-1}, film thickness = 12.5 μm, τ=0.1s and k_{ext}=1×10^{5}s^{-1}, R=10Ω.*

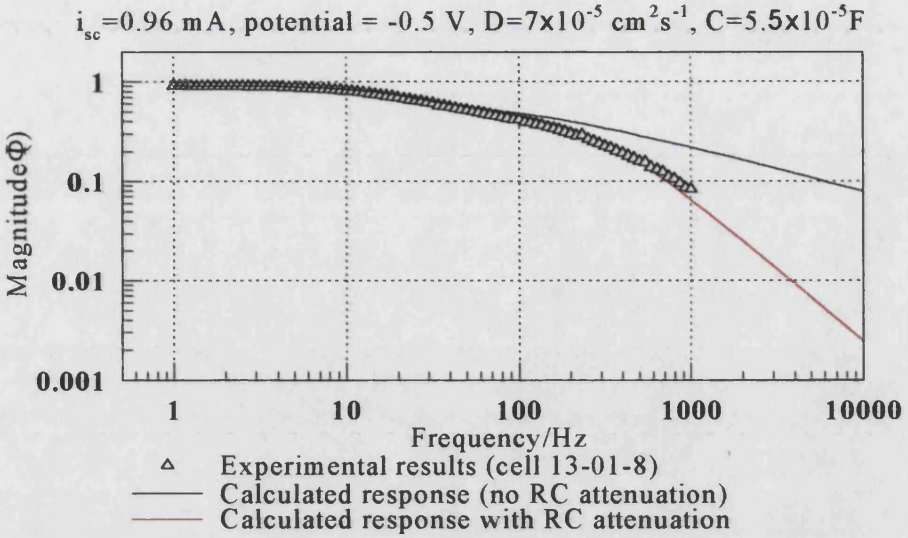

Figure 7.24 *Bode plot of the magnitude (Φ) for substrate side illumination of a dye sensitised solar cell (cell 13-01-8). i_{sc}=0.96mA, potential=-0.5V, D=7×10^{-5}cm^{2}s^{-1} C=5.5×10^{-5}F, α = 2500cm^{-1}, film thickness = 12.5μm, τ=0.1s and k_{ext}=1×10^{5}s^{-1}, R=10Ω.*

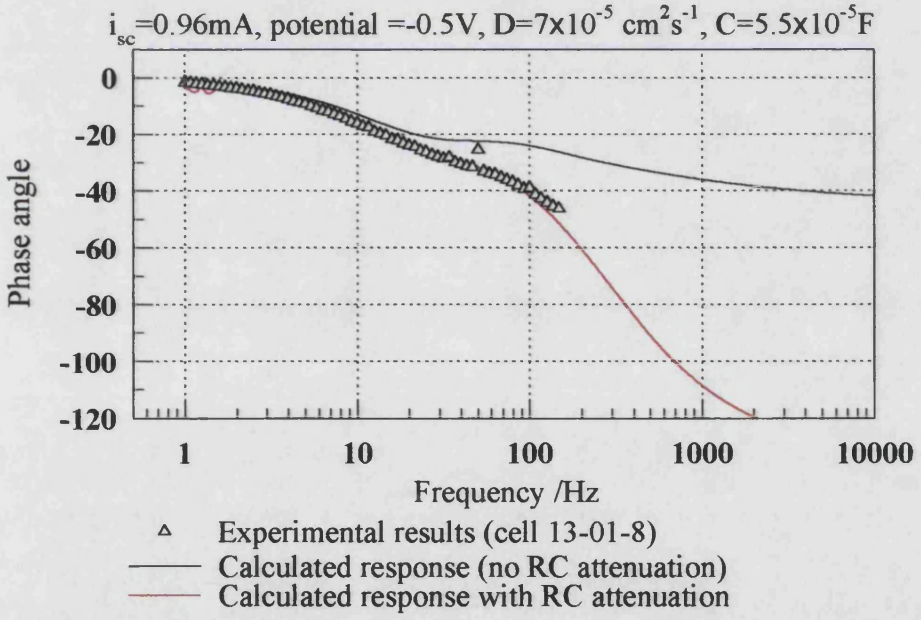

Figure 7.25 *Bode plot of the phase angle for substrate side illumination of a dye-sensitised solar cell (cell 13-01-8). i_{sc}=0.96mA, potential =-0.5V, D=7×10^{-5} cm^2 s^{-1} C=5.5×10^{-5}F, α = 2500cm^{-1}, film thickness = 12.5 μm, τ=0.1s and k_{ext}=1×10^{5}s^{-1}, R=10Ω.*

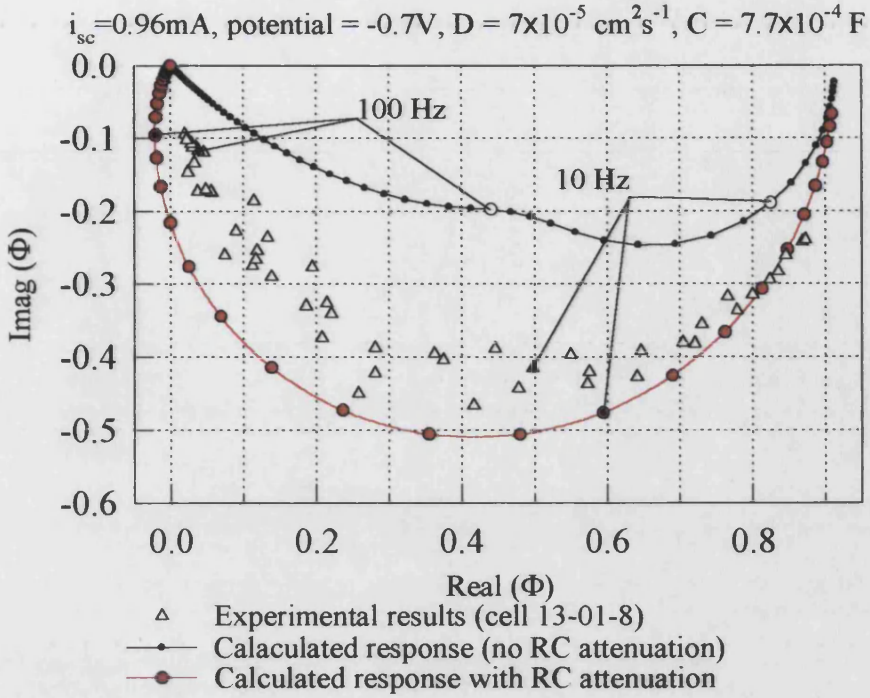

Figure 7.26 *IMPS response for substrate side illumination of a dye sensitised solar cell (cell 13-01-8). i_{sc}=0.96mA, potential =-0.7V, D=7×10^{-5} cm^2 s^{-1} C=7.7×10^{-4}F, α = 2500cm^{-1}, film thickness = 12.5μm, τ=0.1s and k_{ext}=1×10^{5}s^{-1}, R=10Ω.*

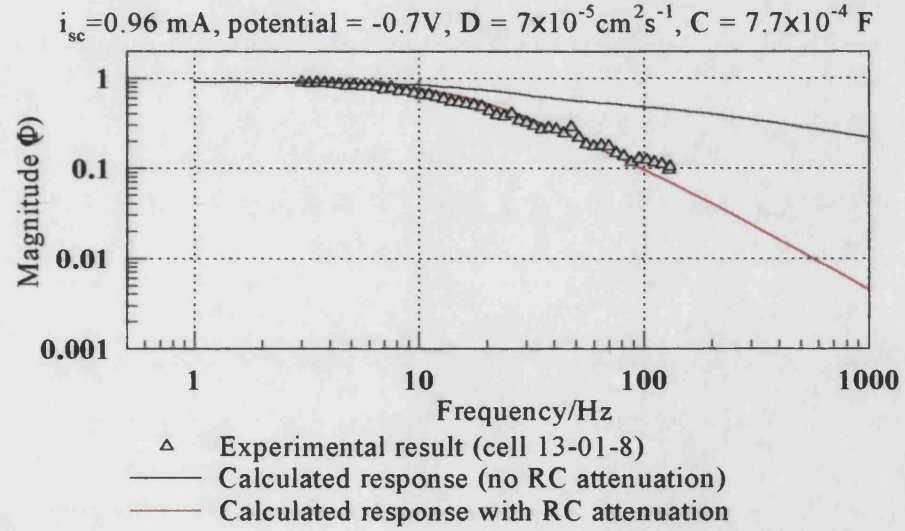

Figure 7.27 *Bode plot of the magnitude (Φ) for substrate side illumination of a dye sensitised solar cell (cell 13-01-8). i_{sc}=0.96mA, potential =-0.7V, D=7×10^{-5}cm^{2}s^{-1} C=7.7×10^{-4}F, α=2500cm^{-1}, film thickness =12.5μm, τ=0.1s and k_{ext}=1×10^{5}s^{-1}, R=10Ω.*

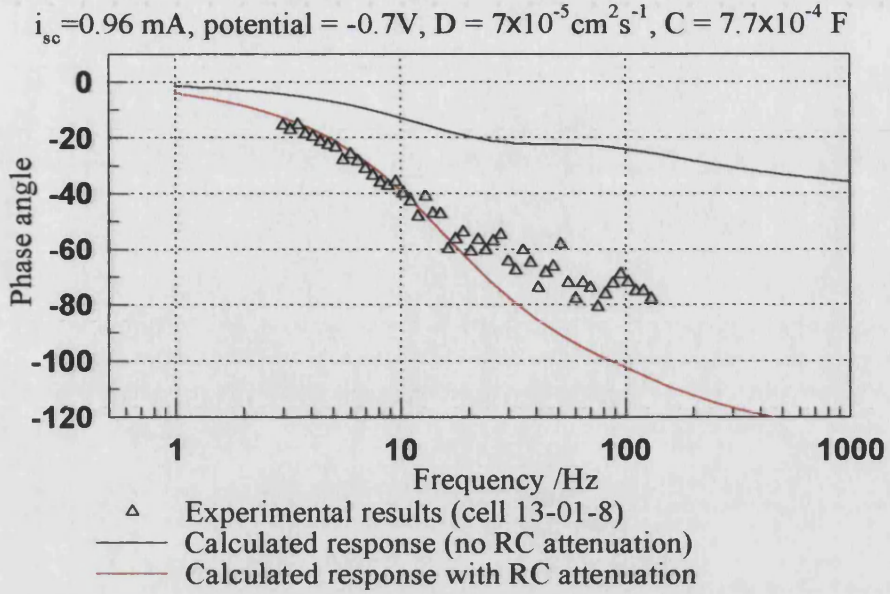

Figure 7.28 *Bode plot of the phase angle for substrate side illumination of a dye-sensitised solar cell (cell 13-01-8). i_{sc}=0.96mA, potential =-0.7V, D=7×10^{-5} cm^2 s^{-1} C=7.7×10^{-4}F, α = 2500cm^{-1}, film thickness = 12.5μm, τ=0.1s and k_{ext}=1×10^{5}s^{-1}, R=10Ω.*

It should be noted in the graphs of different potential that the diffusion coefficient at 0V remains the same at all potentials.

Figure 7.29 shows how f_{min} varies with potential at 2 intensities. This graph shows that at potentials near to open circuit there is little dependence of f_{min} on the intensity.

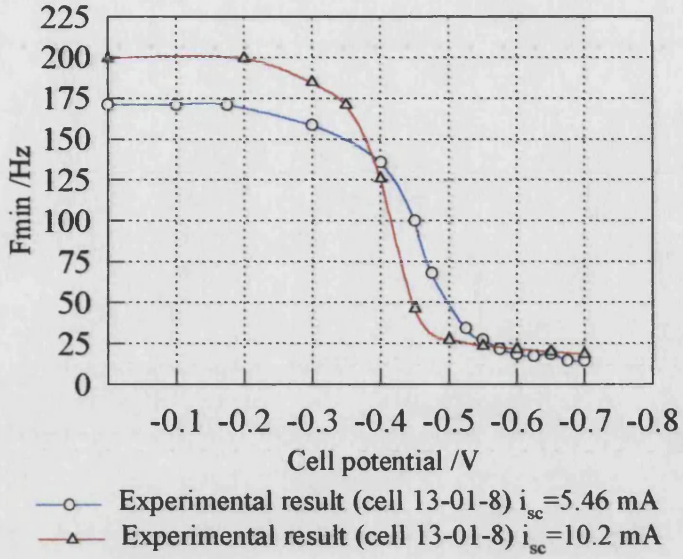

Figure 7.29 *Experimental results taken from IMPS plots showing the potential dependence of f_{min} at two intensities.*

The capacitance calculated from the IMPS measurements and the capacitance derived from the EIS measurements are shown in Figure 7.30.

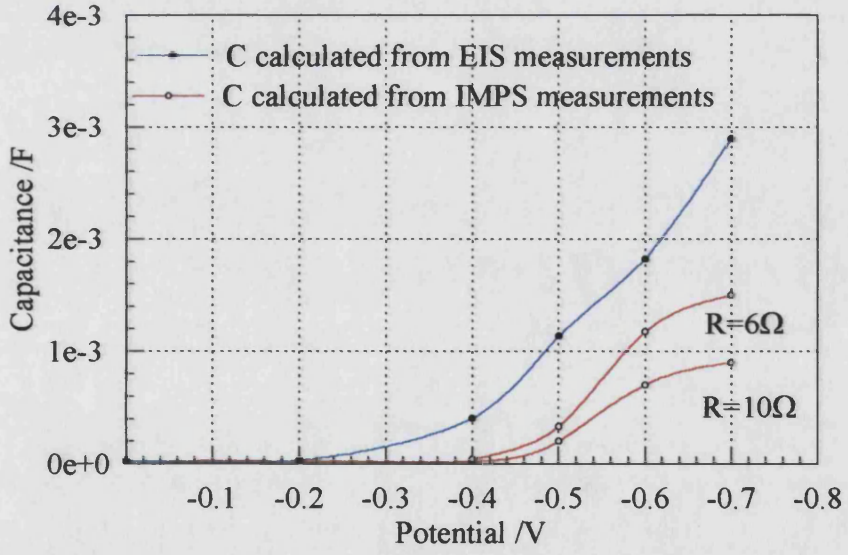

Figure 7.30 *Plot comparing the capacitance calculated from the IMPS and EIS measurements. cell (13-01-8), i_{sc} =5.5mA.*

It can be seen that the capacitance changes by several orders of magnitude as V_{oc} is approached. The values of R used in the IMPS calculations were 10Ω and 6Ω. The EIS

measurements give values of R less than 10Ω this would explain the fact that the EIS measurements show higher capacitances. As we are dealing with a thin film with contacts on the end, a distributed resistance is present and thus assuming a set value for the resistance is not ideal. Non uniform illumination may introduce a range of capacitances and resistances present in different parts of the film, this will lead to an average capacitance and resistance for the whole.

7.2 IMVS results

IMVS measurements have been used to determine the intensity dependence of the electron lifetime (τ_n). It is determined from ω_{min} of the complex plane IMVS response. The electron lifetime at a particular light intensity can be combined with the diffusion coefficient (calculated from the IMPS response) at the same light intensity. The diffusion length (L_n) of the electrons can then be calculated. For the light intensities investigated by both IMPS and IMVS the diffusion length is greater than the film thickness. Typical values for a cell of film thickness 12.5μm the diffusion length is 17μm (under approximately 1mA DC illumination). This indicates that at open circuit the majority of the photoinjected electrons are collected at the back contact and hence the cell has a high conversion efficiency.

7.2.2 Intensity dependence of IMVS

The short circuit current (i_{sc}) is used as a measure of intensity. Figure 7.31 shows the response at an intermediate intensity while Figure 7.32 and Figure 7.33 show results corresponding to a high and low intensity. Measurements at intermediate intensities were also made and the results used to construct the graph shown in Figure 7.34.

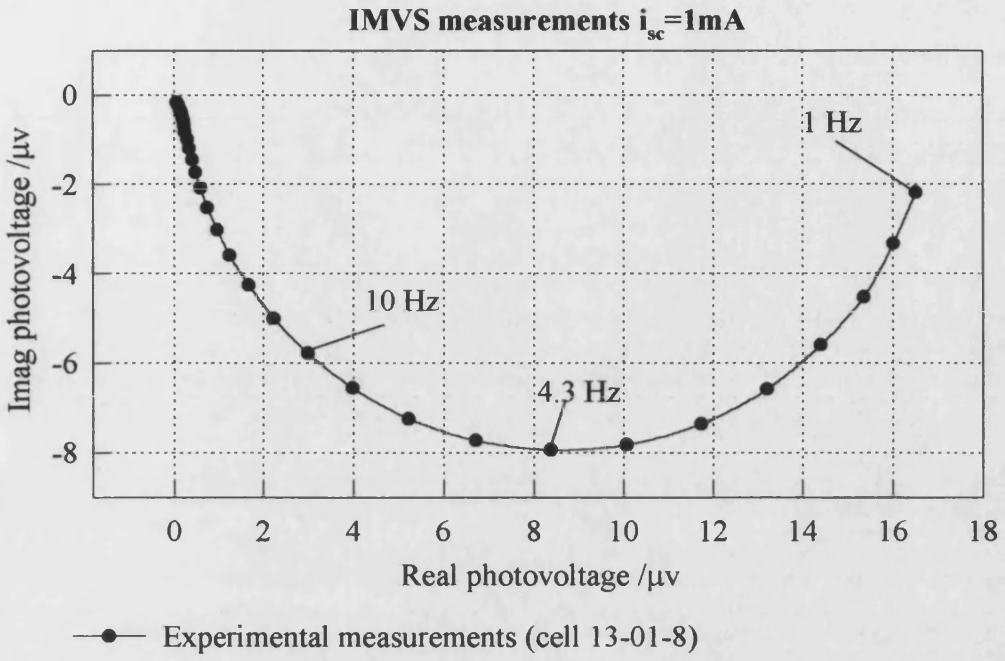

Figure 7.31 *IMVS response for substrate side illumination of a dye sensitised solar cell i_{sc}=1mA (cell number 13-01-8).*

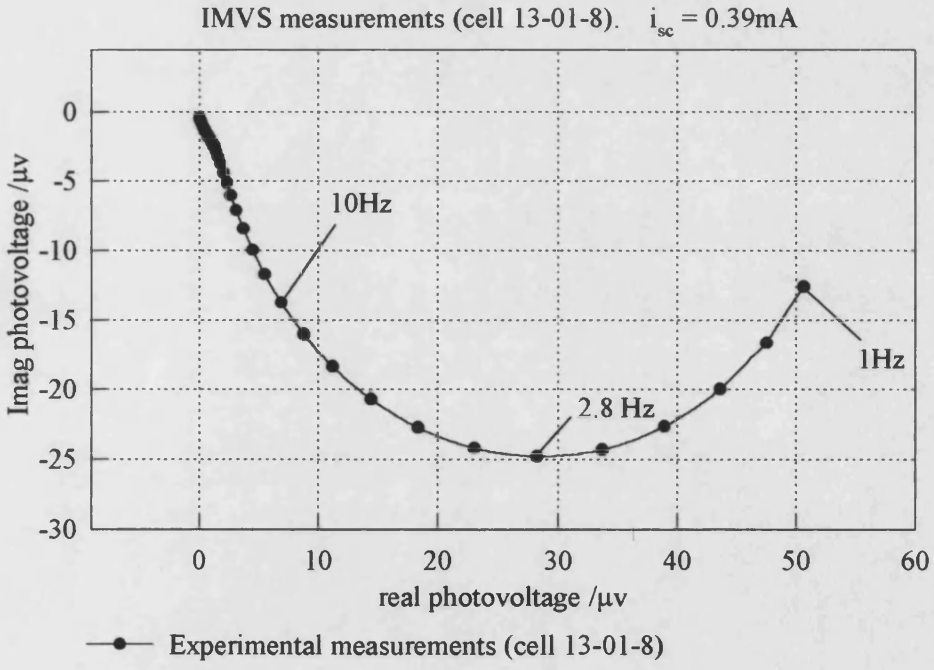

Figure 7.32 *IMVS response for substrate side illumination i_{sc}=0.39 mA (cell 13-01-8).*

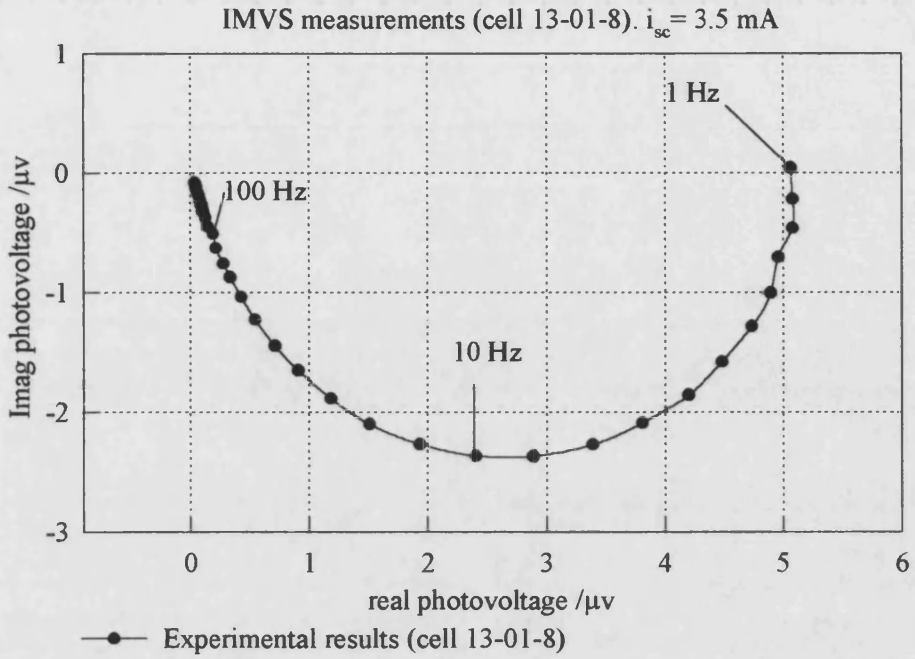

Figure 7.33 *IMVS response for substrate side illumination i_{sc}=3.5 mA (cell 13-01-8).*

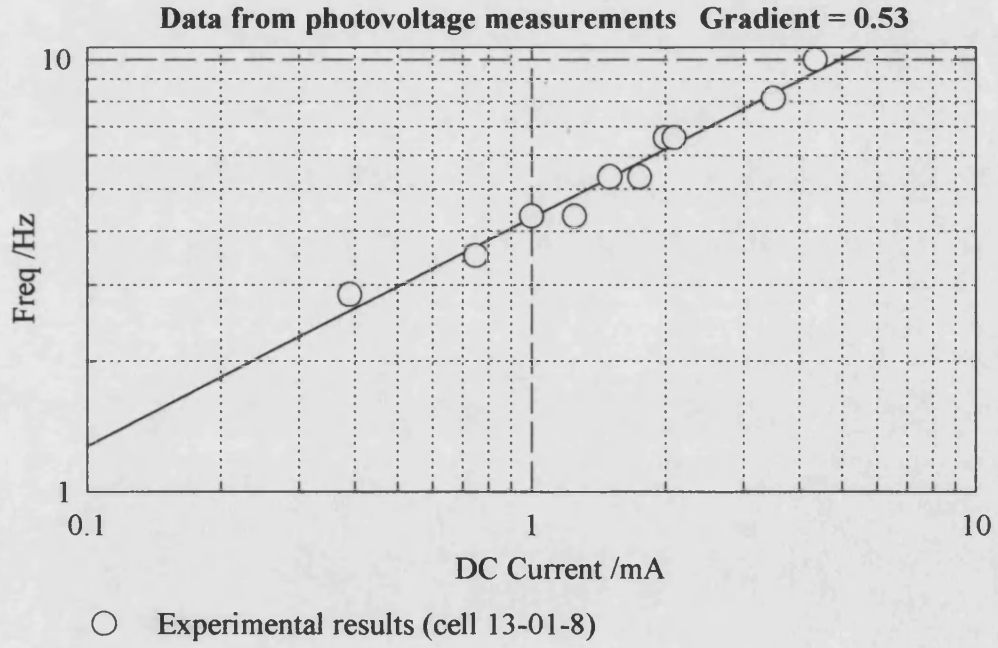

Figure 7.34 *Plot of f_{min} (IMVS) as a function of the short circuit current. (Substrate side illumination, $i_{sc} \propto$ light intensity cell 13-01-8))*

7.3 Discussion

The use of i_{sc} as a measurement of light intensity

The short circuit current (i_{sc}) has been used in preference to the incident light intensity. This gives a relative rather than absolute value of the light intensity. This method gives a more accurate measurement of the light that is actually absorbed by the cell rather than the incident light that may be reflected.

Comparison of the theoretical response and the experimental response for the IMPS plots

Experimental results were obtained for both substrate side and electrolyte side illumination. Fitting the Bode plots was found to be far more satisfactory than fitting the complex plane plot. The phase angle is the most sensitive to any change. In order to obtain a reasonable fit it is essential to include the RC attenuation in the theoretical calculations. For substrate side illumination the fitting was very satisfactory (c.f. Figure 7.3) for electrolyte side illumination the fitting was not quite so good, but in general the correct trend is predicted.

Occasionally scatter is observed on the results at low and high frequency (Figure 7.9). At low frequencies the scatter is attributed to the long acquisition times needed for the measurements. At high frequencies scatter is attributed to the current in this region being very small, the noise therefore has a greater influence on the results *i.e.* the signal to noise ratio is lower. For measurements near to open circuit (*i.e.* Figure 7.28) the current is much smaller than at short circuit and therefore the signal to noise ratio will be lower, hence more scatter will be evident on these measurements.

Fitting deviations may arise from the fact that the RC component is not a simple RC circuit as we have assumed in our calculations, it is in fact a distributed sheet resistance. Secondly the illumination may not be uniform and hence the time constant for diffusion will not be constant. If the illumination is not uniform different areas of the film will have different diffusion coefficients, this will lead to a broadening of the observed IMPS plot and fitting will be less accurate. This would seem a plausible explanation especially as the fitting of IMPS plots from the electrolyte side illumination has in general more deviation. The illumination from the electrolyte side is expected to be

more non-uniform than the substrate side illumination, because the light has more opportunity to be defracted or reflected as it must pass through the platinum coated glass and electrolyte before reaching the TiO_2 layer.

The potential dependence of the experimental results

As the potential approaches the open circuit voltage (V_{oc}) the real component of Φ decreases, the IMPS plot becomes more semicircular and ω_{min} decreases. As noted previously, at monochromatic conversion efficiencies close to 1, both D and τ can influence ω_{min}, however this does not account for the change in shape of the IMPS plot and at the same intensity both D and τ are constant. The best fit by eye results show that by changing only the capacitance it is possible to fit results at all potentials. This indicates that near to V_{oc} the capacitance dominates the IMPS response. The values obtained for the capacitance in these calculations agree with the capacitance obtained from the impedance spectroscopy results.

The decrease in the real component of the photocurrent is due to the decrease in the net electron injection efficiency of the dye into the TiO_2. At potentials near to V_{oc} the reaction of electrons from the TiO_2, with the oxidised state of the dye, increases such that the net electron injection efficiency is 0.3 at open circuit compared to 1 at short circuit [3]. This value of net electron injection efficiency (η) can be used to scale the IMPS output.

The extraction rate constant k_{ext} is also noted to make the plot more semicircular and to decrease ω_{min}, any effect that may be seen due to this is likely to be hidden by the large capacitance. At the open circuit voltage ω_{min} becomes intensity independent, this indicates a uniform distribution of traps within the TiO_2 film.

Intensity dependence of the diffusion coefficient of the IMPS measurements

Diffusion is a means of transport of a molecule, ion or electron through a substrate. For the purpose of this discussion we shall assume it is an electron. Diffusion assumes that the electron can move in any direction from its position and is not influenced by an external electric field. It occurs to smooth out inhomogenities in the concentration gradient of the electrons. If we take an electron at a particular point it can move in any direction by hopping to an adjacent molecule. Once in its new position it can hop again

to any adjacent molecule including back to where it came from this sometimes referred to as 'random walk'. The probability of the time constant of the hop (τ_{hop}) will produce a Gaussian distribution, this is known as normal diffusion and is given by the following equation:

$$D = \frac{\delta x^2}{\tau_{hop}} \qquad (7.1)$$

Here: D = Diffusion coefficient

δx = Distance of hop

τ_{hop} = Time constant for hop (lifetime)

In our case we have traps present on the TiO_2 surface, which trap electrons as they are diffusing. This means that the distribution of lifetimes will not be gaussian. The residence time that the electrons are in the traps depends on the depth of the traps. The deeper the trap the longer the electron will stay there. This is shown in Figure 7.35

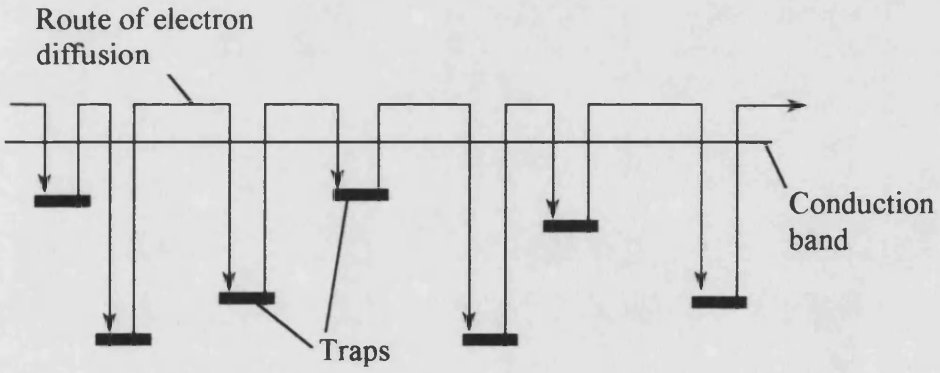

Figure 7.35 *Diagram of the conduction band of TiO_2 showing the route of electron transport when traps are present.*

The release rate (R_{rate}) of the electrons in the traps is given by the following equation:

$$R_{rate} = \nu e^{\frac{-\Delta E}{kT}} \qquad (7.2)$$

Here: ν = Lattice vibrational frequency

ΔE = Trap depth

k = Boltzman constant

T = Temperature

The result of the trap diffusion and the trap filling and releasing is that the distribution of lifetimes is no longer gaussian. The diffusion in this case it termed dispersive.

If the light is on some of the traps within the conduction band will be filled giving a steady state photocurrent. The level that the traps are filled to is the quasi Fermi level. The deeper traps are filled, therefore any electrons diffusing through the film will only get caught in the unfilled low-level traps see Figure 7.36.

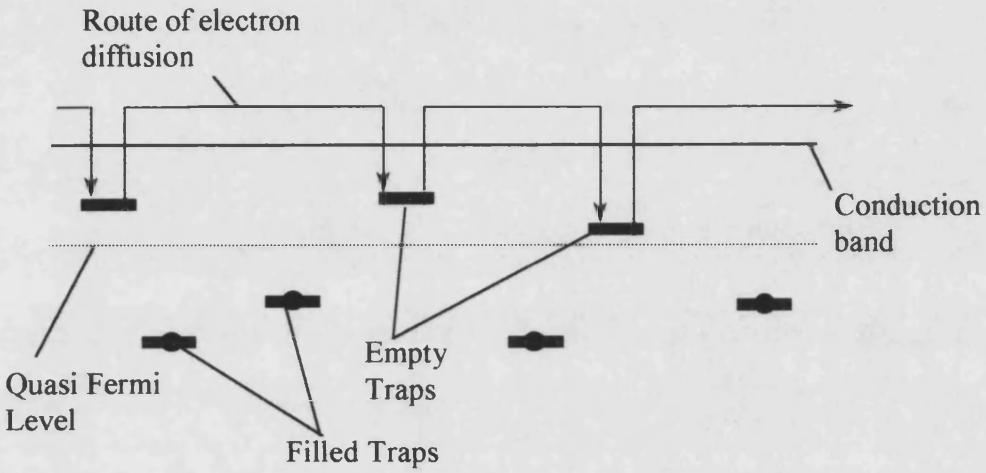

Figure 7.36 *Diagram of the conduction band of TiO_2 showing the route of electron transport under illumination when traps are present and the quasi Fermi level.*

It should be noted that in comparison to Figure 7.35 the same number of traps are present, however due to some of the traps being filled there are fewer traps for the diffusing electron to get caught in. This means the electron should move through the film faster, (*i.e.* high diffusion coefficient). If the illumination intensity is low it will take longer for the electrons to diffuse through the film as there are more traps unfilled.

If one were to illuminate with a high light intensity and then remove the light source (as is the case with pulsed experiments) the number of filled traps would decrease with respect to time. This would cause the time constant for the trapping to increase and consequently the diffusion coefficient would decrease. This causes major problems with pulsed experiments as the diffusion coefficient is constantly changing with time and is

therefore highly non-linear. IMPS avoids this complication by employing bias light that is used alongside the modulated light. The bias light has an intensity much greater than the intensity of the modulated light and hence under illumination the quasi Fermi level is determined by the bias light. The modulated light does not change the quasi Fermi level appreciably. Under these conditions the Diffusion coefficient will be constant and determined by the light intensity.

If the diffusion rate is determined by the trapping/detrapping of electrons in the free traps in the conduction band, then the diffusion coefficient will be proportional to the light intensity. The diffusion coefficients calculated from the experimental results in Figure 7.18 confirm that the effective diffusion coefficient is proportional to light intensity. The gradient is determined by the trap distribution.

The plots of intensity dependence versus ω_{min} and D_n give gradients near to 0.5, which is indicative of light dependent trap filling. [4]. Ideally both the plots should show the same gradient as they both use the same experimental data. The deviation is most likely to be due to the fitting by eye used to obtain the diffusion coefficient. It should be noted that when the lifetime of electrons (τ) in the nanocrystalline cell is large, ω_{min} is only dependent on the diffusion coefficient (D). It can be justified that the electron lifetime is long due to the high quantum efficiency observed with these cells. When obtaining the best fit by eye, the electron lifetime was chosen such that ω_{min} was insensitive to change.

The diffusion coefficient could also be measured by the Monte Carlo method where electrons are put into the film and allowed to hop between traps. This method allows the definition of the distribution of residence times that produce an apparent diffusion coefficient.

Intensity dependence of the IMVS response

The IMVS response shows that the τ_n is dependent on the light intensity. From the graph in Figure 7.34 it is noted that as the illumination intensity increases ω_{min} increases, as ω_{min} is inversely proportional to the lifetime of the electron this means that the electron lifetime decreases as the illumination intensity increases. Once again let us

consider the trap distribution within the conduction band (see Figure 7.36). As stated previously at high light intensity more traps are filled and less are available for the diffusing electrons to be trapped in this case there are more free electrons in the conduction band than at a lower intensity. Free electrons in the conduction band are available to back react with the tri-iodide ions in solution. If there are a high percentage of free electrons the probability of undergoing a reaction with tri-iodide is increased and this will lower the lifetime of the electrons. The model would appear to assume that the electrons could only back react with the tri-iodide ions if they are free to move.

This is not the case with the model created by Schlichthorl et al [5]. They assume that all the electrons injected under illumination eventually react with the iodide, and thas no current in the external circuit is produced. They do not take into account that once injected the electrons may back react with the oxidised state of the dye (this was discussed earlier and the term η the injection efficiency was defined). This factor is important when measuring at open circuit because around 70% of the injected charge back reacts. The authors deduce that only the electrons that are trapped at the surface, which produce the so-called 'surface state' capacitance are able to react with the tri-iodide. However the surface state capacitance includes not only those electrons trapped at the surface but also all electrons that are located with traps within the film. Whilst an electron is located within a trap it may back react, however as mentioned previously, electrons move through the film by a process of trapping and detrapping, the longer an electron is trapped for the higher the probability of recombination.

The diffusion length (L_n) can be calculated from the following equation:

$$L_n = \sqrt{D_n \tau_n} \qquad (7.3)$$

The table below (Figure 7.37) shows the calculated diffusion length from the IMPS and IMVS data.

Intensity	Dn calculated from IMPS	f_{min} (IMVS)	τ_n calculated from IMVS	L_n /cm
0.39	4.5×10^{-5}	2.8481	0.0559	1.586×10^{-3}
0.75	6.2×10^{-5}	3.5122	0.0453	1.676×10^{-3}
1.08	8.0×10^{-5}	4.3288	0.0367	1.700×10^{-3}
1.67	1.0×10^{-4}	5.3386	0.0298	1.720×10^{-3}
1.87	1.2×10^{-4}	6.57	0.0242	1.705×10^{-3}
4.36	1.9×10^{-4}	10.0	0.0159	1.739×10^{-3}

Figure 7.37 *Table of data used to calculate L_n from the IMPS and IMVS response.*

Figure 7.38 shows the logarithmic graph of the calculated L_n values. It should be noted that there is only a slight dependence of L_n on the intensity and this slight dependence is the square root of the difference between the gradients of the graphs in Figure 7.18 and Figure 7.34. The equations below show how the relationship between the intensity and the diffusion length are derived.

$$D_n \propto_{i\,sc}^{0.6} \qquad (7.4)$$

$$\tau_n \propto i_{sc}^{-0.53} \qquad (7.5)$$

Combining the above two equations with equation (7.3) it is possible to see that:

$$D_n\tau \propto i_{sc}^{0.07} \qquad (7.6)$$

hence:

$$L_n = \sqrt{D_n\tau} \propto i_{sc}^{0.035} \qquad (7.7)$$

The results obtained from the IMPS and IMVS measurements show a gradient of 0.0354 which is in strong agreement with the predicted value above. It should be noted at this point that the conversion efficiency of a cell is independent of light intensity.

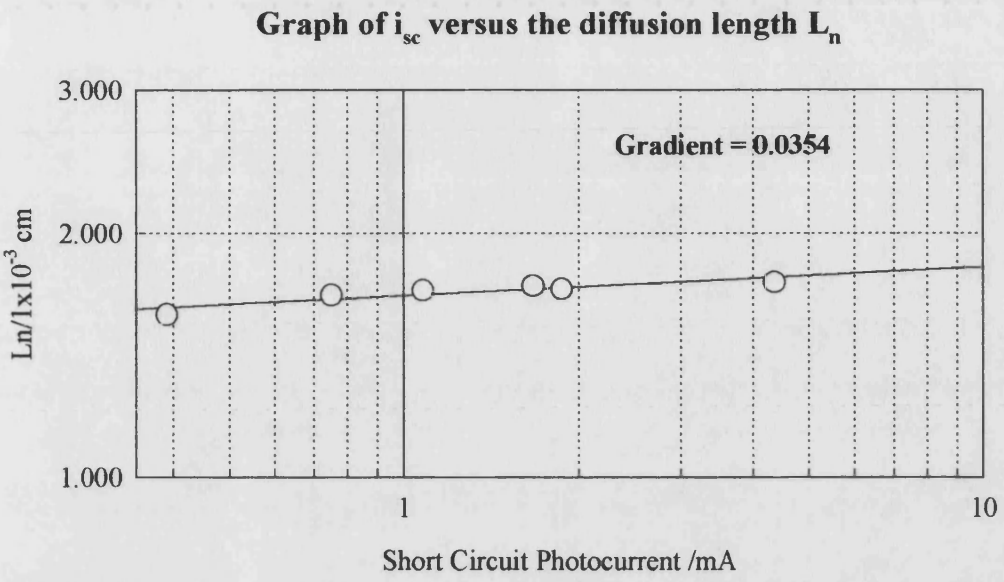

Figure 7.38 *Logarithmic graph of the diffusion length as a function of the light intensity for cell 13-01-8.*

For a cell to work efficiently the diffusion length should be greater than the film thickness (this was discussed in chapter three) so that the maximum amount of electrons will be collected. In the above cell the calculated value of the diffusion length is between 1.5 $\times 10^{-3}$ cm and 1.8 $\times 10^{-3}$ cm (15-18μm). The film thickness of the cell used for the experiments was 1.25e^{-3} cm (12.5μm). A plot of the IPCE as a function of the diffusion length is shown below for both substrate and electrolyte illumination.

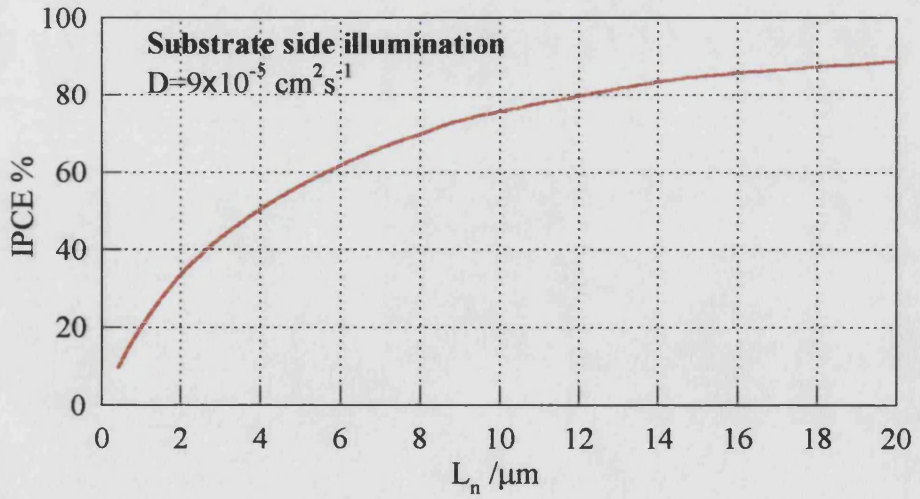

Figure 7.39 *Calculated plot showing the IPCE as a function of the diffusion length for substrate side illumination. $D=9\times10^{-3}$ cm^{2}s^{-1}, $\alpha=2500$cm^{-1}, $k_{ext}=1\times10^{-5}$s^{-1} potential =0V, film thickness = 12.5μm. Value of D determined at short circuit at when $i_{sc}=3.07$mA.*

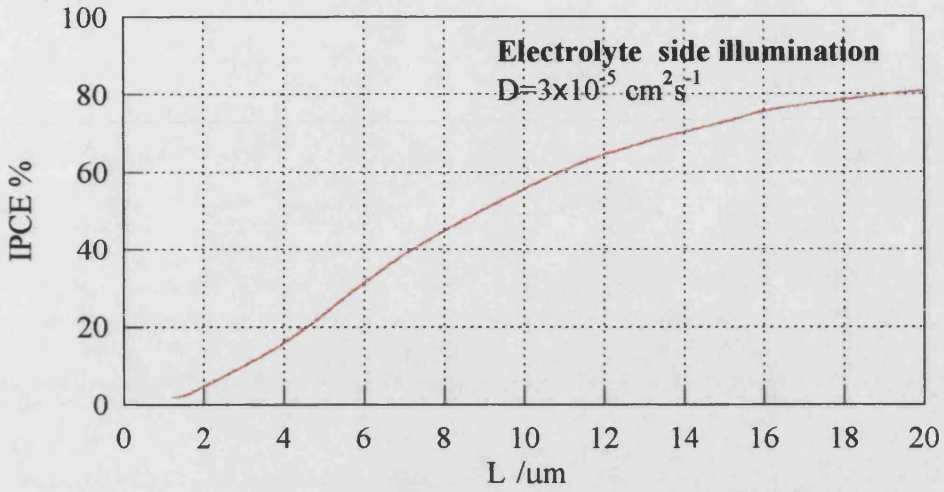

Figure 7.40 *Calculated plot showing the IPCE as a function of the diffusion length for electrolyte side illumination.* $D=3\times10^{-3}$ cm^2s^{-1}, $\alpha=2500cm^{-1}$, $k_{ext}=1\times10^{-5}s^{-1}$ *potential =0V, film thickness = 12.5μm. Value of D determined at short circuit when* $i_{sc}=0.2$ *mA from experimental results.*

In summary, if the diffusion length is greater than or comparable to the cell thickness then the IPCE will be high. If the IPCE is high then the cell is efficient. As the diffusion length of the cells we have used in the experiments is greater than the film thickness, it is possible to say that the cells used are high performance excellent cells.

7.4 References

1. Wijayantha, K. G. U. *Personal communication*, The University of Bath

2. Haque, S. A.; Tachibana, Y.; Klug, D. R.; Durrant, J. R. *J. Phys. Chem. B* **1998**,*102*, 1745

3. Franco, G.; Gehring, J.; Peter, L. M.; Ponomarev, L. M.; Uhlendorf, I. *J. Phys. Chem. B* **1999**, *103*, 692

4. Cao, F.; Oskam, G.; Meyer, G. J.; Searson, P. C. *J. Phys. Chem.* **1996**, *100*, 17021

5. Frank, A.J.; Huang, S. Y.; Schlichthörl, G.; Sprague, J. *J. Phys. Chem. B* **1997**, *101*, 8141

Chapter 8

Conclusions and outlook

Chapter 8 Conclusions and outlook

The results presented in this thesis show that the electron transport in dye-sensitised nanocrystalline cells is remarkably slow and intensity dependent. As the intensity increases the effective diffusion coefficient increases. As the electrons move through the film they are constantly being trapped and released, as the light intensity is increased the deeper traps are filled leaving less unfilled traps. This results in the electrons spending less time in traps and therefore transport through the film is faster at higher light intensities; i.e. the effective diffusion coefficient increases. At a light intensity of 1 sun, Dn is noted to be over 100 times smaller than the diffusion coefficient for electrons in bulk TiO_2.

The lifetime (τ_n) of the photoinjected electrons is also intensity dependent, the lifetime of the electrons decreases as the intensity increases. The reason for this is not clear at present and further work is required. Work to establish a reaction mechanism would also be useful. Further work could include measurements of τ as a function of the iodide and triiodide concentration. The results in this thesis only show a small range of light intensities future work could include extensive studies of τ as a function of the light intensity.

The electron diffusion length (L_n) of the cells determines the incident photon to current conversion efficiency. For an efficient cell L_n needs to be greater than the film thickness so that the maximum number of generated electrons can be collected. If L_n is smaller than the film thickness then most of the photoinjected electrons will not reach the collection contact and thus a small IPCE will result. L_n is characterised by the electron lifetime (τ_n) and the effective diffusion coefficient (D_n) *i.e.* $L_n=(\tau_n D_n)^{1/2}$, as the intensity increases τ_n decreases and D_n increases. The rate at which τ_n decreases and D_n increases are similar and result in L_n being almost independent of light intensity. This raises questions as to weather the I^-/I_3^- redox system is unique and could this be the reason why other redox systems have failed. Clearly more work on the reaction mechanism is needed before it is possible to say for certain.

Impedance measurements of platinum and SnO_2 electrodes in the cell electrolyte which contains I^-/I_3^- show that, on platinum electron transfer occurs on a very fast time scale however on SnO_2 electron transfer is very slow. Electron transfer is also noted to be slow on the TiO_2 film. It is clear to see that the redox system shows differential kinetics which are essential in order for the cell to work efficiently.

As the potential approaches open circuit the capacitance of the film increases. This trend is followed in the dark and under illumination. Under illumination the capacitance at a particular potential is higher than in the dark. Typical values at short circuit are in the μF range however at open circuit values exceeding 3mF have been measured under illumination. The IMPS results also show that that the capacitance of the film dominates as V_{oc} is approached, which confirms the presence of a large capacitance.

Studies within this thesis show that the open circuit voltage of the cell is related to the concentration of tert-butyl pyridine. It is also noticeable that the addition of tert-butyl pyridine appears to increase the fill factor of the cell, more work as to why this occurs is required.

Further work is required to determine the factors that influence the open circuit voltage, the short circuit current and the fill factor of the cell. Once these factors are determined they will enable the construction of optimised cells. An understanding of the reaction mechanism of the I^-/I_3^- redox system would be useful in order to design optimised cells. Work to investigate the factors that influence electron trapping and to determine the possibility of decreasing the trap density within the film is also needed. The film preparation method and the use of alternative oxides could be investigated with a view to reducing the trap density within the film and therefore increasing D_n. Experiments employing alternative dyes focusing on extending the spectral range of the cells would also be useful.